UNCLASSIFIED

AD NUMBER

AD919003

NEW LIMITATION CHANGE

TO

Approved for public release, distribution unlimited

FROM

Distribution authorized to U.S. Gov't. agencies only; test and evaluation; Feb 1974. Other requests shall be referred to AF Flight Dynamics Laboratory [FYA], Wright-Patterson AFB, Ohio 45433.

AUTHORITY

affdl ltr, 27 aug 79

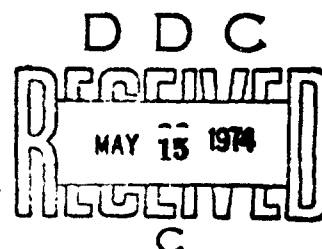# THIS PAGE IS UNCLASSIFIED

AFFDL-TR-73-158

AD919003

JET NOISE REDUCTION FOR MILITARY RECONNAISSANCE/SURVEILLANCE AIRCRAFT

PHASE II: ANALYSIS AND DESIGN OF A QUIET RESEARCH TEST VEHICLE

R. F. SPETH et al

BELL AEROSPACE COMPANY
DIVISION OF TEXTRON

D D C

MAY 15 1974

TECHNICAL REPORT NO. AFFDL-TR-73-158

C

APRIL 1974

REPRODUCTION QUALITY NOTICE

This document is the best quality available. The copy furnished to DTIC contained pages that may have the following quality problems:

- Pages smaller or larger than normal.

- Pages with background color or light colored printing.

- Pages with small type or poor printing; and or

- Pages with continuous tone material or color photographs.

Due to various output media available these conditions may or may not cause poor legibility in the microfiche or hardcopy output you receive.

☐ If this block is checked, the copy furnished to DTIC contained pages with color printing, that when reproduced in Black and White, may change detail of the original copy.

NOTICE

When Government drawings, specifications, or other data are used for any purpose other than in connection with a definitely related Government procurement operation, the United States Government thereby incurs no responsibility nor any obligation whatsoever; and the fact that the government may have formulated, furnished, or in any way supplied the said drawings, specifications, or other data, is not to be regarded by implication or otherwise as in any manner licensing the holder or any other person or corporation, or conveying any rights or permission to manufacture, use, or sell any patented invention that may in any way be related thereto.

Copies of this report should not be returned unless return is required by security considerations, contractual obligations, or notice on a specific document.

JET NOISE REDUCTION FOR
MILITARY RECONNAISSANCE/SURVEILLANCE AIRCRAFT
PHASE II: ANALYSIS AND DESIGN OF A
QUIET RESEARCH TEST VEHICLE

R. F. Speth et al
Bell Aerospace Company
Division of Textron

FOREWORD

ERNEST C. SIMPSON
Director
Turbine Engine Division
AF Aero Propulsion Laboratory

WALTER J. MYKYTOW
Asst. for Research & Technology
Vehicle Dynamics Division
AF Flight Dynamics Laboratory

ABSTRACT

This report presents the results of the analysis and design of a static ground test version of a Quiet Research Test Vehicle (QRTV) utilizing flightworthy propulsion system components. Also included is a discussion of the fabrication of a sufficient number of propulsive struts, employing multiple micro-jets, to propel a Schweizer SGS 2-32 sailplane up to 123 knots airspeed.

The analysis and design encompasses the information required to modify the sailplane structure to incorporate the propulsion system for basic ground tests. The design of the static ground test is not covered completely. Overall consideration of the ultimate QRTV flight version has been a primary goal in the analysis and design phase of this program.

As negotiated originally, the modification to the wing structure necessary to install the spanwise ducts was not a task in Phase II. Late in the program, the analysis and design of the spanwise wing duct installation was added to the program. Furthermore, hot pressure tests of a sample production propulsive strut were also included. Results of these two additional tasks have been incorporated as appendices in this report.

iii

CONTENTS

CONTENTS (CONT)

ILLUSTRATIONS

ILLUSTRATIONS (CONT)

TABLES

LIST OF SYMBOLS AND ABBREVIATIONS

Symbol		Definition
A	-	Area
a	-	Length of panel
b	-	Width
B.M.	-	Bending Moment
C or c	-	Chord
$\mathbb{C}$	-	Centerline
C_{h_α}	-	Flap hinge moment coefficient due to angle of attack
C_{h_δ}	-	Flap hinge moment coefficient due to flap deflection
C_h	-	Total Flap hinge moment coefficient
C_p	-	Pressure coefficient
c_n	-	Section normal force coefficient
C_{N_f}	-	Flap normal force coefficient
c_f	-	Flap chord
CDP	-	Compressor discharge pressure
C_D	-	Discharge coefficient
C_V	-	Velocity coefficient
db or dB	-	Decibels
ds	-	Incremental length
e	-	Eccentricity or distance to flexural center from reference
F_{tu}	-	Stress - tensile ultimate
F_{ty}	-	Stress - tensile yield
F_{cy}	-	Stress - compressive yield

LIST OF SYMBOLS AND ABBREVIATIONS (CONT.)

Symbol		Definition
FF_T	-	Isentropic flow function $\sim \dfrac{w\sqrt{T_T}}{AP_T}$
F_{ir}	-	Inter-rivet buckling stress
F_{bru}	-	Stress - bearing ultimate
$°F$	-	Degrees Fahrenheit
F.S.	- ·	Front spar
f	-	Stress
f_b	-	Bending stress
f_{brg}	-	Bearing stress
f_t	-	Tensile stress
G	-	Material shear modulus
g	-	Acceleration due to gravity
HM_f	-	Flap hinge moment
Hz	-	Hertz
h	-	Height
I	-	Moment of inertia
I_{NA}	-	Moment of inertia at neutral axis
in.	-	Inch
k	-	Coefficient
L	-	Length
ℓ	-	Length (such as panel dimension)
L.E.	-	Leading edge
lb	· -	Pound

LIST OF SYMBOLS AND ABBREVIATIONS (CONT.)

Symbol		Definition
M	-	Moment
M.S.	-	Margin of safety
N	-	Engine spool speed
N_f	-	Flap normal force
P	-	Load, Pressure, or Rivet spacing location
P_D	-	Shear resulting from direct load
P_m	-	Shear resulting from moment
psi	-	Pounds per square inch
psf	-	pounds per square foot
psig	-	Gage pressure
QRTV	-	Quiet research test vehicle
q	-	Shear flow or dynamic pressure
R	-	Reaction
Ref	-	Reference
R.S.	-	Rear spar
°R	-	Degrees Rankine
r	-	Rivet pattern distance - centroid to rivet
rpm	-	Revolutions per minute
Sp	-	Spaces
T	-	Temperature
TIG	-	Tungsten inert gas
T	-	Torque

LIST OF SYMBOLS AND ABBREVIATIONS (CONT.)

Symbol		Definition
T.E.	-	Trailing edge
Temp	-	Temperature
T.O.	-	Takeoff Condition
t	-	Thickness
V	-	Velocity
W	-	Loading
W.L.	-	Waterline
w	-	Running load
$\dot{w}$	-	Weight flow
X	-	Force in y-y axis direction (+Fwd)
Y	-	Force in y-y axis direction (+Left looking fwd)
y	-	Centroid location in y direction
Z	-	Force in z-z direction
%	-	Percent
@	-	At
$\oint$	-	Line integral

LIST OF SYMBOLS AND ABBREVIATIONS (CONT.)

Symbol		Definition

Greek Symbols

θ	-	Ratio of actual temperature to sea level standard temperature, or angle of twist
θ_F or δ_F	-	Flap deflection angle
δ	-	Ratio of actual pressure to sea level standard pressure
δ	-	Deflection
σ_{cr}	-	Tensile stress
σ_F	-	Ultimate compressive stress-ultimate
η	-	Acceleration in "g's"

Subscripts

A,B,C, etc.	-	Location or points on structure
F,L, & R	-	Engine mount points - front, left and right
f	-	Flange
w	-	Web
z	-	Vertical direction (+ up)
y	-	Lateral direction (+ right)
x	-	Drag direction (+ aft)
1	-	Engine low speed spool
2	-	Engine high speed spool

I. INTRODUCTION AND SUMMARY

This program entitled "Jet Noise Reduction for Military Reconnaissance/Surveillance Aircraft" has consisted of two phases. The first phase comprised the analysis, design, development testing, and selection of the basic components of an integrated "quiet" propulsive-wing concept. One task in this first phase dealt with the preliminary design of a static ground test stand. The primary purpose of the test stand was to determine the static propulsion characteristics of a system ultimately to be installed in a Schweizer SGS 2-32 Sailplane. The modified sailplane was designated as a Quiet Research Test Vehicle (QRTV). The test stand however, was conceived in a "boiler-plate" engine installation.

The bench/wind tunnel tests of Phase I of this contract resulted in the selection of the single row of microjet nozzles at the trailing edge of the propulsive struts which will be arranged in closely-spaced multistrut arrays on the upper surface of the wing of the QRTV. Based on the data obtained, the predicted aural detectability of the Quiet Research Test Vehicle will be significantly less than other types of quiet aircraft.

As Phase I approached completion, a decision was made by the Air Force to proceed into Phase II with flightworthy components instead of the "boiler-plate" test stand. From early October 1972 until February 1973, the manner in which Phase II was to be conducted was considered and became established. It was decided that the funds allocated for this phase of the program would be expended mainly in the analysis and design of a flightworthy integrated "quiet" propulsive wing system. It was also decided that a portion of these funds should be used for the fabrication of a sufficient number of propulsive struts for the QRTV.

This report presents the results of the analysis and design of this system as well as a description of the techniques employed in the fabrication of the propulsive struts. It shows that the concept of this particular QRTV is very feasible and presents the detailed analyses of the propulsion system and its structural and weight aspects with regard to the adaptation of this system to the Schweizer SGS 2-32 Sailplane.

A separate contractual item is the complete set of layout and detail drawings showing how this quiet propulsion system can be installed in the QRTV.

Appendices A and B of this report summarize the results of the two tasks added to the contract during the latter part of Phase II. Appendix A contains a summary of the detailed design of the duct installation in the wing of the Schweizer SGS 2 32 Sailplane. The results in Appendix B pertain to the hot pressure testing of a sample production propulsive strut, selected at random, to ascertain the structural integrity of the flightworthy struts. These tests revealed an inadequacy in a secondary structural element caused by the inadvertent choice of incompatible materials and fabrication techniques. An acceptable repair placed the struts in the flightworthy hardware status.

II. ANALYSIS AND DESIGN OF THE QUIET RESEARCH TEST VEHICLE

A.   GENERAL DESCRIPTION

The Quiet Research Test Vehicle (QRTV) may be described as a Schweizer SGS 2-32 Sail-
plane modified to incorporate an integrated "quiet" propulsive wing. This propulsive wing consists
of internal spanwise ducts which supply the mixed exhaust gas from the Williams Research Corp-
oration WR-19 turbofan engine to an arrangement of multiple microjet thrusting struts as depicted
schematically in Figure 1. These struts, installed on the wing of the Schweizer sailplane, will provide
a level of thrust sufficient to propel the aircraft to airspeeds in excess of 120 knots. The nominal
design cruise speed, however, has been set at 60 knots. Figure 2 portrays the general arrangement
of the SGS 2-32 Sailplane with the propulsive struts and engine inlet.

The original primary goal of this Phase II of the program was to analyze and design a system
complete enough to conduct a series of static ground tests to prove the propulsive characteristics of
the flightworthy components of this unique propulsion system. A secondary goal was to obtain
quantitative measurements of the noise environment produced by the engine/propulsion system
installation. However, the negotiated end product of Phase II was to analyze and finalize the design
of this system and to fabricate approximately 500 of the propulsive struts for eventual installation
on the SGS 2-32 Sailplane.

B.   DESIGN

During Phase II of this Jet Noise Reduction Program the layout and detailed design drawings
required to fabricate the integrated "quiet" propulsive wing were generated. These drawings con-
stitute a portion of Item AOOA of the Contractual Data Requirements and are listed in Table 1.
A general discussion of the design aspects of this propulsion system and the required modifications
to the aircraft are contained in this section of this report.

1.   Propulsive Struts and Mounting Plates

Design of the propulsive struts evolved as a result of a Bell Aerospace Company funded
Manufacturing Engineering Development Program. This program proved that the propulsive strut
trailing edge and microjet nozzles could be punched and coined from a preformed blank of 0.032
inch thick 6061-0 aluminum alloy sheet. With the trailing edge and nozzles completed, the airfoil
shape of the strut could be formed by use of an internal mandrel and hydraulic press. The leading
edge and tip of the strut were joined and sealed by the Tungsten Inert Gas (TIG) process. Two
airfoil shaped tension posts were riveted into place at two spanwise locations in the strut to prevent
distortion of the airfoil shape of the strut under the anticipated levels of exhaust gas pressure and
temperature. A flare was provided at the base of the strut for TIG weld attachment of the strut
mounting plates.

The mounting plates were designed in sections to accommodate between 8 and 12 struts
so as not to interfere with the rib structure of the wing. The mounting plates will also be 0.032 inch
thick 6061 aluminum sheet and will be punched to match the airfoil shape of the flared strut base.
The mounting plates, with struts attached, will be sealed with RTV or similar compound and riveted
to the underside of the Titanium backup plate which constitutes the top surface of the spanwise
wing duct.

2

434 STRUTS (217 PER SIDE)
70 - 0.043 IN. DIA HOLES PER STRUT
CLOSE-SPACED; DOUBLE ROW

INDUCED
FLOW

EXHAUST
FLOW

SUPPLY
INFLOW
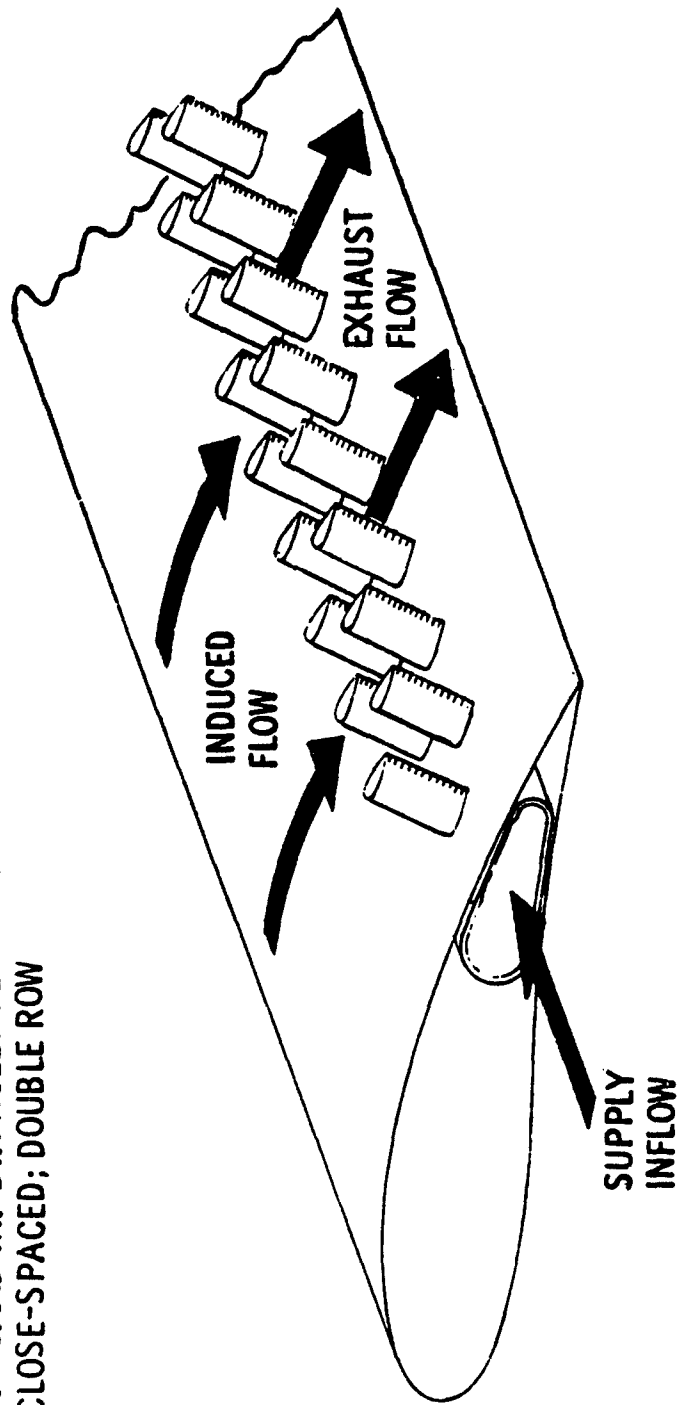
Figure 1. Micro-Jet Propulsive Strut Installation in the QRTV Wing

3

684 (57.0 FT)

84 (7.0 FT)

321 (26.75 FT)
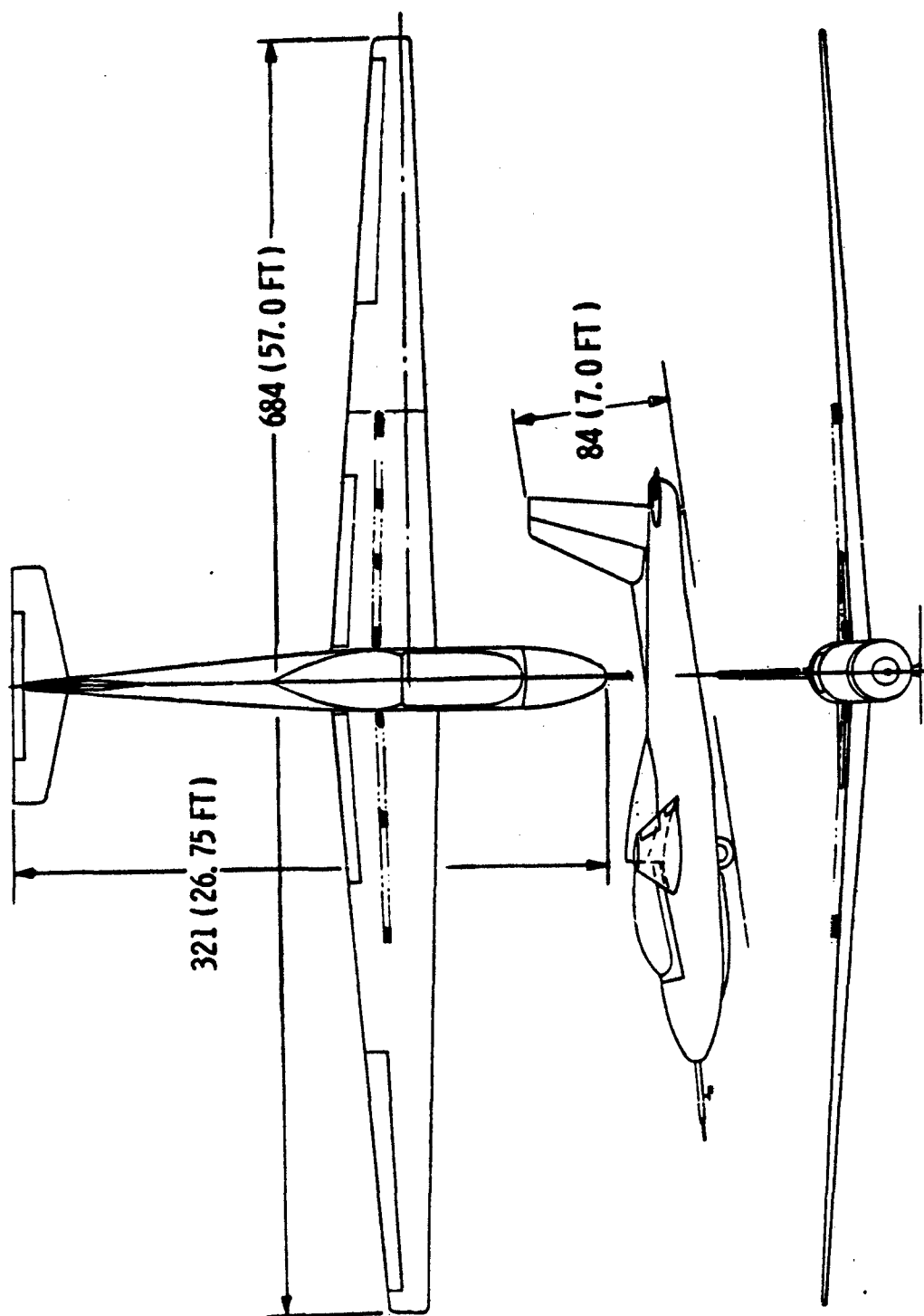
Figure 2. General Arrangement of the QRTV

4

TABLE 1
DRAWING LIST - JET NOISE REDUCTION PROGRAM

7389-430050	Strut Plate Assy. - Jet Noise Reduction
7389-430051	Cover Plate Assy. - Inboard Section - Jet Noise Reduction
7389-430052	Cover Plate Assy. - Center Section - Jet Noise Reduction
7389-430053	Cover Plate Assy. - Outboard Section - Jet Noise Reduction
7389-430054	Exhaust Ducting - Engine - Jet Noise Reduction
7389-430055	Duct Assy. - Inboard Section - Wing - Jet Noise Reduction
7389-430056	Duct Assy. - Center Section - Wing - Jet Noise Reduction
7389-430057	Duct Assy. - Outboard Section - Wing - Jet Noise Reduction
7389-430058	Expansion Joint - Inboard - Wing - Jet Noise Reduction
7389-430059	Expansion Joint - Center - Wing - Jet Noise Reduction
7389-430060	Expansion Joint - Outboard - Wing - Jet Noise Reduction
7389-430062	Duct Installation - Wing - Jet Noise Reduction
7389-430063	Angle - Wing Duct - Jet Noise Reduction
7389-430064	Restraint - Wing Duct - Jet Noise Reduction
7389-430065	Strut Assy. - Jet Noise Reduction
7389-430066	Tee - Wing Duct - Jet Noise Reduction
7389-430067	Support - Wing Duct - Jet Noise Reduction
7389-430068	Link - Wing Duct - Jet Noise Reduction
7389-430070	Propulsion Installation and Fuselage Modification - Jet Noise Reduction
7389-430071	Fuselage Doubler Installation - Wing Root - Jet Noise Reduction
7389-430072	Bulkhead Assy. - Sta. 128.939 - Jet Noise Reduction
7389-430073	Support Installation - Lower - Sta. 129.189 - Jet Noise Reduction
7389-430074	Bulkhead - Upper - Sta. 129.189 - Jet Noise Reduction
7389-430075	Bulkhead - Sta. 153.0 and 154.37 - Jet Noise Reduction
7389-430076	Aft Fuselage (Modified) Glider - Jet Noise Reduction
7389-430077	Truss Installation - Wishbone Structure Replacement - Jet Noise Reduction
7389-430078	Fitting - Wishbone Structure Replacement - Jet Noise Reduction
7389-430079	Support Installation - Engine - Jet Noise Reduction
7389-430080	Mounting Plates - Engine Vibration Mount - Jet Noise Reduction
7389-430081	Engine Mount Pad - Engine Vibration Mount - Jet Noise Reduction
7389-430082	Center Support Assy. - Engine - Jet Noise Reduction
7389-430083	Engine Enclosure - Lower - Jet Noise Reduction
7389-430084	Shear Deck Installation - Engine Mount - Jet Noise Reduction
7389-430085	Engine Enclosure and Inlet Duct - Upper - Jet Noise Reduction
7389-430086	Shear Deck Installation - Sta. 129.189 - Sta. 153.00 - Jet Noise Reduction
7389-430087	Inlet Acoustic Baffle - Assy. and Installation - Jet Noise Reduction
7389-430088	Engine Controls and Instrumentation Installation - Jet Noise Reduction
7389-430089	Flap Geometry - Schweizer Wing - Jet Noise Reduction
7389-430091	Rib Root - Sta. 18.75 - Jet Noise Reduction
7389-430092	Rib Intermediate - Sta. 27.0 - Jet Noise Reduction
7389-430093	Rib Assy - Sta. 34.50 - Jet Noise Reduction
7389-430094	Rib Assy - Sta. 42 - Jet Noise Reduction
7389-430095	Rib Intermediate - Sta. 49.50 - Jet Noise Reduction
7389-430096	Rib Intermediate - Sta. 57.0 - Jet Noise Reduction
7389-430097	Rib Intermediate - Sta. 64.5 - Jet Noise Reduction
7389-430098	Rib Assy - Sta. 72 - Jet Noise Reduction
7389-430099	Rib Assy - Sta. 79.50 - Jet Noise Reduction
7389-430100	Rib Assy - Sta. 87 - Jet Noise Reduction
7389-430101	Rib Intermediate - Sta. 98.0 - Jet Noise Reduction
7389-430102	Rib Intermediate - Sta. 109.0 - Jet Noise Reduction
7389-430103	Rib Intermediate - Sta. 120.0 - Jet Noise Reduction
7389-430104	Rib Intermediate - Sta. 131.0 - Jet Noise Reduction
7389-430105	Rib Intermediate - Sta. 142.0 - Jet Noise Reduction
7389-430106	Rib Intermediate - Sta. 154.0 - Jet Noise Reduction
Sketch No. 1	Cutouts and Reinforcements - Wing - Struts - Jet Noise Reduction
Sketch No. 2	Flap and Ribs - Wings - Jet Noise Reduction

2. Wing Duct and Backup Plates

The spanwise wing ducts which will supply the WR-19 turbofan exhaust gases to the propulsive struts were designed in three sections for each wing panel in order to alleviate growth effects due to exhaust gas temperatures. Each section will be attached to the structure of the ground test stand in the same manner as it eventually will be mounted in the sailplane wing. To achieve this the links and brackets were designed to support the weight of the duct sections and to restrain the duct from movement imposed by the exhaust gas pressure, the propulsive strut thrust, and associated moments.

The duct sections are of a rounded trapezoidal cross-section which taper slightly in the spanwise direction in both width and height. The pressure vessel consists of 0.032 inch thick 6Al-4V titanium with 0.040 inch thick chordwise zee section stiffeners spot-welded to the duct wall at approximately 5 inch spanwise spacing. The zee section stiffeners are 3/4 inch deep and also serve as standoffs for an 0.035 inch thick, porous, sintered stainless steel material known as "Rigimesh" possessing a Rayl Number of 35. This porous material will act as an acoustic damper on the two sides and bottom of the wing ducts.

The top surface of the duct is a 0.10 inch thick sheet of 6Al-4V titanium which is sealed and attached by channel nut plates to titanium angles welded to the fore and aft walls of the spanwise ducts. This sheet constitutes the backup plate for the propulsive strut mounting plates and will be punched with clearance holes to allow the propulsive struts to protrude.

The wind duct sections will be joined and sealed together by means of custom made flexible, silicone rubber joints. The attachment restraints discussed previously will prevent any spanwise movement of the duct sections relative to each oth r. The root chord end of the inboard duct section is similarily joined and sealed to the transistion section of the bifurcated exhaust duct.

3. Fuselage Modifications

In order to incorporate this propulsion system in the SGS-2-32 Sailplane, it will be necessary to remove and replace certain components in the fuselage as well as add some basic structural elements. The following series of nine sketches indicate the nature of these fuselage modifications.

4. Engine Installation

The engine is to be installed behind the aft crew compartment with the inlet facing the rear of the aircraft. This was done in order to locate the bifurcated exhaust duct in the proper position relative to wing to facilitate connection to the spanwise wing duct. Furthermore, this orientation of the engine provided a means for designing an inlet duct with only minor modifications to existing aircraft structure.

Attachment of the engine to the fuselage will be accomplished by utilizing the three mounting pads supplied with the engine bypass duct. Two of these pads provide the primary support and are located on either side of the engine in the plane of the engine centerline just downstream of the main structural frame of the engine. The third mount comprises a stabilizing link on the bottom of the bypass duct just upstream of the flange for attachment of the bifurcated exhaust duct. Additional structural components have been incorporated in the fuselage to transmit engine weight and

FWD

STA
116.39

ADD DOUBLER

WING ROOT
FAIRING FLANGE

7.25 DIA HOLE

WL
11.500

SECTION TO BE
TRIMMED TO
CLEAR 7.25 DIA
HOLE (TYP)

WING ROOT
FAIRING FLANGE
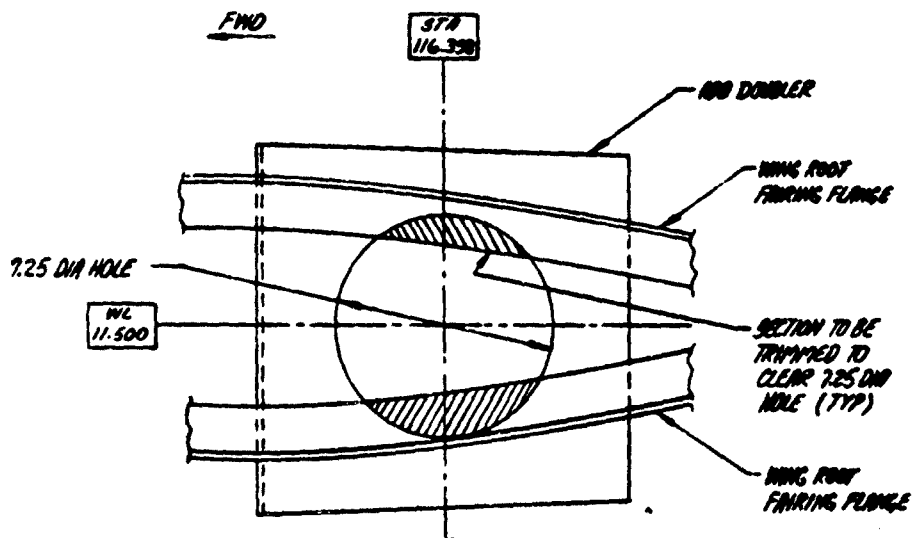
Sketch 1 - Fuselage and Wing Intersection

A hole in the fuselage skin at the fuselage/wing juncture must
be provided to allow passage of the bifurcated exhaust duct into
the wing. As indicated in the sketch, portions of the wing root
fairing flange must also be removed to provide adequate clearance.
The doubler plate shown has been added to provide structural stab-
ility in the fuselage skin in the vicinity of this hole.

FWD

AFT CANOPY DECK ASSY

STA
128.939

WL
26.260

℄ SHIP

A

A

9.9R

WL
26.260

.25

REWORKED DEPTH OF BLKHD

SECTION A-A
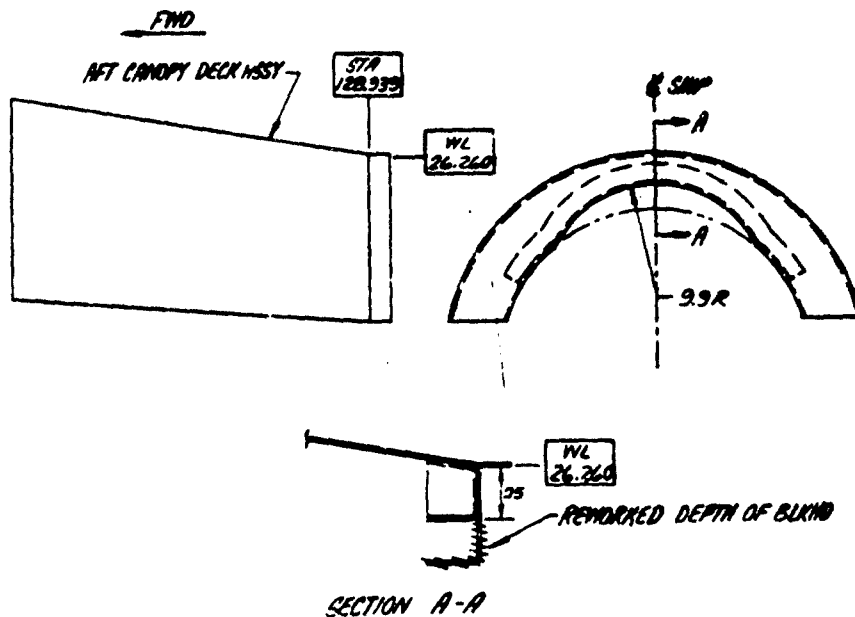
Sketch 2 - Aft Canopy Bulkhead

The existing aft canopy bulkhead at fuselage station 128.939 must
be reworked in the manner shown in the sketch in order to provide
clearance for the top of the engine enclosure

7

Section labels in diagram: REMOVE THIS PORTION OF EXTRUSION, ¢ SHIP, BL 9.750, BL 11.150, END OF EXTRUSION AFTER TRIMMING, ADD SUPPORT, ADD CHANNEL, PICK UP EXISTING RIVETS, A, A, STA 129.18?, 1.00, WL 11.555, 2.00, FWD, .75, ADD 7/8 DIA HOLE, ADD REINF. ANGLE, SECTION A-A, VIEW LOOKING AFT
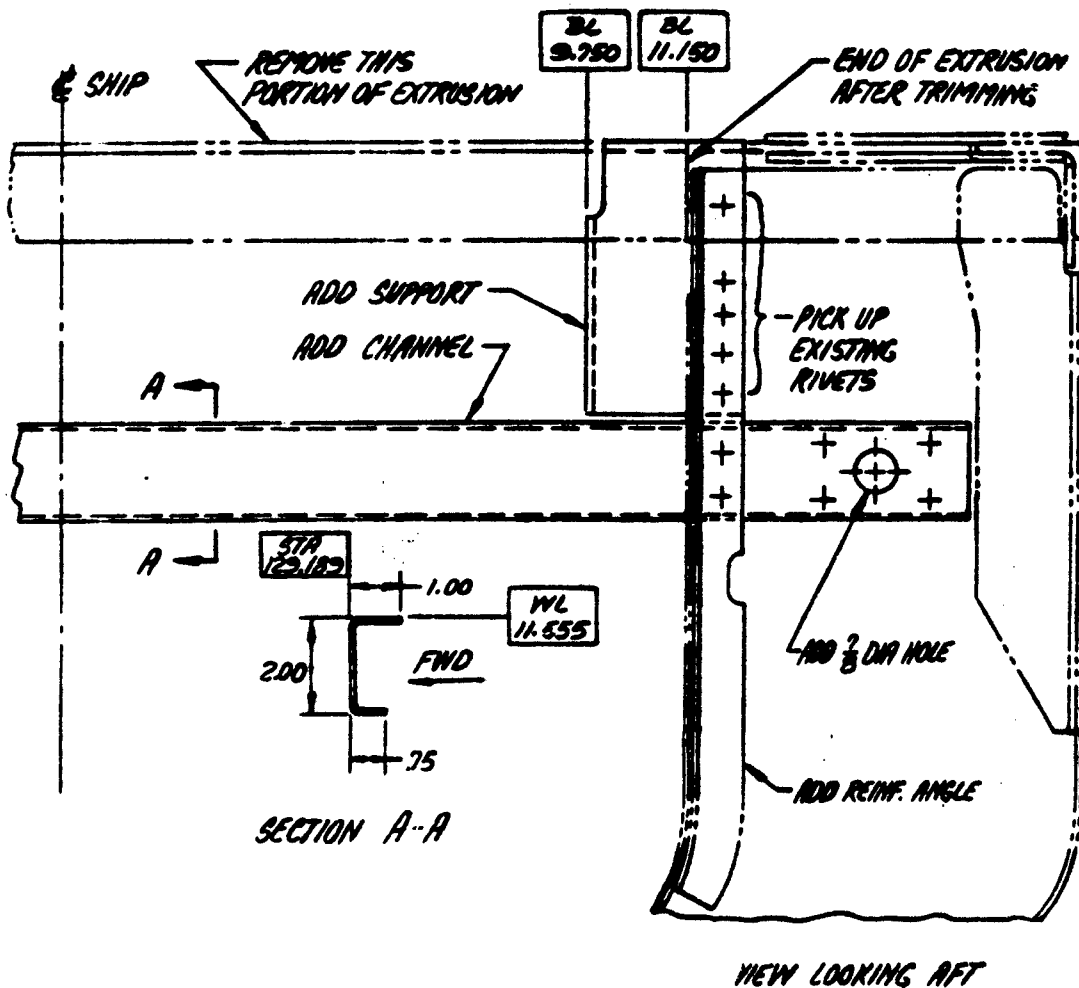
Sketch 3 - Lower Bulkhead; Fuselage Station 129.18?

For installation of the lower portion of the engine enclosure,
it will be necessary to remove that portion of the lateral extrusion
shown in the upper section of sketch between buttock lines 11.150.
The lower channel will be added to maintain structural integrity
at this fuselage station. This added channel will also be employed
as support for the main engine mounts. A flanged shear web will be
added from buttock lines 9.750 and riveted to the existing fuselage
bulkhead. The lower part of the engine enclosure will be attached
to the flange of this shear web. The added 7/8 inch diameter hole
will be provided as a clearance hole for the wing rear beam attach-
ment pin.

8

VIEW LOOKING FWD
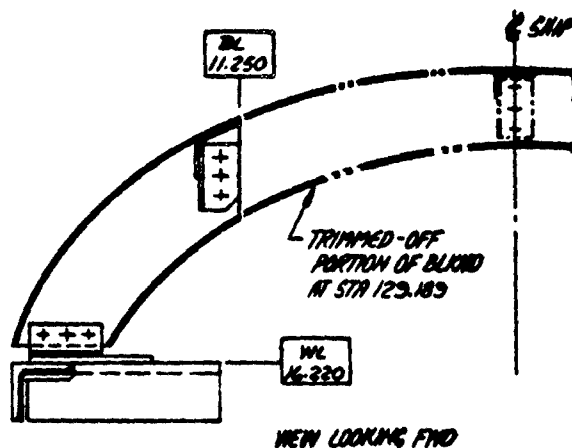
Sketch 4 - Upper Bulkhead, Fuselage Station 129.189

An opening in the top of the aircraft between fuselage stations
129.189 and 153.81 and buttock lines 11.250 for installation
and removal of the upper engine enclosure and inlet. The portion
of the bulkhead at fuselage station 129.189 indicated in the
sketch must be removed for this purpose. This will necessitate
removal of the longitudinal angle shown in end view at the ship
centerline. The gusset and angle shown at buttock line 11.250
will be added on both sides to preserve structural characteristics
of the fuselage in this area.
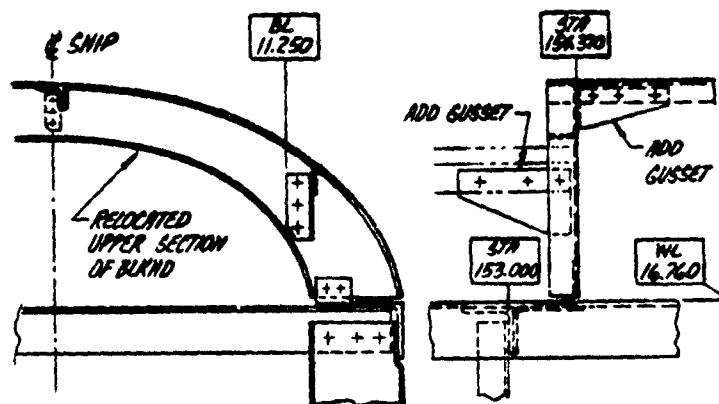
Sketch 5 - Upper Bulkhead, Relocated from Fuselage Station
153.000 to 154.370

It will be necessary to move the upper bulkhead existing at
fuselage station 153.000 to station 154.370 in order to install
the engine enclosure and inlet. This relocated bulkhead provides
the rear attachment point for the new longitudinal angle at buttock
line 11.250 mentioned in the explanatory note for Sketch 4. A
gusset will also be added as a structural attachment at the forward
end of the longitudinal angle on the ship centerline, a portion
of which will be removed to provide the opening at the top of the
fuselage.

9

SECTION A-A
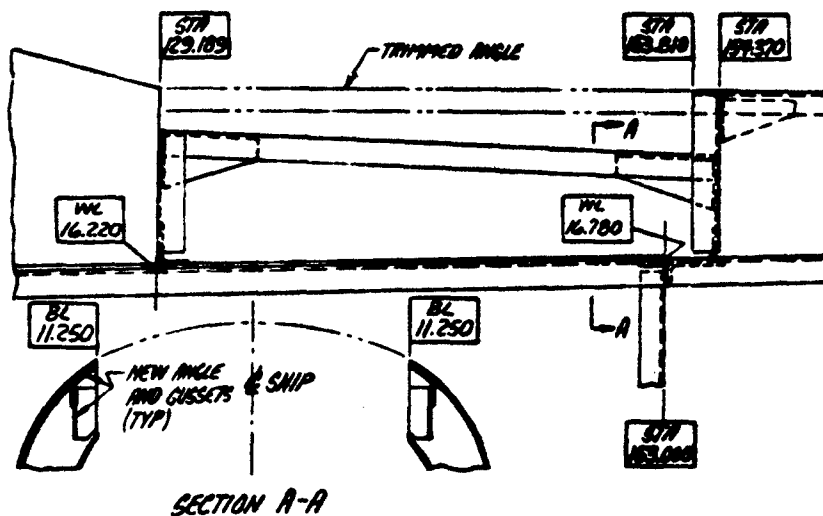
Sketch 6 - Fuselage Frame Assembly (Engine Access)

This sketch portrays the overall fuselage frame assembly discussed
in detail on Sketches 4 and 5. It should be noted that the portion
of the fuselage forward of fuselage station 129.189 and above water
line 16.220 is a presently removable fairing aft of the crew compart-
ment canopy.
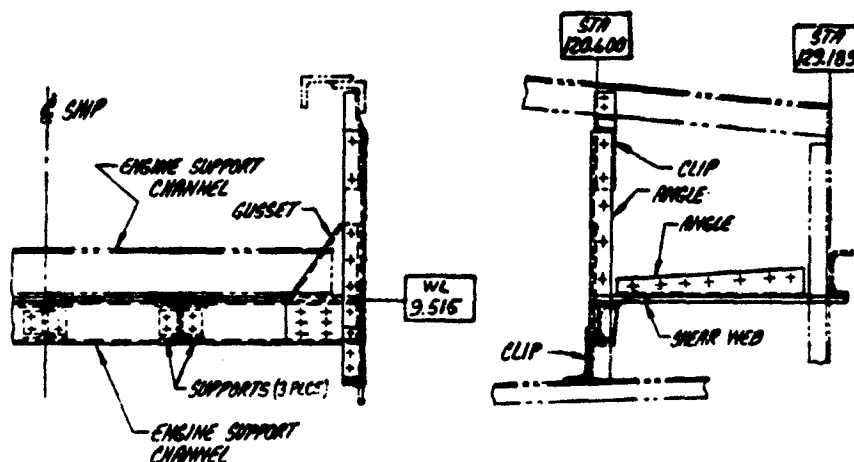
Sketch 7 - Engine Mount Support

This sketch depicts the additional structural members required
to support the engine on the basic aircraft structure. The
lateral channel and vertical angle at fuselage station 120.600
will be added as the structural tie-in for the single rear engine
mount; the channel at station 129.189 will provide support for
the two forward engine mounts. These two lateral channels will
be tied together with the shear web shown. The edges of the shear
web will be stabilized by two angles, which in turn will be
riveted to the fuselage skin. Also included, but not shown in
the sketch, are two compression structural members which will
restrain the engine under a 20g ultimate horizontal load.

10
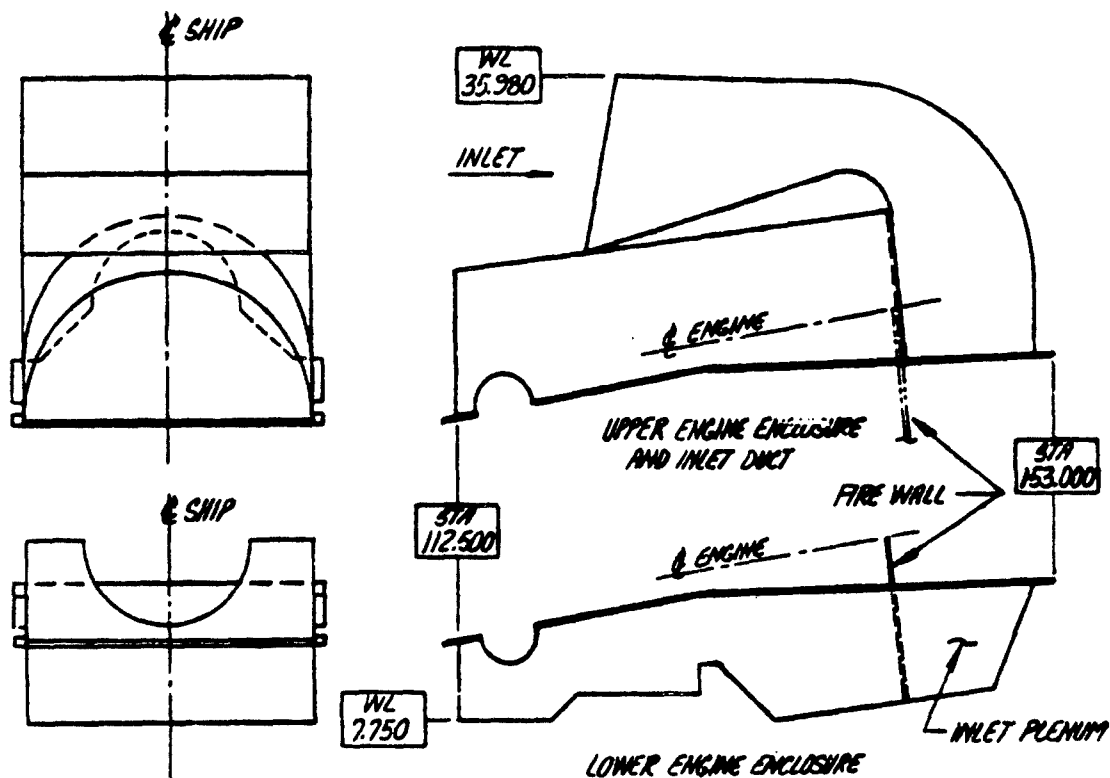
Sketch 8 - Engine Enclosure and Inlet Layout

This sketch depicts the general arrangement of the engine enclosure
and inlet. The lower engine enclosure will be relatively perman-
ently installed in the aircraft; whereas the upper engine enclosure
and inlet assembly will be readily removable for engine maintenance.
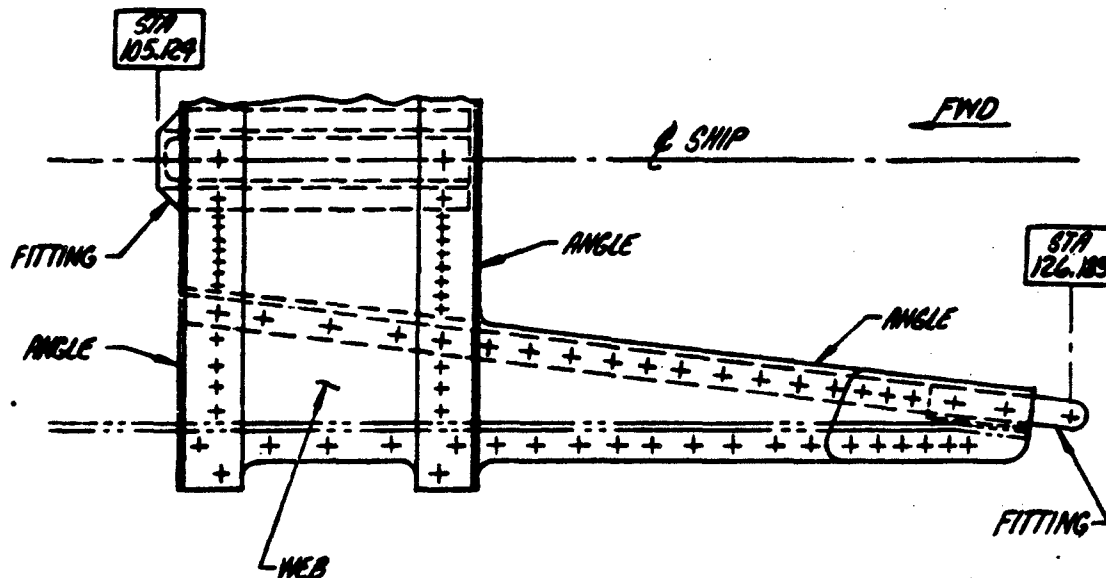
Sketch 9 - Replaced Wing Load Support Structure

The structure shown in the sketch will replace the original wing
load support structure in the aircraft which must be removed to
provide clearance for the engine installation. The fitting located
on the ship centerline wi h the face at fuselage station 105.124
attaches to the wing main carrythrough structure.

thrust reaction loads to primary aircraft structure. A restraining structure has also been designed to be installed and attached to the two primary support pads. This structure consists of two compression members which will restrain engine movement under a 10 g longitudinal impact load.

5. Exhaust Duct and Transition Section

The exhaust duct for the engine in this installation will be bifurcated just downstream of the last turbine stage and each leg will go through a 90 degree bend during which the cross-sectional shape will vary, at constant area, from semi-annular to a 2 to 1 ellipse. Actually, this section of the exhaust duct will be a portion of that used for the Individual Lift Device (Jet Belt) under Contract No. DA23-204-AMC-03712(T). Another short section of duct will provide a means of varying the elliptical section to circular as well as executing a slight bend. This will properly orient the two circular duct sections for attachment to the wing duct by means of the transition section. A Marmon Clamp Flange is to be welded at the downstream ends of these circular ducts as well as at the upstream ends of the transition sections.

The transition section constitutes a slight diffuser and also changes the duct cross-sectional shape from circular to a shape which matches the rounded trapezoidal shape of the spanwise wing ducts. The transition piece will be attached to the wing duct by means of a custom made, flexible silicone rubber joint and to the circular exhaust duct by means of a Marmon clamp. The Marmon clamp joints comprise the disconnect points in the exhaust ducts for removal of the wing ducts from the engine installation in the fuselage. During operation of the system during static ground tests, these joints also allow one foot long circular instrumentation sections to be installed for the purpose of measuring exhaust gas pressures and temperatures. From these data the magnitudes of the exhaust gas velocities and weight flows entering the wing ducts can be ascertained.

6. Engine Enclosure and Inlet Duct

The general appearance of this installation is shown schematically in Sketch 8, page 11. Except for the curvature in the inlet duct entering the plenum chamber at the engine inlet, it can be seen that the engine enclosure and inlet duct are made up of essentially flat 0.040 inch thick aluminum alloy sheet. In the areas of the inlet duct and plenum chamber, where the internal flow velocities will create a slight static pressure differential, these flat panels have been reinforced against undue deflections by properly placed hat section stiffeners. The entire inner surface of the inlet duct and plenum will be lined with a porous (Rayl Number 35), sintered, stainless steel acoustic barrier. This material is held away from the duct wall by approximately 1/2 inch by the hat section stiffeners mentioned previously. The bottom section of the engine enclosure is similarily lined to provide acoustic treatment without the fuel and oil absorption characteristics of fiberglass mat. The exterior of inlet duct, plenum chamber, and lower engine enclosure are to be covered by two layers of 1/4 inch fiberglass mat with a thin lead septum between to act as a noise absorber and dampener. The inner surface of upper engine enclosure is also lined with this fiberglass mat/lead septum material.

The design is such that by removing the existing aerodynamic fairing aft of the crew compartment, the entire inlet duct and upper engine enclosure may be readily removed for easy accessibility.

13

7. Engine Controls and Instrumentation

Once the engine is started and has reached ground idle speed, control of its operation is extremely simple. All accelerations and decelerations of the engine are automatically controlled within the fuel controller. All that is necessary is a throttle quadrant mounted at the left side of the pilot's compartment with the proper detents for ground idle, flight idle and maximum power. This is connected to the throttle lever on the fuel controller by means of a flexible cable and conduit.

Instruments for monitoring engine performance during start and operation will be installed in the existing instrumentation panel of the Schweizer SGS-2-32 Sailplane as depicted in Figure 3. It will be noted that the instruments presently in use on the sailplane will remain in the panel.
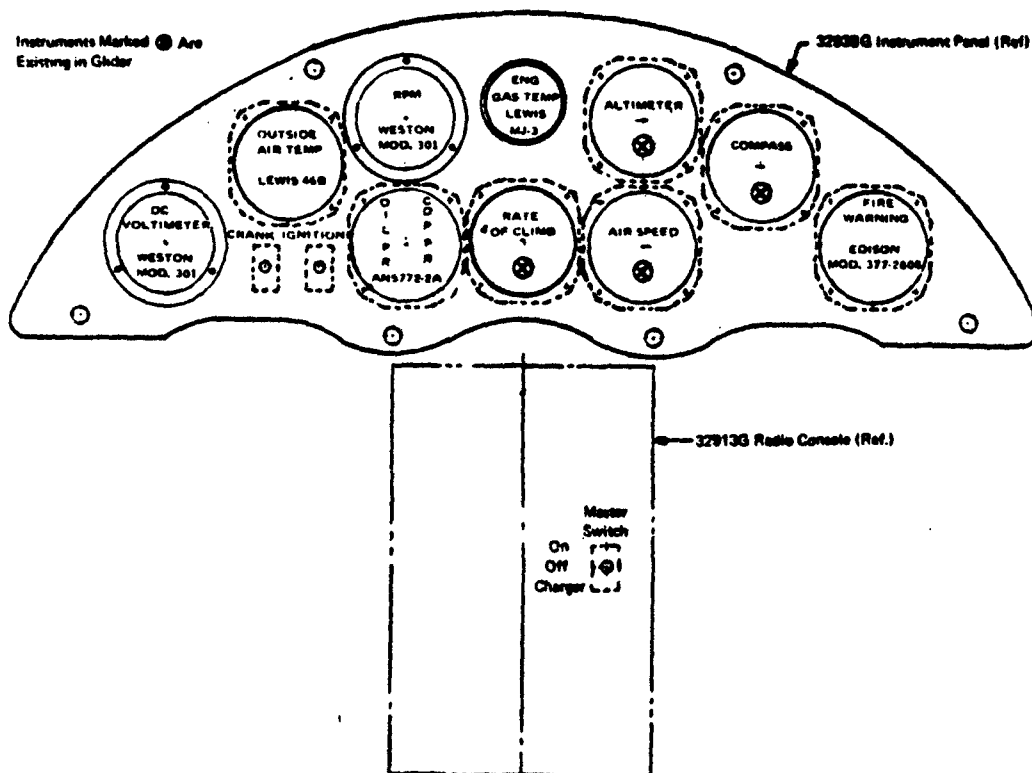
Figure 3. QRTV Instrument Panel and Radio Console

The pilot will perform the operations necessary to air crank and ignite the WR-19 engine and will utilize the normally open momentary switches installed in the panel for these purposes.

Figure 4 contains the schematic diagram for the necessary internal wiring for the QRTV.

It was deemed advisable to provide additional information pertaining to engine operation during the conduct of the static ground tests. Consequently, the external auxiliary instrumentation shown in Figure 5 has been designed from which fuel supply pressure, engine vibration and very accurate high and low pressure spool speeds may be obtained. It is anticipated that this panel will be

14
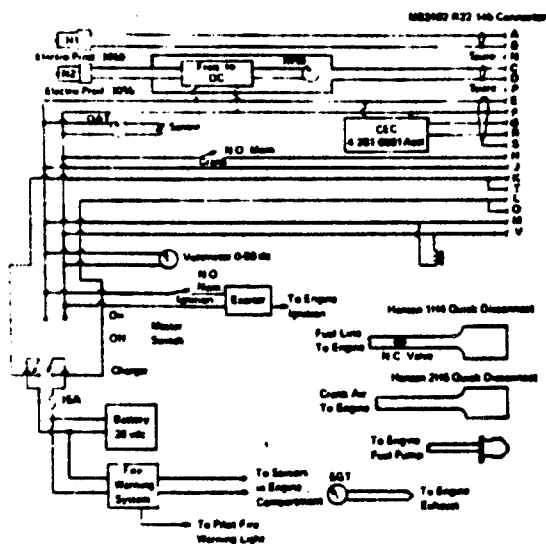
Figure 4. Internal Aircraft Wiring
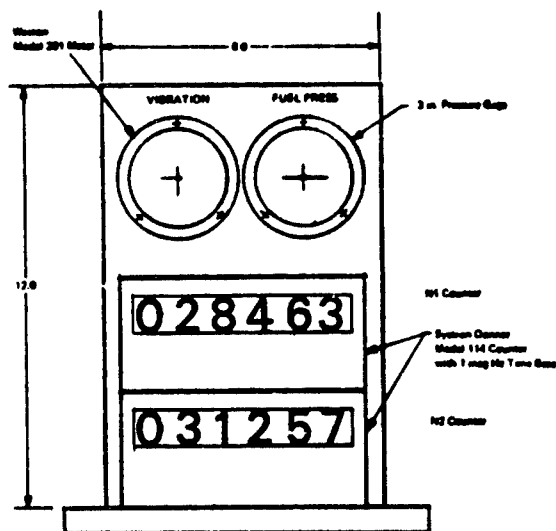
Figure 5. Auxiliary Engine Instrumentation
(Located on Separate Cart)

located such that it may be viewed by the pilot as well as a ground observer. The corresponding wiring schematic for this external panel is contained in Figure 6.
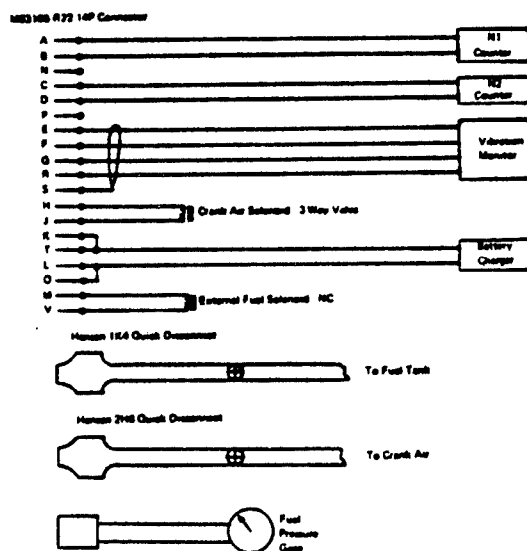
Figure 6. External Instrument Panel Wiring

The WR-19 engine is started by first air cranking the engine up to a nominal ignition speed beyond which it is self-sustaining and will accelerate to the ground idle. The air cranking operation will be accomplished with an external source of compressed "breathing" air which is piped through a filter, regulator, and quick disconnect fitting to a built-in nozzle directed at the high speed turbine. This system, shown in Figure 7, will be employed for cranking the engine during both the static ground tests and the eventual flight tests.
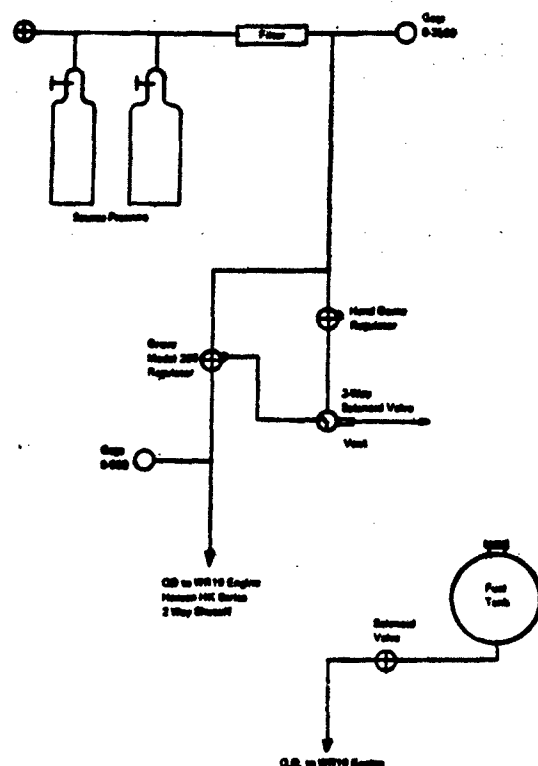
Figure 7. Air Start Cart Schematic

Figure 7 also contains a schematic of a gravity feed external fuel tank with a quick disconnect fitting to the WR-19. This system is for use only during the static ground tests. Space and weight provisions have been included in considerations of the QRTV for an internal fuel tank; however, the design of this system was not planned for this phase of the program.

8. **Static Thrust and Exhaust Flow Instrumentation**

While not a specified task in Phase II of the Jet Noise Reduction Program, it was necessary to take into consideration certain aspects in the design and fabrication of the ground static test stand, as well as the QRTV, in order to analyze and design those components specified in the nine contractual tasks. It had been concluded early in this phase that utilization of the sailplane transport trailer as the basic test stand structure represented the most expeditious approach. By suspending the forward end of the trailer bed on cables arranged to restrict lateral motion and by supporting the aft end on a low friction roller mounted in an adjustable support, the trailer bed will be free to move in the fore and aft direction only. Restraint of this motion by a suitably positioned load cell will provide a direct means of quiet propulsion system thrust measurement.

As discussed in Section II-B-5, the Marmon Clamp joints between the bifurcated exhaust duct and the transition sections to the spanwise wing duct allow installation of a 12 inch long circular duct in each branch for exhaust gas flow instrumentation during the static ground tests. This instrumentation, listed in Tables 2 and 3 consists of an equal area, cruciform total pressure rake with 13 probes, four peripheral static pressure taps, and five thermocouples. Data recorded from these sensors will permit an evaluation of the exhaust gas velocities and weight flows entering each of the

16

TABLE 2. PRESSURE INSTRUMENTATION

Parameter	Visual	Recorded	Range	Accuracy (% Full Scale)
Exhaust Instrumentation Section				
Right Branch				
13 Total		O	0 to 15 psig	±1%
4 Static		O	0 to 15 psig	±1%
Left Branch				
13 Total		O	0 to 15 psig	±1%
4 Static		O	0 to 15 psig	±1%
Engine Monitor Instrumentation				
Ambient	X	TLE	10 to 20 psia	±0.1%
Compressor Discharge	X		0 to 100 psig	±1%
Oil Pump Outlet	X		0 to 100 psig	±2%
Fuel	X		-5 to 50 psig	±2%
Start Bottle	X	TLE	0 to 3000 psig	±2%
Aircrank	X	TLE	0 to 500 psig	±2%

NOTES:

  O   =   Automatic Recording
  TLE =   Manual Test Log Entry

TABLE 3. TEMPERATURE AND MISCELLANEOUS INSTRUMENTATION

Parameter	Visual	Recorded	Range	Accuracy (% Full Scale)
Exhaust Instrumentation Section				
Right Branch				
5 Points		O	0 to 1000°F	±1%
Left Branch				
5 Points		O	0 to 1000°F	±1%
Engine Monitor Instrumentation				
Ambient	X	TLE	0 to 120°F	±1%
Exhaust Gas	X		0 to 1200°F	±1%
Engine Bay				
5 Points	X		0 to 500°F	±1%
Miscellaneous				
Engine Rotor Speed				
High Pressure	X	TLE	0 to 55,000 rpm	±0.1%
Low Pressure	X	TLE	0 to 55,000 rpm	±0.1%
Engine Vibration	X		85 g	±2%
System Thrust	X	TLE	0 to 550 lb	±1%

NOTES:

  O   =   Automatic Recording
  TLE =   Manual Test Log Entry

spanwise wing ducts. For information to the reader these tables also list the instrumentation discussed in Section II-B-7 with the corresponding instrument range and accuracy.

C.   PROPULSION ANALYSIS

1.   Installed Propulsion System Analysis

The propulsion system analysis has been conducted for the purpose of determining the internal flow characteristics from the air intake through the propulsion nozzles. The system has been sized to insure that the WR-19 engine will be operating on or near its design working line and an estimate has been made of the installed thrust. Figure 8 illustrates the propulsion system station numbering system used in the analysis.
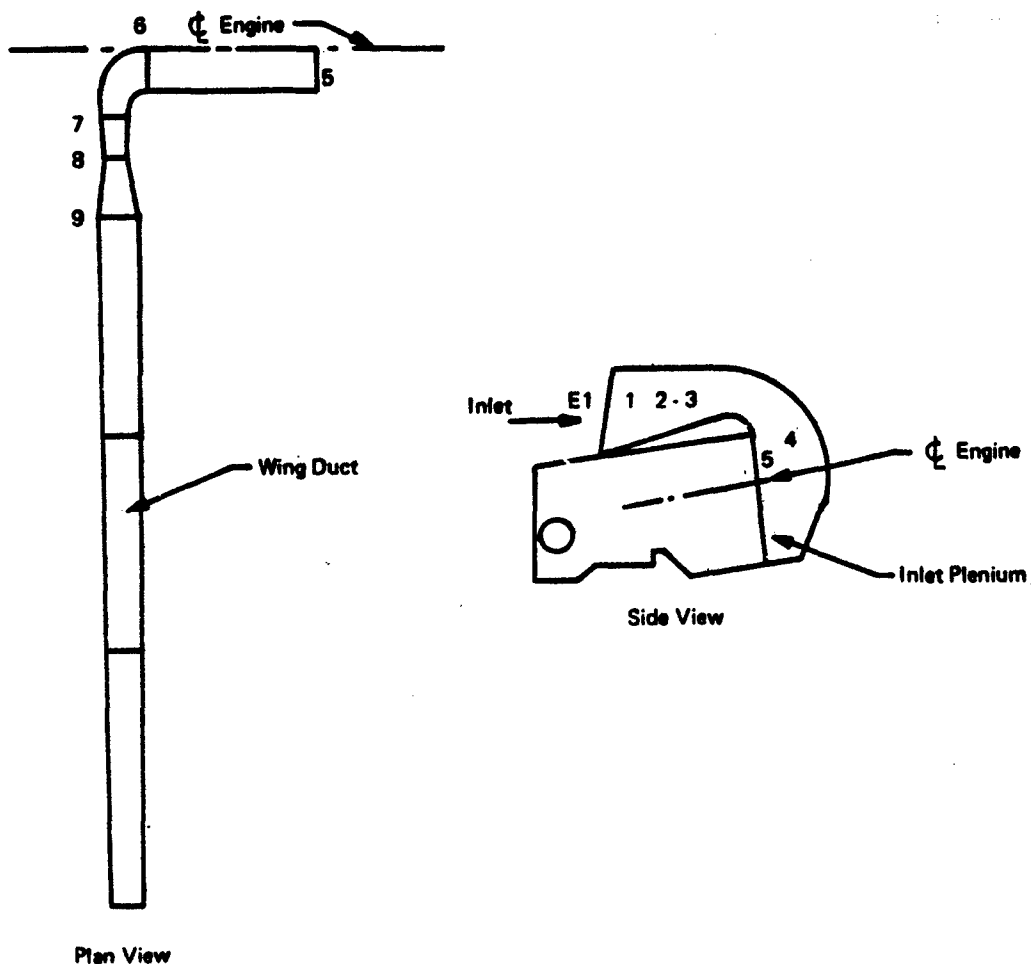
Figure 8. Inlet, Engine, and Exhaust System Schematic

a. Free Stream Conditions

All performance estimates have been made assuming a standard sea level day with no ram pressure recovery in the inlet at airspeeds below 80 knots. The nominal sea level cruise velocity is 60 knots, requiring an engine throttle setting between ground and flight idle. The estimated air capture area at this speed and throttle setting is 125 square inches which will be less than the inlet area. The ram pressure, which will be 0.09 psia at 60 knots, is assumed to be lost in the subsequent diffusion at the engine inlet.

b. Inlet and Inlet Duct

A screen will be placed across the inlet opening for the purpose of filtering out any debris which might clog the microjet exhaust nozzles. This screen will be constructed of woven wire with opening widths of 0.0317 inch. The screen solidity is specified by the manufacturer to be 42.1 percent. The total pressure loss through the screen has been estimated according to the methods suggested in References 1 and 2 and is found to be approximately equal to the air stream dynamic pressure on the upstream side of the screen.

The air will pass the screen and continue through a rectangular inlet passage having a well rounded inlet fairing. A loss of 0.1 of the inlet dynamic pressure at station 1 has been assumed, based on the work reported in Reference 3 . As the inlet Mach number is not expected to exceed 0.123 at this station, the inlet loss between the screen and station 1 will never exceed 0.1 psi.

The inlet passage width will remain constant and the passage height will vary continuously from the entrance to the engine face. The contraction from station 1 to 3 will be gradual and the loss due to this area change has been found to be negligible. The inlet duct walls will be lined with Rigimesh 1510 (Rayl Number 35) approximately one-half inch from the duct wall. The surface of this material, while porous, is very smooth. Even if completely turbulent rough pipe flow is assumed, the total pressure loss due to friction between stations 1 and 3 will be 0.01 psi or less at all engine throttle settings. The contracting section of the inlet passage will cause the air to accelerate to its maximum velocity at station 3. At a takeoff power setting, the Mach number at station 3 will attain a maximum value of 0.18.

The inlet duct will provide air to the engine inlet plenum, within the aircraft fuselage, through a constant width, diffusing 90 degree turn. The loss for this turn (station 3 to 4) has been estimated using the data presented in Reference 3 as a guide. There will be a 50 percent area increase in the turn and the total pressure loss from station 3 to 4 will be approximately 60 percent of the dynamic pressure at station 3. The mean Mach number of the flow at station 4 will have been reduced to 0.12 or less, due to the diffusion occurring between stations 3 and 4.

The air entering the plenum area in front of the engine must again turn approximately 90 degrees into the engine. It is expected that the entire dynamic head at station 4 would be lost in this turn. The computed total pressure at station 5 is, therefore, 96.7 percent of the ambient pressure when the engine is running at its maximum rating.

The foregoing loss analysis was based on using empirically determined loss factors for each inlet subcomponent, computing the loss through each component, and adding the resulting losses. Components in series often produce a different, and usually larger, value for pressure loss than indicated by the sum of the losses estimated for these components individually. To allow for this possibility a total pressure loss 1.5 times the value resulting from the individual component

19

analysis has been assumed for the quiet airplane inlet at less than maximum throttle settings, the total pressure loss has been assumed to vary as the square of the inlet flow rate. The estimated inlet total pressure ratio is shown in Figure 9 as a function of engine high pressure spool speed for all values from ground idle (38,000 rpm) to takeoff (54,000 rpm).
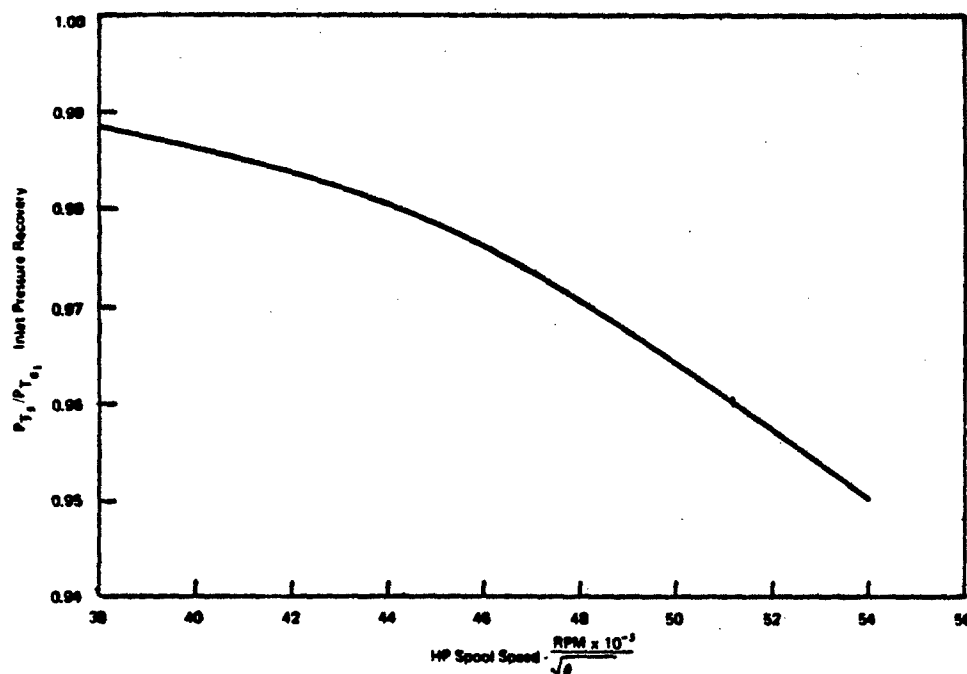
Figure 9. Installed Engine Inlet Pressure Recovery Variation with Engine Speed

c. Engine Operating Characteristics

The propulsion system will be powered by a Williams Research Corporation (WRC) Model WR-19 type engine. Several of these engines were built and tested but no single body of detailed test data exists for these engines. The data, assumed to apply for the engine in this analysis, are a composite taken from that acquired during the Jet Belt Program from engine Serial Number 4, build 8, PFRT and the Serial Number 1 baseline data tests. Contact with WRC has indicated this assumption to be well founded. The inlet airflow, mixed exhaust temperature, fuel flow, and mixed exhaust total pressure used are shown plotted versus the high pressure (HP) spool speed, between the ground idle and maximum rating points as defined by the engine specification. These data are presented in Figures 10, 11, 12 and 13. The engines from which this data was gathered were run with a straight tailpipe of sufficient length to allow the hot and cold exhaust streams to mix. The mixed exhaust was then expelled through a convergent nozzle having an exit area of 30.4 square inches.

d. Bifurcated Exhaust Duct and Transition Section

The bifurcated engine exhaust duct will collect both the engine secondary bypass flow and the primary flow in a common annular passage and will divide the flow into two equal portions to be delivered to each wing. The two branches of the exhaust duct will transition from a

20
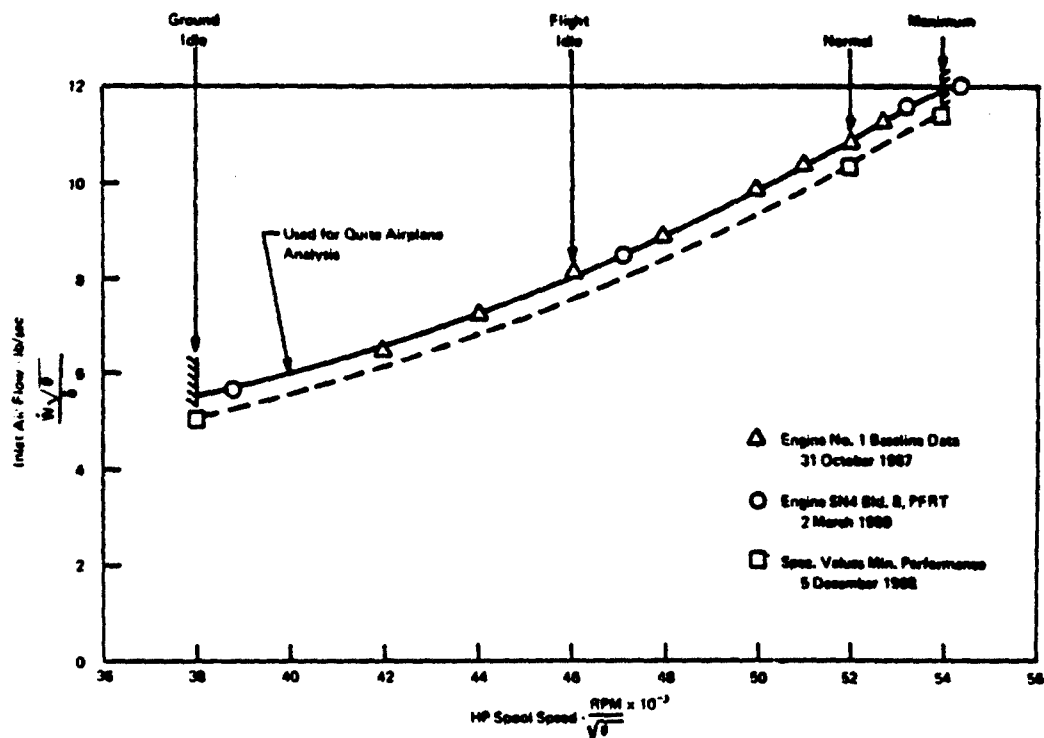
Figure 10. Engine Inlet Corrected Airflow Variation with Engine Speed
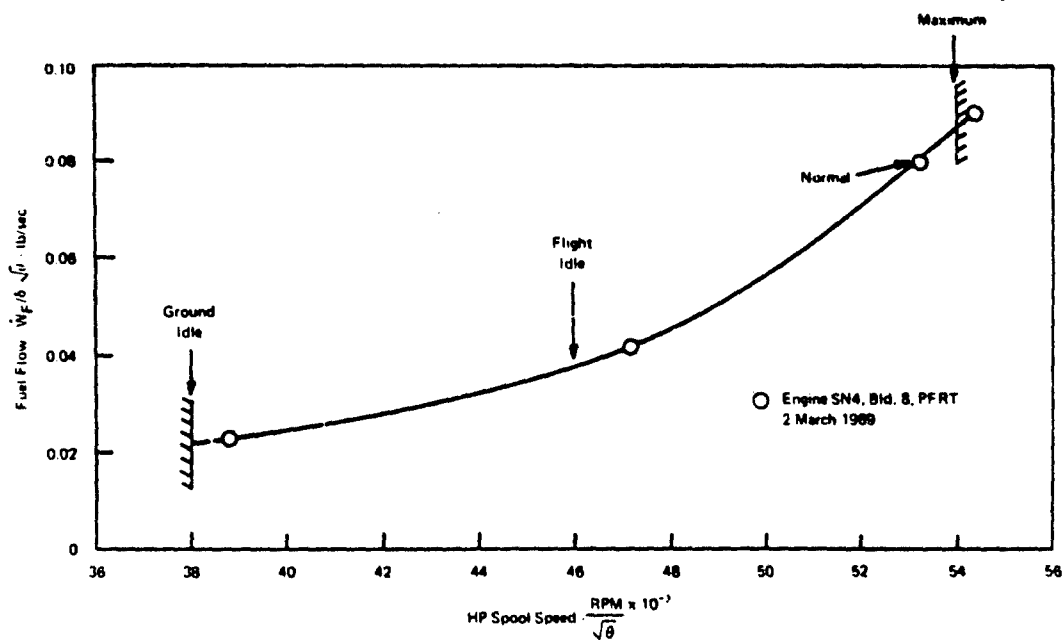
Figure 11. Engine Corrected Fuel Flow Variation with Engine Speed

21
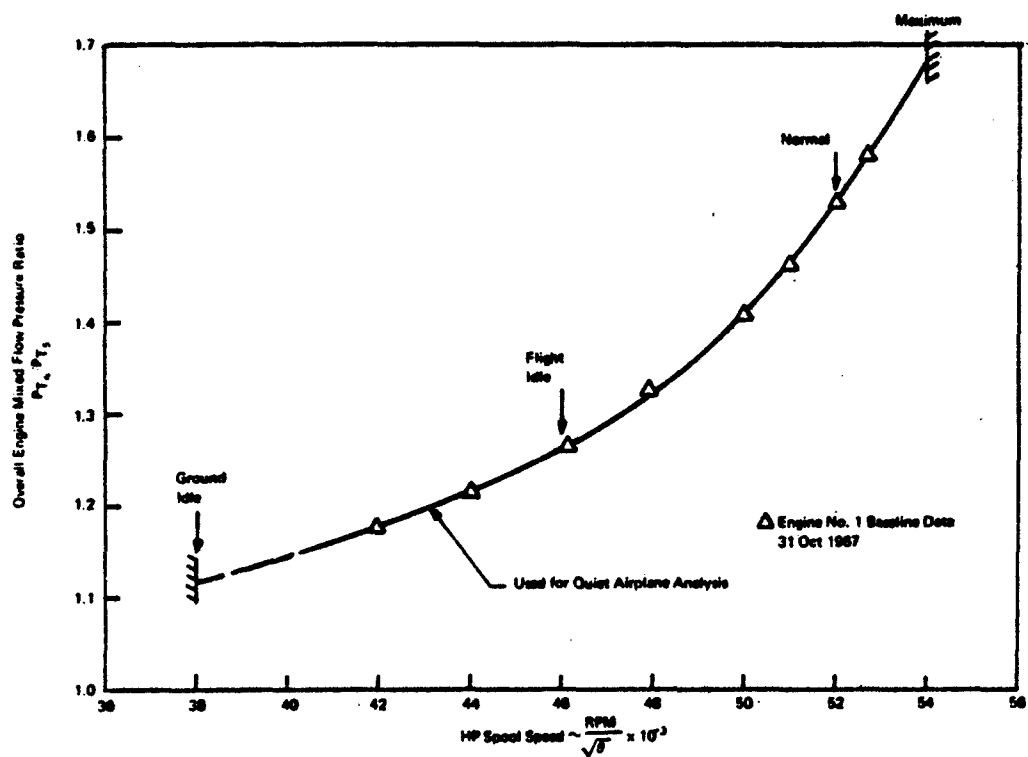
Figure 12. Overall Engine Mixed Flow Pressure Ratio Variation with Engine Speed
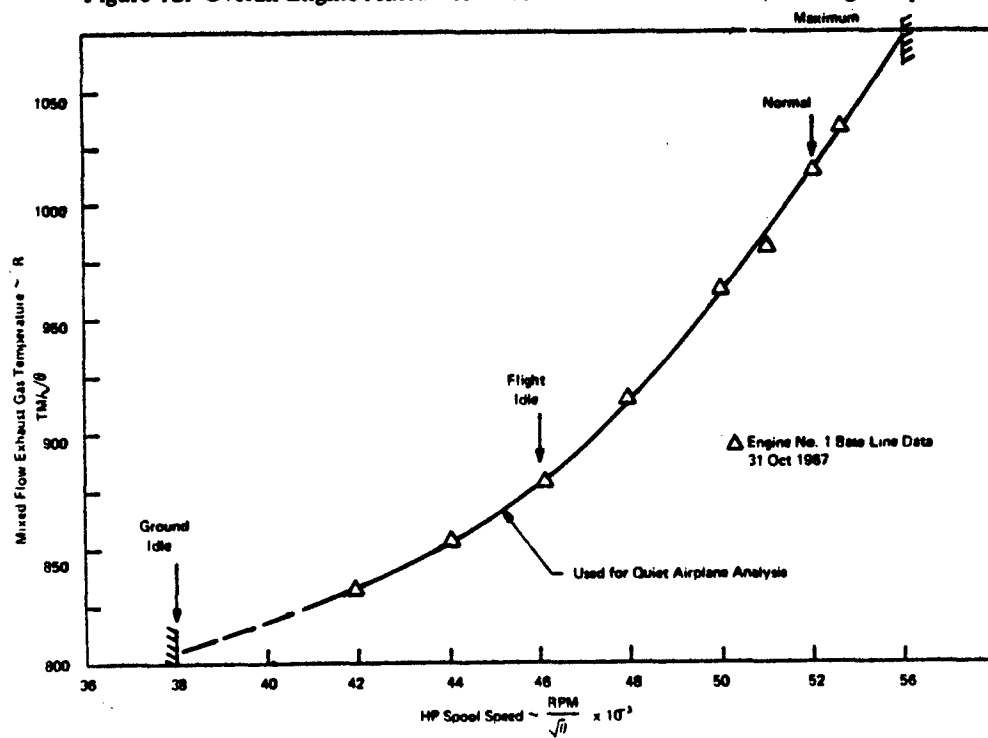
Figure 13. Mixed Flow Exhaust Gas Temperature Variation with Engine Speed

22

sem-annular shape at station 6 to an elliptical shape at station 7. The duct cross-sectional area has been designed to remain constant throughout the transition. Simultaneous with the duct shape transition, the flow in each duct section will be turned approximately 90 degrees toward the wing roots. The duct to be used from station 6 to 7 will be that which was employed on the Bell Jet Belt.

The total pressure loss between stations 6 and 7 will be due to the mixing of the two initially co-axial exhaust streams, to turning the flow 90 degrees, and to wall friction through the complicated transition region. The tests of the Serial Number 1, WR-19 engine show that the mixed total pressure of the engine running at takeoff power can be as high as 23.46 psia. Test experience with the Jet Belt, however, indicates that with the proposed duct arrangement the total pressure at station 7 will be approximately 23.08 psia. A maximum duct Mach number of 0.347 exists at this station.

The ducting will make a constant area transition from an elliptical to a circular cross-section between station 7 and 8. The flow will also be turned an additional 25 degrees aligning it with the spanwise wing ducts. The total pressure will be further reduced by the friction losses in this section. The total pressure is expected to be reduced to 22.98 psia as it reaches station 8.

The duct between stations 8 and 9 will transition from a circular section to an approximate trapezoidal section which will match the shape of the wing duct. In addition to changing shape the duct area will increase by a factor of 1.365.

As the throttle is advanced across its full range from ground idle to maximum, the wing duct mean inlet pressure and mean Mach number will increase from 16.07 psia and 0.140, to 22.73 psia and 0.244 respectively.

e.   Spanwise Wing Ducts

The wing flow channel will initially be trapezoidal in shape and taper along the wing span finally becoming triangular. The wing duct as described in the Design Section II-B-2 will be lined with a stainless steel acoustical damping material known as Rigimesh PMS 1510 which has a Rayl Number of 35 at 3000 feet per hour. This material has a surface finish of 30 to 50 micro-inches and is expected to produce the same pressure loss due to surface friction as a drawn tube of similar hydraulic diameter. The exhaust gases will flow from the wing duct into the propulsion nozzle struts at regular 1.25 inch intervals and the reduction in flow along the span of the duct will be greater than the reduction in duct area due to taper. The net effect on the airflow is assumed to be the same as if the air were flowing through a curved wall conical diffuser of equivalent expansion ratio. At full power the duct total pressure may be expected to vary between 22.73 psia at the inlet, to 22.47 at the end of the span. This will result in less than 2% difference in the airflow through the first and last struts along the span. A mean value has been used for the wing duct total pressure in this analysis. This mean total pressure is estimated to vary between 16.05 and 22.65 psia from ground idle to maximum power setting.

f.   Propulsive Struts

Each propulsive strut will contain 70 small microjet nozzles with contoured inlets and approximately 0.040 inch diameter exits. The 70 nozzles will be arranged in line along the trailing edge of the strut, and will be spaced one mean nozzle exit diameter apart. The geometric exit area of the 70 holes of each strut will be approximately 0.1 square inch. Provisions have been made for up to 434 struts to be mounted along the wings.

23

Tests have been conducted on individual struts connected to a plenum box for the purpose of establishing their discharge coefficients. The discharge coefficient was found to vary with the nozzle throat Reynolds number according to the curve shown in Figure 14. The aircraft propulsion nozzles exit Reynolds number is expected to vary between 5.5×10^3 and 10^4 depending on engine throttle setting and aircraft forward speed. Since the nozzles will be contoured the velocity co-efficient has been assumed to be equal to the discharge coefficient. The determined discharge and velocity coefficients have been replotted as a function of the high pressure spool speed in Figure 15 as a convenience to the reader.

Notes:

1. Determined from data on a single strut mounted on a plenum box.

2. $C_D = \dfrac{\dot{W} \, (T_T)^{1/2}}{A \, P_T \, (FF_T)}$

Where:

W = Measured Flow Rate

P_T = Plenum Box Total Pressure

T_T = Plenum Box Total Temperature

A = Total Nozzle Area

FF_T = Isentropic Flow Function
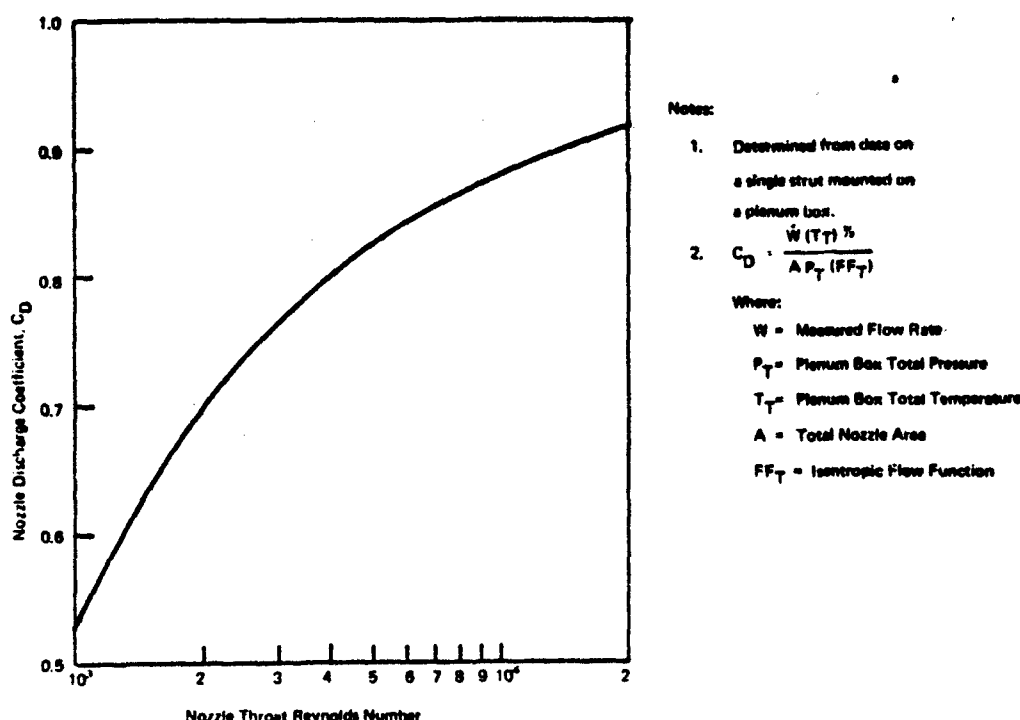
Figure 14. Nozzle Discharge Coefficient Variation with Throat Reynolds Number

The nozzle exit pressure is not expected to deviate significantly from the static ambient value until the aircraft attains some forward speed. At the predicted cruising speed of 60 knots the local static pressure on the upper surface of the wing, at the nozzle strut locations is expected to be 14.56 psia on a standard sea level day.

At the ground idle, flight idle, and maximum engine settings, the nozzle exit areas which will be required to keep the engine operating on its design working line have been computed for zero and 60 knots flight speeds. These points are shown in Figure 16. The required area values differ because the nozzle back pressure changes with forward speed and the nozzle discharge coeffi-cient changes with Reynolds number, and hence, engine throttle setting. Since it would not be practicable to have a varying exhaust nozzle area, and since it has been shown in Reference 4 that the engine will tolerate a change of ±10 percent on the design exhaust area with little change in engine performance, a fixed total nozzle area has been chosen. It is recommended that .366 of the available
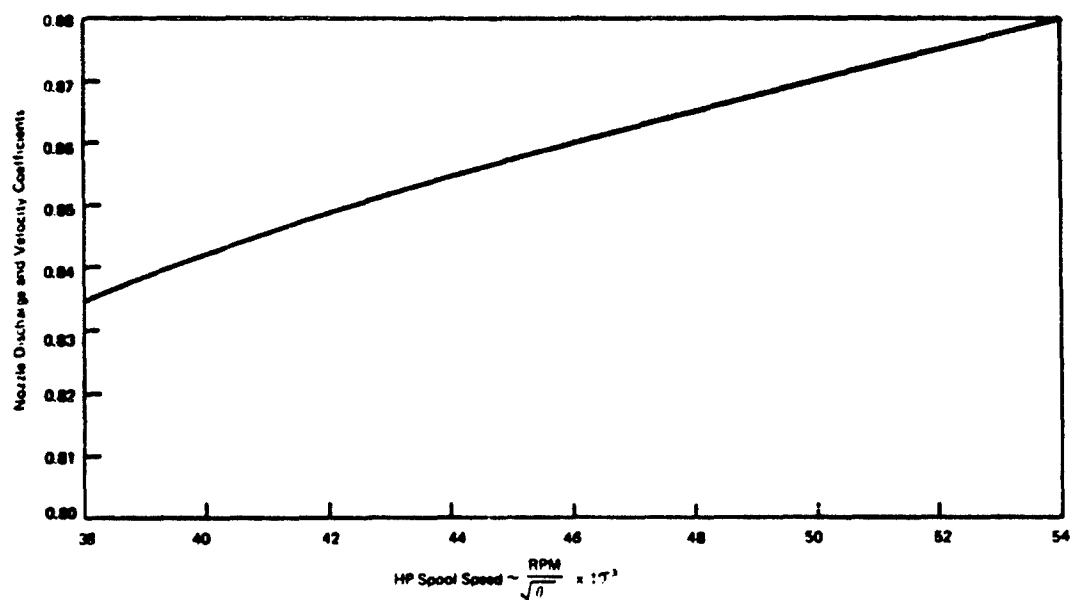
Figure 15. Nozzle C_D and C_V Variation with Engine Speed
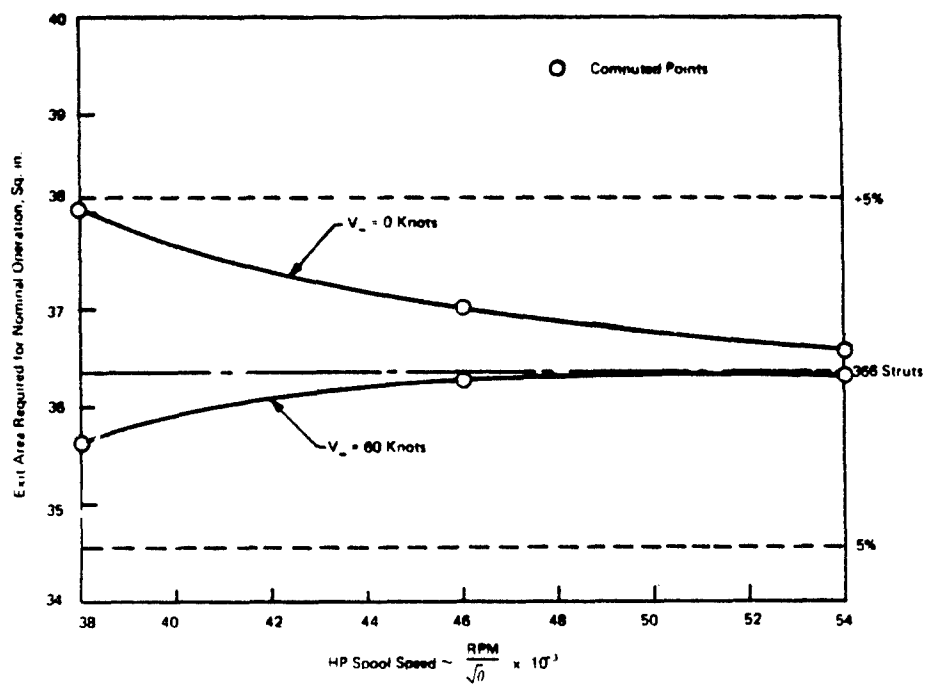
Figure 16. Effect of Flight Speed and Engine Speed on Nominal Exhaust Area

434 exhaust struts be installed. This number should provide a good compromise exit area which will keep the engine operating as though the propulsion nozzle exit area is within 5% of its nominal design value. The available option of using less struts or adding up to 68 struts to the wings, coupled with the demonstrated ability of the engine to run satisfactorily at other than design point operating conditions, gives the system, as designed, enough flexibility to insure that a proper match between the engine and its exhaust system may be achieved in the test phase by merely adding or removing struts from the mounting stations provided.

2. System Performance

Based on the foregoing total pressure loss analysis the system performance has been estimated. The net thrust has been estimated at three ratings, ground idle, flight idle, and maximum, and two speeds, 0 and 60 knots. The decrease in thrust with forward speed was assumed to be linear between 0 and 80 knots. The estimated thrust and drag is shown plotted on Figure 17. The maximum speed attainable will be approximately 123 knots and at the 60 knot cruise speed the engine throttle setting required will be between ground and flight idle. The required high pressure spool speed at cruise will be 42,000 rpm. Table 4 contains a summary of the estimated cruise performance at sea level.
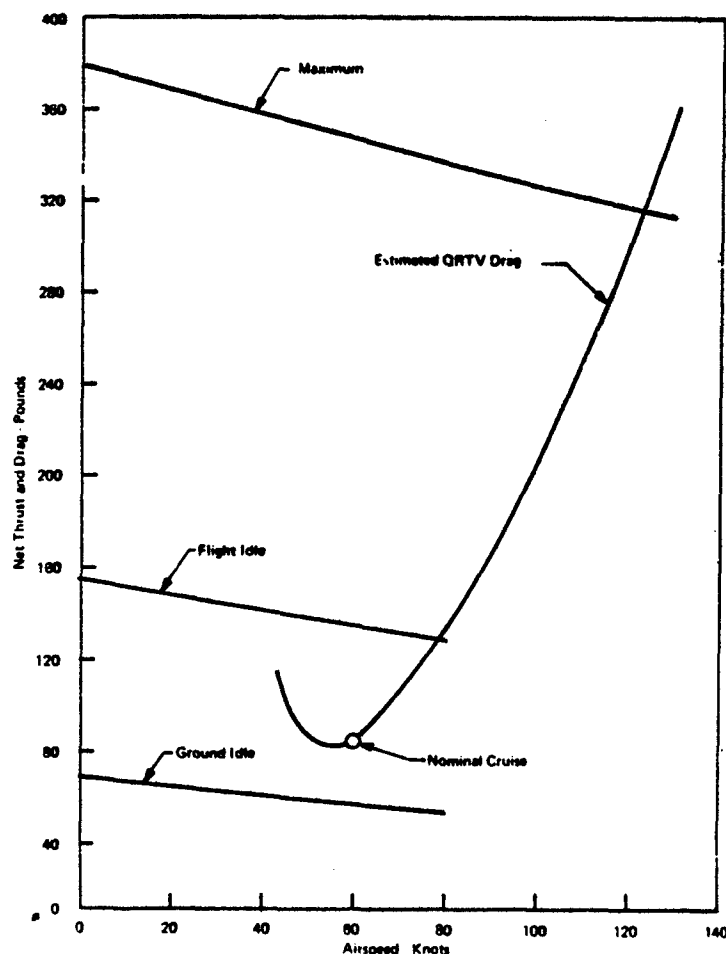
Figure 17. QRTV Estimated Net Thrust and Drag versus Airpseed

26

TABLE 4
ESTIMATED SEA LEVEL CRUISE PERFORMANCE

Flight Velocity	60 knots
High Pressure Spool Speed	42,000 rpm
Exhaust Flow Rate	6.61 lb/sec
Exhaust Velocity (mean)	506 ft/sec
Exhaust Temperature (total)	833 °R
Fuel Flow Rate	101 lb/hr
Gross Thrust	105 lb
Net Thrust	84 lb

The predicted cruise operating point is shown plotted on the WR-19 Gas Generator Characteristics Curve in Figure 18. It has been confirmed by Williams Research Corporation personnel that the engine can operate continuously at this point and that the low pressure compressor surge margin will be acceptable.

The estimated exhaust nozzle exit velocity is shown in Figure 19.

D.   STRUCTURAL CRITERIA AND ANALYSIS

A stress analysis was made of each element of the QRTV test hardware to verify structural integrity in a flight configuration when installed in a Schweizer SGS-2-32 Sailplane. QRTV test hardware includes modification to the fuselage for installing the Williams Research Co. WR-19 engine with bifurcated exhaust duct, engine air intake system, flight test instrumentation and fuel tank. The method of support for the spanwise duct sections with microjet nozzles on the ground propulsion test rig is based on a feasible installation in the sailplane wing. Adequate provisions exist for wing modification and rib reinforcement.

Sailplane design criteria, loads and stress analyses were supplied by the Schweizer Aircraft Corp. Temperatures and pressure data were obtained from the propulsion analysis summarized in Section C.

A summary of the materials used and minimum margins of safety are presented in Tables 5 and 6.

1.   Structural Design Criteria and Loads

The critical design conditions and external loads for each major componet are summarized in Table 7.

The design factors of safety are shown in Table 8.
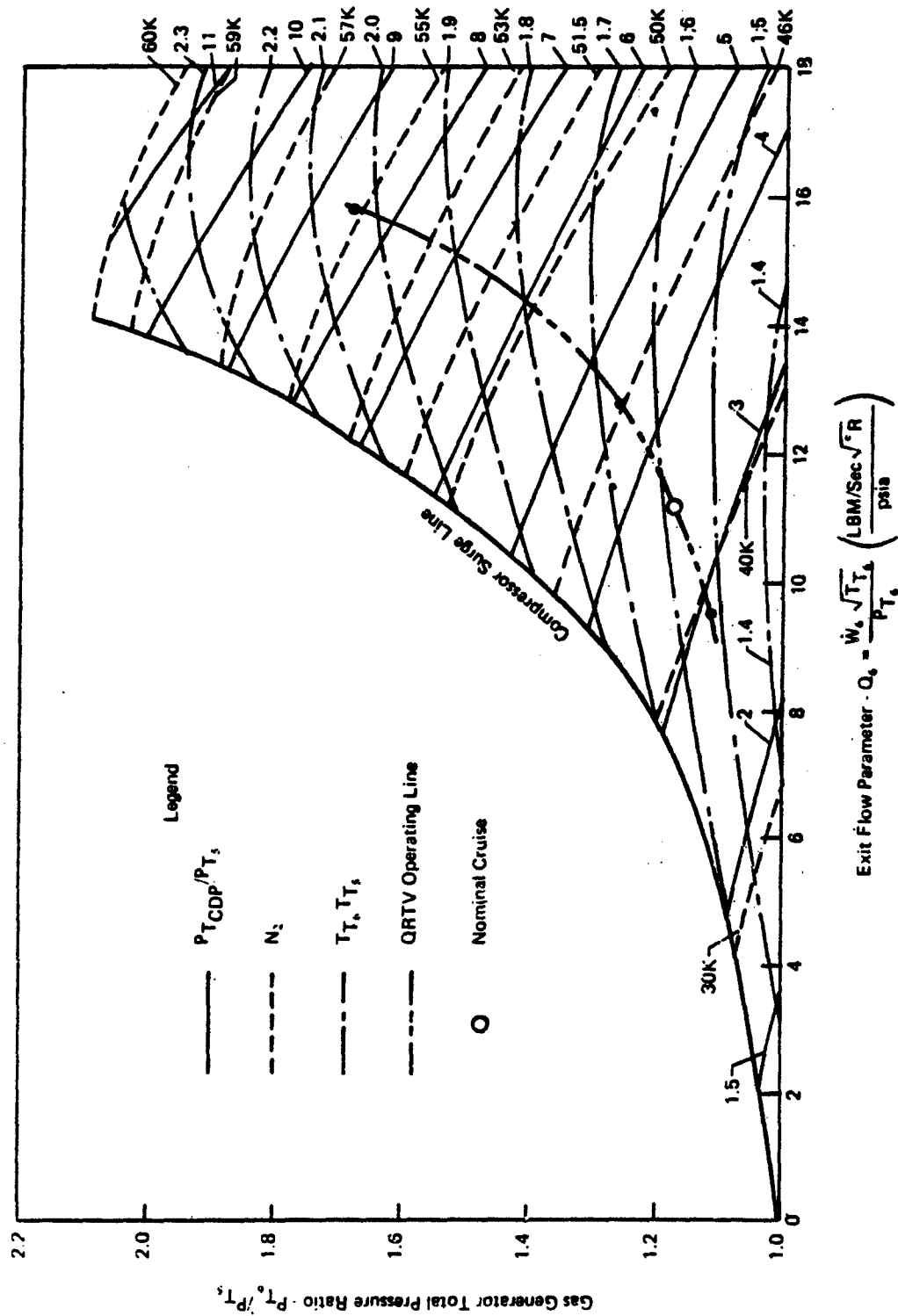
Figure 18. WR-19 Gas Generator Characteristics

28
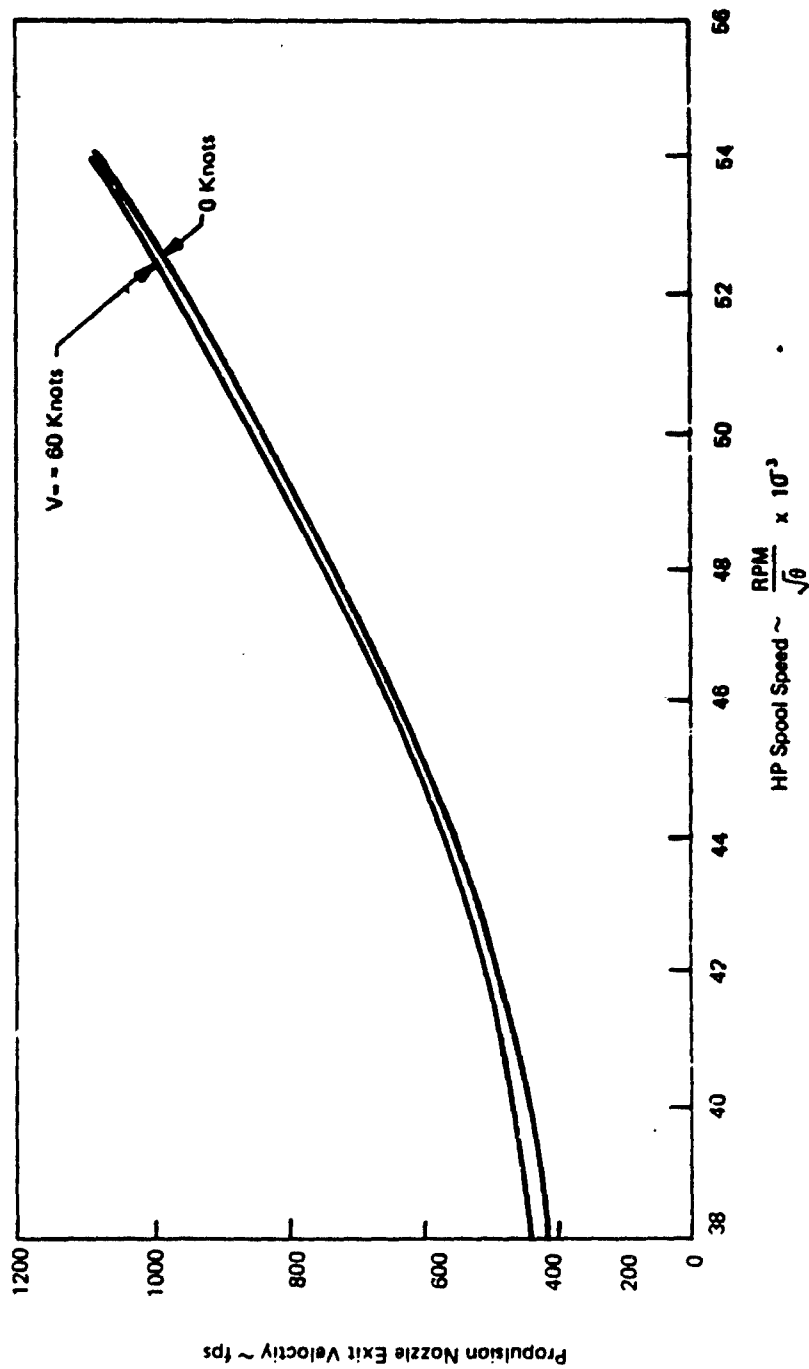
Figure 19. Propulsion Nozzle Exit Velocity Variation with Engine Speed

TABLE 5. SUMMARY OF MATERIAL USAGE

Mechanical and physical properties obtained from Reference 5

Material	Alloy	Form	Spec. No.	Component
2024-T3	Alclad	Sheet	QQ-A-250/5	Engine Support Structure
4130 Steel	125 ksi	Bar	MIL-S-6758	Restraint (Wing Duct)
4130 Steel	90 ksi	Plate	MIL-S-6758	Link and Tee (Wing Duct)
4130 Steel	125 ksi	Sheet	MIL-S-18729	Angle (Wing Duct) Fitting (Wishbone)
4130 Steel	90 ksi	Sheet	MIL-S-18729	Support (Wing Duct)
2024-T4	Alclad	Sheet	QQ-A-250/5	Structure (Wishbone)
2024-T3511		Bar	QQ-A-200/3	Fitting (Wishbone)
2024-T4		Extrusion	QQ-A-200/3	Structure (Wishbone)
6061-T4		Sheet	QQ-A-250/11	Structure (Duct)
2117-T3		Rivet		Struts

TABLE 6. SUMMARY OF MINIMUM MARGINS OF SAFETY

Drawing No.	Component	Critical Condition	Critical Section Location	Material	M.S.	Page Ref.
7389-430084	Restraint (Wing Duct)	A+B	Pt. A	4130 St. 125 ksi	+2.05	40
7389-430063	Angle - Wing Duct	A+B		4130 St. 125 ksi	+0.16	40
7389-430067	Support - Wing Duct	A+B	A-A	4130 St. 90 ksi	+0.57	41
7389-430073-2	Channel	E-1 (Crash)	Pt. A	2024-T3 Alclad	+0.49	49
		E-1 (Crash)	Rivet Attach.	AD 6 Rivets	+0.20	50
7389-430073-3	Channel	E-1 (Crash)	Pt. D	2024-T3 Alclad	+0.15	55
		E-1 (Crash)	Rivet Attach.	AD 6 Rivets	+0.08	56
7389-430084-9	Gusset	E-1 (Crash)	A-A	2024-T3 Alclad	+1.67	58
7389-430079	Bracket	E-1 (Crash)	Rivet Attach.	No. 10 Screws Brg in 2024-T3 Alclad	+0.49	59
7389-430077-9	Fitting	Fl. Cond. I	B-B	4130 St. 125 ksi	+0.05	68
7389-430078	Fitting	Fl. Cond. I	C-C	2024-T3511 Bar	+0.12	70
7389-430077-5	Angle	Fl. Cond. I	A-A	2024-T4 Extr.	+0.13	64
7389-430075-9	Angle	554 lb Ult. Vert. T.L.	A-A	2024-T3 Alclad	+0.08	66
	Rivets	Vert. T.L.	Rivet Attach.	AD 4 Rivets	+0.06	83
7389-430085	Stiffener	Inlet Duct Press.	Mid-Point	6061-T4	+0.12	87
36010 H	Bulkhead	Wishbone Load	WL 11.52	2024-T4 Alclad	+0.00	75

TABLE 7. SUMMARY OF CRITICAL DESIGN CONDITIONS AND EXTERNAL LOADS

Component	Design Condition
a. Spanwise Wing Ducts, Struts and nozzles	Limit Takeoff Condition Pressure = 6.0 psi at 550°F Total exposure = 1/2 hr Limit Cruise Condition Pressure = 3.0 psi at 350°F Total exposure = 100 hr Estimated Thrust Load = 1.5 lb per strut Flight Maneuvering Ref. 6, Page 14 η_z = +5.0, -2.7 g η_y = ±1.0 g η_x = ±2.0 g
b. Engine Installation	Ultimate Crash Load Factors, 10.0 g forward within a 20° semi-angle cone. Flight Maneuvering - same as in a. above.
c. Wishbone Structure	Ultimate Shear Load = 2853 lb applied at Fuse Sta. 104.812 and reacted at Sta. 126.195. Ref. 6 Page 47.
d. Frame at Sta. 129.189 - Dwg. 32010H	Strength loss by eliminating the -7 extrusion. Made up with a frame cap reenforcement and engine support structure. Shear = 1427 lb - (The replaced structure ultimate shear force.)
e. Fuselage Shear and Bending Loads	– 554 lb ultimate vertical tail load applied at Fuse Sta. 280 at a WL to produce a fuselage torque of 25130 in.-lb. Ref. 6 Pages 21 and 22.
f. Sta. 153 Frame	Shear flows from the same critical condition as for fuselage shear and bending loads.
g. Engine Inlet	Limit pressure of 0.70 psi at the engine face varying linearly to zero at the forward inlet face to the outside.

TABLE 8. DESIGN FACTORS OF SAFETY

	Factor	
Structural Component	Yield (1)	Ultimate (2)
Pressurized Ducts and Struts		
Pressure only	1.33	2.00
Combined with other loads	1.10	1.50
General Structure	1.10	1.50

NOTES:
    (1) Yield is where no permanent deflection is occurring that prevents the proper functioning of the unit.

    (2) Ultimate is where no failure occurs.

2. Propulsive Struts

The propulsive strut assembly is shown on BAC Dwg. No. 7389-430065. The strut consists of an 0.032 inch thick 6061-0 aluminum alloy strut formed to the airfoil shape with the trailing edge nozzle holes punched and coined prior to final forming. The leading edge and tip are simply TIG-welded, while the base is TIG-welded to an 0.032 inch thick 6061-0 aluminum alloy seal plate. The chord is approximately 1.69 inches and internal posts are riveted with 3/32 inch diameter 2117-T3 aluminum alloy rivets at the center of the strut to limit deflections when the strut is pressurized.

An element test was conducted on a strut to verify structural integrity. The strut tested had a chord of 1.50 inch instead of 1.69 inch as for the nominal strut. Three posts were placed in the strut with 2-inch spacing, each riveted in place with a single countersunk flat-head rivet, substantially as shown on the drawing of the flight-weight strut, BAC Dwg. No. 7389-430049.

The test procedure included four "tests" as follows:

(a) Cruise condition, 350°F, 3 psig
(b) 2x cruise condition, 350°F, 6 psig
(c) Takeoff condition, 550°F, 6 psig
(d) 1.33 x takeoff condition, 550°F, 8 psig

Each test consisted of 14 pressure cycles (1 minute up, hold 1 minute, 1 minute down) at temperature, with measurements of bulging or permanent set after 1, 4 and 14 cycles. Photos were taken after each test.

There was no permanent set after tests (a) and (b). After tests (c) and (d), the permanent set amounted to 0.004 inch. This amounts to a deflection of 0.0015 of the chord of the strut, for each surface, or 0.0010 of the spacing between rivets. Any bulging was visibly imperceptible, even on the polished strut surfaces.

The net effect on the airfoil shape of the strut is a change in t/c from 15.7% to 16%. A 2% change is considered acceptable from the drag standpoint (less than 3% change in strut drag).

Production struts may have slightly more bulging than the strut tested because:

(a) Chord will be larger by $\frac{1.69}{1.50}$, so (assuming zero fixity at leading and trailing edges) deflection could be larger by $\left(\frac{1.69}{1.50}\right)^3 = 1.42$, or 0.006 inch.

(b) Fixity at the trailing edge will be reduced by a factor of 2 due to the nozzles, but since the difference between zero fixity and infinite fixity contributes less than half to the bulging, this change in fixity means an additional factor of 1.2 at the most.

The increasing deflection due to both of these effects (0.007 inch) would still be less than half of the acceptable bulging. If necessary, a reduction in gage could be considered.

32

Other aspects of this test were also of interest, as follows:

(a)   A minute leak was detected around the upset head of one of the rivets. This would be acceptable from either performance or acoustic standpoints. Nevertheless, if it can be eliminated by painting the rivets with zinc chromate before upsetting them, this would be desirable.

(b)   The process of TIG-welding the tip of the strut, and the base to the seal plate, appears to be completely satisfactory; no leaks were observed.

(c)   The backup plate must have a clearance hole large enough to clear the TIG-weld bead, or else must be countersunk or chamfered.

(d)   The indicated rivet placement appears to be satisfactory from an acoustic standpoint of preventing resonance of the strut skin, without the necessity of viscoelastic damping material. However, the cantilever resonance of the whole strut must be damped, for example, by a viscoelastic (silicone rubber) seal to the wing skin.

3.   Wing Ducts and Backup Plates

Structural details are presented on the following drawings:

Inboard   -   BAC Dwg. No. 7389-430055

Center   -   BAC Dwg. No. 7389-430056

Outboard -   BAC Dwg. No. 7389-430057

The wing ducts and backup plates are critical for combined internal pressurization and flight maneuvering loads. Spanwise shear, bending and torsion loadings due to flight maneuvering are negligible in comparison with the pressurization loadings. At the attachment points, however, inertia loads due to flight maneuvering plus pressurization loads are critical.

Condition A.   Internal Pressurization

- Max. T.O. Thrust = 6.0 psi Limit

- Temp. = 550°F 1/2 hour exposure

- Ultimate Pressure = 10 psi

- Thermal growth shall be unrestrained

Condition B.   Flight Maneuvering

Reference 7, page 14

η_z = +5.0, -2.7 Limit load factor arbitrarily combined with η_y = ±1.0 g and η_x = ±2.0 g.

33

a. **Stiffening Analysis**

Margins of safety are based on the stresses occurring in the inboard section since pressurization loadings are the highest for the largest wing duct. Loadings due to internal pressure are calculated using a conventional strain energy method for frames with a finite element idealization as shown in Figure 20. The internal bending moments in the stiffeners and backup plate are shown in Figure 21.

The bottom section of each wing duct consists of 0.032 inch thick skin stiffened by 0.040 inch thick zee section stiffeners at 5.0 inch spacing, attached by spot-welding. A formed 0.125-inch thick angle is continuously welded on one flange to the skin at each end. The backup plate is mechanically fastened to the other flange of the angle thus forming the top section of each duct. The struts are attached to the backup plate by the strut seal plate with rivets. Material used for all elements of the wing ducts is 6Al-4V titanium sheet.

The minimum margins of safety occurs in the stiffener with effective skin and is calculated as follows:
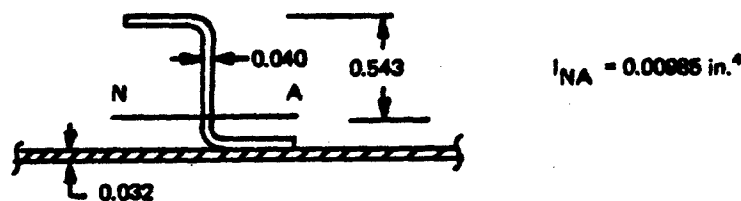
Maximum moment = 150 in.-lb/in. Reference Figure 21
Stiffener spacing = 5.0
Design moment on Stiffener = 150 x 5.0
$$= 750 \text{ in.-lb}$$

$$f_b = \frac{750 \times 0.543}{0.00985} = 41200 \text{ psi}$$

b/t of flange = 0.480/0.040 = 12 $\sigma_{CR} = 45000$ psi Reference 5

M.S. = 45000/41200-1 = +0.095

b. **Attachment Analysis**

The attachment loads for the inboard and center wing ducts are summarized in this section. The center section is included because the arrangement is different. The outboard section arrangement is the same as the inboard section with lower attachment loads due to its lighter weight and size. Based on the critical attachment loads presented, the strength of the attachment brackets is summarized.

34
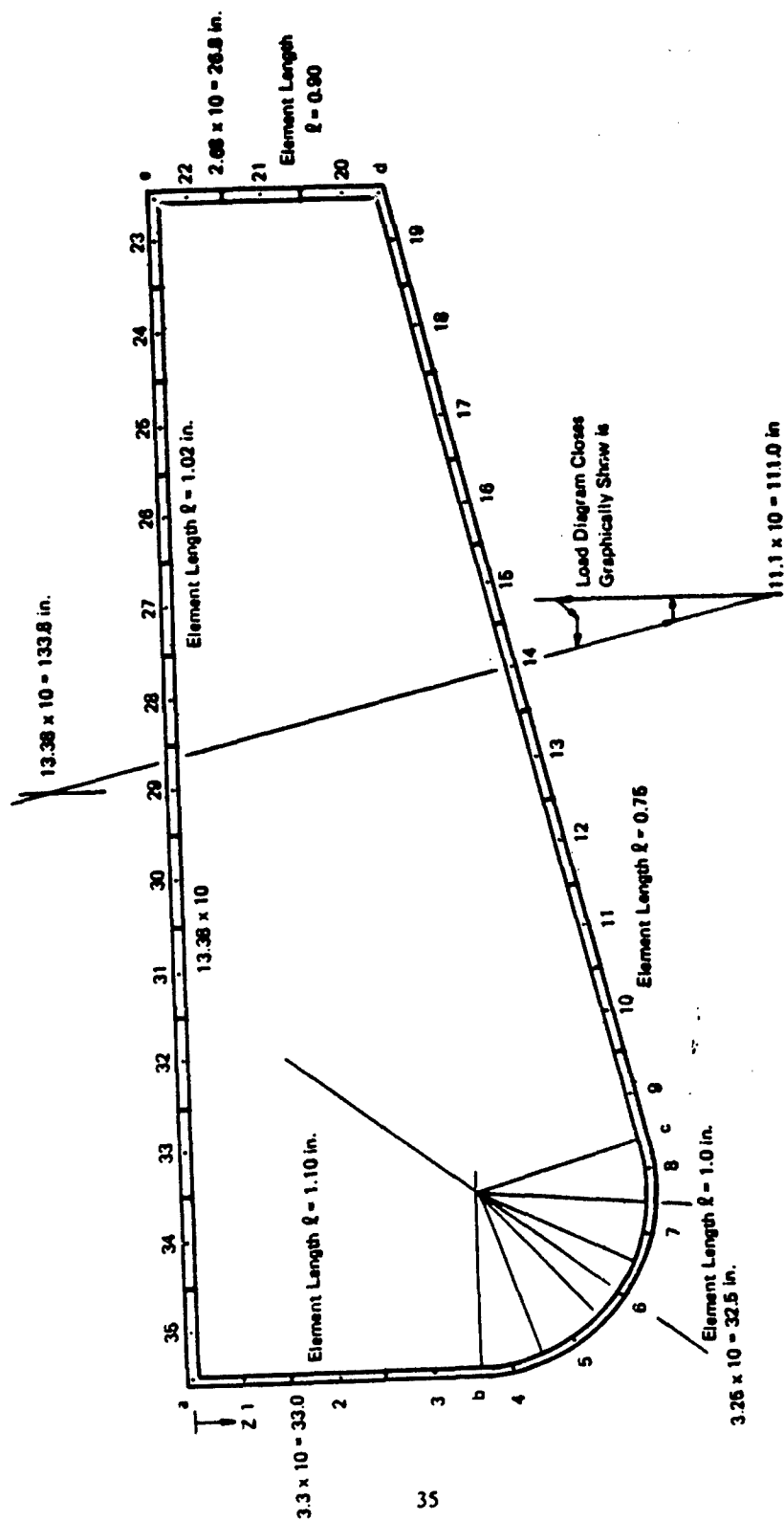
Figure 20. Wing Duct Stiffening Frame Finite Element Idealization

2.69 x 10 = 26.9 in.

Element Length ℓ = 0.90

13.38 x 10 = 133.8 in.

Element Length ℓ = 1.02 in.

13.38 x 10

Load Diagram Closes Graphically Show is

11.1 x 10 = 111.0 in.

Element Length ℓ = 0.75

Element Length ℓ = 1.10 in.

3.3 x 10 = 33.0

Element Length ℓ = 1.0 in.

3.25 x 10 = 32.5 in.

35

Increment Location Around Duct - Inches

Moments - in. - lb/in.
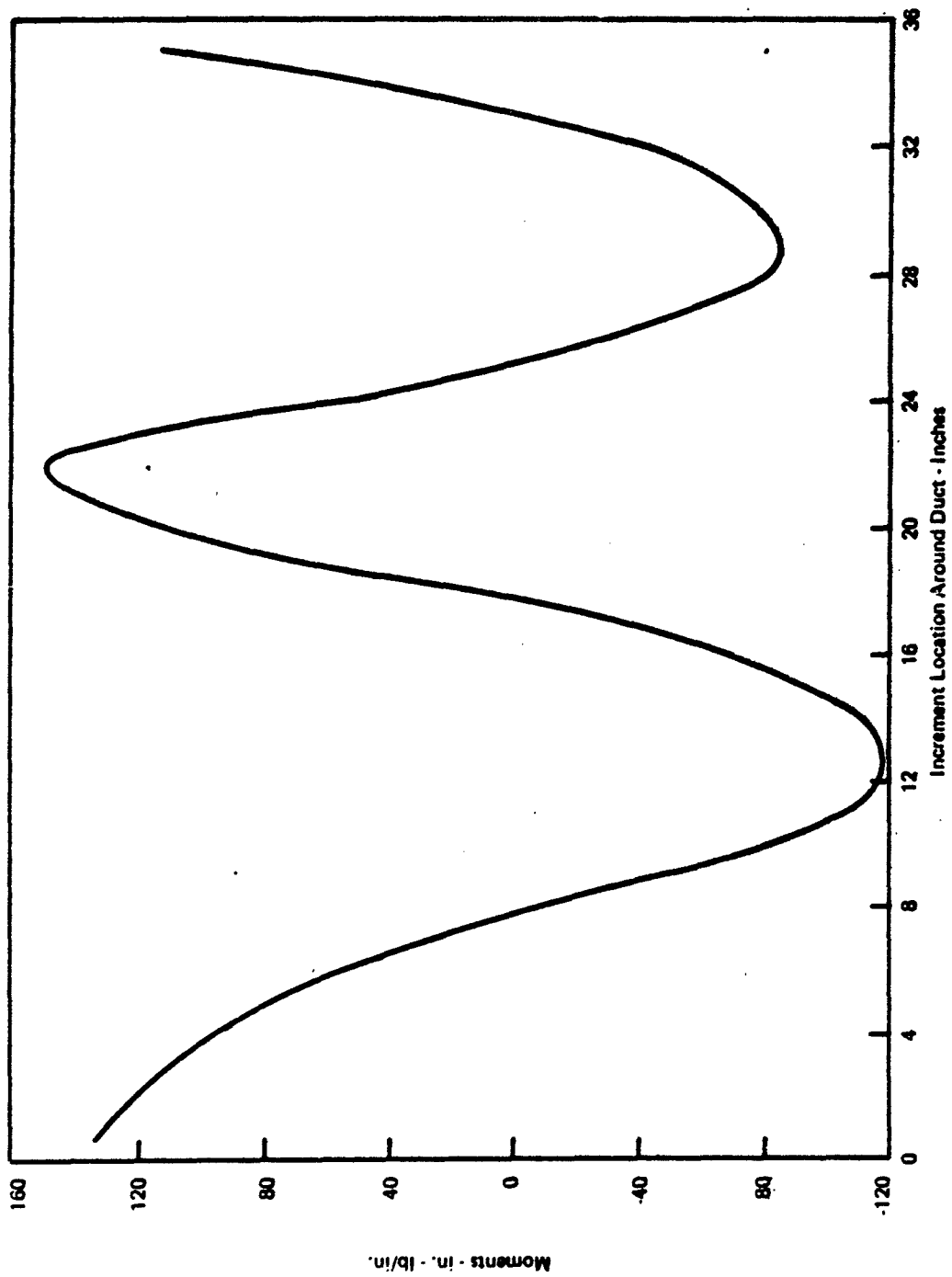
Attachment and applied load nomenclature and geometry are shown in Figures 22 and 23 for the inboard and center sections, respectively. Total inertia loads at the center of gravity, thrust load and reacting attachment loads for the critical conditions are shown in Figures 24 and 25.

A stress analysis of each support bracket is presented on pages 40 to 41.
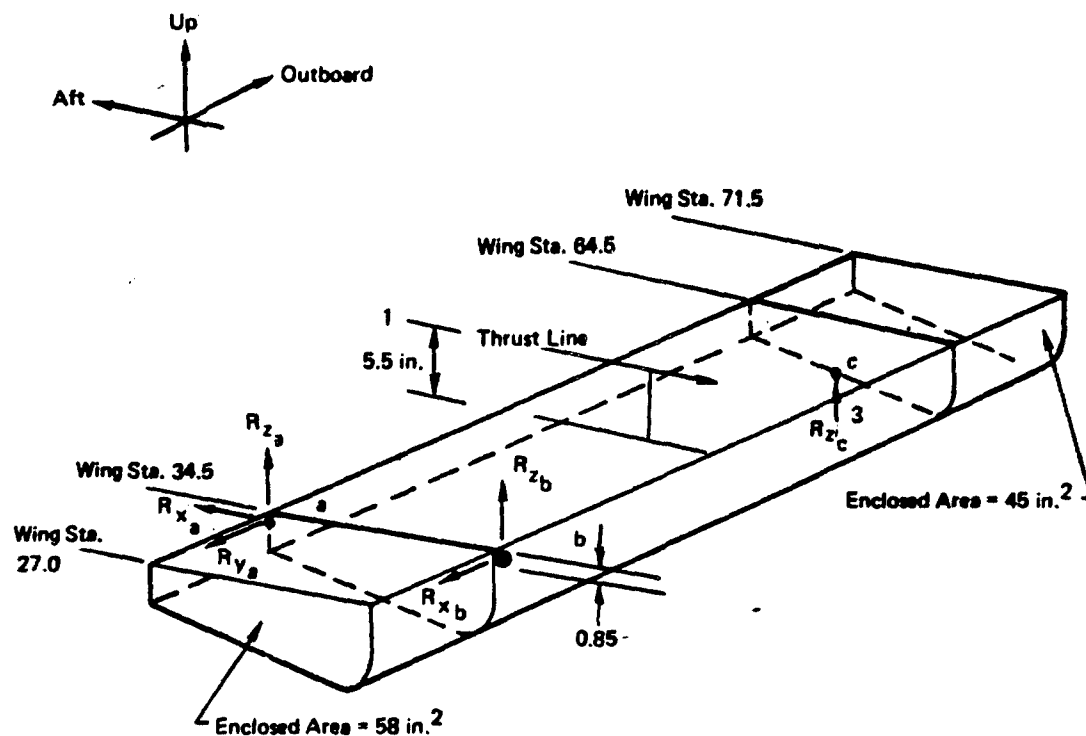
Note:
(1) The Thrust Line of Action is 5.5 in. Above Duct Top Plate
(2) Points a and b Line Along Wing Sta. 34.5 and 0.85 in. Below Duct Top Plate
(3) Point c lies on Wing Sta. 64.5 on Duct Bottom Surface

Figure 22. Inboard Wing Duct Assembly
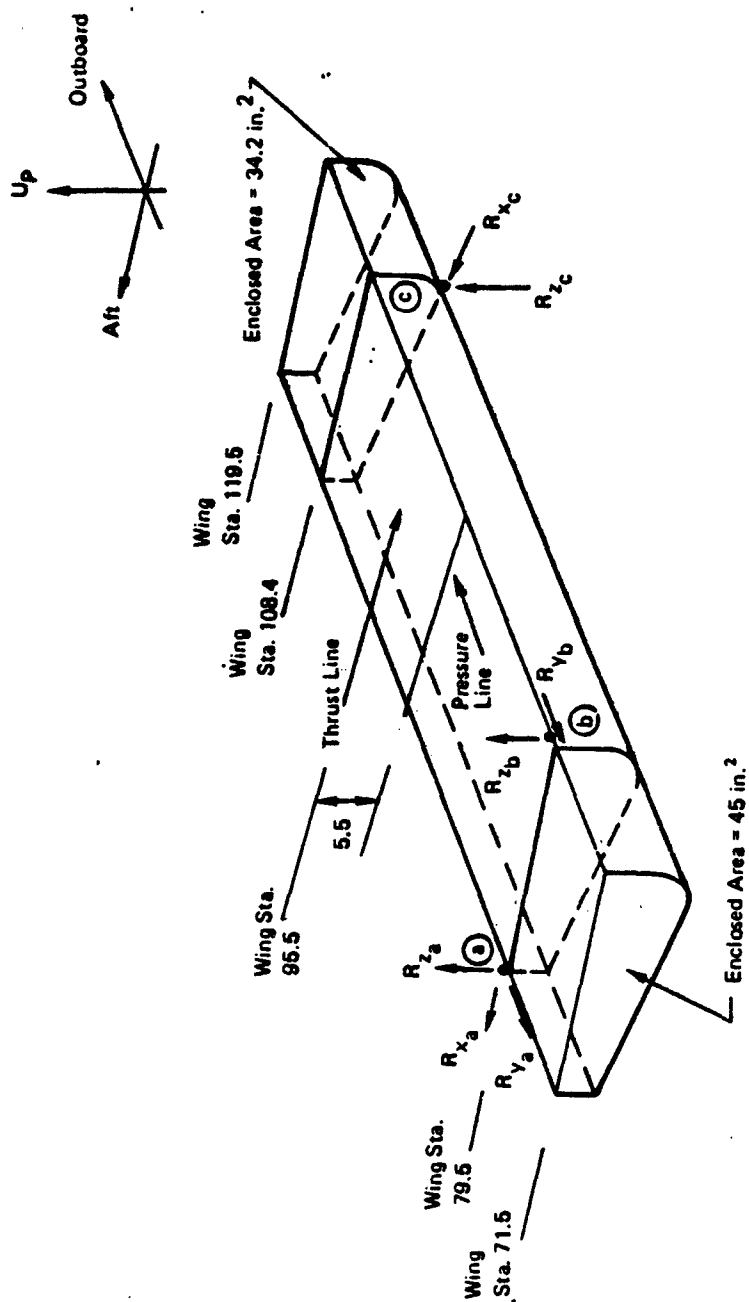
Note:

1. Pt a taken as reference point.

2. Pt b, Sta. 80.1, 13.8 in. forward and 0.0 in. below pt. a.

3. Pt c, Sta. 108.4, 12.6 in. forward and 4.5 in. below pt. a.

   $R_{x_c}/R_{z_c} = \tan(14°) = 0.249$

4. Pressure force is 8.7 in. forward and 2.90 in. below pt. a.

Figure 23. Center Wing Duct Assembly

38
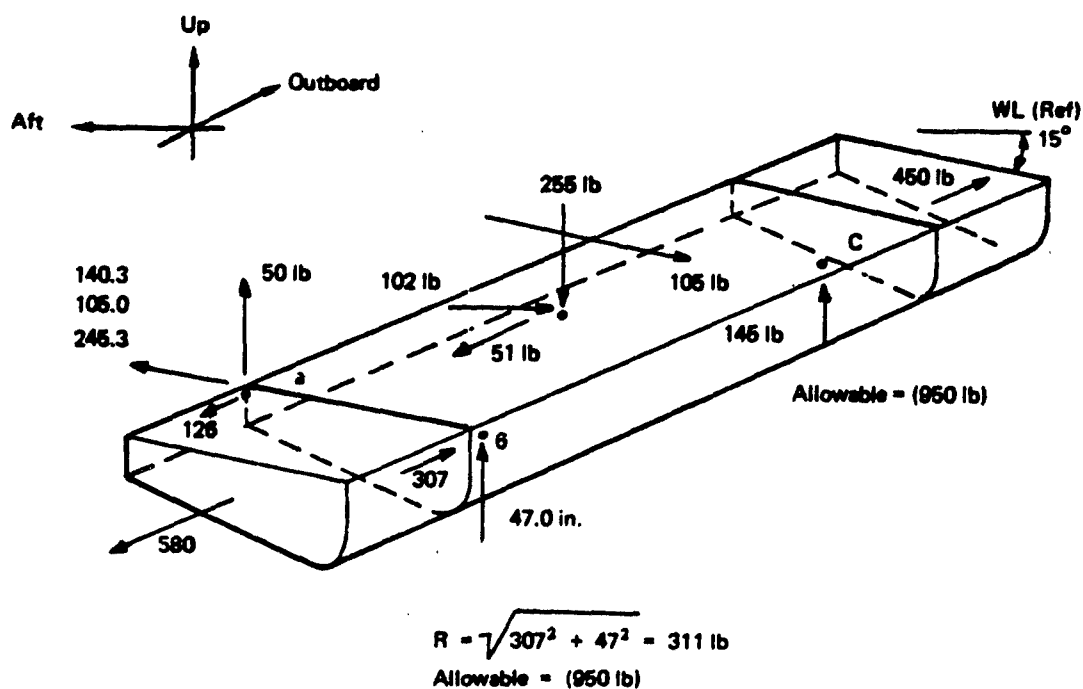
Figure 24. Inboard Wing Duct Attachment Loads - Condition A and B

$$R = \sqrt{307^2 + 47^2} = 311 \text{ lb}$$

Allowable = (950 lb)

$$R_c = 150.8 + 37.6$$
$$= 155.4 \text{ lb}$$

$$R_b = 254.9 + 43.6$$
$$= 258.6 \text{ lb}$$
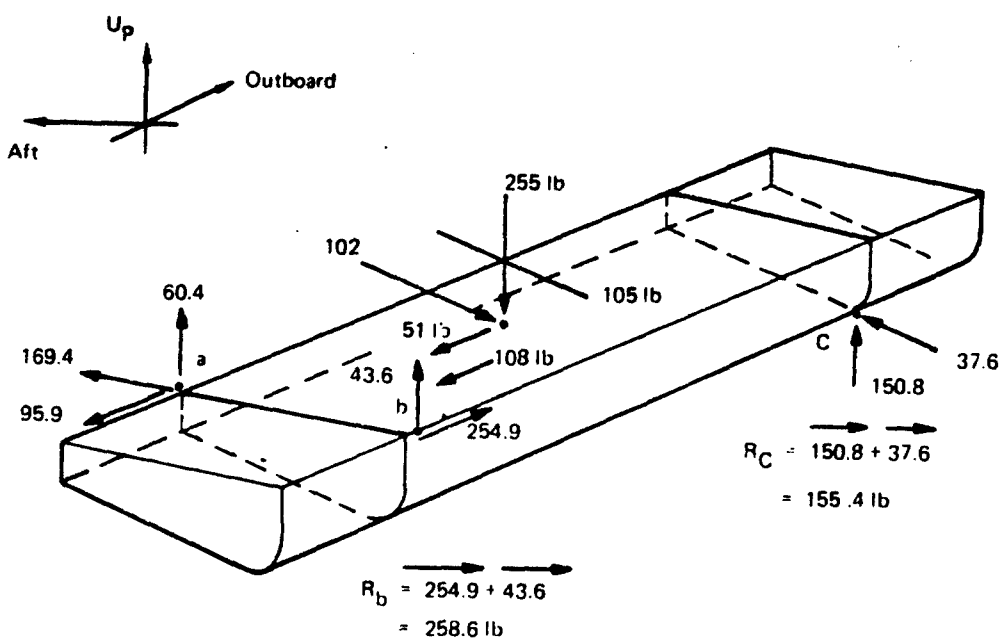
Figure 25. Center Wing Duct Attachment Loads - Condition A and B

Point (b) - Drawing No. 7389-430064 on inboard duct.
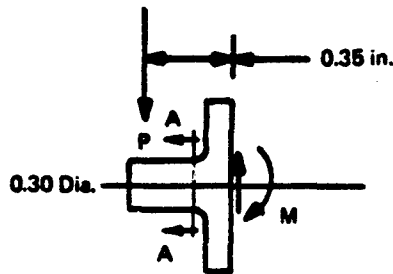
Material = 4130 steel 125 ksi.

Allowable P is based on the bending strength of Section A-A.

$$I = \frac{\pi}{64}(0.30)^4 = 0.000398 \text{ in.}^4$$

Allowable moment $= 125,000\left(\dfrac{0.000398}{0.15}\right) = 332$ in-lb

Allowable P = 332/0.35 = 948 lb

Applied P = 311 lb Ref. Figure 24

$$M.S. = \frac{948}{311} - 1 = +2.05$$

Point (c) - Drawing No. 7389-430068 and 7389-430066 on inboard duct single shear link.

No. 10 screw and 0.100 in. thick 4130 steel plate 90 ksi.
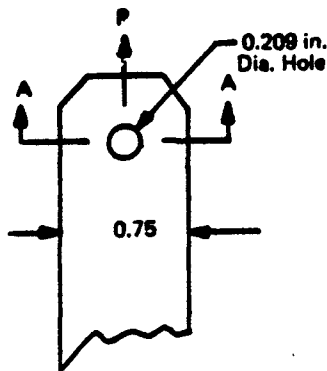
Allowable P is based on the strength of Section A-A.

$A = (0.750 - 0.209)\,0.10 = 0.0541$ in.^{2}

Eccentricity at load $= \dfrac{0.10}{2} = 0.05$ in.

Applied P = 145 lb, Ref. Figure 24.

$f_t = 145/0.0541 = 2670$ psi

$f_b = \dfrac{145(0.05)\,6}{0.541\,(0.10)^2} = 8050$ psi

$$M.S. = \frac{70,000}{(2670 + 8050)} - 1 = + \text{High}$$

Point (a) - Drawing No. 7389-430063 on both inboard and center ducts.

Max. bending moment = (245 x 60) + (126 x 0.55) = 216.5 in.-lb (Ref. Figure 24).

The angle clip, 4130 - Heat treated to 125,000 psi, has a thickness of 0.10 with 0.60 in. and 0.55 in. eccentricities.

$$f_b = \frac{6M}{bt^2} = \frac{6(216.5)}{(1.40 - 0.19)(0.1)^2} = 107,500 \text{ psi}$$

M.S. = (125/107.5) -1 = +0.16

40

Point (c) - Drawing No. 7389-430067 on center duct.
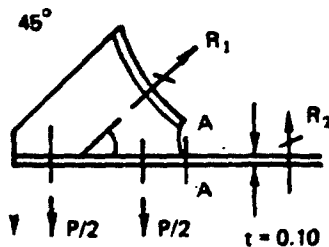
Material: 4130 F_{tu} = 90 ksi

P = 155.4 lb (Ult.), Ref. Figure 25.

R_1 = $P/2$ [2.075 + 3.175]/(3.147 x 0.707)

R_1 = 1.108P

R_2 = P [1/2 + 1/2 - 0.707 (1.108)] = 0.166P

ℓ' = 1.70

M_{A-A} = $R_2 \ell'$ = 0.166(155.4)(1.70) = 43.8 in.-lb (Ult.)

b = 0.65 - 0.19 = 0.46 in.

σ = 6(43.8)/(0.46 x 0.10²) = 57,200 psi

$M.S.$ = $\dfrac{90}{57.2}$ -1 = +0.57

4.   Engine Installation

Alterations to the fuselage and additional structure must be incorporated in the Schweizer SGS 2-32 Sailplane to provide support for the Williams Research Co. WR-19 Jet Engine Installation. To accomplish this, it is necessary to remove the upper fuselage cowling (Fuse Sta. 129 to Sta. 153) and to add structural channel cross members, brackets, shear decks and gussets to support the engine. Mounted at three points, the engine attachment is a determinate configuration allowing unrestrained expansion of the engine and duct system.

Based on the load factors specified in Table 7 for the engine installation, two conditions are critical at the three engine support points. A unit load solution for inertia loads applied at the engine c.g. and the ultimate loads for the two critical conditions (designated conditions E1 and E2) are summarized in Figure 26 and Table 9.

The two aft engine mount points are supported by 2024-T3 Alclad channel section brackets riveted together to form vertical plane truss members which in turn are attached by screws to 2024-T3 Alclad channel section cross fuselage beams. Assuming the truss members to be pin ended, the truss transfers the forces as axially loaded members to both cross fuselage channels to be beamed to existing fuselage frames. The forward attachment fitting is supported at the midpoint of the forward cross ship channel. Load restraint is provided at this point in the vertical direction only. Resulting vertical load at this point is beamed to both ends concurrently with loads introduced by the two aft mount fittings. The riveted attachment of beams to frames is analyzed for a fully fixed end condition. Figures 27, 28 and 29 show the fuselage engine support structural arrangement including drawing numbers of major parts. The internal load distribution, critical sections, stresses and minimum margins of safety are summarized in Section (a) through (c).
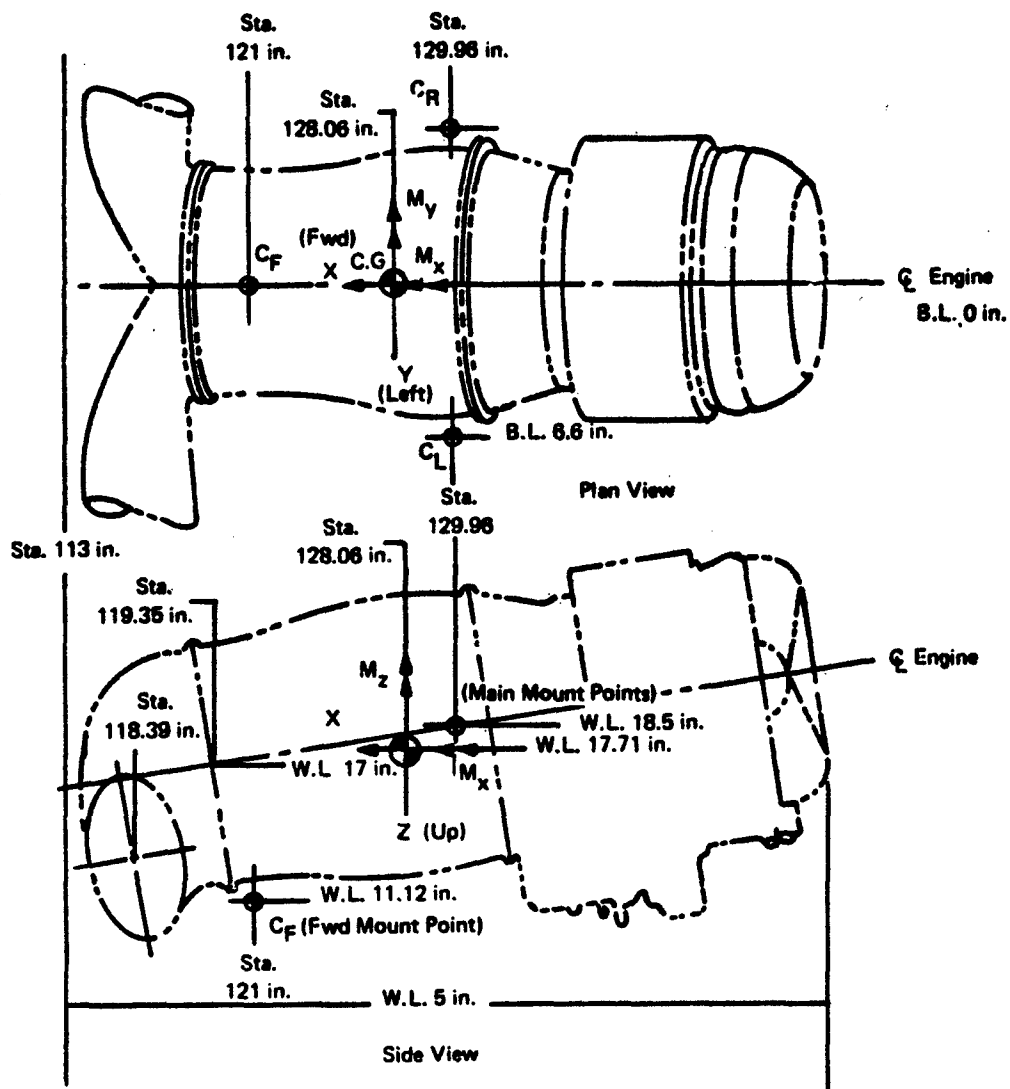
Figure 26. Engine Mount Schematic

42

TABLE 9. SUMMARY OF ENGINE ATTACHMENT LOADS

Load	Reactions $A_T C_F$			$A_T C_L$			$A_T C_R$		
(Unit Cond)	X_F	Y_F	Z_F	X_L	Y_L	Z_L	X_R	Y_R	Z_R
X = 1 lb			-0.0882	-0.5000		+0.0441	-0.5000		+0.0441
Y = 1 lb				+0.1439	-1.000	-0.1439	-0.1439		+0.1439
Z = 1 lb			-0.2121			-0.3940			-0.3940
M_X = 1 in. lb				-0.0758			+0.0758		
M_Y = 1 in. lb			-0.1116			+0.0558			+0.0558
M_Z = 1 in. lb				+0.0758			-0.0758		
Cond. E1 X = 1400 lb Y = 210 lb Z	Ultimate		-123.48	-700 +30.22	-210	+61.74 -30.22	-700 -30.22		+61.74 +30.22
Total			-123.48	-669.78	-210	+31.52	-730.22		+91.90
Cond. E2 X = 210 lb Y = 140 lb Z = 1120 lb	Ultimate		-18.52 +237.55	-105.0 +20.15	-140	+9.26 -20.15 +441.28	-105.0 -20.15		+9.26 +20.15 +441.28
Total			+219.03	-84.85	-140	+430.39	-125.15		+470.69

(Flight Maneuver) (Crash)

NOTES:
(a) Force and Moment Signs are Positive as shown. (Right Hand Rule)
(b) Conditions of Restraint: (See Sketch)
(c) Condition E1: Crash; E2 Flight Maneuvering
(d) IG Wgt of Engine and Support Accessories

43

Up

Left

Fwd

7389-430079-9
Bracket

C_R

7389-430073-2
Channel

C_L

0.050 in.

7389-430079-10
Bracket

C_F

7389-430084-5
Shear Web

7389-430079-11
T (Extrusion) Clip

0.050 in.

7389-430084-3
Channel
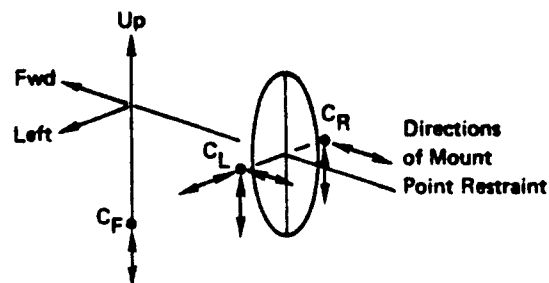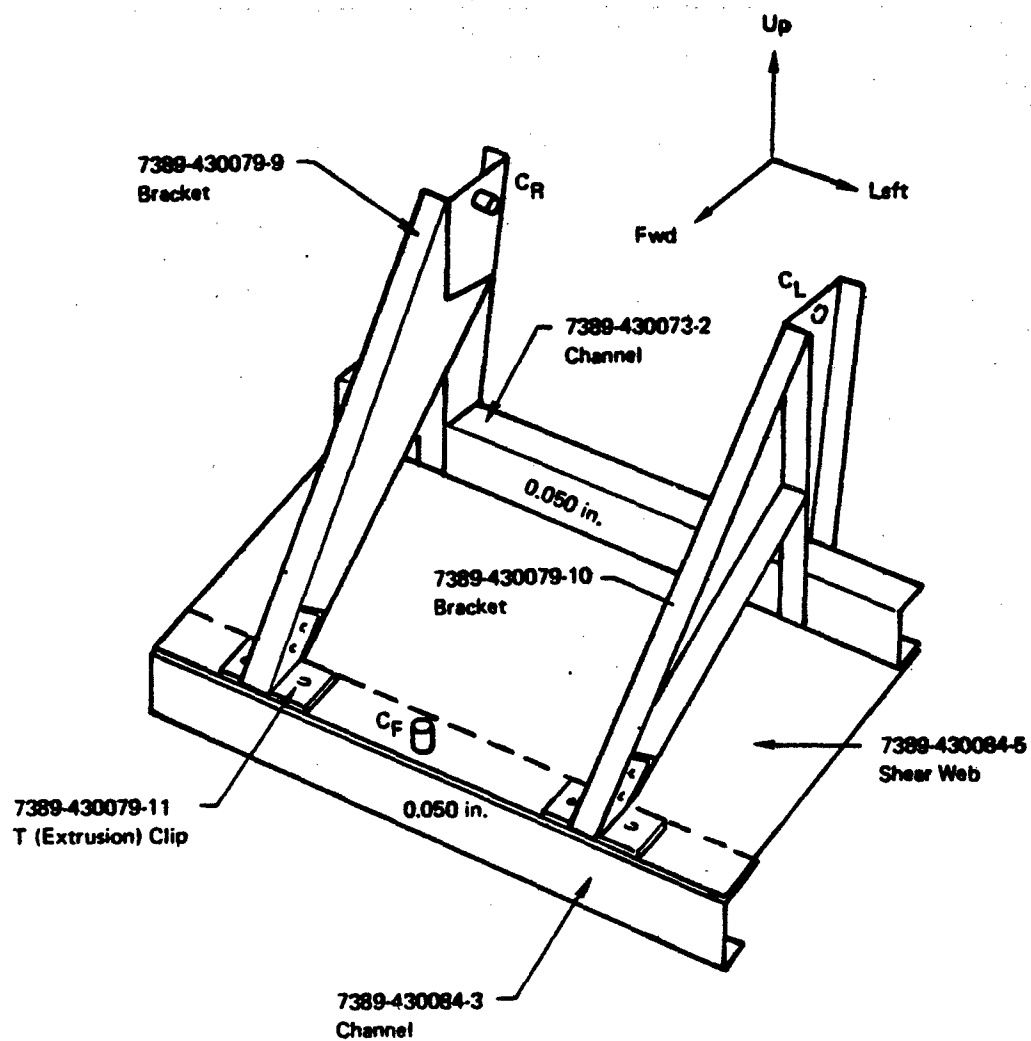
Figure 27. Fuselage Engine Support Structure Arrangement
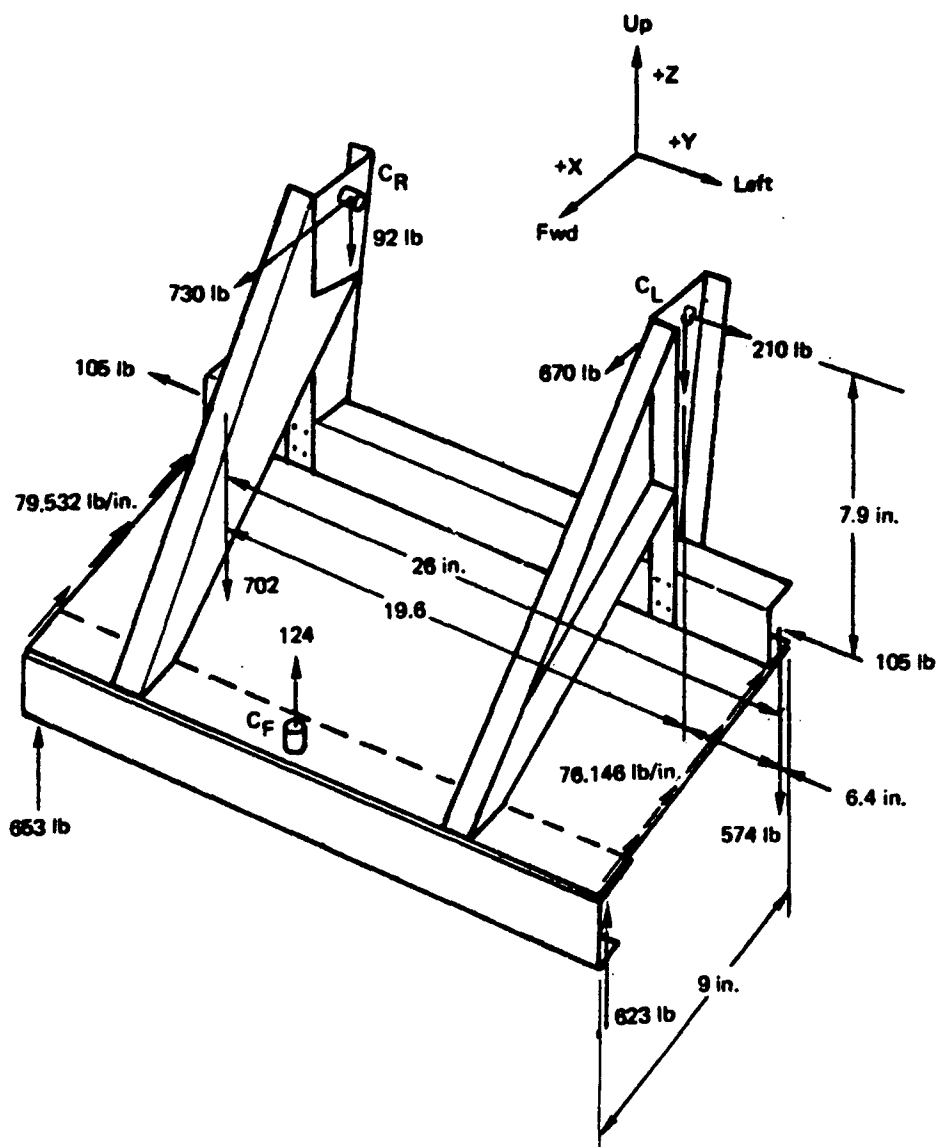
Figure 28. Summary of Fuselage Engine Support Loads
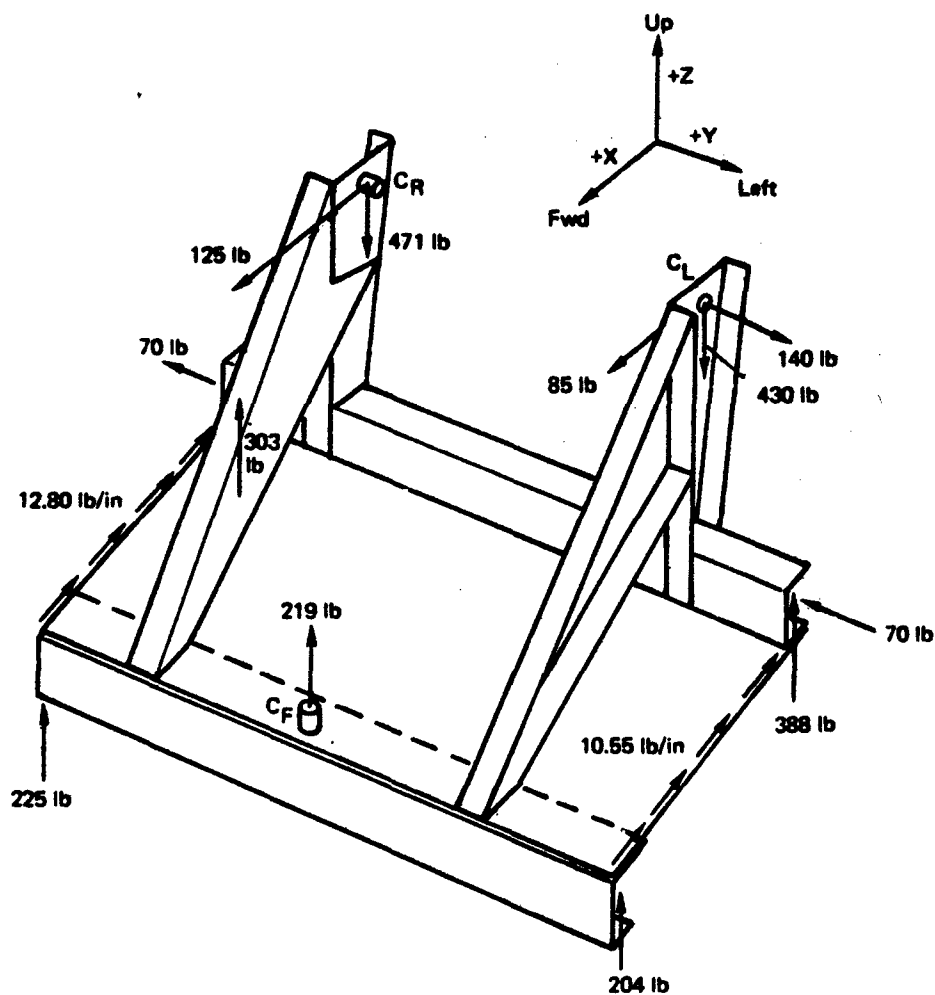
Figure 29. Summary of Fuselage Engine Support Loads

(a) Support Installation - Lower Fuselage Sta. 129.189 - Drawing No. 7389-430073.

-2 Channel
Condition: E1 (Crash) is critical
Material 2024-T3 alclad QQ-A-250/5 Ref (5)

$$F_{tu} = 60,000 \text{ psi}$$
$$F_{cy} = 36,000 \text{ psi}$$

$b_1 = a_1 = 6.4$ in.
$a_2 = b_1 = 19.6$ in.

A = 0.2125 in.^{2}
$\bar{y}$ = 0.9529 in.
I_{NA} = 0.1415 in.^{2}
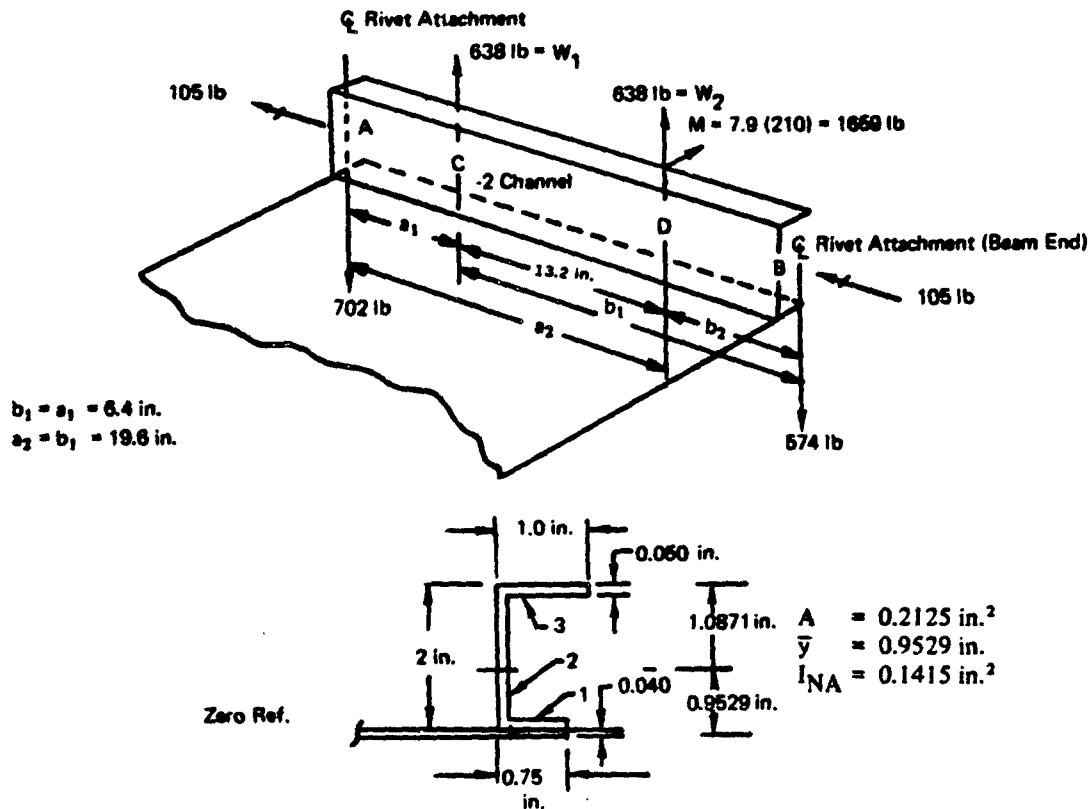
Sketch of the -2 channel as shown above does not show the riveted end attachment of the beam to the existing glider structure. The beam end rivet pattern provides end fixity for which the rivet pattern must be designed. Maximum B.M. and fixed end moments are calculated here. (Ref. 9).

Fixed end moment at Point "A":

$$M_A = - \frac{W_1 a_1 b_1^2}{\ell^2} - \frac{W_2 a_2 b_2^2}{\ell^2} - \frac{M}{\ell^2} [4\ell a_2 - 3a_2^2 - \ell^2]$$

$$= - \frac{638(6.4)19.6^2}{26^2} - \frac{638(19.6)6.4^2}{26^2} - \frac{1659}{26^2} [4 \times 26 \times 19.6 - 3(19.6^2) - 26^2]$$

$$= - 3593 \text{ in.-lb.}$$

47

$$M_B = -\frac{W_1 a_1 b_1^2}{\ell^2} - \frac{W_2 a_2 b_2^2}{\ell^2} + \frac{M}{\ell^2}(2\ell a_2 - 3a_2^2)$$

$$= -2320 - 758 + \frac{1659}{26^2}(2 \times 26 \times 19.6 - 3 \times 19.6^2) = -3405 \text{ in.-lb}$$

Peak moments along the channel will occur at Points "C" or "D."

$$M_C = +\frac{W_1 a_1 b_1^2}{\ell^2} - \frac{W b_1^2}{\ell^3}(3a_1 + b_1)a_1 + \frac{W_2 a_2 b_2^2}{\ell^2}$$

$$- \frac{W_2 b_2^2}{\ell^3}(3a_2 + b_2)a_1 + \frac{M_O}{\ell^2}(4\ell a_2 - 3a_2^2 - \ell^2)$$

$$- 6\frac{M_O}{\ell^3}(a_2 \ell - a_2^2)a_1$$

$$M_C = \frac{638(6.4)19.6^2}{26^2} - \frac{638(19.6^2)}{26^3}(3 \times 6.4 + 19.6)6.4$$

$$+ \frac{638(19.6)6.4^2}{26^2} - \frac{638(6.4^2)}{26^3}(3 \times 19.6 + 6.4)6.4$$

$$+ \frac{1659}{26^2}(4 \times 26 \times 19.6 - 3 \times 19.6^2 - 26^2)$$

$$6\frac{1659}{26^3}(19.6 \times 26 - 19.6^2)6.4 = -874 \text{ in.-lb}$$

$$(-)M_D = 2320 - 3392 + 753 - 620 + \frac{M_O}{\ell^2}(4\ell a_2 - 3a_2^2 - \ell^2)$$

$$6\frac{M_O}{\ell^3}(a_2 \ell - a_2^2)a_2$$

$$= -934 + \frac{1659}{26^2}(4 \times 26 \times 19.6 - 3 \times 19.6^2 - 26^2)$$

$$- 6\frac{1659}{26^3}(19.6 \times 26 - 19.6^2)19.6 = -1814 \text{ in.-lb.}$$

$$(+)M_D = -1814 + 1659 = -155 \text{ in.-lb.}$$

Bending at Point "A" on -2 Channel:

BM_{max} = 3593 in.-lb at Point "A"

$$f_b \text{ (compression)} = \frac{-3593\,(0.9529)}{0.1415} = -24,200 \text{ psi}$$

Ref. Figure 170.04.1.1 - Page 170.04.1-3 of Ref. 8.

$$\frac{b_w}{b_f} = \frac{1.95}{0.725} = 2.69 \quad , \quad \frac{t_w}{t_f} = \frac{0.050}{0.050} = 1 \quad , \quad K_f = 0.895$$

$$\Upsilon_{cr} = \frac{K_f \pi^2 \eta E}{12(1-0.3^2)} \left(\frac{t_f}{b_f}\right)^2 = \frac{0.895\,\pi^2 \times 10.2 \times 10^6}{12(1-0.3^2)} \left(\frac{0.050}{0.725}\right)^2 = 39,242 \text{ psi} .$$

$$39,242 > F_{CY} = 36,000 \text{ psi}$$

$$M.S. = \frac{36,000}{24,200} - 1 = +0.49$$

Analysis of Riveted End Attachment of -2 Channel (AD6 Rivets - Six Required)
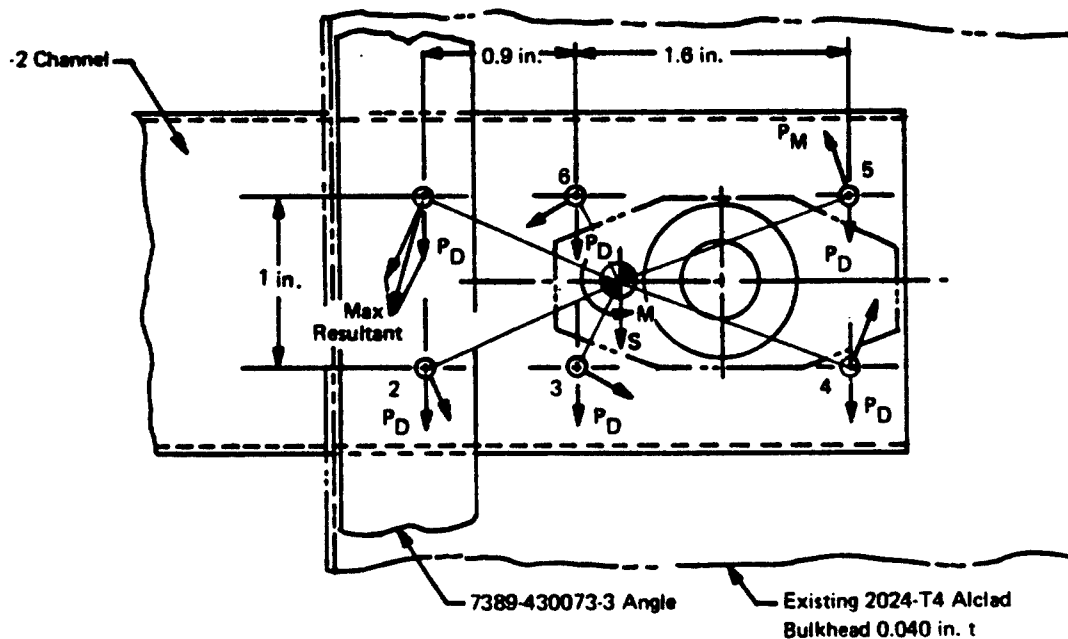
$$y = \frac{0.9(2) + 2.5(2)}{6} = 1.133 \text{ in.}$$

$$P_D \text{ (Direct Shear/Riv.)} = \frac{709}{6} = 118 \text{ lb.}$$

49

Rivet	Z	Z²	Y	Y²	r²=Z²+Y²	r	P_m
1	0.5	0.25	-1.133	1.2837	1.5337	1.2384	561 lb
2	-0.5	0.25	-1.133	1.2837	1.5337	1.2384	561 lb
3	-0.5	0.25	-0.233	0.0543	0.3043	0.5516	250 lb
4	-0.5	0.25	+1.367	1.8687	2.1187	1.4556	660 lb
5	0.5	0.25	+1.367	1.8687	2.1187	1.4556	660 lb
6	0.5	0.25	-0.233	0.0543	0.3043	0.5516	250 lb
					7.9134		

Moment Reacted Through Bolt Pattern = 3693 in.-lb.

$$P_m \text{ (Shear/Riv. Resulting From M)} = \frac{M\,r}{\Sigma(r^2)} = \frac{3593\,r}{7.9134} = 454\,r \text{ lb}.$$

Maximum Resultant-Measured Graphically - Is at No. 1 and No. 2

= 670 lb at Each.

Allowable Single Shear - AD6 Rivets = 862 lb

All Brg. of AD6 in -2(0.050 in.) Alclad Channel

$$\frac{121,000}{100,000}\,(955) = 1150 \text{ lb}.$$

All Brg. of AD6 in Existing 0.040 in. Bulkhead Web

$$= \frac{119,000}{100,000}\,(764) = 910 \text{ lb}.$$

Shear Strength Correction Factor = 0.933 (Ref. Table 8.1.2.1(b) of Ref. 5).

$$\text{Min. M.S. at No. 1 and No. 2} = \frac{862(0.933)}{670} - 1 = +0.20$$

(b) Shear Deck Installation Engine Mount - Drawing 7389-430084 (-3 Channel) (Fwd.)

Determination of fixed end moment, B, moments and reactions on -3 channel for 2 conditions (Ref. 9):

Condition E-1
(Crash)

50
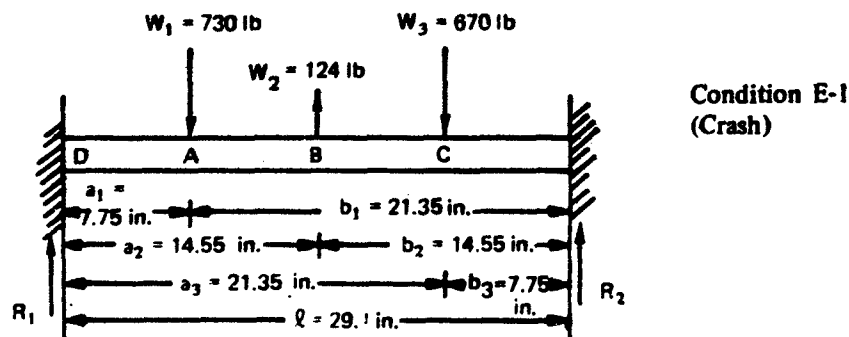
$$R_1 = \frac{W_1 b_1^2}{\ell^3}(3a_1 + b_1) - \frac{W_2}{2} + \frac{W_3 b_3^2}{\ell^3}(3a_3 + b_3)$$

$$= \frac{730(21.35^2)}{29.1^3}(3 \times 7.75 + 21.35) - \frac{124}{2} + \frac{670(7.75^2)}{29.1^3}(3 \times 21.35 + 7.75)$$

$$= +657 \text{ lb.}$$

$$R_2 = \frac{W_1 a_1^2}{\ell^3}(3b_1 + a_1) - \frac{W_2}{2} + \frac{W_3 a_3^2}{\ell^3}(3b_3 + a_3)$$

$$= \frac{730(7.75^2)}{29.1^3}(3 \times 21.35 \times 7.75) - \frac{124}{2} + \frac{670(21.35^2)}{29.1^3}(3 \times 7.75 + 21.35) = +618 \text{ lb.}$$

$$M_1 = \frac{W_1 a_1 b_1^2}{\ell^2} - \frac{W_2}{8} + \frac{W_3 a_3 b_3^2}{2} = \frac{730(7.75)21.35^2}{29.1^2} - \frac{124(29.1)}{8}$$

$$+ \frac{670(21.35)7.75^2}{29.1^2} = 3609 \text{ in.-lb}$$

$$M_2 = \frac{W_1 a_1^2 b_1}{\ell^2} - \frac{W_2 \ell}{8} + \frac{W_3 a_3^2 b_3}{\ell^2} = \frac{730(7.75^2)21.35}{29.1^2} - \frac{124(29.1)}{8}$$

$$+ \frac{670(21.35^2)7.75}{29.1^2} = 3449 \text{ in.-lb}$$

$$M_A = \frac{W_1 a_1 b_1^2}{\ell^2} + \frac{W_1 b_1^2}{\ell^3}(3a_1 + b_1)a_1 - \frac{W_2}{8}(4a_1 - \ell)$$

$$- \frac{W_3 a_3 b_3^2}{\ell^2} + \frac{W_3 b_3^2}{\ell^3}(3a_3 + b_3)a_1$$

$$= \frac{730(7.75)(21.35^2)}{29.1^2} + \frac{730(21.35^2)}{29.1^3}(3 \times 7.75 + 21.35)\,7.75$$

$$- \frac{670}{8}(4 \times 7.75 - 29.1) - \frac{670(21.35)7.75^2}{29.1^2} + \frac{670(7.75^2)}{29.1^3}(3 \times 21.35$$

$$+7.75)\,7.75 + = +1358 \text{ in. lb}$$

$$M_B = -\frac{W_1 a_1 b_1^2}{\ell^2} + \frac{W_1 b_1^2}{\ell^3}(3a_1 + b_1)a_2 - W_1(b_2 - a_1)$$

$$-\frac{W_2}{8}(4a_1 - \ell) - \frac{W_3 a_3 b_3^2}{\ell^2} + \frac{W_3 b_3^2}{\ell^3}(3a_3 + b_3)a$$

$$= -\frac{730(7.75)21.35^2}{29.1^2} + \frac{730(21.35^2)}{29.1^3}(3 \times 7.75 + 21.35)14.55$$

$$- 730(14.55 - 7.75) - \frac{124}{8}(4 \times 7.75 - 29.1) - \frac{670(21.35)7.75^2}{29.1^2}$$

$$+ \frac{670(7.75^2)}{29.1^3}(3 \times 21.35 + 7.75)\ 14.55 = +1416\ \text{in.-lb.}$$

$$M_C = \frac{W_1 a_1 b_1^2}{\ell^2} + \frac{W_1 b_1^2}{\ell^3}(3a_1 + b_1)a_3 - W_1(a_3 - a_1)$$

$$- \frac{W_2}{8}(3\ell - 4a_3) - \frac{W_3 a_3 b_3^2}{\ell^2} + \frac{W_3 b_3^2}{\ell^3}(3a_3 + b_3)a_3$$

$$= -\frac{730(7.75)21.35^2}{29.1^2} + \frac{730(21.35^2)}{29.1^3}(3 \times 7.75 + 21.35)21.35$$

$$- 730(21.35 - 7.75) - \frac{124}{8}(3 \times 29.1 - 4 \times 21.35) - \frac{670(21.35)7.75^2}{29.1^2}$$

$$+ \frac{670(7.75^2)}{29.1^3}(3 \times 21.35 + 7.75)\ 21.35 = +1356\ \text{in.-lb.}$$

W_1 = 125 lb   W_2 = 219 lb   W_3 = 85 lb
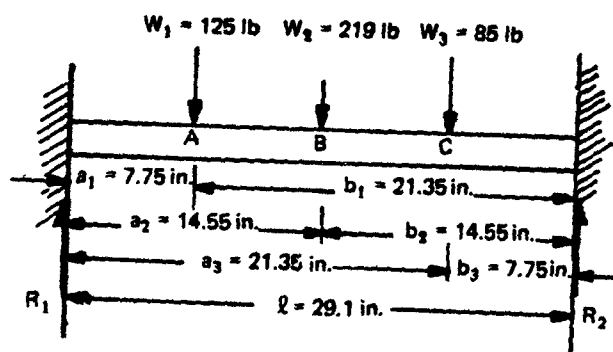
Condition: E2
(Flight Maneuvering)

$a_1 = 7.75$ in. $b_1 = 21.35$ in.
$a_2 = 14.55$ in. $b_2 = 14.55$ in.
$a_3 = 21.35$ in. $b_3 = 7.75$ in.
$\ell = 29.1$ in.

52

$$R_1 = \frac{W_1 b_1^2}{\ell^3}(3a_1 + b_1) + \frac{W_2}{2} + \frac{W_3 b_3^2}{\ell^3}(3a_3 + b_3)$$

$$= \frac{125(21.35^2)}{29.1^3}(3 \times 7.75 + 21.35) + \frac{219}{2} + \frac{85(7.75^2)}{29.1^3}(3 \times 21.35 + 7.75)$$

$$= 103 + 110 + 15 = +228 \text{ lb.}$$

$$R_2 = \frac{W_1 a_1^2}{\ell^3}(3b_1 + a_1) + \frac{W_2}{2} + \frac{W_3 a_3^2}{\ell^3}(3b_3 + a_3)$$

$$= \frac{125(7.75^2)}{29.1^3}(3 \times 21.35 + 7.75) + \frac{219}{2} + \frac{85(21.35^2)}{29.1^3}(3 \times 7.75 + 21.35)$$

$$= 20 + 110 + 70 = +200 \text{ lb.}$$

$$M_1 = \frac{W_1 a_1 b_1^2}{\ell^2} + \frac{W_2 \ell}{8} + \frac{W_3 a_3 b_3^2}{\ell^2} = \frac{125(7.75)21.35^2}{29.1^2} + \frac{219(29.1)}{8}$$

$$+ \frac{85(21.35)7.75^2}{29.1^2} = 521 + 797 + 129 = 1447 \text{ in.-lb.}$$

$$M_2 = \frac{W_1 a_1^2 b_1}{\ell^2} + \frac{W_2 \ell}{8} + \frac{W_3 a_3^2 b_3}{\ell^2} = \frac{125(7.75^2)21.35}{29.1^2} + \frac{219(29.1)}{8}$$

$$+ \frac{85(21.35^2)7.75}{29.1^2} = 189 + 797 + 355 = 1341 \text{ in.-lb.}$$

$$M_A = \frac{-W_1 a_1 b_1^2}{\ell^2} + \frac{W_1 b_1^2}{\ell^3}(3a_1 + b_1)a_1 + \frac{W_2}{8}(4a_1 - \ell)$$

$$- \frac{W_3 a_3 b_3^2}{\ell^2} + \frac{W_3 b_3^2}{\ell^3}(3a_3 + b_3)a_1 = -\frac{125(7.75)21.35^2}{29.1^2}$$

$$+ \frac{125(21.35^2)}{29.1^3}(3 \times 7.75 + 21.35)7.75 + \frac{219}{8}(4 \times 7.75 - 29.1)$$

$$- \frac{85(21.35)7.75^2}{29.1^2} + \frac{85(7.75^2)}{29.1^3}(3 \times 21.35 + 7.75)7.75$$

$$= -521 + 799 + 52 + 129 + 115 = +316 \text{ in.-lb.}$$

53

$$M_B = -\frac{W_1 a_1 b_1^2}{\ell^2} + \frac{W_1 b_1^2}{\ell^3}(3a_1 + b_1) a_2 - W_1(a_2 - a_1)$$

$$+ \frac{W_2}{8}\left(4 \times \frac{\ell}{2} - \ell\right) - \frac{W_3 a_3 b_3^2}{\ell^2} + \frac{W_3 b_3^2}{\ell^3}(3a_3 + b_3) a_2$$

$$= -\frac{125(7.75)21.35^2}{29.1^2} + \frac{125(21.35^2)}{29.1^3}(3 \times 7.75 + 21.35)\,14.55$$

$$- 125(14.55 - 7.75) + \frac{219}{8}\left(4 \times \frac{29.1}{2} - 29.1\right) - \frac{85(21.35)(7.75^2)}{29.1^2}$$

$$+ \frac{85(7.75^2)}{29.1^3}(3 \times 21.35 + 7.75)\,14.55 = -521 + 1500$$

$$- 850 + 797 - 129 + 216 = +1013 \text{ in.-lb.}$$

$$M_C = \frac{-W_1 a_1 b_1^2}{\ell^2} + \frac{W_1 b_1^2}{\ell^3}(3a_1 + b_1) a_3 - W_1(a_3 - a_1) + \frac{W_2}{8}(3\ell - 4a_3)$$

$$- \frac{W_3 a_3 b_3^2}{\ell^2} + \frac{W_3 b_3^2}{\ell^3}(3a_3 + b_3) a_3$$

$$= \frac{-125(7.75)21.35^2}{29.1^2} + \frac{125(21.35^2)}{29.1^3}(3 \times 7.75 + 21.35)\,21.35$$

$$- 125(21.35 - 7.75) + \frac{219}{8}(3 \times 29.1 - 4 \times 21.35)$$

$$- \frac{85(21.35)7.75^2}{29.1^2} + \frac{85(7.75^2)}{29.1^3}(3 \times 21.35 + 7.75)\,21.35$$

$$= -521 + 2202 - 1700 + 52 - 129 + 318 = +220 \text{ in.-lb.}$$

Analysis of -3 Channel

$A = 0.2315 \text{ in.}^2$

$\overline{y} = 1.267 \text{ in.}$

$I_{NA} = 0.1456 \text{ in.}^4$

Material: 2024-T3 Alclad QQ-A-250/5

(Ref. 5) $F_{tu} = 60,000$ psi

$F_{cy} = 36,000$ psi

54
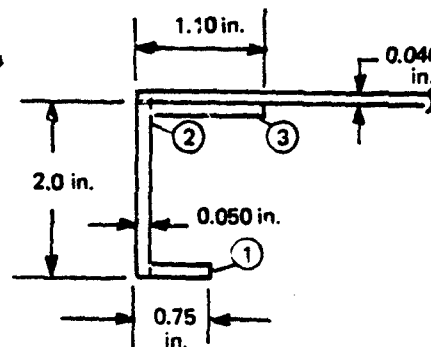
BM (max) $= 3609$ in.-lb (at point "R"), Ref. Page 39.

$$f_b = \frac{3609(1.267)}{0.1456} = 31,400 \text{ psi}$$

$$\frac{t_w}{t_f} = 1 \quad , \qquad \frac{b_w}{b_f} = \frac{2 - 0.05}{0.75 - 0.025} = \frac{1.95}{0.725} = 2.69$$

$$K_f = 0.9 \quad (\text{Ref. 8, Figure 170.04.1-1})$$

$$\sigma_{cr} = \frac{0.9 \, \pi^2 \, \eta \, 10.5 \times 10^6}{12 \, (1 - 0.3^2)} \left(\frac{0.05}{0.725} \right)^2 = 40,623 \text{ psi}$$

$$\sigma_{cr} > F_{CY} \ (= 36,000)$$

$$\text{M.S.} = \frac{36,000}{31,400} - 1 = +0.15$$

Analysis of Riveted End Attachment of -3 Channel

Condition E-1
(Crash)

$$\text{Direct Shear/Rivet} = \frac{657}{6} = 110 \text{ lb}$$

55
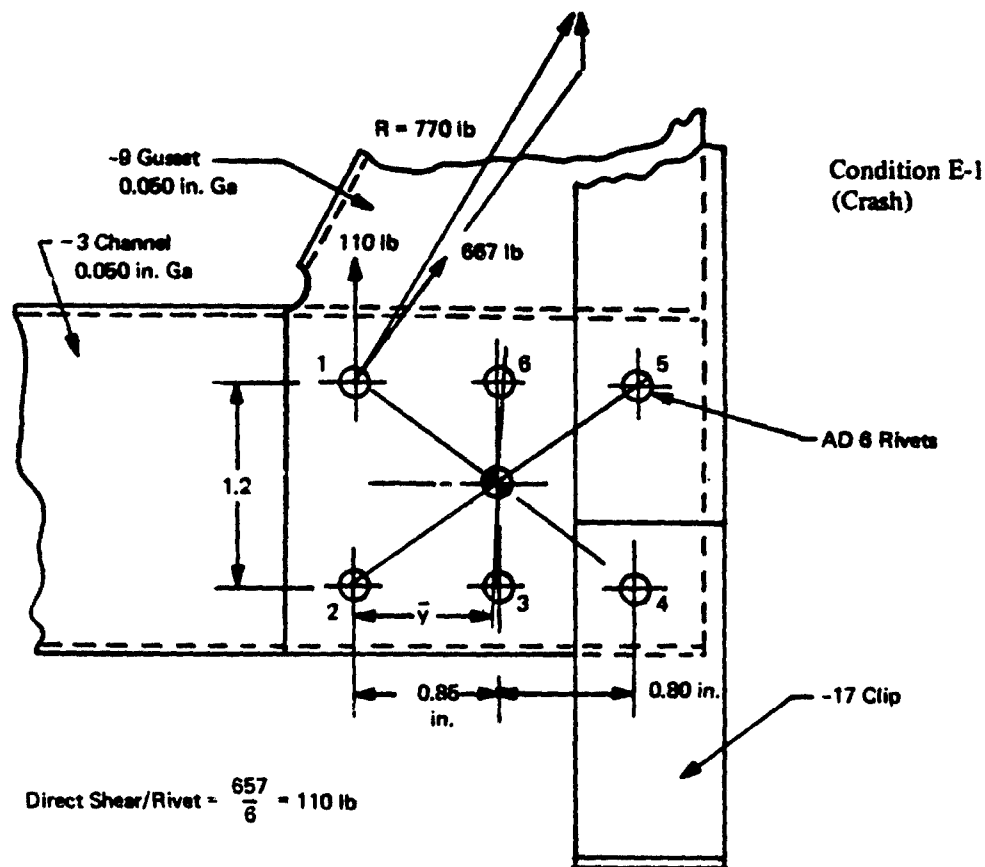
$$y = \frac{\Sigma y}{6} = \frac{5}{6} = 0.833$$

M_1 = 3609 in.-lb (Moment Reacted through Rivet Pattern)

$$\text{Direct Shear/Rivet} = \frac{657}{6} = 110 \text{ lb.}$$

Rivet No.	z	z^2	y	y_1	y_1^2	$r^2 = z^2 + y_1^2$	r	m
1	+0.6	0.36	0	-0.833	0.6939	1.0539	1.0266	667 lb
2	-0.6	0.36	0	-0.833	0.6939	1.0539	1.0266	667 lb
3	-0.6	0.36	0.85	+0.017	0.00029	0.3603	0.6002	390 lb
4	-0.6	0.36	1.65	+0.817	0.6675	1.0275	1.0137	659 lb
5	+0.6	0.36	1.65	+0.817	0.6675	1.0275	1.0137	659 lb
6	+0.6	0.36	0.85	+0.017	0.6675	1.0275	1.0137	390 lb
			Σ y · 5.00			5.5506		

$$P_m \text{ (Shear Resulting from } M_1 \text{)} = \frac{M_1 r}{r^2} = \frac{3609\, r}{5.5506}$$

Maximum Resultant - Measured Graphically - is at No. 1 or No. 2 = 770 lb.

Allowable Single Shear/AD6 Rivet = 862 lb.

Allowable Brg. of AD6 in 0.050 in. Ga of -3 Channel or -9 Gusset

$$= 955 \times \frac{121,000}{100,000} = 1155 \text{ lb.}$$

Shear Correction Factor = 0.970 (Ref. Table 8.1.2.1(b) of Ref. (5)).

$$\text{M.S.} = \frac{862(0.970)}{770} - 1 = +0.08.$$

Analysis of -9 Gusset

-9 Gusset
Material: 2024-T3 Alclad
$F_{tu} = 60,000$ psi
QQ-A-250/5
Ref (1)

(R = 770 lb)   (R = 770 lb)

660

1   390 lb   6   5
387

1.2 in.

660 lb

0.8 in.

390
3   lb   4

660 lb

387   2
lb

-3 channel

1.25 in.

57
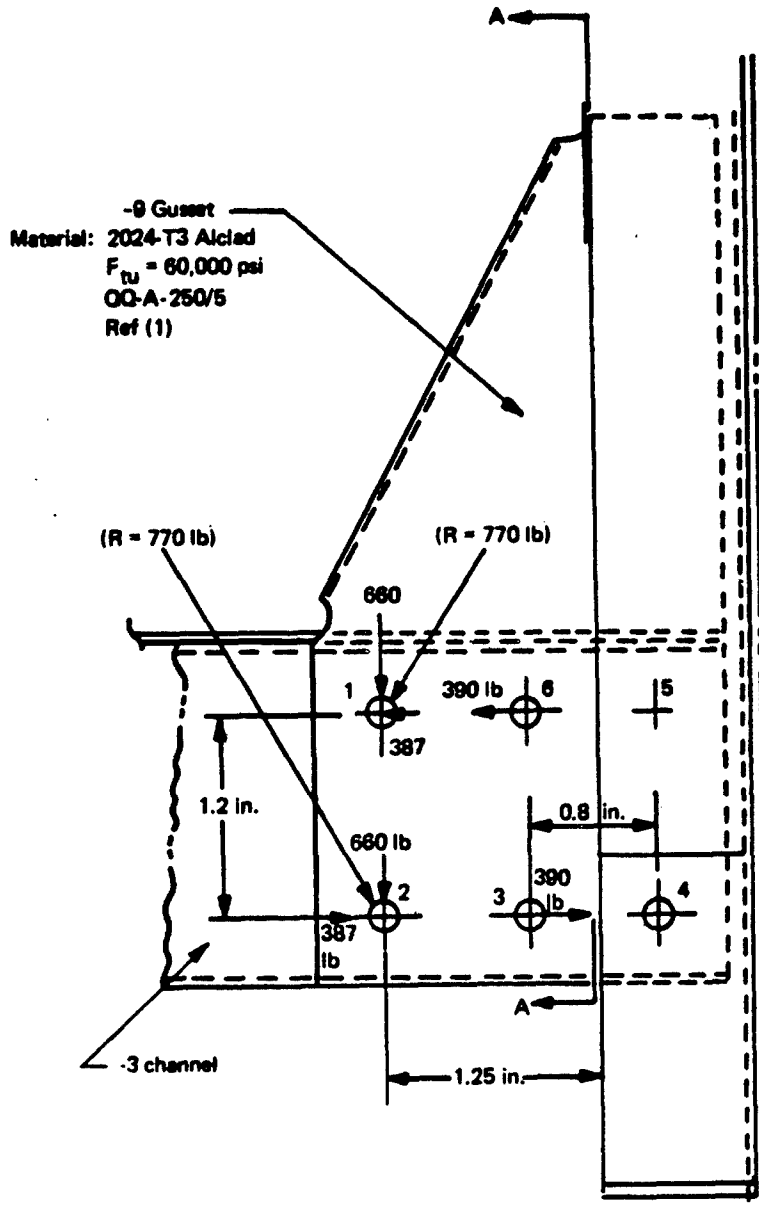
SECTION A-A
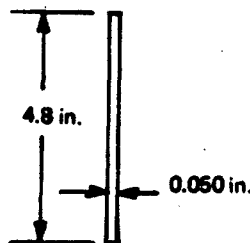
$$\frac{I}{y} = \frac{0.050(4.8)^2}{6} = 0.192 \text{ in.}^3$$

$$BM = 660(2)1.25 + (387 + 390)1.2 = 2575 \text{ in.-lb.}$$

$$f_b = \frac{2575}{0.192} = \pm 13,400 \text{ psi.}$$

Inter-rivet buckling stress between rivets at No. 3 and No. 4:
(Ref. (10) - page C7.14, Figure C7.19)

$$\frac{P}{t} \quad \frac{\text{(Rivet Spacing)}}{\text{(Sheet t)}} = \frac{0.8}{0.050} = 16.$$

F_{ir} (Inter-Rivet Buckling Stress) = 35,800 psi

$$M.S. = \frac{35,800}{13,400} - 1 = +1.67$$

(c) Support Installation-Engine - Drawing 7389-430079

Analysis: Bracket 7389-430079-9 Attachment to Channel No. 7389-430084-3.

58
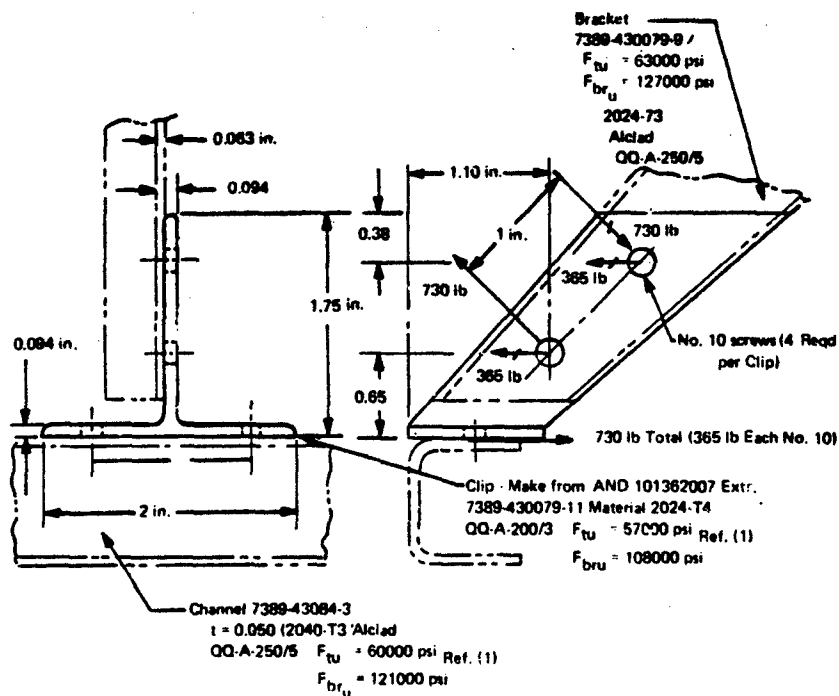
Maximum resultant load on above screws (solved graphically) = 1015 lb

Allowable Brg. on 7389-430079-9 Bracket = 127,000(0.190)0.063 = 1517 lb

Allowable S. Shear on No. 10 Screws = 2126 lb

Allowable Brg. of No. 10 on 7389-430079-11 Clip = 108,000 (0.190) 0.094 = 1930 lb

Allowable Brg. of No. 10 on 7389-430084-3 Channel = 121,000 (0.190)0.050 = 1147 lb

$$\text{Min. M.S.} = \frac{1517}{1015} - 1 = +0.49$$

Condition: E-1 (Crash)

Assume that all Mom resulting from transfer of 210 lb to the 4 No. 10 Screws:

$$M = 210(7.945) = 1675 \text{ in.-lb.}$$

Another vertical component = 670 - 32 = 638 lb Tension. This equals 158 lb/ attachment point.

- 3 Bracket
0.063 in
2024-T3 ALC.
QQ-A-25015/5
$F_{tu} = 63000$ psi
Ref. (1)

210 lb

7.945 in.

158 lb   R = 610 lb

53 lb   455

53 lb   1   53 lb   4

53 lb   2   53 lb   3

59
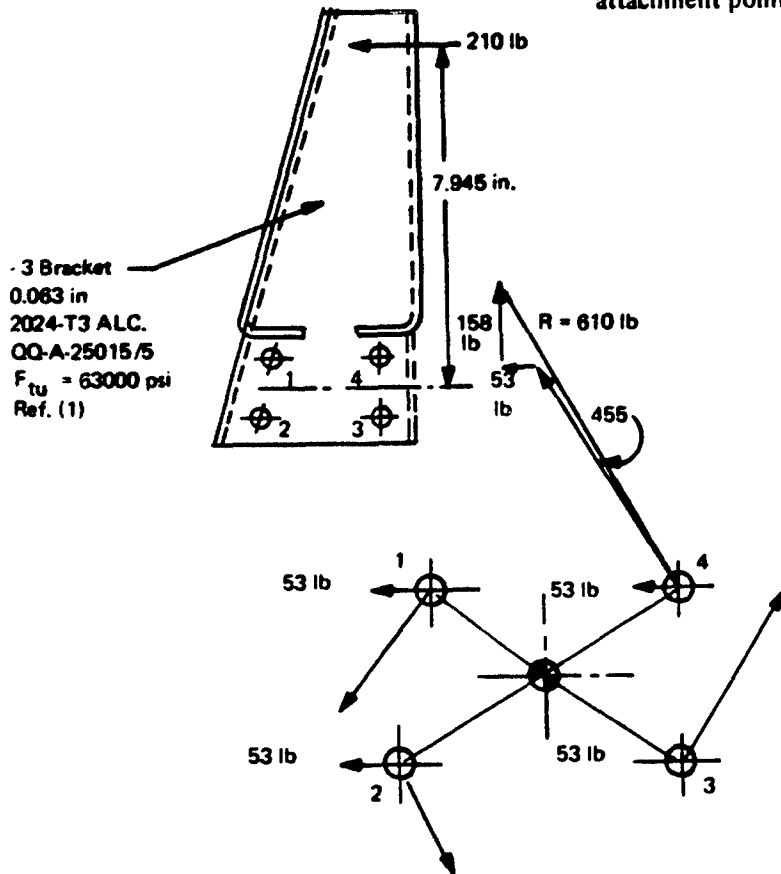
	$\bar{y}$	y_1	y_1^2	z	z_1	z_1^2	$r^2 = y_1^2 + z_1^2$	r
1	–	-0.6715	0.4509	1.00	0.50	0.25	0.7009	0.8372
2	-0.188	-0.8595	0.7387	0	-0.50	0.25	0.9887	0.9943
3	1.437	0.7635	0.5829	0	-0.50	0.25	0.8329	0.9126
4	1.437	0.7635	0.5829	1.00	0.50	0.25	0.8329	0.9126
	2.686			2.00			$\Sigma = 3.3554$	

$$\therefore \bar{y} = 0.6715 \qquad\qquad \therefore \bar{z} = 0.5$$

$$\text{Direct Shear/Rivet} = \frac{210}{4} = 53\,\text{lb} \quad : \quad \text{Mom Shear} = \frac{Mr}{\Sigma(r^2)}$$

No.	Moment Shear
1	420 lb
2	496 lb
3	455 lb
4	455 lb

Maximum resultant shear is at No. 4 and = 620 lb (solved graphically).

Allowable S. Shear on No. 10 screws = 2126 lb.

Allowable Brg. of No. 10 on 0.050 in. ga 7389-430073-2 Channel

$$= 955 \left(\frac{121}{100} \right) = 1150.$$

$$\text{Min. M.S.} = \frac{1150}{620} - 1 = +0.85.$$

5. Fuselage Modification

The Wishbone Structure required a replacement redesign because of interference with the WR-19 engine and exhaust duct installation. This structure is designed to carry the unbalance load from the wing for a critical wing roll condition. The design load for this structure is shown in Table 7.

Due to the upper cowl removal described in Section II, paragraph D.4, a redistribution of shear flow must be determined for the aft side of bulkhead at Fuselage Station 153. The resulting shear flow values are not critical by comparison with values shown in Reference 6; consequently no analysis is made in this section. Modification to the upper portion of bulkheads at Stations 153 and 154.37 are required because of the upper cowl removal.

The lower engine enclosure between Fuselage Stations 153 forward to Station 129.189 in conjunction with the shear deck installation shown on BAC Dwg. No. 7389-430086 forms a

closed section with the existing fuselage 0.025 inch thick skin. A bending and shear analysis is made in this region to determine fuselage skin and engine enclosure shear flows.

The Wishbone replacement structure consists of two triangular truss type structural members which are symmetrical about the fuselage center line (extending between Fuselage Station 126.195 and a cross ship structural beam which is centered at Fuselage Station 108.653). The chord members of both trusses are made up of 2024-T4 angle extrusions. Existing longeron members form one boundary of these structures. Attached to the angle extrusions is an 0.040 inch 2024-T4 Alclad web riveted on all sides. The cross ship beam centered at Station 108.653 consists of two 1 in. x 1¼ in. x 0.125 in. 2024-T4 extruded angles. The 0.040 inch truss web extends forward and is trimmed to such a configuration as to form a web for the cross ship built up beam member. The web is riveted to these angles. Forces applied by the truss members to the built up cross beam are beamed laterally and reacted by existing sail plane structure.

    a.   Truss Installation - Wishbone Structure Replacement Jet Noise Reduction Drawing 7389-430077
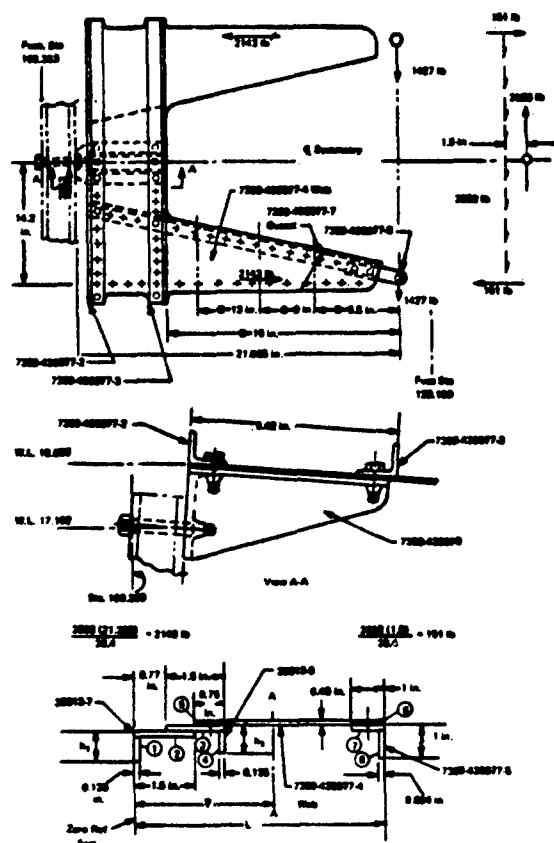
Distance from Pt of Load Application (D)	h₁	h₂	L	ȳ	I_{NA}
5.5 in.	1.2 in.	0.55 in.	4.13 in.	1.8451 in.	7.7302 in.⁴
9 in.	1.28 in.	0.89 in.	4.95 in.	2.0713 in.	2.7098 in.⁴
13 in.	1.38 in.	1.27 in.	5.89 in.	2.2981 in.	4.10035 in.⁴
15 in.	1.42 in.	1.48	6.37 in.	2.4061 in.	4.95102 in.⁴

Section at D = 15 in.

B.M. $\quad = \quad 15(1427) = 21,400$ in.-lb

$I_{NA} \quad = \quad 4.951$ in.⁴

y (to compression edge) = 3.9639 in.

f_b (maximum compression) $= \dfrac{-21,400\,(3.9639)}{4.951} = -17,100$ psi.

$\dfrac{b}{t} = \dfrac{1.0 - 0.047}{0.094} = 10.10$

Ref. Figure 80.04.2-5 of Ref. (8), Page 80.04.2-4.

Material of 7389-430077-5 Angle is 2024-T4
Spec: AND 10133-1002 and QQ-A-200/3 (extrusion).

$F_{cy} \quad = 34,000$ psi (flange allowable)

M.S. $= \dfrac{34,000}{17,100} - 1 = +0.99$

Section at D = 9 in.

B.M. $\quad = \quad 9(1427) = 12,830$ in.-lb.

$I_{NA} \quad = \quad 2.7098$ in.⁴

y (to compression edge) = 4.95 - 2.0713 = 2.8787 in.

f_b (maximum compression) $= \dfrac{-12,830(2.8787)}{2.7098} = -13,580$ psi.

Flange dimensions are same as above ∴ F_{cy} will be used as allowable stress.

M.S. $= \dfrac{34,000}{13,530} - 1 = +1.51$

62
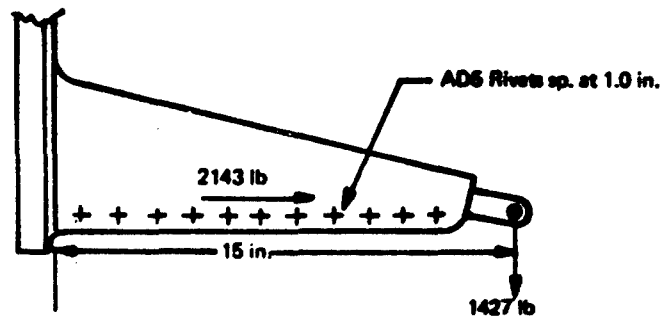
Shear of 2143 lb is reacted in rivets along 15 in.

$$\therefore q = \frac{2143}{15} = 143 \text{ lb/in.}$$

S. Shear/Rivet = 388 x 0.996 = 386 lb.

All brg. of $\frac{5}{32}$ in. Rivet on 2024-T4 Alclad

$$= \frac{119,000}{100,000} \ (636) = 758 \text{ lb}$$

$$\text{M.S.} = \frac{386}{143} - 1 = +1.70.$$

Calculating the Structure as a Truss:
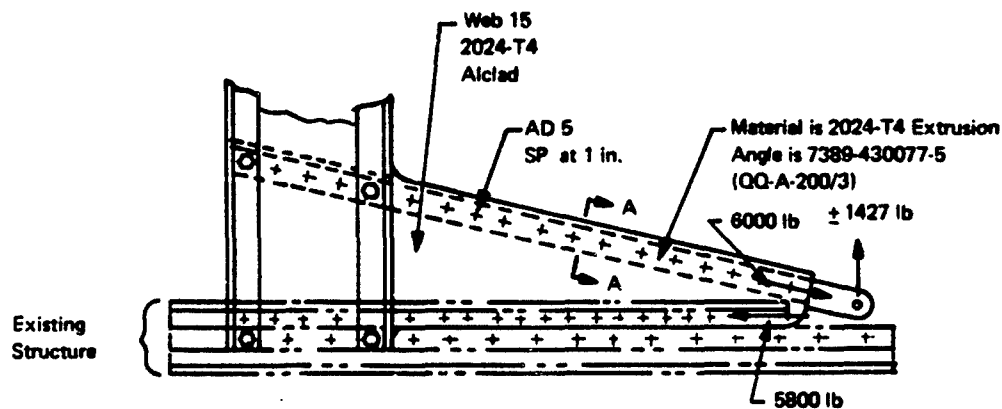
Section Across A-A

$$\text{Area} = (1 + 0.906)0.094 + 0.040(1) = 0.219 \text{ in.}^2$$

$$\frac{P}{A} = \frac{6000}{0.219} = 27,400 \text{ psi.}$$
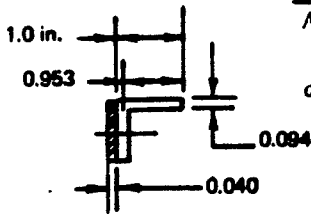
$$\sigma_{cr} \text{ (Ref. (8), Figure 90.02.3.1-5)} = \frac{K_2 \, \pi^2 \eta E}{12(1 - \mu^2)} \left(\frac{t_2}{b_2}\right)^2$$

$$= \frac{0.435 \, \pi^2 \times 10.3 \times 10^6}{12(0.91)} \left(\frac{0.094}{0.953}\right)^2 = 39,393 \text{ psi} > F_{cy} = 34,000 \text{ psi.}$$

$$\text{M.S.} = \frac{34,000}{27,400} - 1 = +0.24$$

Check of Rivet Spacing - Web to Above Angle:

$$F_{ir} \text{ (Inter-Rivet Buckling Stress)} = \frac{\pi^2 E_t}{(p/0.58t)^2}$$

(for clamped ends - Ref. (10)

Equ. C7.22 Page C7.12 - See Fig. C7.19.
Page C7.14 for F_{ir} plotted).

F_{ir} (Ref. Figure C7.19 - Page C7.14 of Ref. (10) at t = 0.040 and SP. at 1 in. = 31,000 psi.

$$\text{M.S.} = \frac{31,000}{27,400} - 1 = +0.13.$$

7389-43077-2

7389-43077-3

$P_R = 3501$

5800 lb

29.50

2853

1427 lb

19.50 in.

₵ Symm
₵ Ship

3.5 in.

5800 lb

1427 lb

A   A

$P_L = 3501$
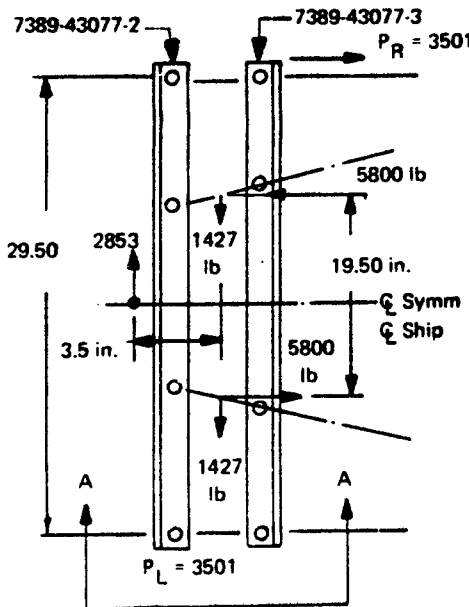
$$P_L = P_R = \frac{5800(19.5)}{29.50} - \frac{2854(3.5)}{29.50}$$

$$= 3840 - 339 = 3501 \text{ lb.}$$

$$\frac{P_L}{2} = \frac{P_R}{2} = \text{Shear/AN4 Bolt (each end)}$$

$$= \frac{3501}{2} = 1750 \text{ lb.}$$

All S. Shear/AN4 Bolt = 3681 lb.

All Brg. of 1/4 inch bolt in 0.125 in. t angles
= 119,000 (1/4) 0.125 = 3720 lb.

$$\text{M.S.} = \frac{3681}{1750} - 1 = +1.10$$
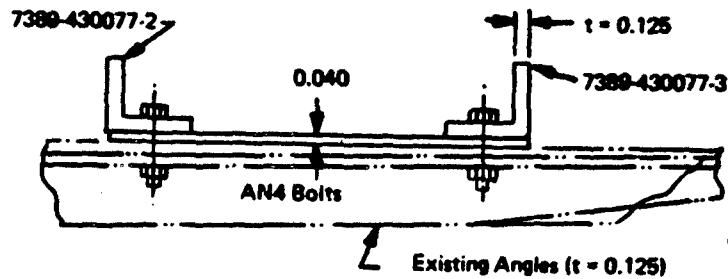
Maximum B.M. in beam consisting of 2 angles and 0.040 in web = 3501(5.25) = 18,400 in.-lb.
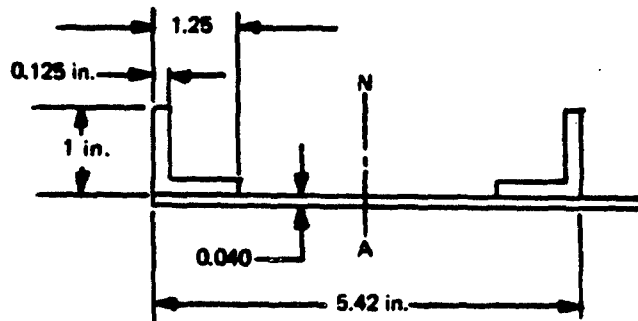
$$I_{NA} = \frac{1.04(5.42^3)}{12} - \frac{0.875(5.17^3)}{12} - \frac{0.125(2.92^3)}{12} = 3.4635 \text{ in.}^4$$

$$f_b = \frac{18,400(2.71)}{3.4635} = \pm14,430$$

$$\frac{b_2}{b_1} = \frac{0.9375}{1.1875} = 0.797 \qquad \frac{t_2}{t_1} = 1$$

$$K_2 = 0.315: \quad \sigma_{cy} = \frac{K_2 \pi^2 \eta E}{12(1-0.3^2)} \left(\frac{t_2}{b_2}\right)^2 = \frac{0.315 \, \pi^2 \, 10.3 \times 10^6}{12(1-0.3^2)} \left(\frac{0.125}{0.9375}\right)^2$$

$$= 52,131 \text{ psi} > F_{cy} = 34,000$$

$$M.S. = \frac{34,000}{14,430} - 1 = +1.35.$$

65

Fitting - 7389-430077-9

0.125 in.

2.35 in.

0.50 ← 1.85 in. →

1.37

0.9 in.

0.5 in. 0.5 in.

B

Material is: 4130 Steel
Spec: MIL-S-18729
HT 125,000 psi

AN5 Bolt

2 Bolts AN4

1.0 in.

B

1.40 in.

1427 lb
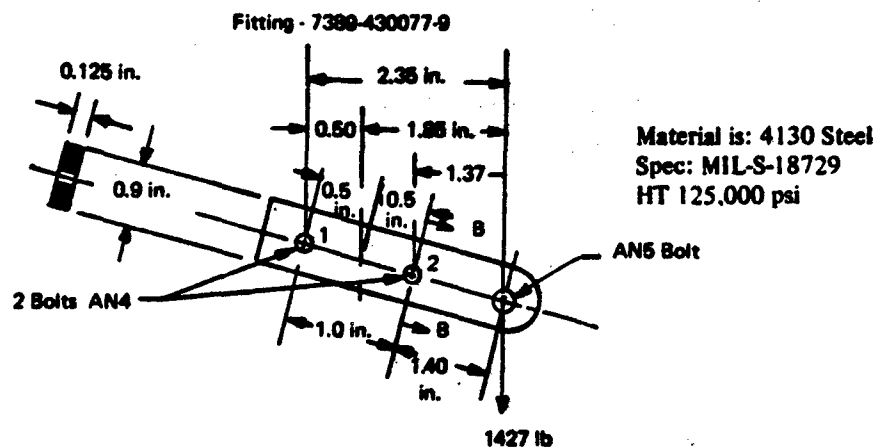
Max. bolt load is at Bolt No. 2: $P = \dfrac{1427(2.35)}{(2.35 - 1.37)} = 3420 \text{ lb}$

Bolt load at Bolt No. 1 = 3420 - 1427 = 1993 lb

Allowable Single Shear/AN4 Bolt = 3680 lb.

$M.S. = \dfrac{3680}{3420} - 1 = +0.08$

$F_{bru}(4130 \text{ Steel}) = 194,000 \text{ psi}$

$f_{br} = \dfrac{3240}{0.25(0.125)} = 103,500 \text{ psi}$

$M.S. = \dfrac{194,000}{103,500} - 1 = +0.87$

Section at B-b

$I_{NA} = \dfrac{0.125(0.9^3 - 0.25^3)}{12} = 0.00743 \text{ in.}^4$

$BM = 1.37(1427) = 1955 \text{ in.-lb}$

$f_b = \dfrac{1955(0.45)}{0.00743} = 118,800 \text{ psi}$

$M.S. = \dfrac{125,000}{118,800} - 1 = +0.05.$

7389-430077-7 GUSSET ATTACHMENT

The rivet attachment of the -4 Web and -7 gusset to the structural members (consisting of 11 3/16 rivets) shall be made good to transfer the 1427 lb fitting load and its resulting moment due to its transfer to the rivet pattern controid.

66

Gusset
7389-430077-7
Material is 2024-T4
Alclad QQ-A-250/5

Resultant = 927 lb

1427 lb
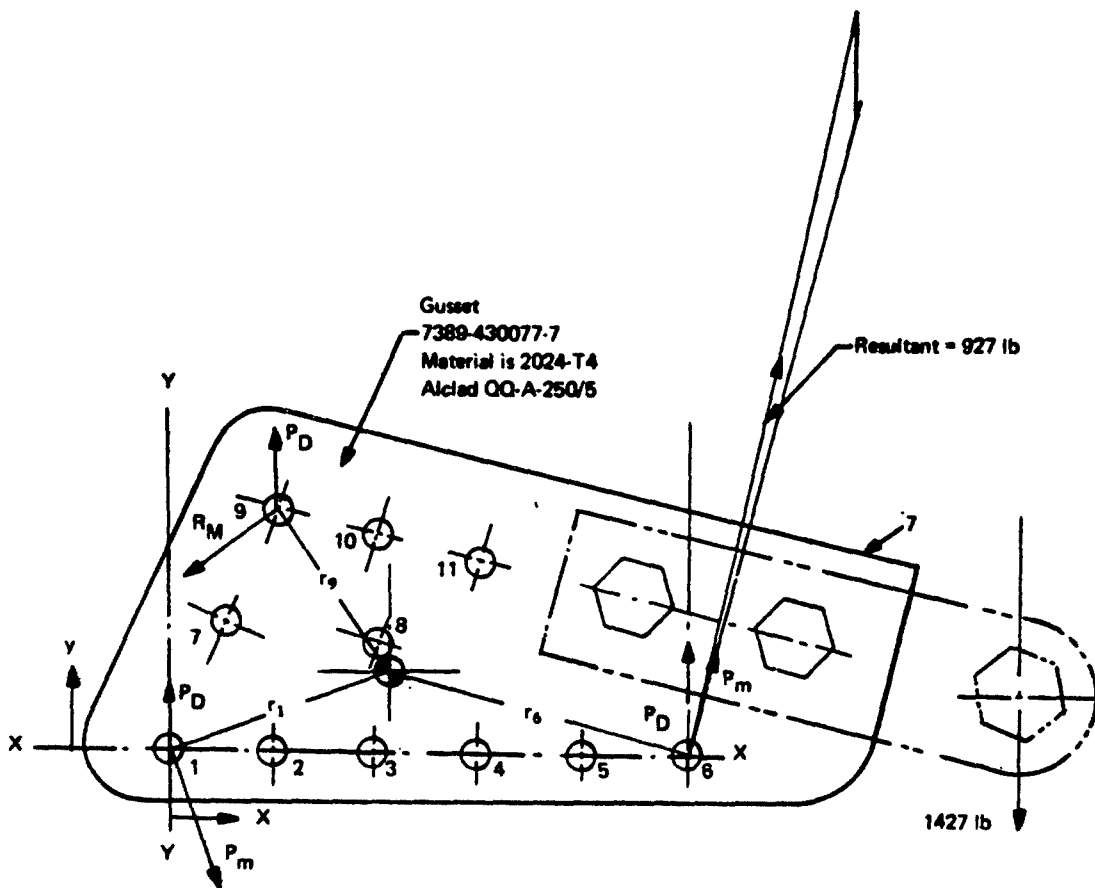
Rivet No.	X	X_1	X_1^2	y	y_1	y_1^2	r^2	r
1	0	-1.37	1.876	0	-0.493	0.243	2.119	1.456
2	0.64	-0.73	0.533	0	-0.493	0.243	0.776	0.881
3	1.28	-0.09	0.008	0	-0.493	0.243	0.251	0.501
4	1.92	0.55	0.303	0	-0.493	0.243	0.546	0.739
5	2.56	1.19	1.416	0	-0.493	0.243	1.659	1.288
6	3.20	1.83	3.348	0	-0.493	0.243	3.591	1.895
7	0.34	-1.03	1.061	0.79	0.297	0.088	1.149	1.072
8	1.30	-0.07	0.005	0.65	0.157	0.025	0.030	0.173
9	0.65	-0.72	0.518	1.48	0.987	0.974	1.492	1.221
10	1.29	-0.08	0.006	1.33	0.837	0.700	0.706	0.840
11	1.92	0.55	0.303	1.17	0.677	0.458	0.761	0.872
	15.10			5.42			13.080	

$$\bar{X} = 15.10/11 = 1.37 \qquad \bar{y} = 5.42/11 = 0.493 \qquad r^2 = X_1^2 + Y_1^2$$

$$P_D \text{ (Direct Load/Rivet)} = \frac{1427}{11} = 130 \text{ lb}$$

$$P_m \text{ at rivet No. 6} = \frac{M \text{ at } CG(r_6)}{\Sigma r^2} = \frac{5490 (1.895)}{13.080} = 796 \text{ lb}$$

$$M \text{ at } CG = 3.85 (1427) = 5490 \text{ in. lb}$$

Maximum rivet load is at No. 6 (solved graphically) = 927 lb

Allowable Single Shear of DD-6 = 1180 lb
Allowable Brg. of 3/16 in. rivets in (.040 in + .063 in.)

2024 -T4 Alclad Sheets

$$= \frac{764 (119)}{100} + \frac{1203 (125)}{100} = 2415 \text{ lb}$$

$$M.S. = \frac{1180}{927} - 1 = +0.27$$
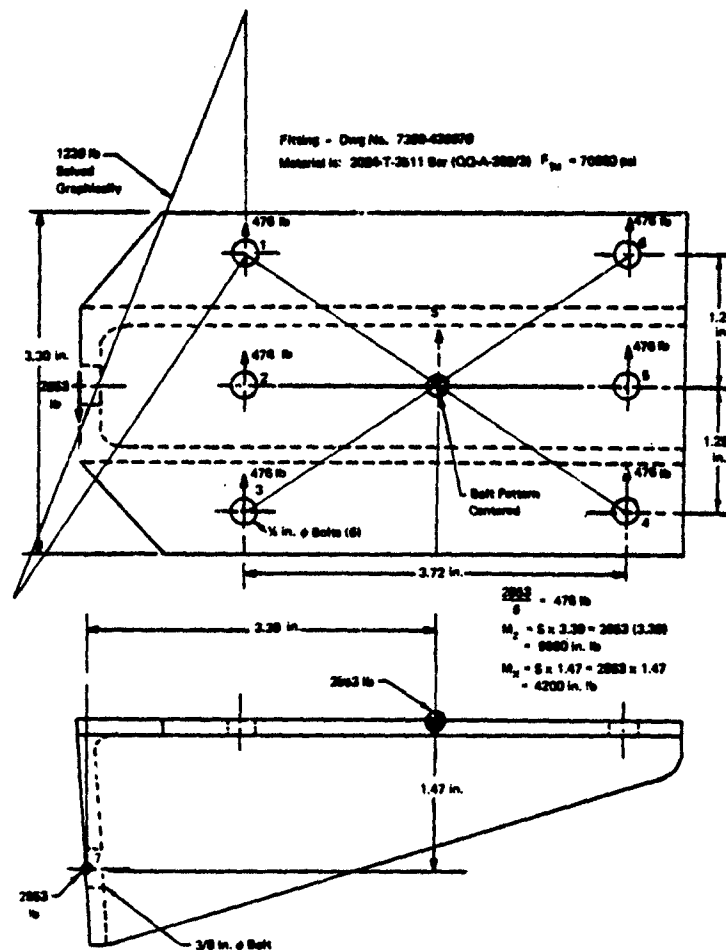
Moment Loads (P_m) at 6 Bolts Due to M_Z									
Bolt	x	x_1	x_1^2	y	y_1	y_1^2	r^2	r	P_m
1	0	-1.86	3.46	2.50	1.25	1.56	5.02	2.24	803
2	0	-1.86	3.46	1.25	0	0	3.46	1.86	665
3	0	-1.86	3.46	0	1.25	1.56	5.02	2.24	803
4	3.72	+1.86	3.46	0	1.25	1.56	5.02	2.24	803
5	3.72	+1.86	3.46	1.25	0	0	3.46	1.86	665
6	3.72	+1.86	3.46	2.50	1.25	1.56	5.02	2.24	803
	11.16			7.50			27.00		

$$\bar{x} = \frac{11.16}{6} = 1.86 \qquad \bar{y} = \frac{7.50}{6} = 1.25 \qquad r^2 = x_1^2 + y_1^2$$

$$\bar{x} = \frac{11.16}{6} = 1.86 \qquad \bar{y} = \frac{7.50}{6} = 1.25 \qquad r^2 = x_i^2 + y_i^2$$

$$P_M \text{ (Moment load due to } M_Z) = \frac{M_Z r}{\Sigma r^2} = \frac{9660r}{27.00} = 358r$$

$$P_T \text{ (Tensile load in each bolt at No. 1 and No. 6)} = \frac{4200}{2(1.65 \times 2/3 + 1.25)} = 895 \text{ lb}$$

$$\text{Max } \rho \text{ lb/in.} = \frac{4200}{2(1.65 \times 2/3 + 1.25)} \frac{2}{1.65}$$

$$= 1082 \text{ lb/in.}$$
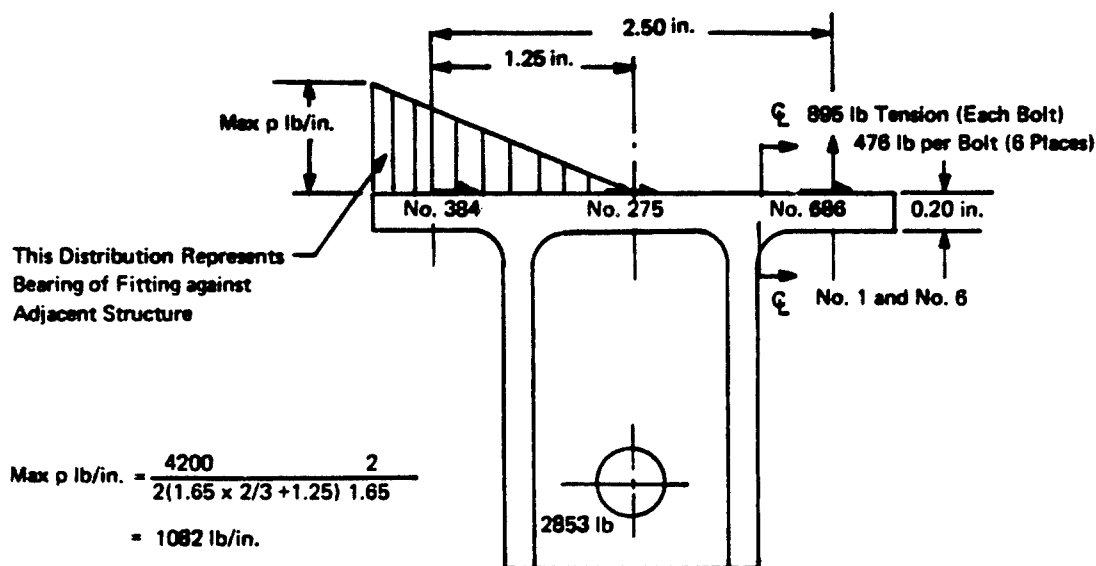
SECTION AT C-C

The bolt tensile load at No. 1 and No. 6 will fan out at 90° from the bolt $\underset{L}{C}$ to Section C-C. The flange length at C-C assumed to carry each tensile bolt load = 1.0 in (See sketch below).

Due to restraint resulting from clamping action of bolt head and nut, the bolt tension shall be applied at a point designated as pt. "a" (see sketch).

BM at C-C = 895 (0.334)
= 298 in. lb.

$$\frac{I}{Y} = \frac{1 (0.2^3)}{6} = 0.00665$$
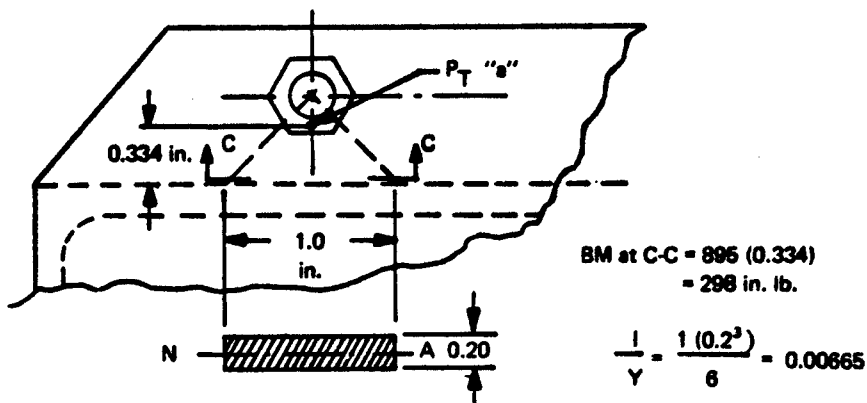
$$f_b = \frac{298}{0.00665} = \pm 56,000 \text{ psi}$$

Brg. stress of bolt on fitting due to 1230 lb load

$$f_{brg} = \frac{1230}{0.25 (0.2)} = 24,600 \text{ psi}$$

Apply the 1230 lb as $\frac{P}{A}$ at Section C-C to combine with the bending stress

$$+ f_t = \pm 56,000 + \frac{1230}{1. (0.2)} = \pm 56,000 + 6150 = + 62,150 \text{ psi}$$

$$\text{M.S.} = \frac{70,000}{62,150} -1 = + 0.12 .$$

Brg. stress at bolt No. 7 $= \frac{2853}{0.375 (0.187)} = 40,700 \text{ psi}$

$$\text{M.S.} = \left[\frac{109,000}{40,700} \right] -1 = + 1.68$$

b.   Fuselage Shear Aft of Fuselage Sta. 153.0

BULKHEAD GEOMETRY - AFT SIDE OF BULKHEAD FUSE STA. 153

REFERENCE: Drawing 32042 G

554 lb ———————— Vertical Tail Side Load · Applied at W.L. 46.361

71
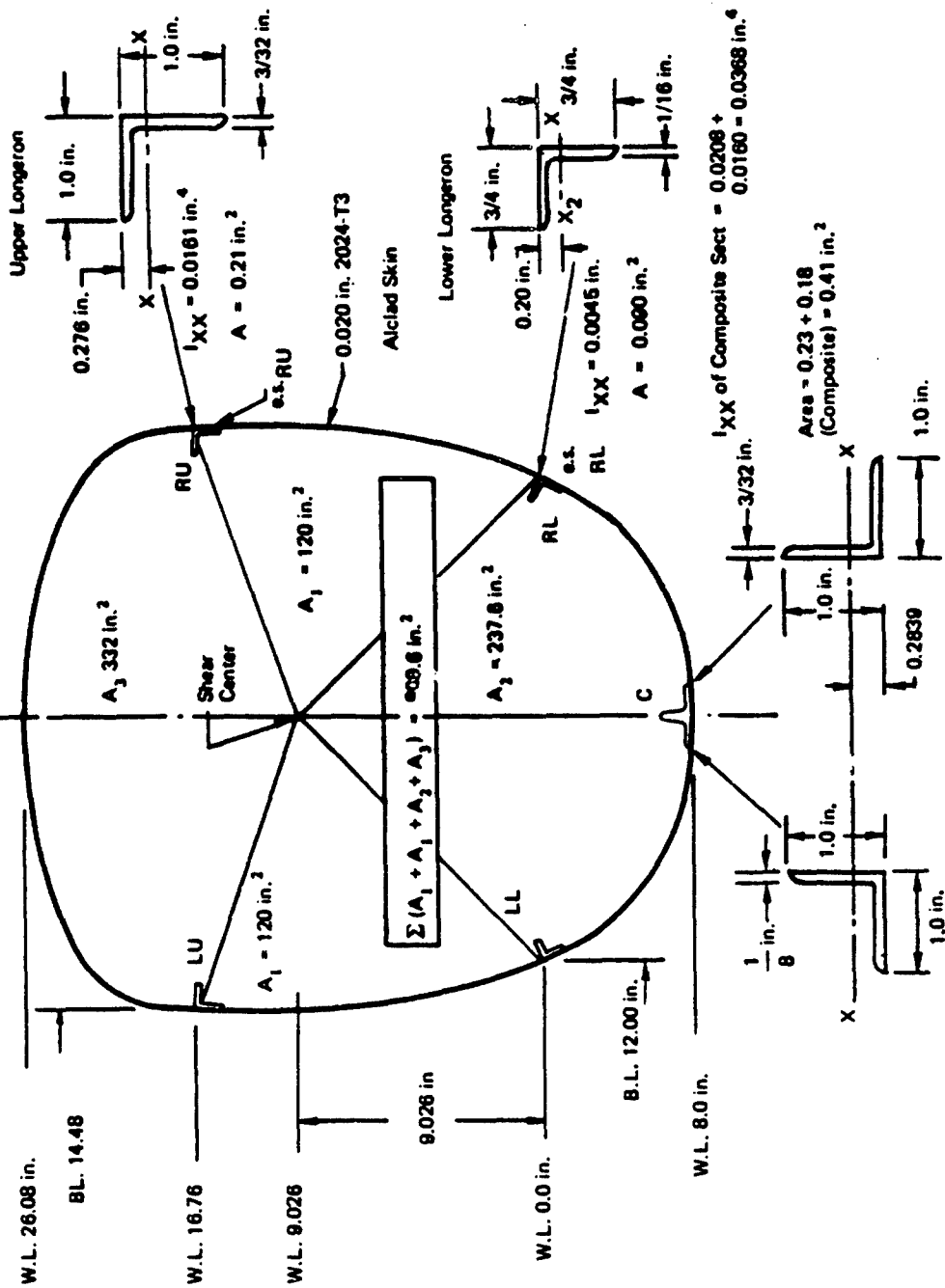
All longerons 2024.T4 AL.AL. Extrusions
All Skin 0.020 in. t 2024-T 3 Alclad
e.s. represents effective skin - subscripts represent location.

SHEAR CENTER LOCATION - AFT SIDE OF FUSE STA. 153

$$e = \frac{E_1 I_1 X_1 + E_2 I_2 X_2 + E_3 I_3 X_3 \cdots \frac{E_n I_n X_n}{}}{E_1 I_1 + E_2 I_2 + E_3 I_3 \cdots \cdots \frac{}{E_n I_n}}$$

To closely approximate the I and X of the skin portion of the structure, an equivalent circle of skin with the same periphery as the bulkhead contour and with its center at a point 1/2 of the bulkhead height.

Peripheral length around bulkhead (measured) = 51.2 in. (=C)

Diameter of equivalent circle = $\frac{C}{\pi}$ = $\frac{51.2}{\pi}$ = 16.3 in.

I of equivalent circle = $\pi R^3 t$ = $\pi(8.15^3) 0.020$ = 34.0136 in^4.

X of equivalent circle = $\frac{26.08 + 8}{2}$ = 17.04 in.

E of Alclad Skin = 10.5×10^6

E of Alum. Extrusions = 10.8×10^6

$$\therefore e = \frac{10.5(34.0136) 17.04 + 10.8(0.0368) 0.2839 + 10.8(0.009)(8-0.2) + 10.8(0.0322)(16.76+8-0.276)}{10.5(34.0136) + 10.8(0.0368) + 10.8(0.009) + 10.8(0.0322)}$$

$$= \frac{6095.099}{357.985} = 17.026 \text{ in. above W.L. - 8.0 in.}$$

e = 17.026 in -8.0 = 9.026 in. above W.L. 0.0 in.

SHEAR FLOW - AFT SIDE OF BULKHEAD FUSE STA. 153

72
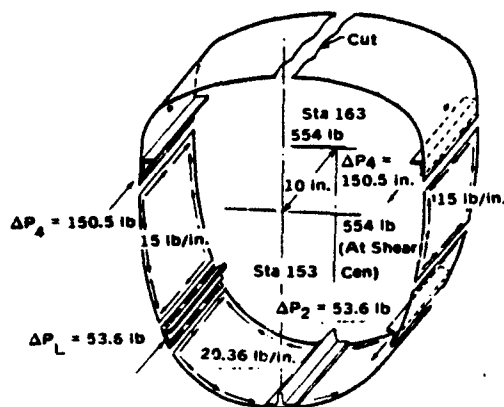
SECTION PROPERTIES AT STA. 153 - NEGLECTING SKIN

	Area	y	ΔY	ΔY²	i_{oo}
LU	0.21	14.204	2.983	42.368	0.0161
RU	0.21	-14.204	-2.983	42.368	0.0161
LL	0.09	11.80	1.062	12.532	0.0045
RL	0.09	-11.80	-1.062	12.532	0.0045
	0.60	$\bar{y} = 0$	0	109.80	0.0412

$$I_{NA} = 109.8 + 0.0412 = 109.8412 \text{ in.}^4$$

B.M. at fuselage Sta. 153 resulting from 554 lb
Side load on vertical tail applied at fuse.
Station 280 in. = (280 - 153) 554 = 127 (554) = 70358 in. lb.

$$\text{Upper longeron loads} = \pm \frac{My(A_{LU \text{ or } RU})}{I}$$

$$= \pm \frac{70358 \,(14.201) \,0.21}{109.8} = \pm 1911.35 \text{ lb}$$

$$\text{Lower longeron loads} = \pm \frac{My(A_{LL \text{ or } RL})}{I}$$

$$= \pm \frac{70358 \,(11.8) \,0.09}{109.8} = \pm 680.51 \text{ lb}$$

Using $\Delta L = 10$ in.
$$\Delta P_U = \pm \frac{5540}{70358} \,(1911.35) = \pm 150.5 \text{ lb}$$

$$\Delta P_L = \pm \frac{5540}{70358} \,(680.51) = \pm 53.6 \text{ lb}$$

Unbalanced shear flow in Sta. 153 aft side developed from ΔP loads stated above. (view looking forward)

Torque represented by shear flow adjacent (unbalanced mom):

$$T = 2 \,(15) \, A_1 \,(2) + 2 \,(20.36) \, A_2$$
$$= 60 \,(122.08) + 40.72 \,(237.6)$$
$$= 7320 + 9650 = 16970 \text{ in. lb.}$$

Torque at E.A. from 550 lb side tail load at W.L. = 45.361 in.
$$= 554 \,(45.361 - 9.026) = 20130 \text{ in. lb.}$$

73
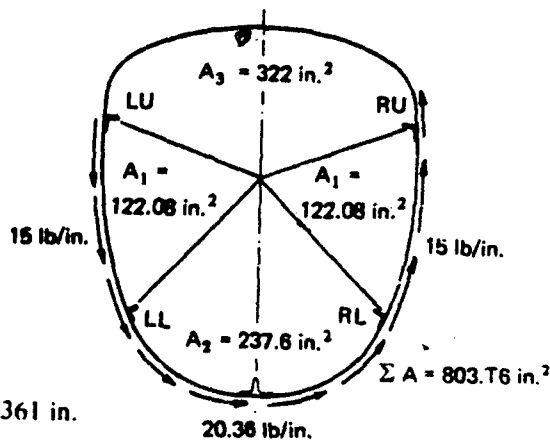
Shear flow resulting from T = 20130 in. lb.

$$q_2 = \frac{T}{2A} = \frac{20130}{2\,(803.76)} = 12.52 \text{ lb/in.}$$

q_3 resulting from unbalance moment of 16970 in. lb:

$$q_3 = \frac{16970}{2\,(803.76)} = 10.57 \text{ lb/in.}$$

NOTE: These Values of q_2 and q_3 Act Clockwise Looking Forward

RESULTANT SHEAR FLOWS - AFT SIDE OF STA. 153

$q_{LU \text{ to } RU}$ = 12.52 + 10.57 $\quad$ = 23.09 lb/in.

$q_{RU \text{ to } RL}$ = 12.52 + 10.57 - 15 $\quad$ = 8.09 lb/in.

$q_{RL \text{ to } LL}$ = 12.52 + 10.57 - 20.36 $\quad$ = 2.73 lb/in.

$q_{LL \text{ to } LU}$ = 12.52 + 10.57 - 15 $\quad$ = 8.09 lb/in.

q = 23.09 lb/in.

LU   RU   Summary: View Looking Fwd.

8.09 lb/in.

q' = 8.09 lb/in.   LL   RL

2.73 lb/in.
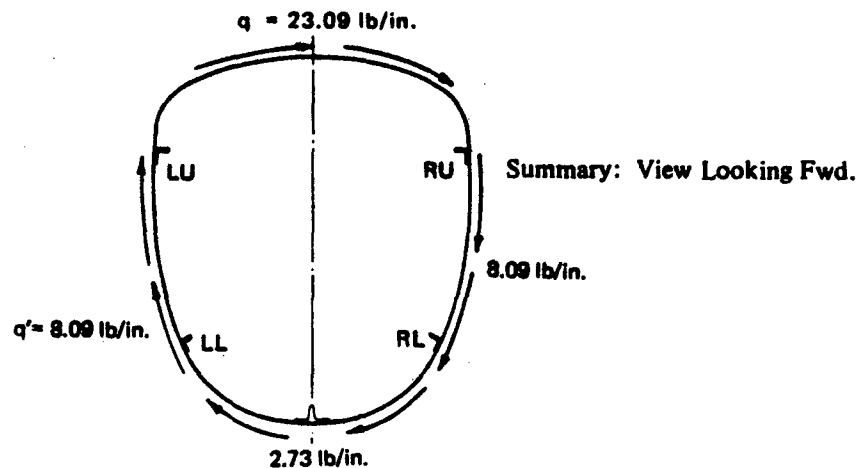
c. Station 129.189 Frame Analysis

Frame loads due to redistribution of shear flows applied from the aft side (Sta. 129.189 to 153) and the fwd side (Sta. 113 to 129.189) are not critical by inspection. These shear flows relieve one another.

Shear from the Wishbone Structure for the wing tip landing condition makes the upper portion of the frame critical.

The lower frame sections are critical for landing wheel load distribution (Reference ⁻).

74

1427 lb (Wishbone Load) Ref. Table 7; Item C

A   A   4.7 in.

32,010 H Bulkhead (Sta. 129.189)

7389-430073-2
Channel
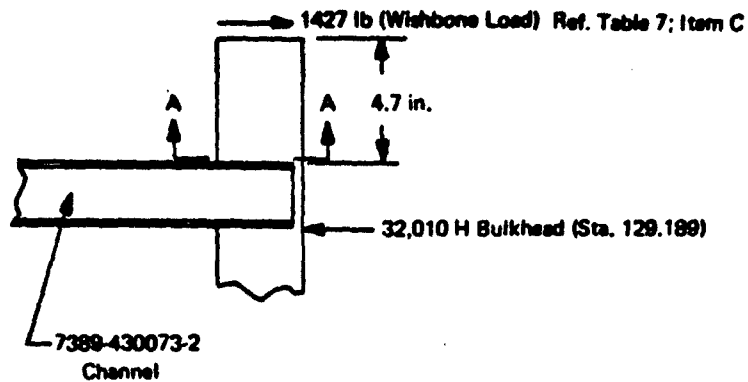
M at A-A = 4.7(1427) = 6707 in. lb

SECTION ACROSS A-A

1 in.   0.091

1.25

4.75
X   X

0.040
0.063

0.7
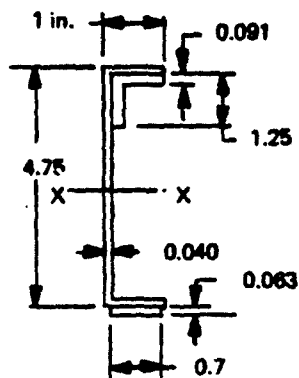
$$\frac{1}{y} \text{ at xx} = \frac{1.8129}{3.148} = 0.576$$

$$f_b = \frac{6707}{0.576} = -11630 \text{ psi}$$

$$\frac{hw}{b_f} = \frac{4.71}{0.98} = 4.6 \qquad \frac{tw}{t_f} = \frac{0.040}{0.040} = 1 \therefore K = 0.755$$

(Ref. Fig. 170.04.1-1 Page 170.04.1-3 of Ref. 8)

$$\sigma_{cr} = \frac{K_f \pi^2 \eta E}{12(1-\mu^2)} \left(\frac{t_f}{b_f}\right)^2 = \frac{0.755 \pi^2 \times 10.2 \times 10^6}{12(1-0.3^2)} \left(\frac{0.040}{0.98}\right)^2 = 11587 \text{ psi}$$

$$M.S. = \frac{11587}{11630} - 1 = +0.00$$

75

d. Bending and Shear Analysis - Fuselage Sta. 129.189 to 153.0

The analysis is based on an average cross section as follows:

CONTOUR OF BULKHEAD AT FUSELAGE STATION 129.189

76

Shear Center Location at Fuse Station 129.189

$$e = \frac{E_1 I_1 X_1 + E_2 I_2 X_2 + E_3 I_3 X_3}{E_1 I_1 + E_2 I_2 + E_3 I_3} \qquad \frac{E_n I_n X \eta}{E_n I_n}$$

$$E_1 = E_2 = E_3 \quad \text{etc.}$$

$$e = \frac{0.01697(2)(16.22 - 0.2845) + 0.00485(2)(-2.17 - 0.2106) + 0.0396(-10.17 - 0.7502)}{0.03394 + 0.00969 + 0.03959}$$

$$= \frac{0.54085 - 0.00414 - 0.43232}{0.03394 + 0.00969 + 0.03959} = 1.254$$

Fuselage Station 129.189 Bending Moment of Inertia at Z-Z

Item		Area	y	Δy	Δy^2	I
③	RU	0.17871	+15.716	+2.8086	44.1400	0.01697
⑤	RL	0.08985	+13.589	+1.2210	16.5918	0.00484
⑨	LU	0.17871	-15.716	-2.8086	44.1400	0.01697
⑪	LL	0.08985	-13.589	-1.2210	16.5918	0.00484
⑥	C	0.60831	0	0	0	0.03959
		1.1454	$\overline{y} = 0$	0	121.4636	0.08321

$$I_{NA} = 121.5468 \text{ in.}^4$$

B.M. at Fuselage Station 129.189 resulting from 554 lb Side Load on Vertical Tail applied at Fuselage Station 280 in.

$$\text{B.M.} = 554 (280 - 129.189) = 83,549 \text{ in. lb}$$

$$\text{Longeron Loads} = \pm \frac{M_y (A_{longeron})}{I}$$

$$\text{Upper Longeron Loads} = \pm \frac{83549 (15.716) 0.17871}{121.547}$$

$$= \pm 1923 \text{ lb}$$

$$\text{Lower Longeron Loads} = \pm \frac{83549 (13.5894) 0.08985}{121.547}$$

$$= \pm 831 \text{ lb}$$

77

Longeron Loads for $\Delta BM = 5540$ in. lb

$$\text{Upper Longeron} = \frac{5540(1923)}{83549} = \pm 127.5 \text{ lb}$$

$$\text{Lower Longeron} = \frac{5540(831)}{83549} = \pm 55.1 \text{ lb}$$

Torque at E.A. at Station 129.189 = 554 (45.361-1.254) = 24435 in. lb
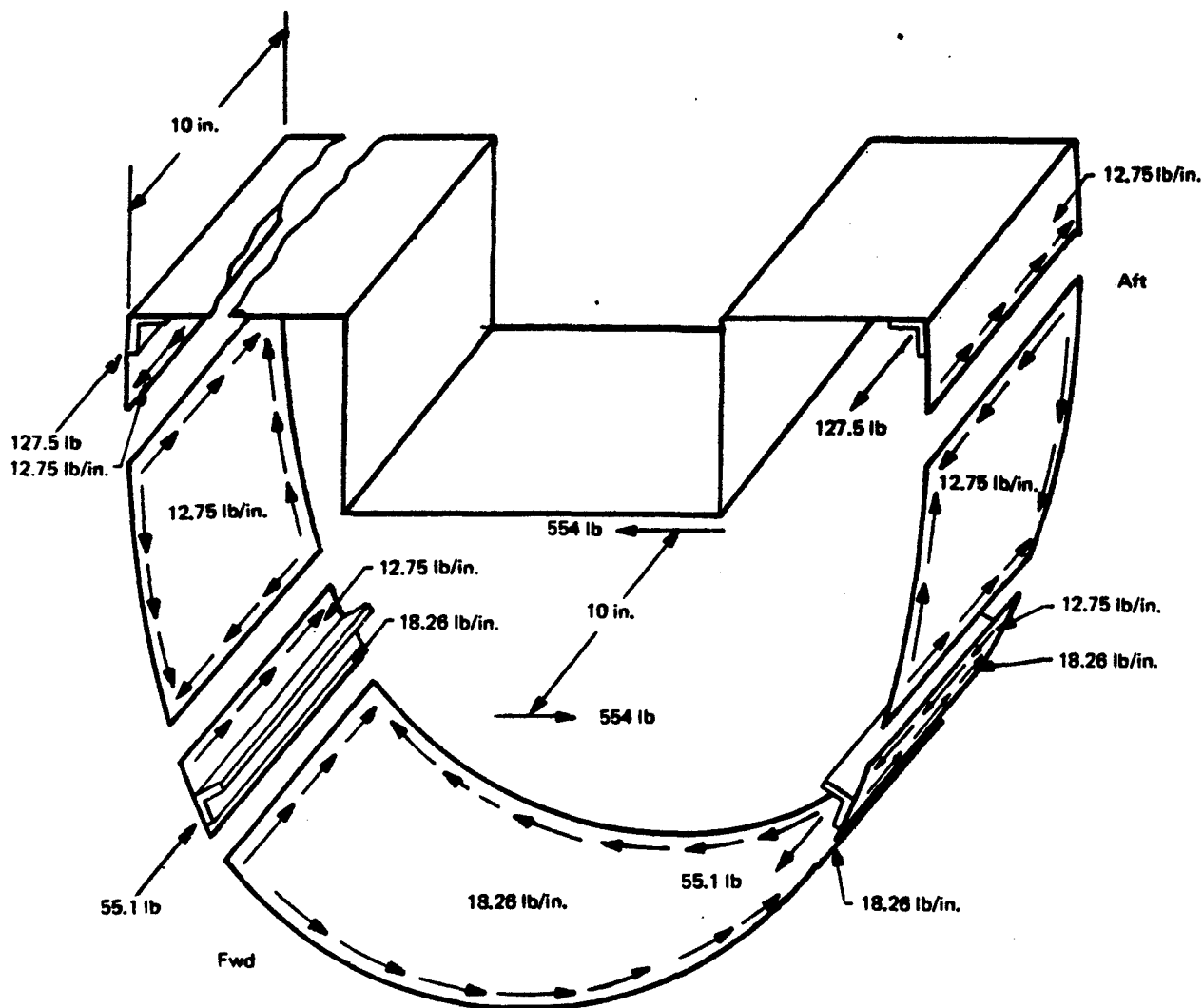
The Enclosed Area of the Previous Section:

$$A = \frac{\pi (16^2)}{2} + 10.39 (32) - 19.50 (8.47) = 569.44 \text{ in.}^2$$

CONTOUR OF BULKHEAD AT FUSELAGE STATION 129.189 IN.
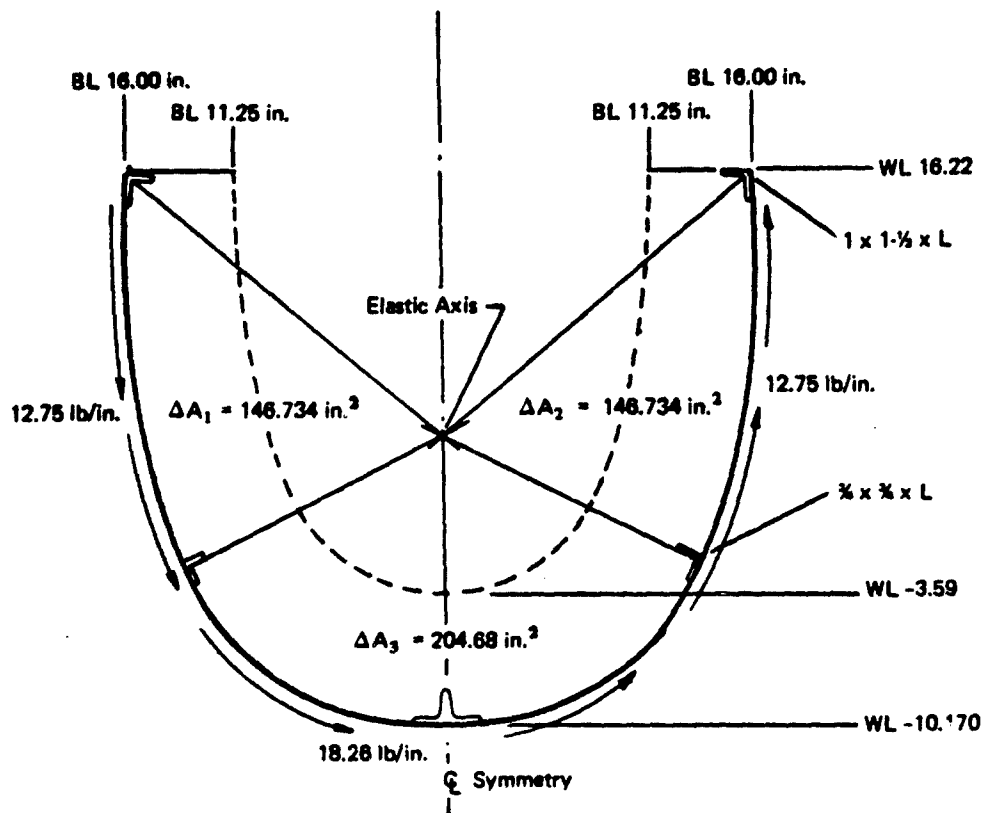
Torque Represented by Area Increments ΔA_1, ΔA_2 and ΔA_3

$$T = 2q_1 (\Delta A_1) + 2q_2 (\Delta A_2) + 2q_3 (\Delta A_3)$$

$$= 2(12.75)(146.734) + 2(12.75) 146.734 + 2(18.26) 204.68$$

$$= 3742 + 3742 + 7475 = 14959 \text{ in. lb} \quad \text{(This is an unbalanced Moment)}$$

Torque imposed by 554 lb Side Load on Vertical Tail:

$$T = 554(45.361 - 1.254) = 24435 \text{ in. lb}$$

q Developed by Unbalanced Moment and the External Moment Resulting from Side Load on Vertical Tail:

$$q = \frac{14959}{2(569.44)} + \frac{24435}{2(569.44)} = 13.13 + 21.40$$

$$= 34.59 \text{ lb/in.}$$

SUMMARY OF SHEARS AROUND SECTION:

q_{Lu} To Ru = 34.59   = 34.59 lb/in.

q_{Ru} To RL = 34.59 - 12.75 = 21.84 lb/in.

q_{RL} To LL = 34.59 - 18.26 = 16.33 lb/in.

q_{LL} To Lu = 34.59 - 12.75 = 21.84 lb/in.

LU   RU

34.59 lb/in.

21.84 lb/in.

21.84 lb/in.

LL   RL

16.33 lb/in.
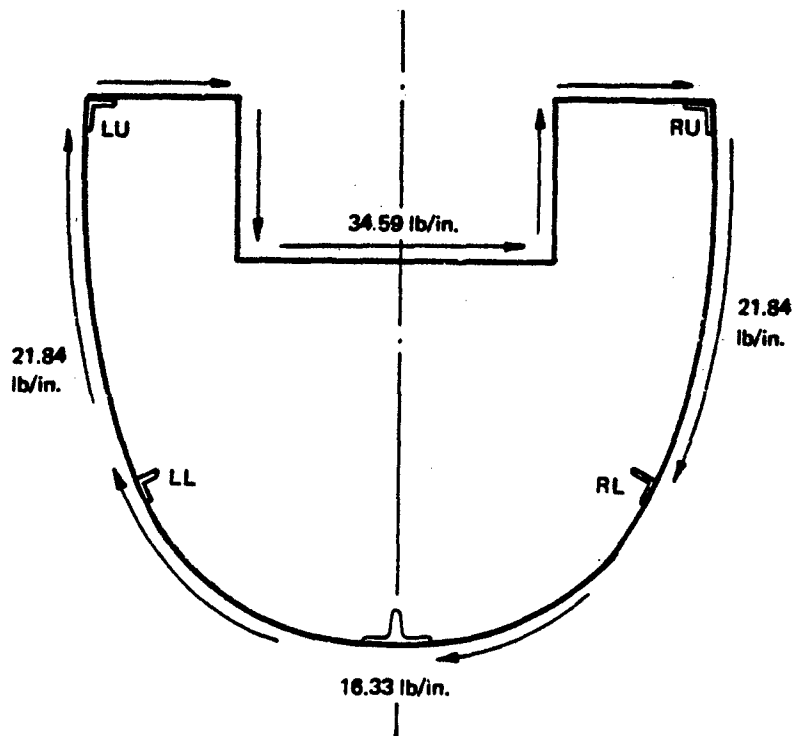
e. Bulkhead Sta. 153. an 154.37 Jet Noise Reduction DRG. in. 7389-430075
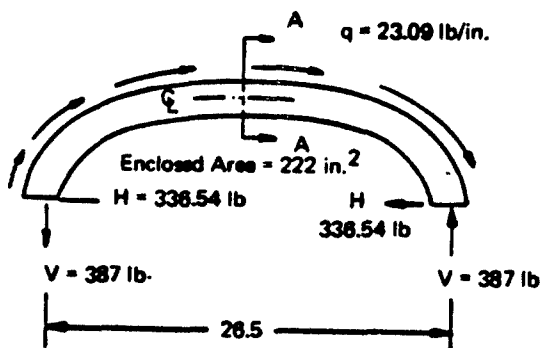
$$H = \frac{23.09\,(29.15)}{2} = 336.54 \text{ lb}$$

$$V = \frac{T}{26.50}$$

$$T = 2Aq = 2(.22)\,23.09$$
$$= 10252 \text{ in. lb}$$

$$V = \frac{10252}{26.50} = 387 \text{ lb}$$

At Section A-A
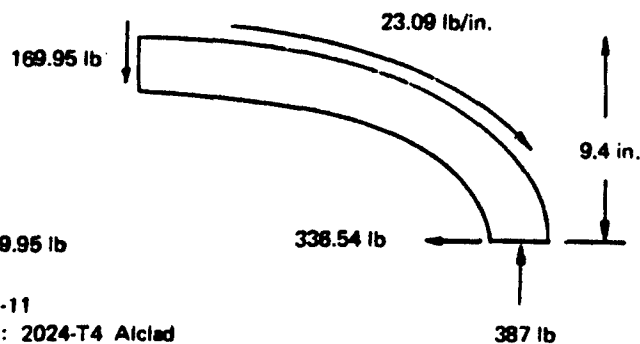
Shear at A-A = 387 · 23.09 (9.4) = 169.95 lb

32042G-11
Material: 2024-T4 Alclad

t = 0.025 in.
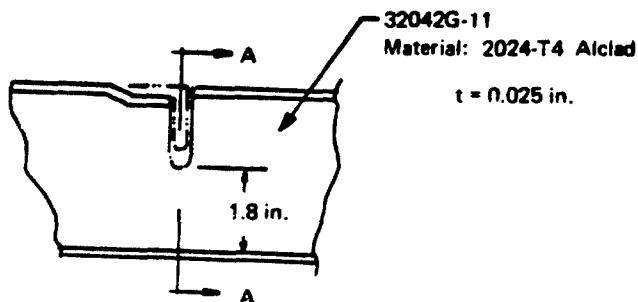
$$f_s = \frac{169.95}{1.8\,(0.025)} = 7550 \text{ psia}$$

$$F_{su} = 37,000$$

$$MS = \pm \text{Large}$$

81

CHECK OF JOINT

Filler Plate

336.54 lb

387 lb

Loads at Joint

AD 4 Rivets

A

A

0.063

0.33

0.45
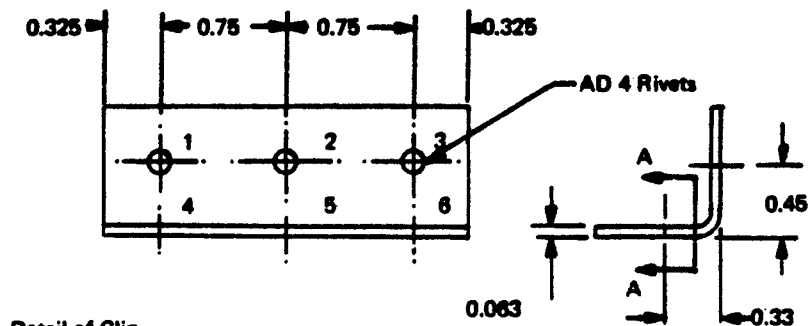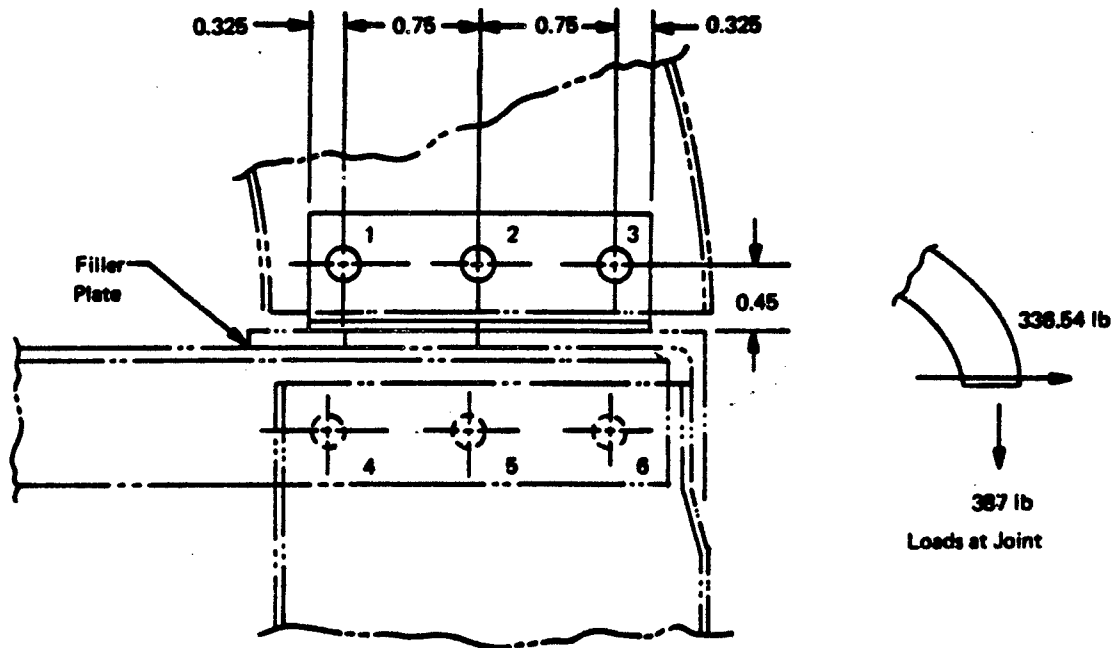
Detail of Clip
Material is 2024-T3 Alclad
QQ-A-250/3

BENDING AT SECTION A-A
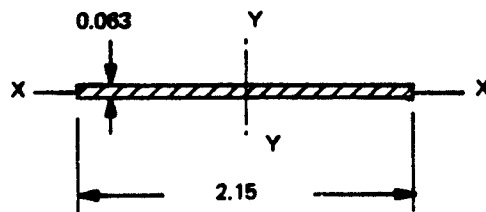
$$\frac{I_{xx}}{y} = \frac{2.15\,(0.063^2)}{6} = 0.00142$$

$$\frac{I_{yy}}{y} = \frac{0.063\,(2.15^2)}{6} = 0.0485$$

$$\text{Area} = 2.15\,(0.063) = 0.135$$

82

$$BM_{xx} = (439.26) \, 0.177 = 77.9 \text{ in. lb}$$

$$BM_{yy} = (336.45) \, 0.177 = 59.5 \text{ in. lb}$$

$$P = 286.2$$

$$f_{b_{xx}} + f_{b_{yy}} + \frac{P}{A} = \frac{77.9}{0.00142} + \frac{59.5}{0.0485} + \frac{286.2}{0.135} = 58206 \text{ psi}$$

Restraint Effects of Screw Head on Bending have been Neglected

$$MS = \frac{63000}{58206} \; 1 = +0.08$$

Check of AD 4 Rivets

Combining Shear and Tension in AD 4 Rivets:

Allowable Single Shear in AD 4 = 388 lb

Allowable Tensile Load in AD 4 = $\frac{388}{2}$ = 194 lb

Shear Load in No. 4 = 174 lb
Tensile Load in No. 4 = 194 lb

$R_T = \frac{159}{194} = 0.82$ $R_s = \frac{174}{388} = 0.449$ - Refering to Fig. 1.5.3.5 of Ref (5) Page 1-23
and using Curve $R_1^2 + R_2^2 = 1$ then $R_{Ta} = 0.87$

$$M.S. = \frac{0.87}{0.82} \; -1 = +0.06$$

Allowable Bearing of 1/8 in. Rivets on 0.025 2024 - T4
Alclad = 321 (1.19) = 382

Max Rivet Shear = 210.15 in.

$$M.S. = \frac{382}{210.15} \; -1 \quad +0.81$$

6. Engine Inlet and Enclosure

The rectangular inlet duct opening is formed of 0.040 inch 6061-T4 aluminum alloy material and contains aft from Fuselage Station 121.720 to Fuselage Station 124.840. At approximate Fuselage Station 137.770, the duct goes into a curved configuration and mates with the upper surface of the upper 0.040 inch thick 6061-T4 engine container segment. The lower edge of the engine inlet and upper enclosure is flanged and bolts to the flange of the lower 0.040 inch thick 6061-T4 container and a shear deck installation between Station 129.189 and Station 153. The flanges of the upper and lower containers bolt together between Stations 129.189 and 112.5.

The engine inlet flat 0.040 inch 6061-T4 sides and 0.040 inch 6061-T4 upper flat panels are broken into smaller panels by formed 0.040 inch thick 6061-T4 hat section stiffeners spot welded through both flanges to the panels. The stiffeners are analyzed as beam columns because the internal negative duct pressure produces compressive end loads on the stiffeners. Side load is provided by the normal panel loading as described on page 85. All corners of the inlet duct are reinforced with 0.071 inch thick 6061-T4 formed angles spot welded to the duct skin.

All bottom, side and end plates of the lower container are assembled by spot welding to 0.040 inch thick 6061-T4 formed corner angles. The engine inlet and enclosure is assembled with an inner shell of 0.032 inch nonstructural acoustic metal weave material separated from the inlet and enclosure by rivet and sleeve spacer standoffs for purposes of acoustical damping.

The design is based on the pressure loadings presented in Table 7.

a. Engine Inlet Loads

The engine inlet pressure is -0.70 psi at the engine face, tapering linearily along the inlet passage to zero at the forward edge where the air enters. A limit to ultimate factor of 1.50 will be used. The effects of pressure are to be combined with inertia loadings for flight and landing maneuvers and crash conditions.

19.50 in.

10 in. Max.

p yield = 0.70 psi
p ult   = 1.05 psi
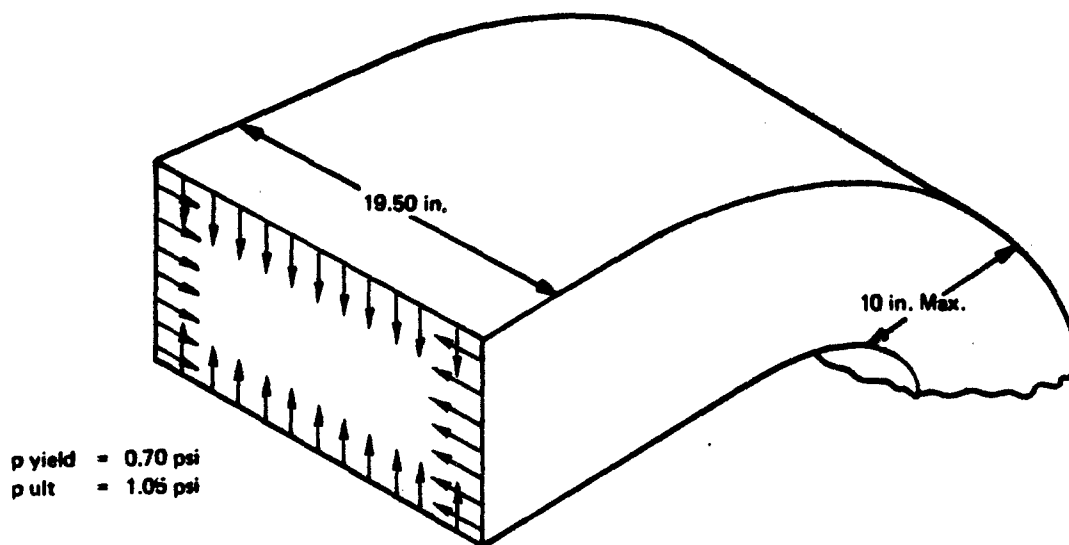
ENGINE ENCLOSURE UPPER AND INLET DUCT
JET NOISE REDUCTION - DWG 7389-430085
CONTINUED

DUCT - TYPICAL CROSS SECTION

$$\ell^3 = 7415$$
$$\ell_1^3 = 1000$$
$$P_{ult} = 1.05 \text{ psi}$$

ℓ = 19.5 in.

ℓ₁ = 10 in.

Pressure = -1.05 psi
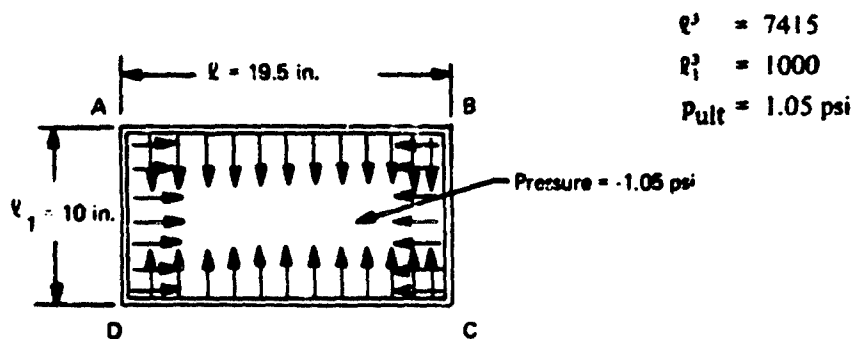
For this case, all moments at A, B, C and D are equal with:

$$M = \frac{P(\ell^3 + \ell_1^3)}{12(\ell + \ell_1)} = \frac{1.05(7415 + 1000)}{12(29.5)} = 25 \text{ in. lb}$$

(Reference - (11) Page 329)

CHECK OF HAT SECTION STIFFENER BETWEEN A AND B

Stiffener Spacing = 6 in.
p = 1.05 psi (Ultimate)
w (Running Load/Inch of Span) = 1.05(6) = 6.3 lb/inch

Loads & Moments
in Stiffener Sections
Around Duct

R at End of Short Side
$$= \frac{1.05(10)6}{2} = 31.5 \text{ lb}$$

R at End of Long Side
$$\frac{1.05(19.5)6}{2} = 61.5 \text{ lb}$$
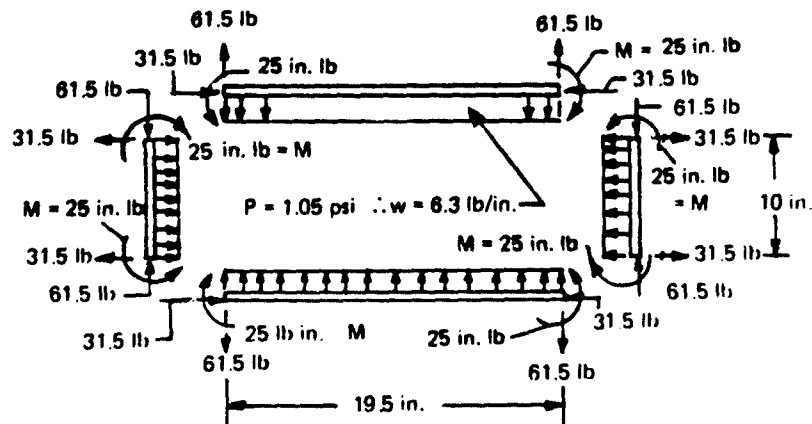
61.5 lb
31.5 lb
25 in. lb
61.5 lb
31.5 lb
25 in. lb = M
M = 25 in. lb
P = 1.05 psi ∴ w = 6.3 lb/in.
31.5 lb
61.5 lb
25 lb in. M
31.5 lb
61.5 lb

61.5 lb
M = 25 in. lb
31.5 lb
61.5 lb
31.5 lb
25 in. lb = M
10 in.
M = 25 in. lb
31.5 lb
61.5 lb
61.5 lb
31.5 lb
25 in. lb

19.5 in.

CHECK OF HAT SECTION STIFFENER AB AS A BEAM COLUMN
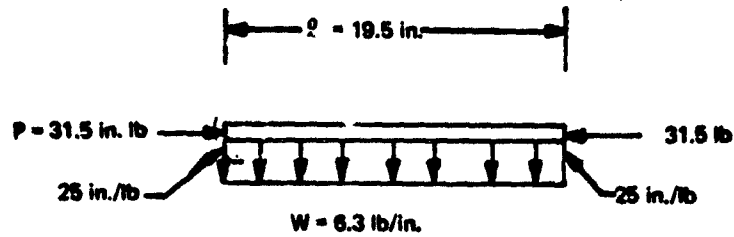
$$j = \sqrt{\frac{EI}{p}} = \frac{9.9 \times 10^6 \times 0.00828}{31.5} = 2602.20 = 51.01$$

where E   For 6061-T4 $= 9.9 \times 10^6$

I $= 0.00828$ in.^{4} (Ref. Page 87)

$$D_1 = M_1 - \omega j^2 = 25 - 6.3 (2602.2) = -16369$$

$$\cos \frac{x}{j} = \cos \frac{\frac{19.5}{2}}{51.01} = \cos 0.1911 = 0.9818 \quad (\text{Ref. (2) Page A5.24})$$

$$M_{max} = \frac{D_1}{\cos \frac{x}{j}} + \omega j^2 = \frac{-16369}{0.9818} + 6.3 \ (2602.2) = -279 \text{ in. lb}$$

(At Mid Point)

86
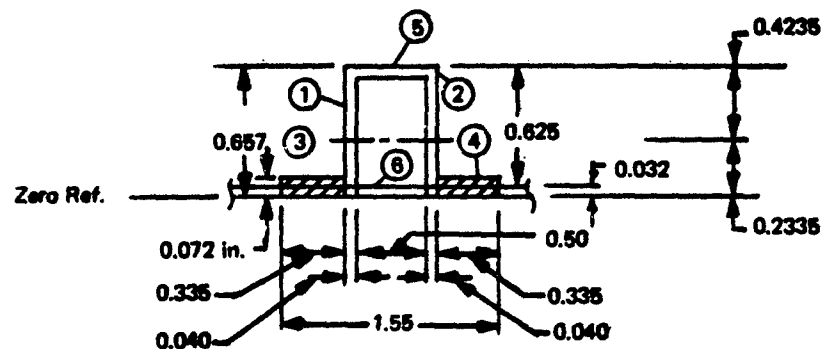
ENGINE ENCLOSURE UPPER AND INLET DUCT ~ JET
NOISE REDUCTION ~ DWG. 7389-430085~CONTINUED

STIFFENER SECTION PROPERTIES

Item		Area	y	Ay	Ay^2	I$_{oo}$
1	0.657 (0.040) =	0.0263	0.3285	0.0086	0.002835	0.000945
2	0.657 (0.040) =	0.0263	0.3285	0.0086	0.002835	0.000945
3	0.335 (0.072) =	0.0241	0.036	0.00087	0.000031	
4	0.335 (0.072) =	0.0241	0.036	0.00087	0.000031	
5	0.500 (0.040) =	0.0200	0.637	0.01274	0.008115	
6	0.500 (0.032) =	0.0160	0.016	0.00026	0.000004	
	Σ	0.1368	$\overline{y}$ = 0.2335	0.03194	0.01385	0.00189

$$I_{NA} = 0.00189 + 0.01385 - 0.2335 \, (0.03194) = 0.00828 \text{ in.}^4$$

$$f_b = \frac{279(0.4035)}{0.00828} = 14220 \text{ psi}$$

$$\frac{b_w}{b_s} = \frac{0.657 - 0.02 - 0.016}{0.5 + 0.04} = 1.15 \qquad \frac{t_w}{t_s} = 1$$

$$K_s = 5.2 \quad (\text{Ref. (8) Fig. 170.04.1-4})$$

$$\sigma_{cr} = \frac{K_s \, \pi^2 \, \eta \, E}{12 \, (1-\mu^2)} \left(\frac{t_s}{b_s}\right)^2 = \frac{5.2 \, \pi^2 \, (9.9 \times 10^6)}{12 \, (1-\mu^2)} \left(\frac{0.040}{0.54}\right)^2 > F_{cy}$$

$$F_{cy} = 16000 \text{ psi}$$

$$\text{M.S.} = \frac{16000}{14220} - 1 = +0.12$$

ENGINE ENCLOSURE UPPER AND INLET DUCT ~ JET NOISE
REDUCTION ~ DWG 7389-430085 ~ CONTINUED

MAX. STRESS IN TYPICAL SKIN PANEL~

Maximum Stress in Typical Skin Panel will be at Mid Point of Long Side ~ Parallel to Short Side.
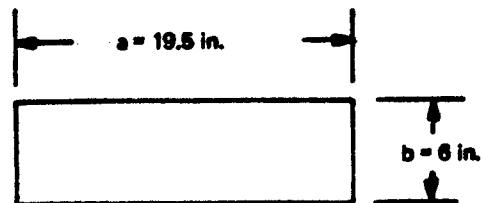
$$\frac{a}{b} = \frac{19.5}{6} = 3.25 \qquad \frac{b}{2t} = \frac{6}{0.064} = 93.7$$

$\sigma_t = 6800$ psi   (Ref. Fig. 7.9 Page 294 of Ref. (12))

M.S. = + Large

ENGINE ENCLOSURE UPPER AND INLET DUCT – JET
NOISE REDUCTION – DWG. 7389-430085 – CONTINUED
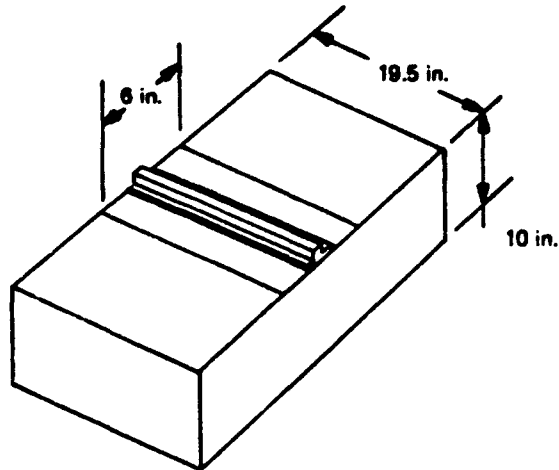
**Maximum Permissable Deflection in Either Skin Panels or Frame Stiffeners
Equals 0.5 in. from the Static (Zero Load) Structural
Positioning. This Will Be a Combination of Stiffener Bending
Deflection Plus Skin Panel Center Point Deflections Resulting
From Normal Pressures.**
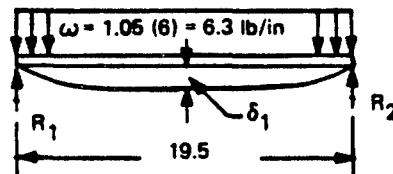
**Stiffener Deflection Formula For Simply
Supported Beam Uniformly Loaded:**

$$\delta_1 = \frac{5W\ell^3}{384EI} = \frac{5wb\ell^4}{384EI}$$

ENGINE ENCLOSURE UPPER AND INLET DUCT – JET
NOISE REDUCTION – DWG. 7389-430085 – CONTINUED

Skin panel deflection at center point for 6 in. x 1.95 in. panel 0.032 in. thick loaded uniformly with a pressure ult of 1.05 psi will be calculated: (Ref. (12), page 293).

$$\frac{b}{t} = \frac{6}{0.032} = 187 \text{ using this value and } p = 1.05 \text{ psi.}$$

Figure 7.7 of Reference 12 indicates the skin panel category to be a thin plate.

$$\frac{a}{b} = \frac{19.5}{6} = 3.25; \text{ Figure 7.8, page 293 of Reference 12 gives} \frac{\delta_2}{t} = 2.15$$

$\Delta \delta_2$ is deflection at center point on panel

$$\therefore \Delta \delta_2 = 2.15 (0.032) = 0.069 \text{in.}$$

$$\delta_{Total} = 0.5 \text{ in. permissable} = \Delta \delta_1 + \Delta \delta_2 = \Delta \delta_1 + 0.069 \text{ in.}$$

$$\therefore \Delta \delta_1 = 0.50 - 0.069 = 0.431 \text{ in. maximum permissable deflection of hat section stiffener only.}$$

$$\Delta \delta_1 = \frac{5wb\ell^4}{384EI} \text{(using I of hat section} = 0.00593)$$

$$\Delta \delta_1 = \frac{5 (1.05) 6 (19.5^4)}{384 (9.9 \times 10^6) 0.00593} = 0.2020 \text{ in.}$$

ENGINE ENCLOSURE UPPER AND INLET DUCT - JET
NOISE REDUCTION   DWG. 7389-430085 - CONTINUED

CHECK OF BENDING SECTION AT CORNER

1.34 in. Flange

1.0 in.

0.62

Spot Welds

A

A B

Hat Section 6061-T4

0.040 in. Structural Inlet Duct

C

0.032 in. Acoustic Metal Weave

A

0.071 in. Corner Angle

6061-T4

$F_{tu} = 30,000$ psi

$F_{ty} = 16,000$ psi

SECTION ACROSS A-A

3.5

0.071 in.

N

A

$$\frac{I}{y} = \frac{3.5\,(0.071^2)}{6} = 0.002950$$
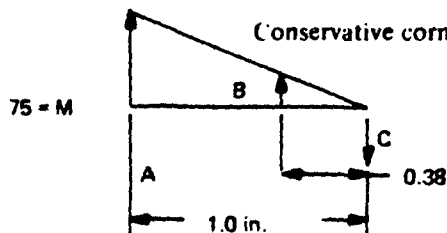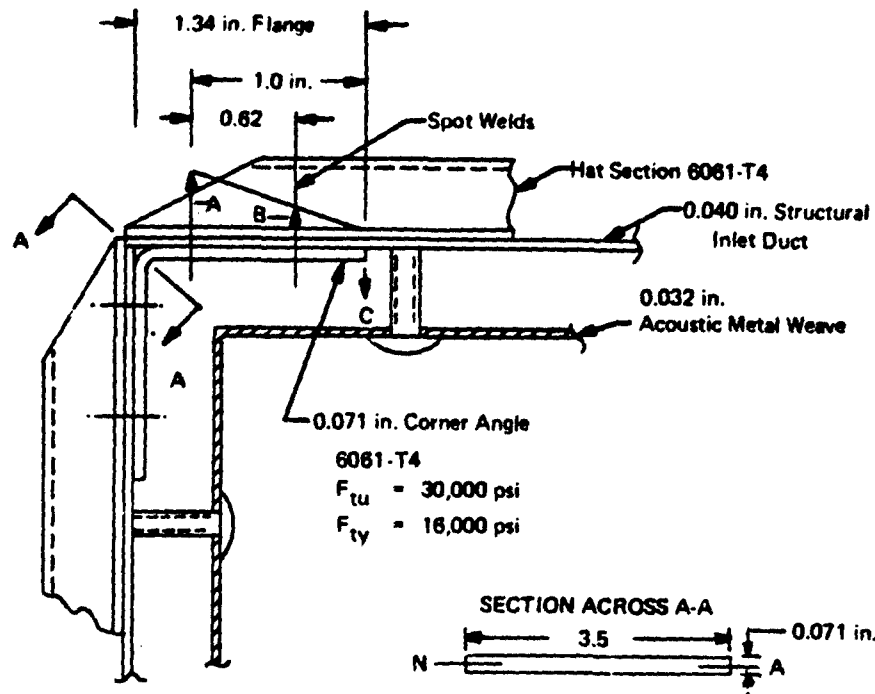
Conservative corner moment assumed to be $25 \times 3 = 75$ in.-lb

$75 = M$

B

C

A

0.38

1.0 in.

$$f_b = \frac{75}{0.00295} = 25424 \text{ psi}$$

$$M.S. = \frac{30000}{25424} - 1 \qquad\qquad +0.18$$

Loads in spot weld attaching ends of hat sections:

$$\Sigma M: \ 0.38\,B + A(1) = 75$$
$$\Sigma F: \ A + B = C$$

$$\frac{A}{1} = \frac{B}{0.38} \therefore B = \frac{0.38A}{1} = 0.38A$$

$$0.38A \times 0.38 + A = 75 \qquad \therefore A = 65.5$$
$$\therefore B = 0.38\,(65.5) = 24.1 \text{ lb}$$
$$\therefore C = 65.5 + 24.1 = 89.6 \text{ lb}$$

91

ENGINE ENCLOSURE — LOWER JET NOISE REDUCTION
DWG. NO. 7389-430083
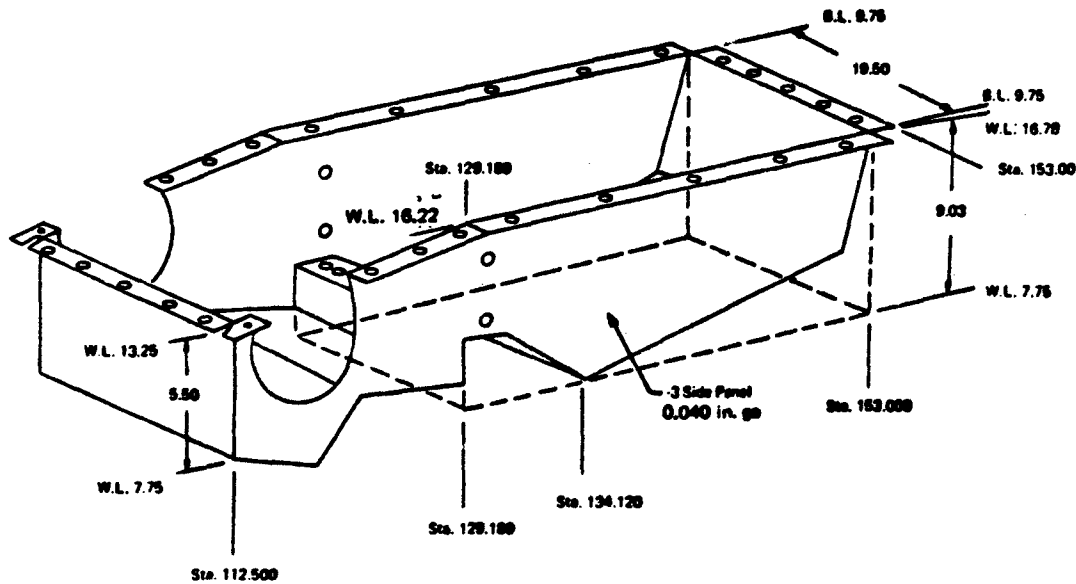
For Purposes of Analyzing the Side Sheet on Above Structure —
Assume the Lower Deck of Engine Enclosure to be at A Constant
Elevation Between Stations 129.189 in. and 153.000 in.

ANALYSIS OF SIDE PANEL -3
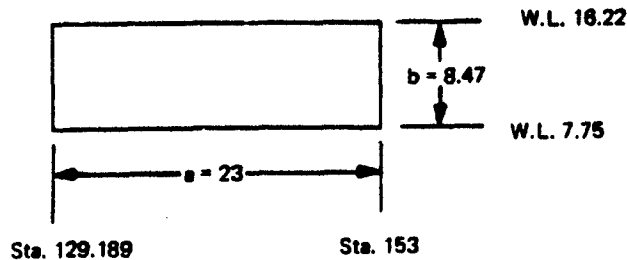
$$\frac{b}{a} = \frac{8.47}{23} = 0.368$$

$K_S = 6$ (Ref (8) Fig. 110.02.1.1-1)

$$\tau_{cr} = \frac{K_S \pi^2 \eta E}{12(1-u^2)}\left(\frac{t}{b}\right)^2 = \frac{6\pi^2 (9.9 \times 10^6)}{12(1-0.3^2)}\left(\frac{0.040}{8.47}\right)^2 = 1181 \text{ psi}$$

$$f_s = \frac{q}{t} = \frac{34.59}{0.040} = 865 \text{ psi}$$

M.S. = + Large

92

7.   Bifurcated Exhaust Duct and Transition Section

The bifurcated exhaust duct section of this engine exhaust system installation is an already proven and flight tested design previously used with the WR-19 engine on the Bell jet flying belt. Material used is A286 heat resistant steel alloy. The transition duct section, made of the same material, is required for expansion of diameters from the bifurcated exhaust end to the spanwise wing duct inlet end.

The aft end of the bifurcated ducting is rigidly attached to the jet engine. Expansion joints between the bifurcated section and the adjacent outboard transition sections permit growth due to temperature. The flexible joints are fiber glass sleeves impregnated with silicone.

Being that the pressure and temperature environment for the proposed Schweizer sail plane installation is the same as the jet belt the structural integrity is considered to be adquate. However, the outboard section transitions the duct from the round cross-section in the bifurcated region to the flat upper and lower cross sections of the spanwise duct. Being flat and also the widest, stresses due to pressure are investigated herein.

The transition exhaust duct section located between the round bifurcated duct section outlet and the spanwise wing duct section has been analyzed using the General Purpose MAGIC III Program which utilizes the finite element concept. Sketches follow to indicate the node point and element numbering system (Figure 29a) used in analysis programing.

Results from MAGIC III provide element deformations and stresses. Maximum deformation and stresses and minimum margins of safety are summarized and tabulated in Table 9a.
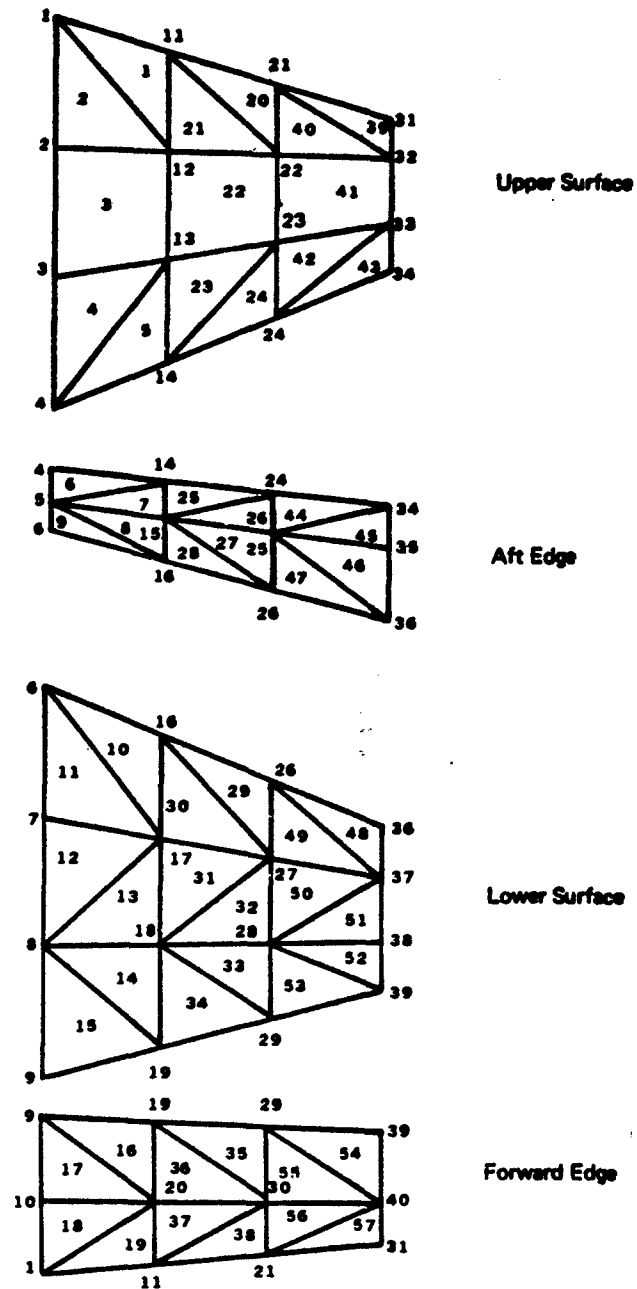
Figure 29a. Node Points and Elements Used in MAGIC III Program - Transition Duct Between
Bifurcated Duct and Spanwise Wing Duct - Pressure Analysis

94

TABLE 9a. SUMMARY OF EXHAUST DUCT TRANSITION SECTION DEFLECTIONS' STRESSES AND MARGINS OF SAFETY

Ultimate design pressure - 10 psi
Computer output values

Element No.	Node Points	Limit Deflection (in.)	Ultimate Stress (psi) (1)	Margin of Safety (2)
3	3, 13, 12, 2	0.072	65220	+1.17
22	13, 29, 22, 12	0.152	115321	+0.23
41	29, 33, 32, 22	0.085	70150	+1.02
31	17, 18, 27	0.063	60322	+High
27	15, 26, 25	0.092	58732	+High
36	19, 20, 30	0.043	42300	+High

Notes:

(1) Ultimate stress is the sum of membrane plus bending stresses.

(2) Margin of safety is calculated using a material allowable for A-286 steel of 140,000 psi as equal to (140,000/ultimate stress -1).

E. WEIGHTS ANALYSIS

Weight and balance analyses have been conducted during the design phase of the Jet Noise Reduction program as applied to the Schweizer glider, Model SGS 2-32. These analyses supported the design activities by assuring that the glider, when modified, will exhibit safe weight and balance characteristics during the flight test phase of the program. Due to the acoustic aspects of the flight tests, the aircraft will only be flown on relatively calm days in controlled maneuvers made possible since it is a powered aircraft. Thus, maneuver loads will be less than those encountered as a glider and design load factors may be reduced in order to permit test operations at gross weights higher than in the FAA Type Certificate, No. G1EA.

Center of gravity limits for the glider are taken as Fuselage Sta. 101.08 to 105.18 at the gross weight of 1768 pounds shown in Table 10. These limits are the same as those given for the glider in the Type Certificate for the maximum weight condition. In the configuration represented by the estimates in Table 10, an additional 44.0 pounds of nose ballast (24 pounds is in the delivered weight) and a 50 pound battery located at Fuselage Station 20 are installed in order to present an acceptable c.g. location.

The weight data in Table 10 are based on either Schweizer Aircraft Corporation or Bell Aerospace drawings or estimates as noted. Actual weight data for Model SGS 2-32, Serial No. 37 was obtained from Reference 13. These data are intended to represent the estimated weight and balance in a flight test configuration. Prior to actual flight testing additional definition of the estimated weights will have been made from drawing analyses and an actual weight and balance measurement will be determined. Assurance that the aircraft will be safely configured will be provided by these means. Since the data in Table 10 is of a summary nature, a detailed breakdown of the Bell drawing weights is presented in Table 11 for additional information.

TABLE 10. MODIFIED SCHWEIZER GLIDER WEIGHT AND BALANCE

Item	Data Source	Weight lb	Arm Fuse Sta.	Moment in. lb
Model SGS 2-32, No. 37,	Form I 4356, 11 July 1966			
Weight Empty	Schweizer Aircraft Corp.	915.0	113.08	103,468
Less:				
Variometer	Schweizer Aircraft Corp.	-1.5	37.0	-56
Oxygen System	Schweizer Aircraft Corp.	-17.0	19.9	-338
Delivered Weight Empty		884.0	116.11	102,637
Test Configuration Modifications:				
Deletions:				
Wing Elements	Estimated	-47.5	120.0	-5,700
Aft Seat	Schweizer Air. Corp.	-6.5	102.0	-663
Upper Fuse. Skin	Schweizer Air. Corp. Dwg.	-1.2	141.0	-169
Wishbone Struct.	Schweizer Air. Corp. Dwg.	-1.5	116.0	-174
Additions:				
Exhaust Duct - Transition	Bell Dwg. 7389-430064	6.0	116.4	698
Duct Install - Wing	-430062	213.0	116.3	24,760
Propulsion Install &	-430070	195.5	131.1	25,629
Fuselage Mods				
Engine Controls and	-430068	85.0	44.0	3,735
Instruments				
Fuel Tank	Estimated	12.4	91.0	1,128
Fuel Tank Supports	Estimated	10.0	91.0	910
Wing Rib Strengthening	Estimated	17.3	120.0	2,076
New Trailing Edge Flap	Estimated	23.0	120.0	2,760
Flap Controls	Estimated	3.0	115.0	445
Inlet Fairing	Estimated	24.0	147.0	3,528
Ballast-Nose	To give takeoff c.g. at Sta. 104	44.0	15.0	660
Test Configuration Weight Empty		1473.0	110.45	162,697
Plus Pilot with Chute	Estimated (170 + 25)	195.0	61.9	12,071
Gross Weight less Fuel		1668.0	104.78	174,697
Plus Fuel		100.0	91.0	9,100
Gross Weight		1768.0	104.0	183,868

TABLE 11. DETAILED WEIGHT BREAKDOWN - JET NOISE REDUCTION MODIFICATIONS

Bell Drawing	Item	Weight, lb	
7389-430054	Transition Duct	1.76	
	Exhaust Duct Assy (GFP)	2.69	
	Clamp	1.56	
	Total		6.01
7389-430062	Inboard Duct Assy	31.16	
	Center Duct Assy	30.14	
	Outboard Duct Assy	25.92	
	Inboard Struts and Plate	36.00	
	Center Struts and Plate	33.82	
	Outboard Struts and Plate	31.20	
	Joints, Seals, Attachments	24.76	
	Total		213.00
7389-430070	Fuselage Modifications	6.69	
	Engine Enclosure	88.82	
	Engine (Williams WR-19)	67.00	
	Engine Ducting, Clamps, Supts	32.50	
	Attachments	0.45	
	Total		195.46
7389-430088	Exciter and Start Tubing	10.50	
	Fuel Line Tubing	3.00	
	24-Volt NI-CAD Battery	50.00	
	Battery Supports	4.00	
	Throttle System	4.00	
	New Instruments	6.00	
	Wiring	7.50	
	Total		85.00

97

F. DYNAMIC STRUCTURAL ANALYSIS

The cantilever vibration modes of the struts were calculated for the base rigidly fixed; they are 138, 882, 2429, 4764, 7875 Hz. However, the strut mounting plate is only 0.032 inches thick and the fundamental 'cantilever' mode of the (rigid) strut on the rotational stiffness of the mounting plate, along the root-chord line, was estimated to be 50 Hz. Since this bending frequency is quite low, and the first torsional mode of the strut is estimated to be much longer than the bending mode, the strut was checked for susceptability to bending-only flutter. Reference 14 indicates that this bending-only flutter is impossible for zero-sweepback. Even though the struts are 'swept' 11.5° with respect to the vertical, they have no sweepback relative to the local airflow and thus should be stable.

The strut cantilever modes will be suppressed considerably by the silicone rubber air-seal around each strut at the wing upper skin.

The tubular type construction of the ducts should preclude any adverse beam-bending vibration. The spanwise natural frequency of the duct segments on the wing structure or the ground test rig supports have not been calculated since these installations have not been finalized. However, the organ-pipe frequencies of the duct (all 3 sections) with 800°R gas inside were calculated to be 27.7, 83.1, 138.5, 193.9, 249.3 Hz, etc. for the odd half-wave harmonics. These frequencies should be avoided in the duct installation.

The nominal engine speeds of 30 krmp and 54 krpm for the low pressure and high pressure sections, respectively, correspond to frequencies of 500 and 900 Hz respectively; these frequencies should not be transmitted beyond the engine itself due to the small unbalance forces involved (small rotors and good balance) and the fact that the engine mounts will isolate very well at these high frequencies.

The fuel line, throttle linkage, and other controls or sensors connected to the engine should be supported in soft rubber bushings and grommets to prevent transmission of engine vibration to the fuselage structure.

The sheet-metal engine enclosure and intake airscoop are extensively treated with acoustical linings which will also suppress mechanical vibration of these panels.

G. ACOUSTIC ANALYSIS

1. Wing Ducts

The wing ducts are acoustically treated to minimize the radiation of upstream noise through the microjet nozzles and to reduce the buildup of acoustic modes. Upstream noise consists mainly of fan-discharge and compressor noise, engine combustion noise and duct-flow noise.

The acoustic treatment and wing-duct sections are shown in BAC Drawing No. 7389-430055, 056 and 057. Both the chordwise and spanwise sections are free of parallel surfaces to reduce susceptibility to acoustic normal mode buildup. Approximately 60% of the wing duct chordwise perimeter is acoustically treated with a porous sintered-metal facing sheet (35 Rayl Rigimesh) offset 0.75 inches from the duct wall. This type of treatment is most effective in the 800-8000 Hz range, and is particularly suited to suppressing the fan-discharge and compressor noise.

98

The limited wing-duct cross-sectional area and duct-flow velocities (up to about Mach 0.15) preclude the application of treatment significantly effective at frequencies below 800 Hz. A low-frequency resonant absorber would require an unacceptably deep core and/or extremely thick facing sheet (Reference 15,)and a viscous absorber would not be suitable at the anticipated duct-flow velocities.

Parameters affecting the duct attenuation as a function of frequency are duct height and length, number of walls treated, composition and flow resistance of the porous facing sheet, core depth (offset of facing sheet from duct wall) and duct-flow Mach number. Extensive investigation of the effects of these parameters is reported in Reference 16. The attenuation of the QRTV wing ducts was predicted by empirically modifying the attenuation of the closest corresponding case in Reference 16. This data is for a 6 x 10 in. rectangular cross-section duct, 22 in. length, lined on the two 10-in. duct walls with a 30-rayl polyimide fiberglass facing sheet, 0.75-in. core depth, at a Mach 0.15 duct-flow velocity. Corrections were made to conform to the QRTV parameters - 10 x 3 x 10 x 1 in. trapexoidal duct cross-section, treated on all but one 10-in. side with a sintered metal facing sheet instead of polyimide, and a 350°F duct temperature.

The resulting predicted sound attenuation in a 22-in. length of wing duct is shown in Figure 30. The treatment is most effective in the 2-3 kHz range, with attenuation exceeding 20 dB. Significant attenuation is maintained at higher frequencies, being about 5 dB at 10 kHz. At frequencies below the peak frequency the attenuation drops off rapidly and is negligible below 800 Hz.

The effect of duct length on attenuation was studied in Reference 16. Attenuation in dB at the peak frequency is nearly a linear function of duct length; if the peak attenuation for a 22-in. duct is 21 dB, then a 44-in. duct would have about 40 dB attenuation at the peak frequency. Attenuation increases less rapidly with duct length at other frequencies; for example, the one-octave bandwidth attenuation (centered at the peak frequency) increases about 3-4 dB for each additional 10 in. of duct.

Internal wing-duct noise is radiated through the microjet nozzles continuously along the wing span. It is thus evident that one cannot simply define the effectiveness of the wing-duct acoustic treatment as the attenuation of the full-length duct because the noise at each strut is based on a different duct length. Further testing and analysis must therefore be performed to determine:

1. Radiation characteristics of internal duct noise propagating through the microjet nozzles, including effects of flow.

2. Effect of strut-base openings on the wing-duct attenuation.

3. Local flow-noise generation at the base of each strut.

2. Inlet, Engine Enclosure, and Exhaust Duct

It is necessary to reduce the engine and fan noise such that these sources will not contribute to aural detectability of the aircraft. The inlet duct must be lined to reduce upstream propagation of fan noise, and the engine and bifurcated exhaust duct must be enclosed by a sound barrier to attenuate case-radiated jet noise and combustion noise.

This analysis is presented in two parts, discussing first the lining of the inlet duct and then the sound-barrier engine/exhaust duct enclosure.

99
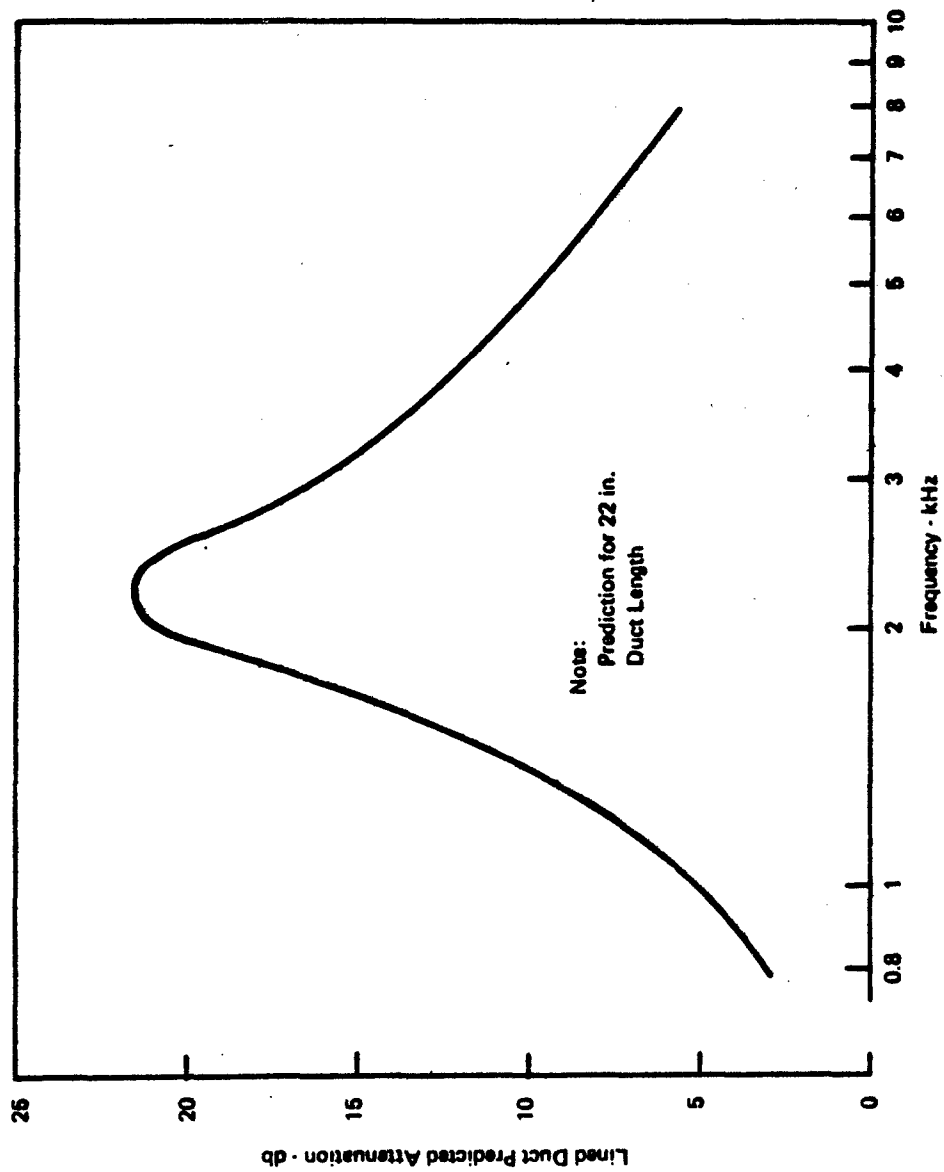
Figure 30. Predicted Attenuation of Wing Ducting

100

a. Inlet Duct Lining

At cruise power, the fundamental blade-passage frequency of the WR-19 fan is approximately 9 kHz. Interaction with the stator and the compressor blades will generate subharmonics in the 1-5 kHz range. Although lower in amplitude than the 9 kHz fan-blade tone, the subharmonics will likely be the greater problem because sound at 1-5 kHz is less favorably attenuated by the atmosphere.

The predicted inlet-duct attenuation is computed from duct-lining attenuation data and parameter-variation studies given in Reference 16. The acoustically-lined inlet duct, detailed in BAC drawing 7389-430085 and illustrated in Figure 31, consists basically of four 'sections', each with different acoustic properties. Starting from the WR-19 engine inlet and proceeding in the upstream direction, these sections are:

		Length (in.)	Cross-Section (in.)
1.	Lined Plenum at Engine Inlet	15	8.5 x 18
2.	Lined 90-degree Bend	10	6.5 x 18
3.	Lined Splitter Section	6.5	3 x 18 (each, 2 Sections)
4.	Lined Air-Intake Section	8	8.5 x 18

(All dimensions are approximate)

An accurate sound attenuation prediction for this four-section inlet is difficult to achieve because the length of each section is in each instance less than the largest cross-sectional dimension. To be most effective, a lined duct should be several diameters long; the duct sections tested in Reference 16 were generally 2.2 times their width.

As a result, the predicted attenuations of the individual sections were not summed directly for the complete duct. The procedure used was, first, to predict the attenuation of each duct section over the 800 kHz - 8 kHz range using Reference 16 by extrapolating attenuation data for a 22 inch long duct, 6 inch by 10 inch rectangular cross-section, acoustically treated only on the 10 inch sides. Then, at each frequency, the total attenuation of the four sections was computed by adding the attenuation of the best section to one-half the sum of the attenuations of the remaining three sections. The results are as follows (attenuation in db):

Section	Frequency in kHz							
	0.8	1	1.5	2	2.5	3	4	8
Plenum	3db	3	6	12	11	9	5	2
90° Bend	2	4	8	14	19	23	20	17
Splitter	2	3	5	9	13	18	16	5
Intake	1	2	3	8	10	8	5	1
'Sum' for Complete Inlet Duct	5db	8	15	29	36	41	33	21

101
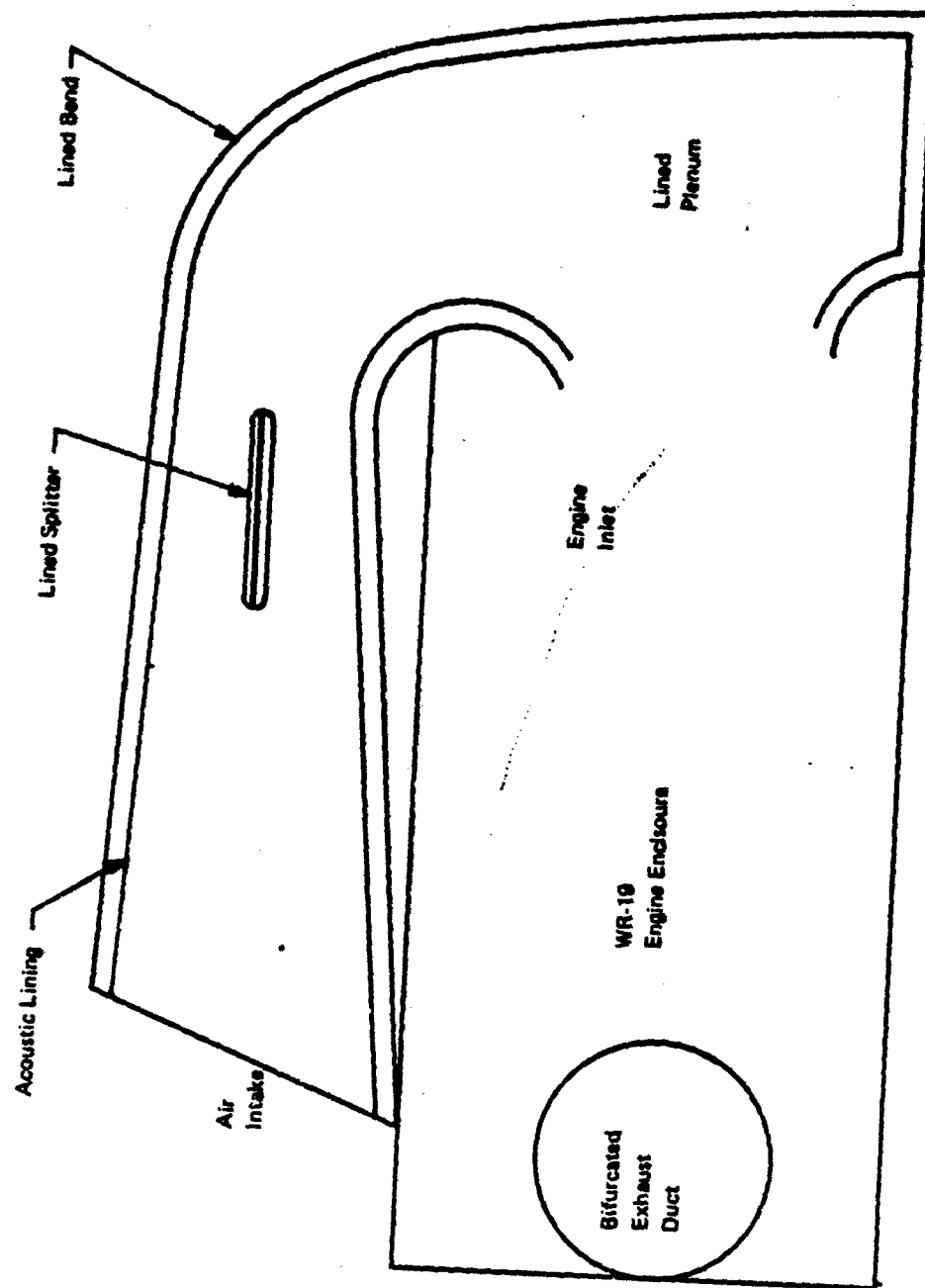
Figure 31. Schematic of Engine Inlet Duct Acoustic Treatment

Lined Bend

Lined Splitter

Acoustic Lining

Air Intake

Engine Inlet

Lined Plenum

WR-19 Engine Enclosure

Bifurcated Exhaust Duct

Of the four duct sections, the 90-degree bend is the most effective, followed closely by the splitter section. The intake section is least effective, because of its short length and relatively greater height.

The predicted attenuation for the complete inlet duct is plotted in Figure 32. Greater than 10 db attenuation is predicted above 1.1 kHz, and above about 1.5 kHz the attenuation exceeds 20 db. Peak attenuation of 41 db occurs at 3 kHz.

A firm conclusion regarding the effectiveness of the inlet acoustic treatment cannot be made without measured or reliably predicted inlet noise levels for the bare WR-19 engine, presently unavailable. If the static propulsion tests of the QRTV indicate a requirement for additional attenuation, this could likely be achieved by some increase in duct length and greater utilization of lined splitters.

b. Engine and Exhaust Enclosures

The engine and bifurcated exhaust ducts (BAC drawing 7389-430085) are enclosed with a sound-barrier sandwich consisting of two quarter-inch thick fiberglass mats (Exactomat) separated by a thin lead sheet septum. A plastic spray coating is applied to the outer face of the sandwich to protect the fibreglass from erosion. The sound barrier is applied generally on the external surface of the enclosures, except on the sides and top of the engine enclosure where it is affixed to the inside surface to provide internal sound absorption to the engine box in order to minimize reverberant noise buildup.

The sound transmission loss of the enclosure with noise barrier is predicted from a method described in Reference 17 that considers both mass-law and coincidence effects, and is plotted in Figure 33. The 0.040-in. aluminum skin is itself quite effective, exceeding 20 db transmission loss (T.L.) above 0.8 kHz. With the sound barrier attached, the T.L. is at least 7 db greater at all frequencies.

Sound radiated downward and laterally from the engine must pass through both the sound-barrier-on-aluminum-skin engine enclosure and the outer skin of the fuselage. Together the system provides more than 35 db T.L. at 500 Hz, and over 60 db T.L. at 2 kHz. Upward-radiated sound transmitted through the inlet duct wall is attenuated by sound-barrier duct wrapping.

3. Radiated Noise of the QRTV

The predicted flyover noise of the QRTV for 1500 ft altitude at 50 knots flight speed is shown in Figure 34. Two dominant noise sources are present, the glider aerodynamic noise and the jet noise from the strut array.

The glider noise spectrum is extrapolated from flyover noise measured in Phase I, Task 6 (Ref. 28) at 125 ft altitude and 94 ft/sec flight speed. Predicted jet noise is taken directly from Reference 18, page 133 and is based on noise measurements from a 45-strut array blown with compressed air. The maximum 1/3-octave band SPL is 24.5 db, in the 315 Hz band, which is essentially identical with the results shown in Figure 77 of Reference 18. Therefore, the inclusion of the results of Reference 28 (Glider Flight Test) has not changed the predicted detectability of the QRTV-72.

103
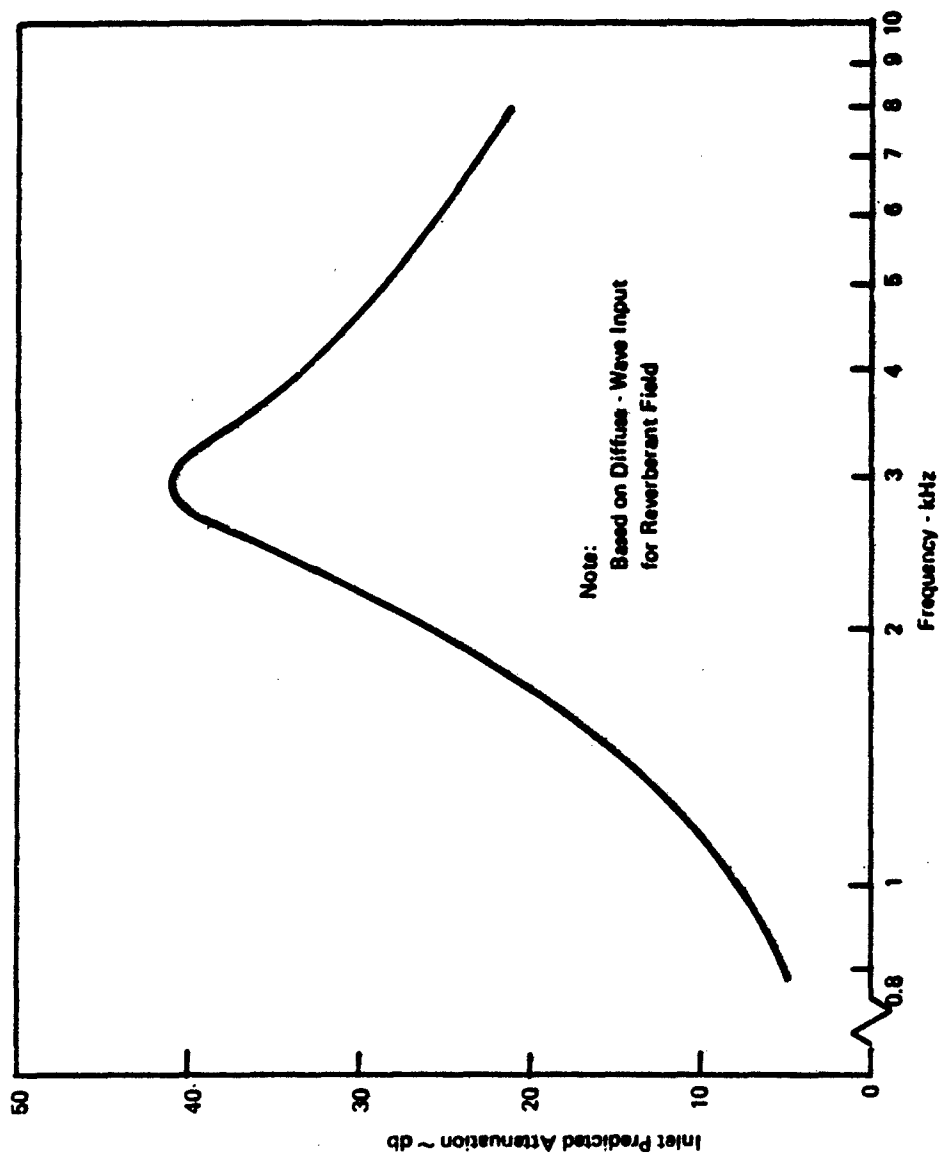
Figure 32. Predicted Noise Attenuation of Acoustically Treated Engine Inlet Duct
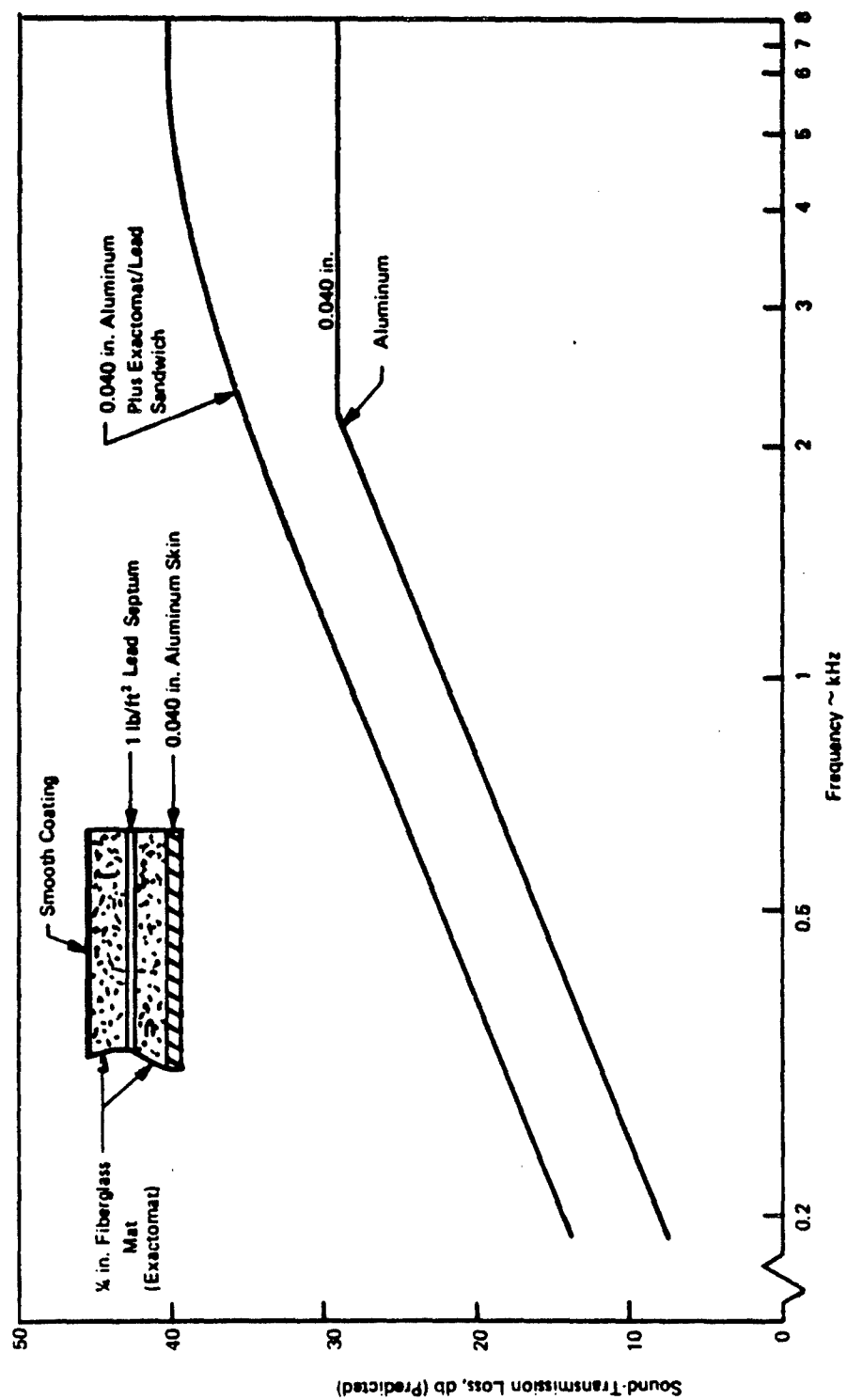
Figure 33. Predicted Sound-Transmission Loss of Sound-Barrier Treatment

105
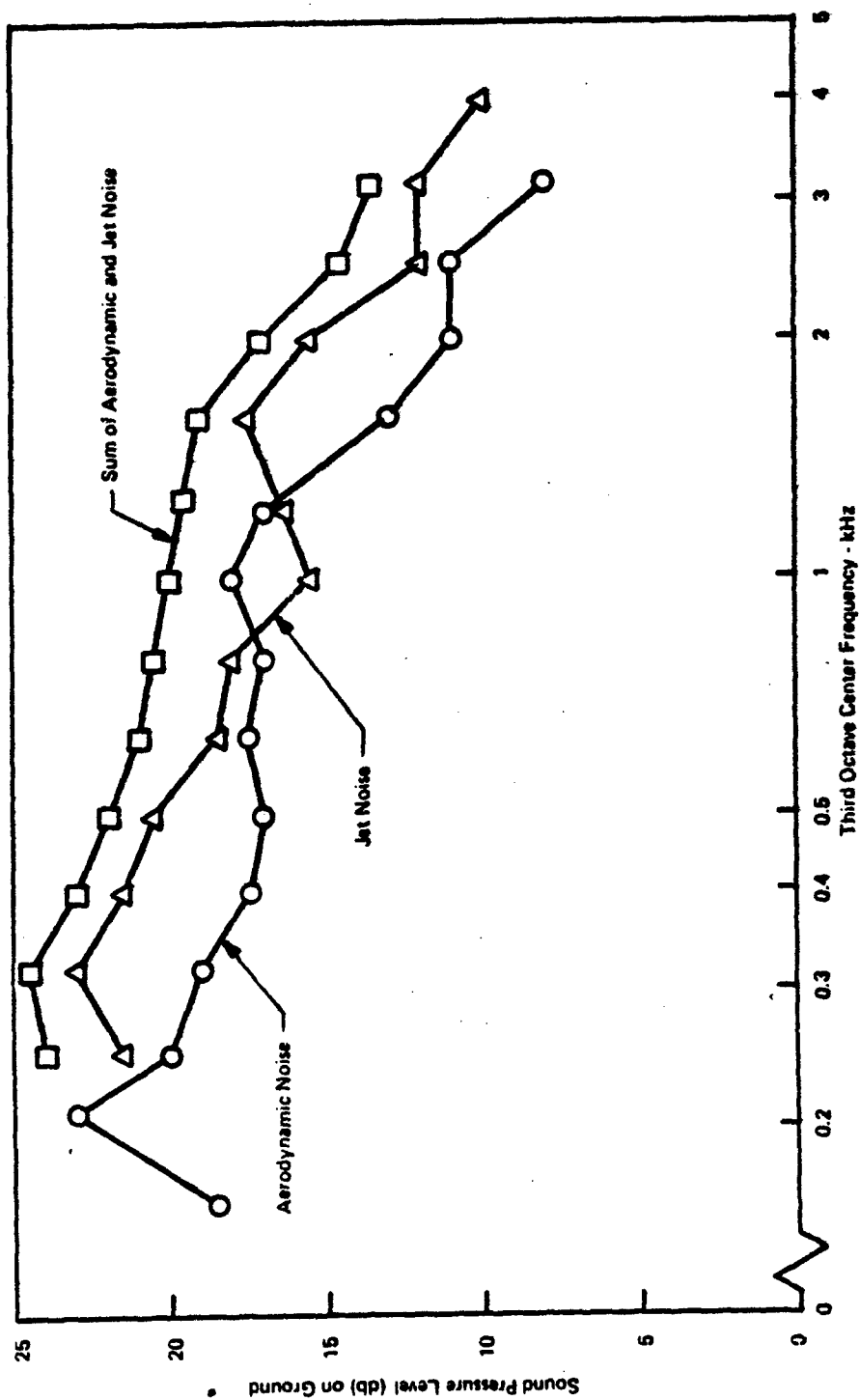
Figure 34. Predicted Jet and Aerodynamic Noise of QRTV at 50 Knots 1500-Foot Flyover

106

It is anticipated that the engine and inlet noise will be suppressed by proper acoustic treatment, and thus will be inaudible relative to the jet and aerodynamic noise.

An approximate test to demonstrate the adequacy of these acoustic treatments would be to duct the exhaust gas from the wing-feed ducts to acoustic "dump", and measure the remaining engine noise of the aircraft at a horizontal range of 15 feet with the engine operating at "ground idle". If the 1/3-octave measurements do not exceed the "sum" levels shown in Figure 34 by more than 35 db, the suppression is almost certainly adequate. If levels more than 45 db above the "sum" curve are observed at 15 feet (horizontal), more suppression will definitely be required. If levels between 35 and 45 db over the "sum" curve are encountered, either more careful measurements (accounting for ground reflection and directivity) will be required, or more attenuation should be applied to eliminate these noises as possible sources of problems.

III. FABRICATION OF TOOLS AND PROPULSIVE STRUTS

Of the nine tasks negotiated to be accomplished during this Phase II of the Jet Noise Reduction Program, only one pertained to the fabrication of the flightworthy hardware components for use on the ground static propulsion test stand. This task involved the development of techniques and the tools required to fabricate a sufficient number of propulsive struts to equip one Quiet Research Test Vehicle.

Results of preliminary propulsion analysis indicated that a total of 434 struts (217 per wing panel) would provide a sufficient excess in total propulsion nozzle area to assure satisfactory operation of the WR-19 engine during ground tests. Hence, the installation of this number of struts was provided for during the design of the spanwise wing ducts. With an allowance of 36 struts for attrition during system fabrication and of 10 struts for engineering testing, a total of 482 struts were planned for fabrication.

A.   FABRICATION OF TOOLS

Phase I of this program was concerned with the development of a multiple microjet nozzle configuration and arrangement and a series of bench and wind tunnel tests to verify the characteristics of the selected propulsive strut design. Fabrication techniques employed to fabricate these development struts were effective and produced very satisfactory struts with consistent propulsive characteristics. However, as Phase II began, it became evident that these techniques would prove too costly for a production type process. A Bell Aerospace Company-funded manufacturing development program resulted in a strut fabrication technique which promised to be much more economical. The primary innovation in this technique pertained to the manner in which the strut trailing edge and microjet nozzles were formed. The previous method consisted of forming a trailing edge piece, drilling the nozzles by the EDM process, and fitting this piece to an airfoil shaped strut with an open trailing edge. The present method utilizes a punch and coin tool and die which punches the nozzles and coins the strut trailing edge in a flat sheet blank of the complete strut.

1.   Punch and Coin Tool and Die

The punch and coin tool was fabricated from a pre-machined and heat treated piece by the electric discharge machining (EDM) process. To do this, it was first necessary to machine a female electrode from a copper-tungsten alloy to the desired contours of the punch and coin tool. Figure 35(a) shows this electrode in which the row of seventy holes which formed the nozzle punch and internal contours may be seen. Figure 35(b) depicts the electrode mounted in the EDM fixture. In the middle of the photograph the heat treated punch and coin tool may be seen in the partially machined state. Once completed the tool was dressed, polished, and mounted on the die shoe as portrayed in Figure 35(c).

Meanwhile a "Vee" shaped female die was machined to the desired contour of the strut trailing edge and jig-bored to match the nozzle punch pattern of the punch and coin tool. This die is shown in Figure 35(d) mounted on the die shoe matching that on which the punch was mounted. Stripper tools are mounted on either side of the die block to strip the formed and punched part from the tool.

(a) EDM Electrode

(b) Tool in EDM
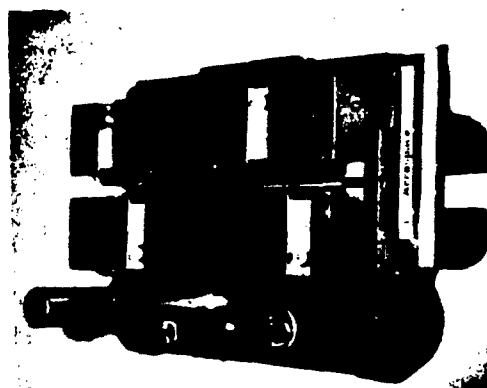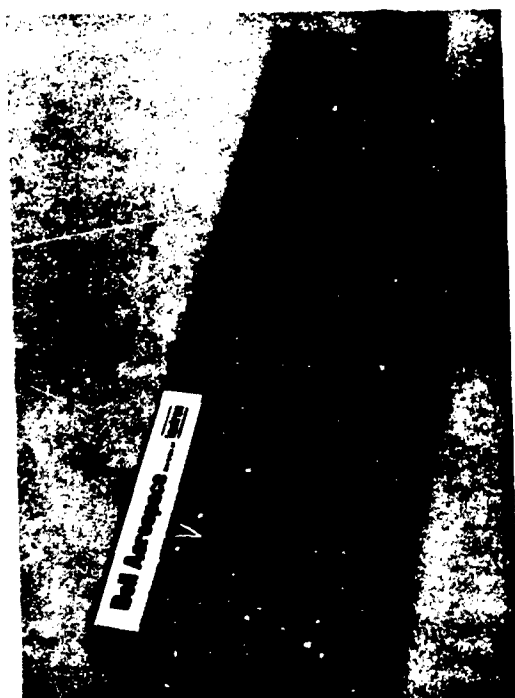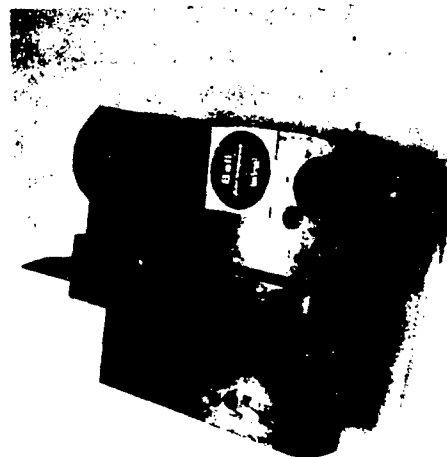
(c) Tool Mounted on Die Shoe

(d) Matching Female "V" Die

Figure 35. Punch and Coin Tool and Die

2. Other Strut Fabrication Tools

Several other tools and manufacturing aids were required to successfully manufacture consistent propulsive struts. Some of these are contained in Figure 36. The strut development template is depicted in Figure 36(a). This is a flat plate development of the airfoil shaped strut and rounded tip which is used to shear strut blanks from flat sheet and form the rounded tip.

During development of the strut fabrication technique, it was found necessary to fold the strut blank into a vee along the trailing edge prior to the punch and coin operation. This folding tool is shown in Figure 36(b).

Once the strut trailing edge and nozzles were formed, the airfoil shape of the strut was obtained by use of the forming mandrel in Figure 36(c). An additional tool (see Figure 39a) was employed to finalize the leading edge shape and reduce the closure for TIG welding. After the welding operation, the strut was placed in the fixture portrayed in Figure 36(d) to drill the holes for riveting the airfoil shaped tension posts in place inside the strut. Locating and holding the posts during the riveting process utilized another special manufacturing aid (see Figure 41c).

The flare at the base of the strut was formed by hand using a custom made flaring tool.

B. FABRICATION OF THE PROPULSIVE STRUTS

The fabrication of the propulsive struts consists of fifteen basic manufacturing operations accompanied by several minor tasks. The fifteen operations are:

1. Shear strut blanks and shape tip area
2. Pre-fold trailing edge
3. Anneal part
4. Punch and coin trailing edge and nozzles
5. De-burr exterior nozzle edges
6. Liquid hone internal nozzle contours
7. Visually inspect nozzle contours
8. Form airfoil shape and strut tip
9. TIG weld leading edge and tip
10. Clean up weld seam
11. Perform die penetrant check
12. Drill and countersink for tension posts
13. Insert post and rivet
14. Flare strut base
15. Buff cleanup of completed strut.

A series of figures have been prepared which photographically illustrate the majority of these operations. Figure 37(a) portrays the result of Operation 2 during which the strut flat blanks were folded along the trailing edge. The folding process work-hardened the strut in the trailing edge region

110

(a) Strut Development Template

(b) Strut Blank Folding Tool

(c) Strut Forming Mandrel

(d) Strut Post Drill Fixture

Figure 36. Additional Fabricational Tools

111

(b) Punch and Coin Operation

(a) Pre-folded Strut Blanks

(c) Folded Blank in "Vee" Die

(d) Formed Trailing Edge and Nozzles

Figure 37. Strut Trailing Edge and Nozzle Forming

to the extent that the part had to be annealed prior to punching and coining the trailing edge and nozzles. Figure 37(b) shows the punch press operator inserting the annealed folded blank into the "Vee" die under the strippers. The following Figure 37(c) shows the part in position for the actual punching and coining. The finished part shown in Figure 37(d) has actually undergone the de-burring of Operation 5.

During the punch and coin operation, a certain amount of material was extruded into the clearance between the hole punch and die. This material constituted the exterior burr which had to be removed. In addition, some of this extruded material adhered to the punch and was drawn back into the nozzles as the part was stripped from the punch. This undesirable debris was readily removed by the liquid hone Operation 6 depicted in Figure 38(a). The struts were visually inspected individually for acceptance under magnification in the manner illustrated in Figure 38(b). In order to verify the general shape of the nozzle interior contour, one of these formed trailing edges was sectioned and photographed under approximately 10 power magnification. This is portrayed in Figure 38(c). At this point the accepted parts proceeded to Operation 8 during which the airfoil shape of the strut was formed. This is illustrated in Figure 38(d) which shows the strut body on the forming mandrel lying on a thick pad of relatively hard rubber in an hydraulic press. A similar rubber pad, out of camera view, was attached to the descending part of the press. Operation of the press forced the soft aluminum sheet to form around the mandrel into the desired airfoil shape. A slight spring-back and insufficient forming near the leading edge required some manual forming to reduce the gap as illustrated in Figure 39(a). This operation was followed by the manual forming of the tip portrayed in Figure 39(b). The part was next mounted in the weld fixture and Operation 9 was performed wherein a continuous weld was made along the strut leading edge and tip as shown in Figure 39(c). The part on the left in Figure 39(d) depicts the leading edge seam after welding. The part on the right shows how the leading edge looked after the weld seam cleanup of Operation 10 which is shown in steps in Figures 40 (a) (b) and (c). Following cleanup the weld seams were subjected to a dye penetrant quality inspection check to detect any cracks or other flaws (See Figure 40(d)). In all cases the defects were repairable and were reworked in the weld shop.

With the strut bodies complete and accepted by the Quality Assurance Department, Operations 12 and 13 were accomplished. These consisted of drilling and countersinking holes in the strut and riveting the airfoil shaped tension posts in place. These operations are illustrated in Figures 41(a) (b) (c) and (d). Prior to the rivet operation the hole in the strut and post were first coated with zinc chromate. This was done to prevent leakage of exhaust gases from the strut.

During Operation 14 the base of the struts were flared. This is depicted in Figure 42(a) with the completed flare shown in Figure 42(b). The final Operation 15 comprised a buffing cleanup portrayed in Figure 42(c) which removed slight surface scratches which occurred during fabrication as well as any zinc chromate residue on the strut surface.

113

(a) Liquid Honing Nozzles

(b) Nozzle Visual Examination

(c) Cross-Section of Nozzle Contour

(d) Forming Strut Airfoil Shape

Figure 38. Further Manufacturing Steps

114

(b) Tip Forming

(d) Strut Welded and Dressed Up

(a) Improving Leading Edge Closure

(c) TIG Welding in Fixture

Figure 39. Final Forming and Welding of Strut

115

(a) Rough Clean-Up

(b) Fine Clean-Up of Leading Edge

(c) Fine Clean-Up of Tip

(d) Application of Die Penetrant
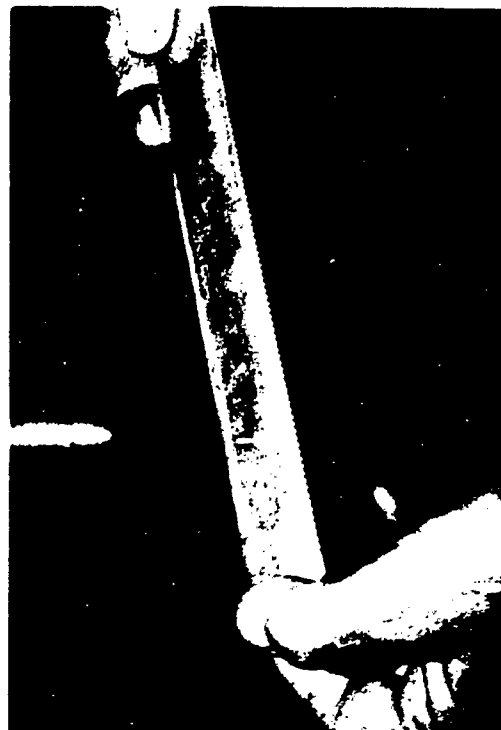
Figure 40. Weld Clean-Up and Die Penetrant

116

(a) Drilling Rivet Holes

(b) Countersinking Rivet Holes

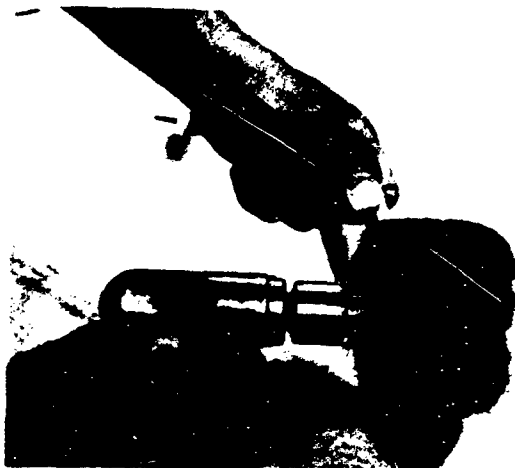(c) Inserting Tension Posts

(d) Installing Rivets

Figure 41. Installation of Tension Posts

117

(a) Flaring Strut Base

(b) Completed Flare
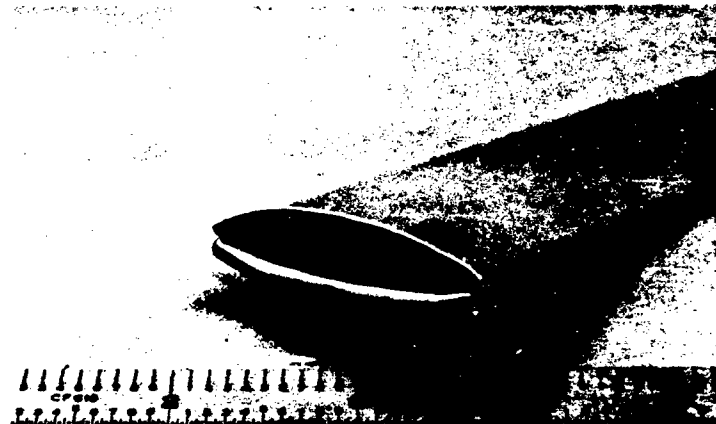
(c) Final Buffing Clean-Up

Figure 42. Completion of the Propulsive Strut

IV. CONCLUSIONS

As a result of the Bench/Wind Tunnel Tests and Flight Tests of Phase I of this contract, certain technical conclusions were made which had a direct bearing on Phase II efforts.

1.   A single row of N circular nozzles in a line, spaced 2 diameters center-to-center, when measured in the broadside direction, show noise levels not significantly different from N individual nozzles, and when measured in the axial direction, a few dB quieter.

2.   Closely-spaced multi-strut arrays generally produce less noise than an equal number of widely-spaced single struts at high frequencies, and more noise at low frequencies. For arrays of 15 struts or more the noise at all frequencies and in the important directions appears to be proportional to the number of struts, within experimental error.

3.   The noise of individual jets increases linearly with frequency (the peak of the jet noise frequency spectrum is well above 20 kHz). The higher frequencies are reduced by the combined effects of (a) reduction of shear in a multi-strut array, (b) shielding of strut-nozzle noise due to reflection and refraction off the surface of the wing, and (c) atmospheric attenuation. This decrease in the high-frequency noise results in critical aural detection bands for a QRTV at 500 Hz or lower, even in the presence of moderate aircraft maneuvers.

4.   A useful QRTV can be produced by modification of a sailplane, using a GFE fanjet engine.

5.   The predicted aural detectability of a Quiet Research Test Vehicle is significantly less than other types of quiet aircraft.

6.   A Quiet Research Test Vehicle could also demonstrate the aerodynamic advantages of improved lift and resulting short takeoff obtained with this concept.

7.   The predicted static jet propulsion noise in the lowest bands exceeds the aerodynamic noise of the sailplane at the best speed for quiet cruise (50 knots). At 70 knots, the two noise components are about equal.

8.   The flight test evaluation of "dummy" propulsive struts installed on the upper surface of a glider wing (Phase I, Task 6) showed that the overall noise and detectability of the aircraft was not adversely affected by the strut installation even though the "dummy" produced a drag increment larger than that of the actual propulsive struts.

During Phase II the concept of a ground static test of the complete flight-weight propulsion system installed in the test aircraft was introduced, reduced to a concrete approach, and incorporated as a redirection to the contract. The analysis and detailed design of the installation of the quiet propulsive system in the Schweizer SGS 2-32 Sailplane was completed and showed that the test aircraft modification can be accomplished in a safe and serviceable manner. The fabrication of the flight-worthy propulsive struts was achieved by employing a punch and coin process which proved to be much more economical and producible that the EDM process originally contemplated.

The purpose of this contract was to resolve technical questions in acoustics, propulsion, structures, and aerodynamics in order to assess the feasibility of adapting the concept of propulsive microjet struts to produce a Quiet Research Test Vehicle. All of the technical questions have been

119

satisfactorily resolved to the degree possible short of a full scale installation and flight test. The major remaining questions are: (1) does the jet engine produce noise (e.g., low-frequency combustion noise) than can be attenuated in a feasible flight-weight engine/ducting installation; and (2) will the flow of turbulent mixed air from the propulsive struts over the upper surface and trailing edge of the wing in flight produce more noise than that measured during the static tests or than that of the wing itself? There appears to be no way of answering these questions in a definitive manner other than the proposed full scale static propulsion tests and flight tests.

In addition to assuring the feasibility of the original concept, the contract has provided sufficient data to indicate directions in which the original concept could be improved. In particular, it has been shown that the proposed strut array produces low-frequency noise which is much greater than that extrapolated from individual nozzles or single strut tests. Also, the drag of the present strut array is sufficient to seriously affect the dash speed capability of the aircraft. It appears likely that it will be possible to accept slightly greater noise from single struts (by employing larger nozzles or more rows of nozzles per strut) in order to reduce both the drag of the strut array and the low-frequency noise of the strut.

The feasibility of this noise reduction concept could be demonstrated by means of a static propulsion system test followed by flight tests of the complete QRTV.

120

V. APPENDICES

APPENDIX A

DETAILED DESIGN OF THE SCHWEIZER SGS 2-32
SAILPLANE WING MODIFICATION FOR INSTALLATION
OF THE SPANWISE DUCT

I. GENERAL

The specific goal of this task was to achieve an expeditious modification of the Schweizer SGS 2-32 wing to incorporate the spanwise duct which will supply engine exhaust gases to the propulsive struts on the upper surface of the wing. In order to achieve this goal, it was necessary to conduct a detailed structural analysis of the modified wing. In addition, certain other pertinent factors were considered to the extent necessary to ensure overall safety in flight of this wing modification. These factors involved (1) The effects of temperature conditions within the wing produced by the hot exhaust gases flowing through the wing duct, (2) The change in wing loads produced by the installation of the trailing edge flap with the propulsive struts blowing, (3) The change in wing flutter characteristics produced by the duct installation, and (4) The possible changes in the operational limit load factor of the aircraft required due to the altered wing structure and associated flight loads.

A. THERMAL ANALYSIS

Under conditions of maximum engine operation, the mixed exhaust gas temperatures from the WR-19 will be approximately $550°F$. Since these gases are distributed to the propulsion struts located on the wing surface by means of a duct within the aluminum wing structure, heating of the wing structure to temperatures in excess of $300°F$ was a possibility, with the associated detrimental effect on the structure. Consequently, a study was conducted which has three primary objectives: (1) predict the design structural temperatures of wing for both idle and maximum power conditions, (2) design a thermal protection system to maintain all structural temperatures to less than $300°F$ and (3) verify the final design.

The basic wing structure consists of 0.025 inch aluminum skin riveted to a 1.0 inch high "zee" section spaced 7.5 inches apart. In the vicinity of the 6AL-4V titanium exhaust duct, the "zee" sections are fabricated from two 0.75 inch x 0.75 inch x 0.032 inch angles riveted together.* Except for a few supports along the duct there is a 0.15 inch gap between the wing ribs and the duct. During idle operation, the exhaust gas flows through the duct at a mach number of 0.1 and a temperature of $350°F$. During maximum power condition, these values increased to 0.2 and $550°F$ respectively.

For purposes of the thermal analysis, only the upper wing structure was analyzed. In the region of the "zee" sections heat flows from the duct to the "zee" sections by the combined modes of radiation and conduction across the 0.15 inch air gap. Convection was not permitted in the gap since the gap width is too narrow to allow natural convection currents to develop. The heat then flows by conduction through the two riveted joints to the aluminum skin. Natural convection from both sides of the "zee" was considered. In the region between the wing ribs, the heat flows from the duct to the aluminum skin by natural convection and radiation. The space between the duct and the wing was conservatively assumed to be sealed from the external air stream hence this

---

*The thickness of the added angle was in most cases increased during the subsequent structural analysis. Increased thickness and conductivity will lower the temperature of the inner flange, making the analysis as presented here slightly conservative.

temperature stabilizes at some value between the duct and outer skin temperature. In the actual system, leakage of external boundary layer into this space will definitely exist and will tend to reduce the predicted structural temperatures. The conditions of the external air stream were specified as 70°F and 30 feet per second. Consequently, forced convection from the outer skin to the air stream was considered as a primary heat transfer mechanism.

On the basis of this thermal arrangement, equilibrium temperatures of the wing structure were predicted using a finite difference steady state computer program for the ground idle mode of operation. Figure A-1 presents these results. The temperatures shown in this figure were then used as the initial temperatures for the maximum power mode of operation. This assumed that because of system checkout and taxiing, the time in the idle mode of operation would be greater than the time required for the temperatures to stabilize. Figure A-2 presents the predicted temperature time histories for some of the more critical locations in the wing structure. The temperature of the lower flange exceeds 300°F after 19 seconds in this condition. Since this time is less than anticipated duration in this condition, this structural arrangement must be modified in order to reduce the structural temperatures.

A comparison of the amount of heat flow to the aluminum skin indicated that a considerable fraction of the total heat flow is a result of convection and radiation to the aluminum skin in the area between the wing ribs. By eliminating this heat flow, the structural temperatures will be below the 300°F allowable. Employment of 1/2 inch of 6 pounds per cubic foot Dynaflex or equivalent insulation will satisfy this condition. With this thermal structural arrangement, even the stabilized temperatures will be less than 300°F. Figures A-3 and A-4 present the equilibrium temperatures for the idle operational mode and maximum power operational mode, respectively.

This brief thermal analysis will probably require review and refinement at some future stage of the wing design. One area which should be further considered is the wing-skin-and-doubler in the area between the struts. Also it may be desirable to re-examine the postulated 70°F ambient air temperature, and the possible necessity of considering full solar radiation on the upper skin, both of which depend on the extent and nature of the intended flight test program.

B.   WING LOADS DUE TO FLAP

Installation of the spanwise wing duct and propulsive struts precluded the use of the existant dive brake on the SGS 2-32 Sailplane. In order to provide a desirable speed control device, provisions were made to incorporate a plain, unbalanced, trailing edge flap extending from the wing-fuselage juncture to just outboard of the span of the propulsive struts (see Figure A-8). This flap will permit low speed flight (reduced noise) with a suitable stall margin. In the deflected position, it may produce a reduction in the trailing edge noise usually present with the struts blowing over the upper surface of the wing.

The aerodynamic loads introduced on the wing by this flap were estimated by calculating the chordwise wing load distribution for an NACA 63_3618 airfoil equipped with a 16 percent chord flap. These distributions are applicable to the QRTV and include the effect of strut blowing as determined by the information in Reference (19) for estimating pertinent lift and angle of attack relationships. The basic airfoil pressure distribution with the added loads due to flap deflection were predicted using the methods contained in Reference (20). The derivatives of hinge moment as functions of angle of attack and deflection were estimated in accordance with the methods of Reference (21).

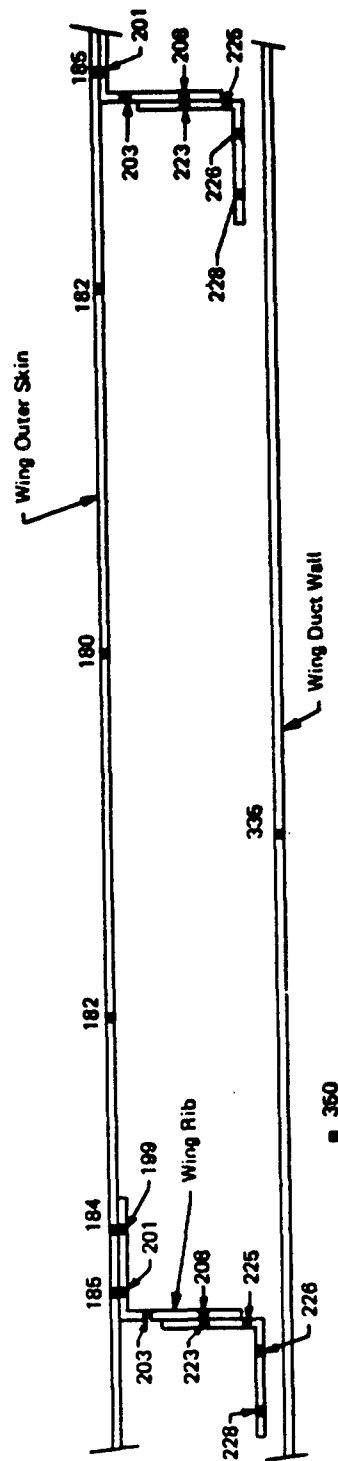Figure A-1. Equilibrium Temperatures for QRTV Wing Structure Without Insulation, Idle Power Operation

123
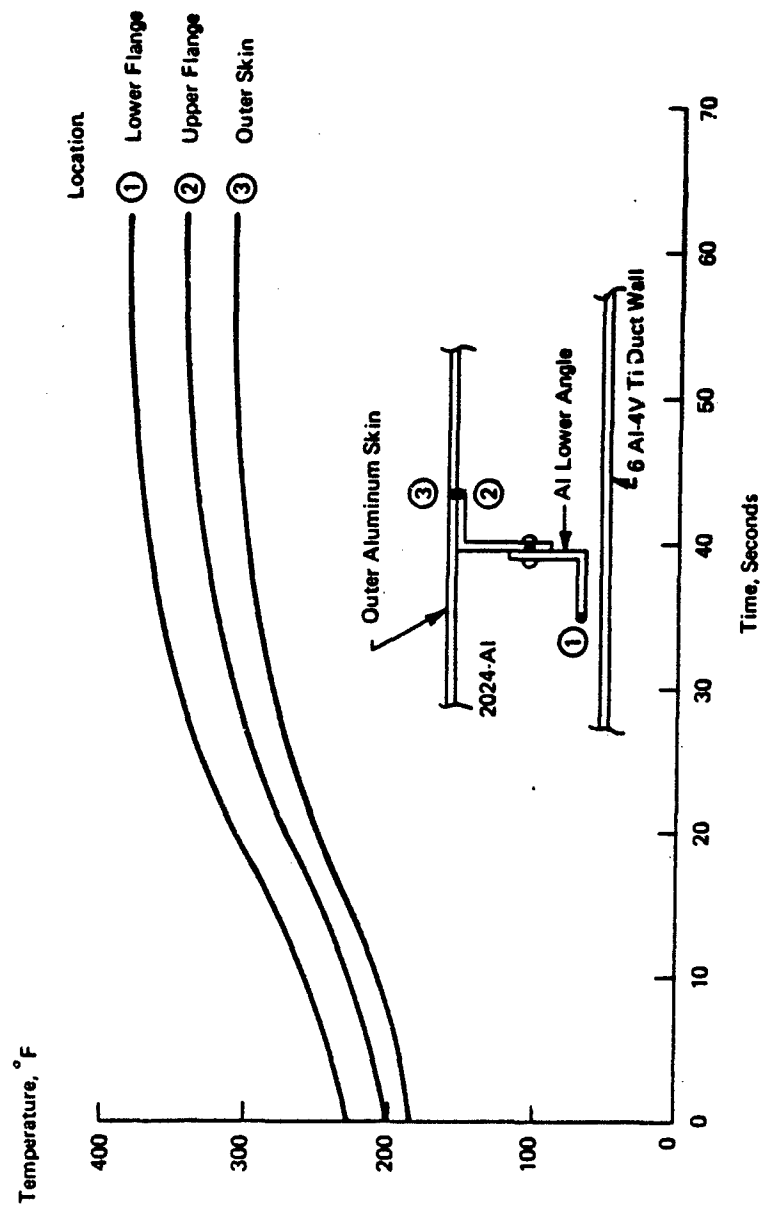
Figure A-2. Temperature History of Critical Locations Within QRTV Wing Structure

124
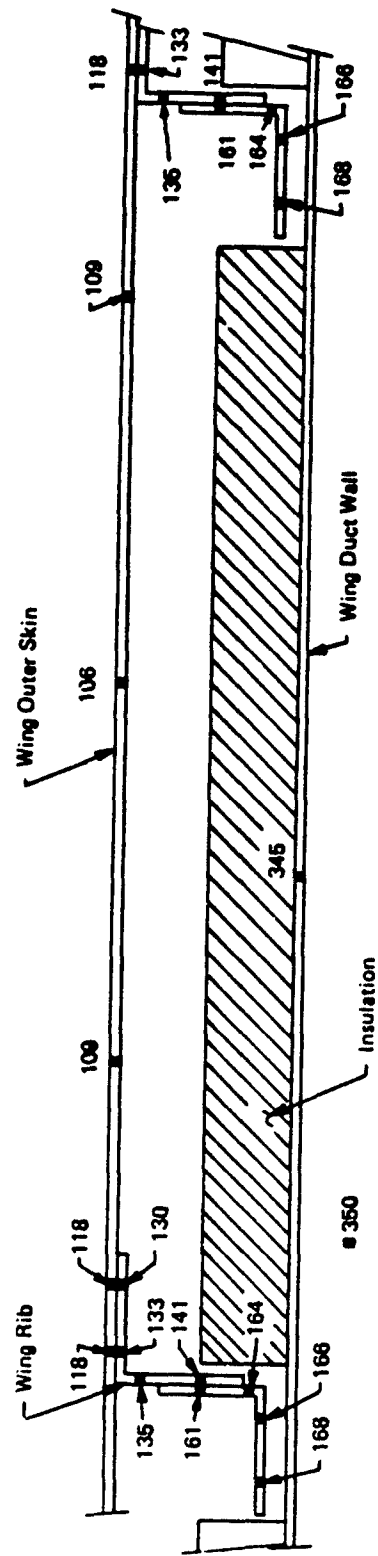
Figure A-3. Equilibrium Temperatures for QRTV Wing Structure with Insulation, Idle Power Operation
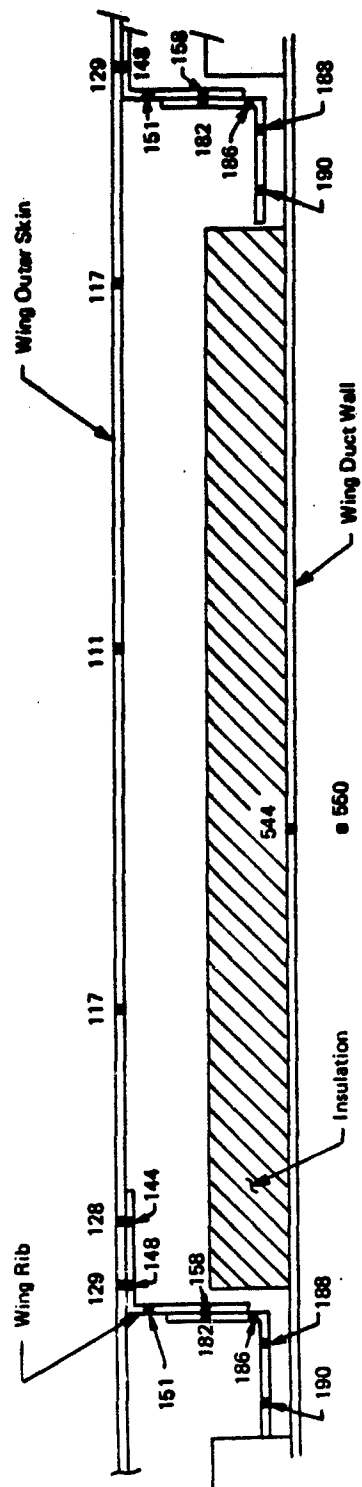
Figure A-4. Equilibrium Temperatures for QRTV Wing Structure with Insulation, Maximum Power Operations

126

Two flight conditions at a 5 g (limit) load factor were investigated. Positive high angle of attack (PHAA) was chosen to be approximately 18° which is near stall for the blown condition. Positive low angle of attack (PLAA) was selected to be that corresponding to a maximum speed of 100 knots.

Shown in Figure A-5 are pressure distributions of the basic unflapped airfoil for three different angles of attack. Figure A-6 presents the total load distribution for the PHAA condition with 30" flap deflection. Figure A-7 gives the load distribution for the PLAA condition with 30° flap deflection.

Table A-I gives the flight conditions for which distributions are calculated and Table A-II the hinge moment variation with flap deflection for a given q, including the flap normal force at 30° deflection as determined from the load distribution.

These aerodynamic loads were employed in the structural analysis to ascertain the structural integrity of the modified wing.

TABLE A-1. GLIDER FLIGHT CONDITIONS

Weight   = 1800 lb
Wing Area   = 180 sq ft
Flap Span (One Side) = 156 inches
Mean Flap Chord = 7.45 inches

Flight Condition	δ_f (deg)	V (kt)	q (lb/sq ft)	α (deg)
PHAA	0	77.1	20.22	18
	30	66.5	15.06	18
PLAA	0	98	32.7	11
	30	100.8	34.5	2

TABLE A-2. FLAP HINGE MOMENT VARIATION WITH FLAP DEFLECTION

Flight Condition	δ_f	V (kt)	C_{h_α}	C_{h_δ}	C_h	HM_f (ft-lb)	C_{N_f}	N_f (lb)
PHAA	0	66.5	-0.00547	-0.0121	-0.0985	-7.43		
	15	66.5	-0.00547	-0.0121	-0.280	-21.1		
	30	66.5	-0.00547	-0.0121	-0.4615	-34.8	1.2	145.9
	45	66.5	-0.00547	-0.0121	-0.643	-48.5		
	60	66.5	-0.00547	-0.0121	-0.8245	-62.2		
PLAA	0	100.8	-0.00547	-0.0086	-0.0109	-1.88		
	15	100.8	-0.00547	-0.0086	-0.1399	-24.2		
	30	100.8	-0.00547	-0.0086	-0.268	-46.3	1.6	445
	45	100.8	-0.00547	-0.0086	-0.3979	-68.7		
	60	100.8	-0.00547	-0.0086	-0.5269	-91.0		
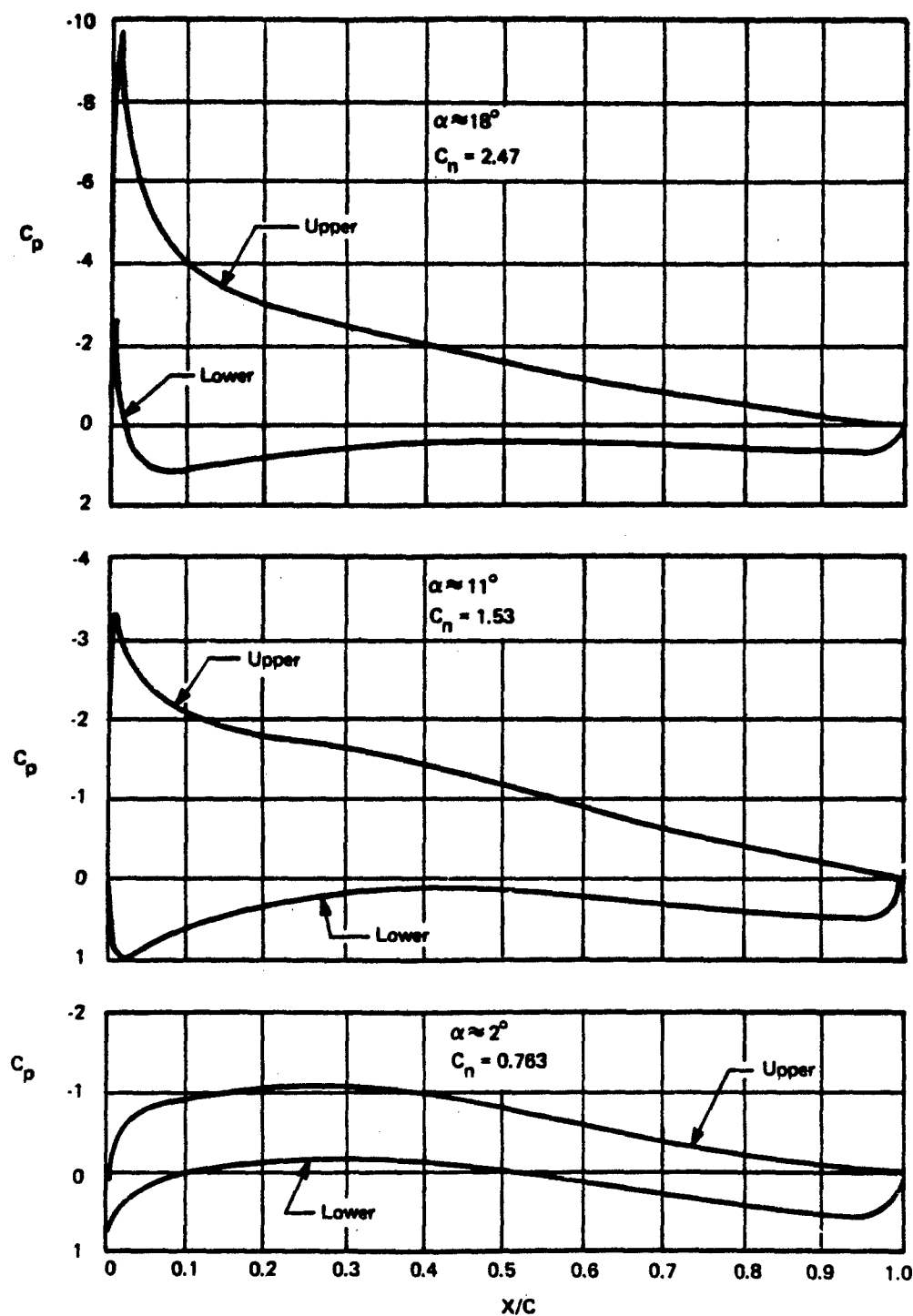
Figure A-5. Pressure Distribution, NACA 63₃618 Airfoil with Blowing Struts, $\delta_f = 0°$

Unflapped Airfoil Section Normal Force $c_n = 2.47$

Flapped Airfoil Section Normal Force $c_n = 3.32$

Flap Section Normal Force $c_{n_f} = \dfrac{n_f}{q\, c_f} = 1.2$

$\alpha \approx 18°$

$c_n = 3.32$
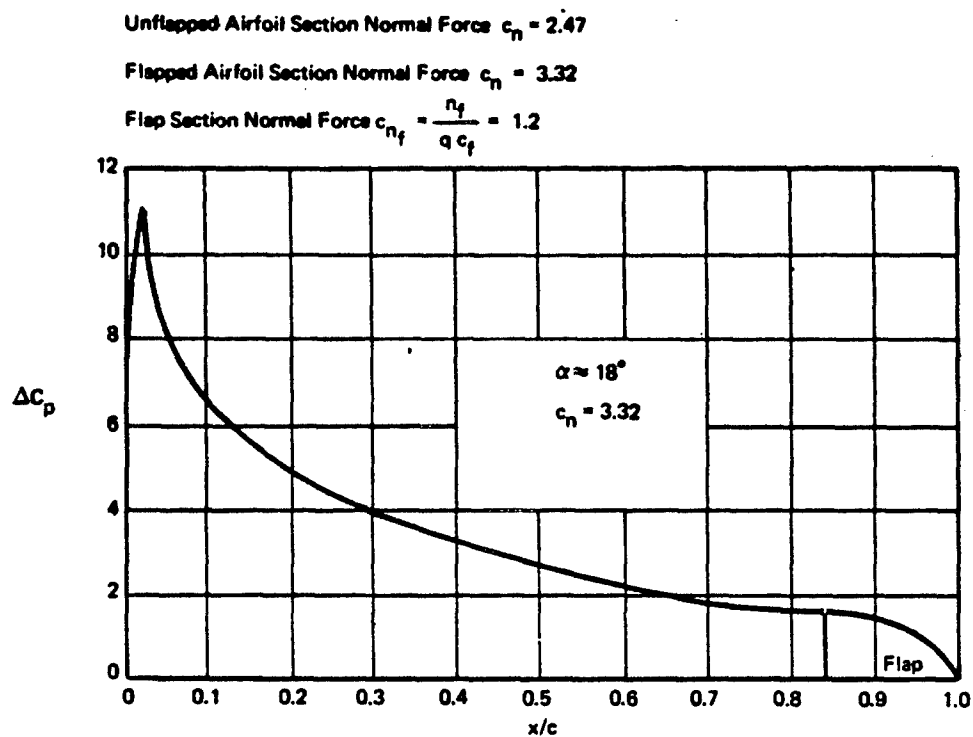
Figure A-6. Load Distribution, NACA 63_3 618 Airfoil with Blowing Struts, $\delta_f = 30°\ \alpha \approx 18°$

Unflapped Airfoil Section Normal Force $c_n = 0.76$

Flapped Airfoil Section Normal Force $c_n = 1.45$

Flap Section Normal Force $c_{n_f} = \dfrac{n_f}{q\, c_f} = 1.6$

$\alpha \approx 2°$

$c_n = 1.45$
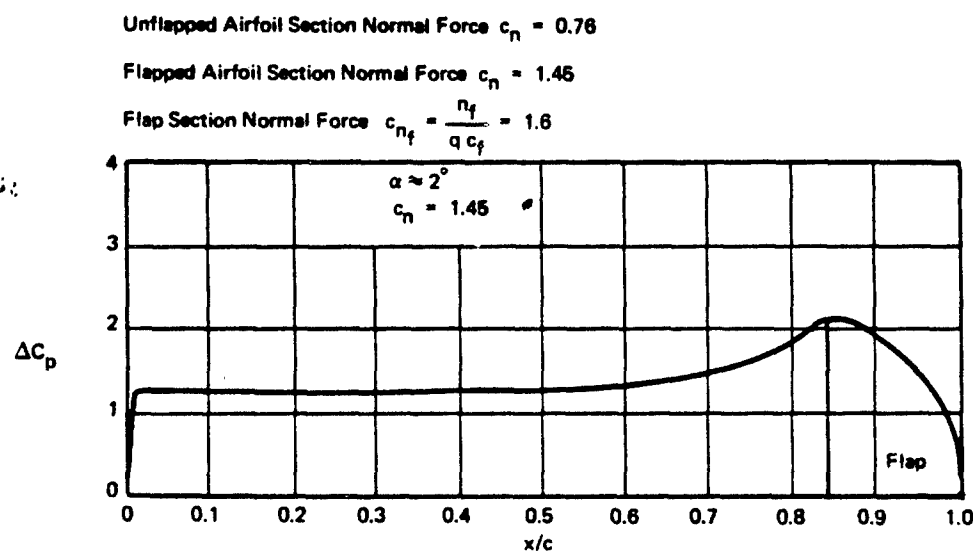
Figure A-7. Load Distribution, NACA 63_3 618 Airfoil with Blowing Struts, $\delta_f = 30°\ \alpha \approx 2°$

129

C. WING FLUTTER CHECK

Because of the rather extensive modifications necessary to install the spanwise duct and trailing edge flap in the wing of the SGS 2-32 Sailplane, a general check of the flutter characteristics of the resulting configuration was considered advisable. The results of this analysis are summarized in this section.

Basic wing data pertinent to the flutter analysis are:

Span   57 ft.

Wing Area   180 sq ft

Root Chord (C_L)   57 in.

Chord at Wing Sta 16   55.2 in.

Mean Geometric Chord   37.9 in.

Tip Chord   19 in.

Aspect Ratio   18.05

From information contained in Reference 22:

Center of gravity-average axis   37 percent chord

Air load reference axis   26.6 percent chord

Torsional reference axis   33.3 percent chord

From information contained in Reference 23 relative to vibration modes:

Wing bending mode frequency (sym.) $\approx$ 37 rad/sec

Wing torsional mode frequency (sym.) $\approx$ 232 rad/sec

The original wing weight was 430 lb. Parts of the wing which must be removed to achieve the installation of the duct and flap were estimated to be 47.5 lb.

Items to be added were estimated to be:

Duct and installation	213 lb	
Rib reinforcement	17.3 lb	
Trailing edge flap	23 lb	
	253.3 lb	
	- 47.5	{Assumed to be 9 in. from
Added increment	205.8 lb	{c.g. of section

130

For the purposes of this check of wing flutter characteristics, it was assumed that there would be no change in the stiffness properties.

The changes in mass and inertia of the wing in the vicinity of spanwise duct were estimated using average existing wing properties as a basis.

Wing weight per foot = 7.55 lb/ft

Wing inertia per foot = 6.28 lb ft^2/ft

Wing section radius of gyration = 0.912 ft

The incremental increase in these quantities in the area of the spanwise duct as a result of the wing modifications and installations were evaluated to be 7.44 lb/ft and 7.44 lb ft^2/ft, respectively. The corresponding new values for the modified wing in the duct area will be:

Modified wing weight per foot = 14.99 lb/ft

Modified wing inertia per foot = 14.72 lb ft^2/ft

Modified wing section radius of gyration = 0.992 ft

The appropriate ratios between the modified wing and the original wing in the duct area will be:

Weight ratio = 1.98

Inertia ratio = 2.37

Accordingly, the wing bending mode frequency will be reduced to 26 rad/sec and the wing torsional frequency to 150 rad/sec.

Flutter velocities for both the original and modified wing were computed using the approximate formula derived in Reference 24 for this wing with the reference section at wing station 214 and a reference chord of 2.7 feet.

$$\frac{V^2}{\omega_t^2} = \frac{d_3 m_r k^2}{\rho_0 I_\alpha} \frac{\left\{ (d_1 k^2 + \bar{X}^2)(1 - 2\frac{\omega_2^2}{\omega_1^2}) + 4\bar{X}^2 \right\}}{\left\{ (d_1 k^2 + 5\bar{X}^2)y + 4d_3 d_s \bar{X} k^2 \right\}}$$

where:

Symbol	Definition	Original Wing	Modified Wing
d_1	Constants dependent on taper ratio and evaluated from	1.4	1.4
d_3	Reference 22.	1.5	1.5
d_5		0.95	0.95
m_r	Mass per foot run (slugs/ft)	0.234	0.466
k	Radius of gyration ÷ reference chord	0.338	0.367
$\overline{X}$	Distance of c.g. aft of torsional axis ÷ reference chord	0.037	0.081
y	Distance of air load forward of torsional axis ÷ reference chord	0.067	0.067
ω_1	Wing torsional frequency (rad/sec)	232	150
ω_2	Wing bending frequency (rad/sec)	37	26
i_α	Nondimensional lift derivative	2.2	2.2
V	Flutter velocity (ft/sec)	1360	1050

Results of this study indicate a 23 percent reduction in flutter speed of the modified wing from the original sailplane wing. They also confirm the high flutter speed (1300 fps) implied in Reference 23 which considered investigations of the wing torsion/bending flutter unnecessary due to the large separation between the wing bending and torsional frequencies. In the case of the modified wing, the modal frequencies have been estimated to reduce such that they will remain well separated.

Summarizing the results of this study together with the restrictions anticipated in the flight envelope, no wing flutter problems for the modified sailplane are invisioned.

A brief consideration of the flap dynamic stability indicated that the flap will have similar mass and stiffness properties to that of the ailerons except for control surface stiffness, which will be higher for the flap. Hence, the modal frequencies of the flap will be higher than the first and second wing symmetric bending modal frequencies. Because the flap actuator is located at the inboard end only, mass balancing may be required to prevent inertial coupling with the wing torsion modes. Also, ground tests may be required to check flap torsional modal frequencies, circuit stiffness and backlash.

132

D. DESIGN LOAD FACTORS

For wing bending and torsion, the design stress levels in wing spars and skin were taken to be the same as for the unmodified aircraft. For these loads, the design load factors for the modified aircraft were taken to be those of the unmodified aircraft divided by the ratio of the gross weights, (1770/1340) = 1.32. The ultimate load factor is therefore (8.25)/1.32 = 6.25g, and the limit load factor would traditionally be taken as 6.25/1.5 = 4.16g. (If due to subsequent changes the gross weight should increase, these load factors would decrease further.)

The gross-weight ratio gives a slightly conservative estimate since it assumes that the distribution of weight between wings and fuselage is the same for both modified and unmodified aircraft. Since proportionately more weight has really been added to the wings than to the fuselage, the wing bending loads will be slightly lower than indicated by the ratio of gross weights. On the other hand, that portion of the aerodynamic load which is carried by the flap is now applied to the wing structure as point loads at the hinges, rather than as distributed loads. This causes local bending and torsion stresses which could be slightly larger than in the unmodified wing. It is concluded that the simple calculation of load factors based on gross weight ratio is adequate.

The bending and torsion load factors define the requirements for the wing spars and skins. The loads which define the strength requirements of the modified wing ribs, on the other hand, are aerodynamic loads and flap loads, which are considerably different from those of the unmodified wing.

The design loads for the wing ribs are based on a symmetrical aerodynamic load of 5g at 1800 lb gross weight. The structure of the ribs is designed for 1.5 times these loads, corresponding to an ultimate load factor of 7.5g. For different gross weights, this factor should be divided by (gross weight/ 1800 lb). Since this ultimate load factor is larger than that of wing bending, the lower value should govern.

The factor of safety of 1.5 between the ultimate load and the limit load, is used throughout the aircraft industry, by specification, with the tacit or explicit expectation that the structure will be proven by a static structural test to ultimate load. At ultimate loads, permanent deflection and yielding are permitted and expected. In the present case, it would be uneconomic to conduct such a (destructive) test on a modified wing. As an alternative, it is recommended that a factor of 2 between ultimate and limit loads be used. It is felt that this will be an adequate allowance for any inadvertent discrepancies between the analysis and the hardware due to material, workmanship or approximations used in the loads or the analysis. The use of a factor of 2 for ultimate-to-limit loads has been used in lieu of static testing for a number of cases in prototype aircraft by the Air Force.

Using this factor, the limit load factor for the modified wing is $(6.25/2) = 3.22$g, at 1770 lb gross weight. At other gross weights, the limit load factor for the wing will be $3.22\left(\dfrac{1770\ lb}{gross\ weight}\right)$g.

This load factor is only one of the loads needed to define the operating envelope of the aircraft. Other operating limits may exist due to wing or tail loads due to maneuvering or gusts, landing vertical velocity, etc. At the time the aircraft is constructed, a separate report on operating limits must be prepared in order to describe the limits within which test flying must be conducted. At the time of preparation of the operating limits report, formal approval of the factor to be used between ultimate load and limit load should be approved by the agency responsible for the flight test.

133

II. WING DESIGN MODIFICATION

The actual modifications to the SGS 2-32 wing for installation of the spanwise duct and trailing edge flap will be achieved in several sequential steps:

- Deactivation of the existing dive brake.

- Installation of the trailing edge flap and actuation system.

- Removal of a portion of the wing upper skin between spars over the space occupied by the duct.

- Remove the material in those ribs necessary to provide clearance for the duct,

- Installation of the duct,

- Replacement of rib structure with added doublers, and

- Replacement of skin with strut clearance holes, doublers, and flexible seal.

Figure A-8 depicts the general layout of the spanwise duct and trailing edge flap in the left panel of the Schweizer 2-32 Sailplane wing. The duct location will preclude the use of the existing dive brake, which must either be removed or securely fastened down for the QRTV configuration. The actuation system for this dive brake must be disconnected.

The trailing edge flap will replace the dive brake as a speed control device, and may also serve to reduce trailing edge noise in the deflected position. While detailed design of the flap and actuation system was beyond the scope of this task, certain aspects of the design were considered to establish design of the wing modifications. As can be seen in Figure A-8, the flap is made up of two sections – one extending from the wing-fuselage juncture to wing station 79.5, and the other from this station to wing station 172. This division of the flap evolved from evaluation of the wing bending deflection under air load. With a single flap section hinged at each end, the gap at the mid-span of the flap would have become excessive as the wing deflected. Placing a hinge at the midpoint would have introduced binding in one or more of the flap hinges. Dividing the flap in two appropriate sections with hinges at the ends of each section will produce minimal gaps along the flap leading edge as the wing deflects. Pinning the two flap segments together at the trailing edge will tie them together and permit actuation of the flap by means of a bell crank system with the fuselage. Actuation of the flap in this way will produce some windup in the flap along its span. A brief check indicated the degree of windup will not be excessive. Incorporation of a curtain type seal in the flap-wing gap will provide suitable flap effectiveness.

To install the spanwise duct within the wing, it will be necessary to remove the upper wing skin between the two main spars from the wing-body juncture to approximately wing station 172. This will be accomplished by drilling out the flush head rivets which attach the skin to the wing structure.

With this portion of the wing skin removed, the interior of the wing will be accessible which will permit cutting through the rib caps and cutting out that portion of the rib webs necessary to clear the duct cross-sectional shape. A typical wing duct section is shown in Figure A-9. This figure also shows the general construction of the wing duct of formed and welded titanium sheet
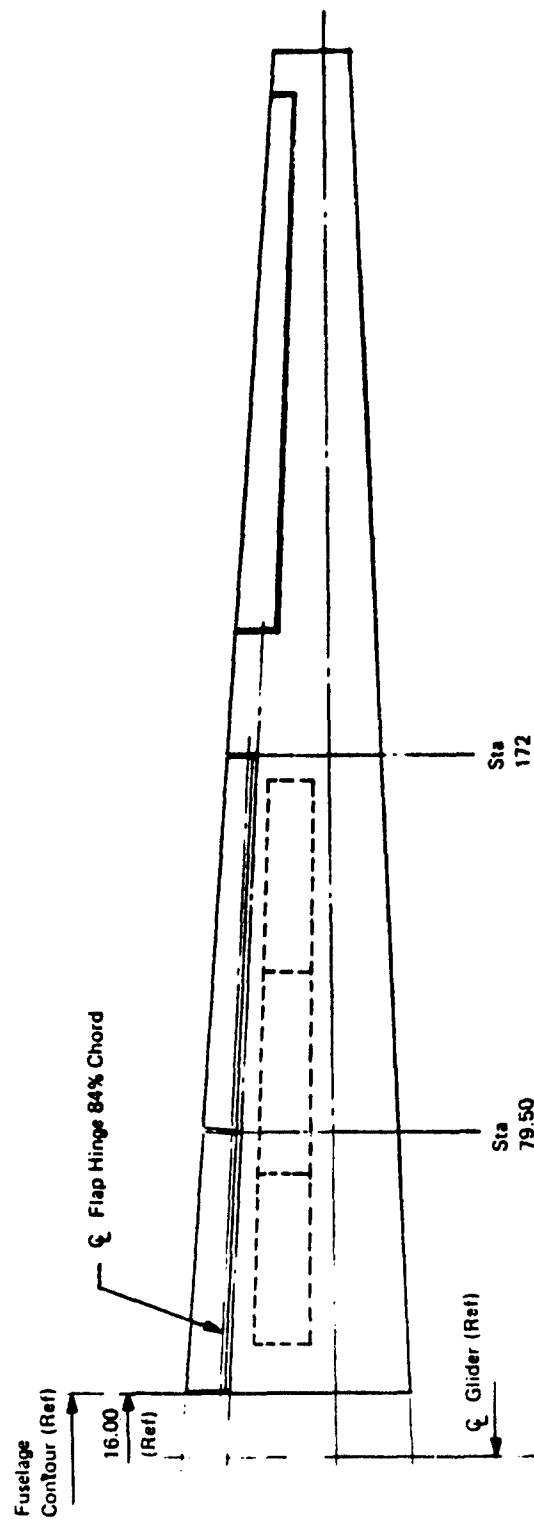
134

Figure A-8. Planform Layout of Spanwise Duct and Trailing Edge Flap
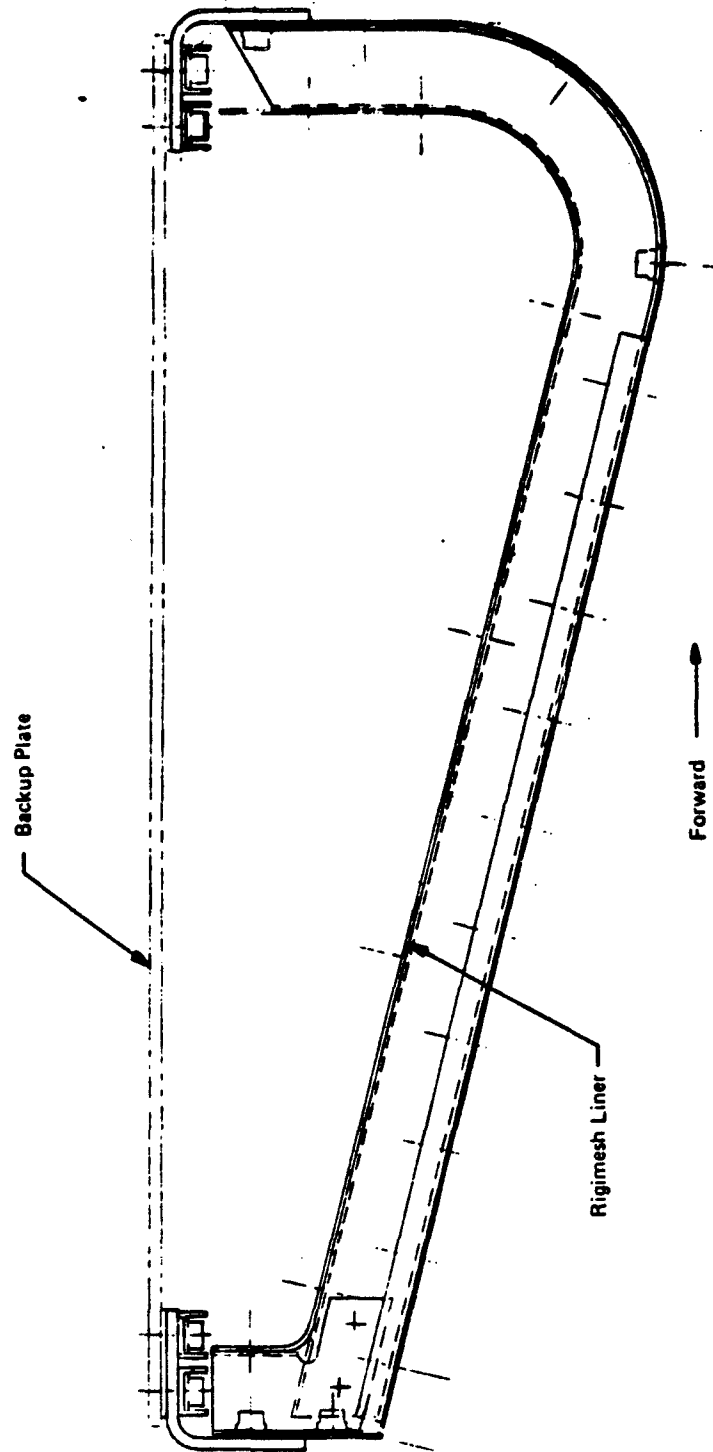
Backup Plate

Rigimesh Liner

Forward ⟶

Figure A-9. Typical Wing Duct Section

136

with the titanium "Z" sections which serve as duct wall stiffeners as well as standoffs for the porous stainless steel acoustic liner. The titanium angles welded to the top of the fore and aft duct walls provide a means of attaching the removable backup plate through which the propulsive struts protrude.

Figure A-10 depicts a typical wing rib as modified to accommodate the spanwise duct. Each duct section is attached to the wing structure by a kinematic suspension which provides freedom for differential expansion of the ducting with respect to the wing, while restraining the duct in six degrees of freedom. This suspension system is designed to absorb duct thrust and pressure loads, permitting normal wing bending without introducing loads into the duct or wing, and isolating duct vibration from the wing structure for acoustic attenuation.

Before installing the duct, reinforcing flanged doublers will be riveted to the fore and aft ends of the rib. The lower rib cap, which comprises a flange on the remainder of the rib web, will be stiffened by means of a formed aluminum angle. After duct installation, the upper rib will be installed together with a formed aluminum stiffener which will extend fore and aft of the cut out section and be riveted to the doubler plates.

The wing upper skin will be replaced by a sheet of the same gage as the original, but per-forated with clearance holes for the propulsive struts. A doubler plate similarily perforated will be riveted to the underside of the skin to maintain skin shear strength. Before attaching this doubler, a thin elastomeric sheet, slotted to the same pattern as the strut array, will be adhered to both the underside of the skin and the upper surface of the doubler plate. This sheet will provide a seal around each strut to keep moisture and dirt out of the wing interior. The skin will be installed by sliding it down over the struts and fastening it in place. The resulting overall arrangement of this unique quiet jet propulsion system is shown schematically in Figure A-11.
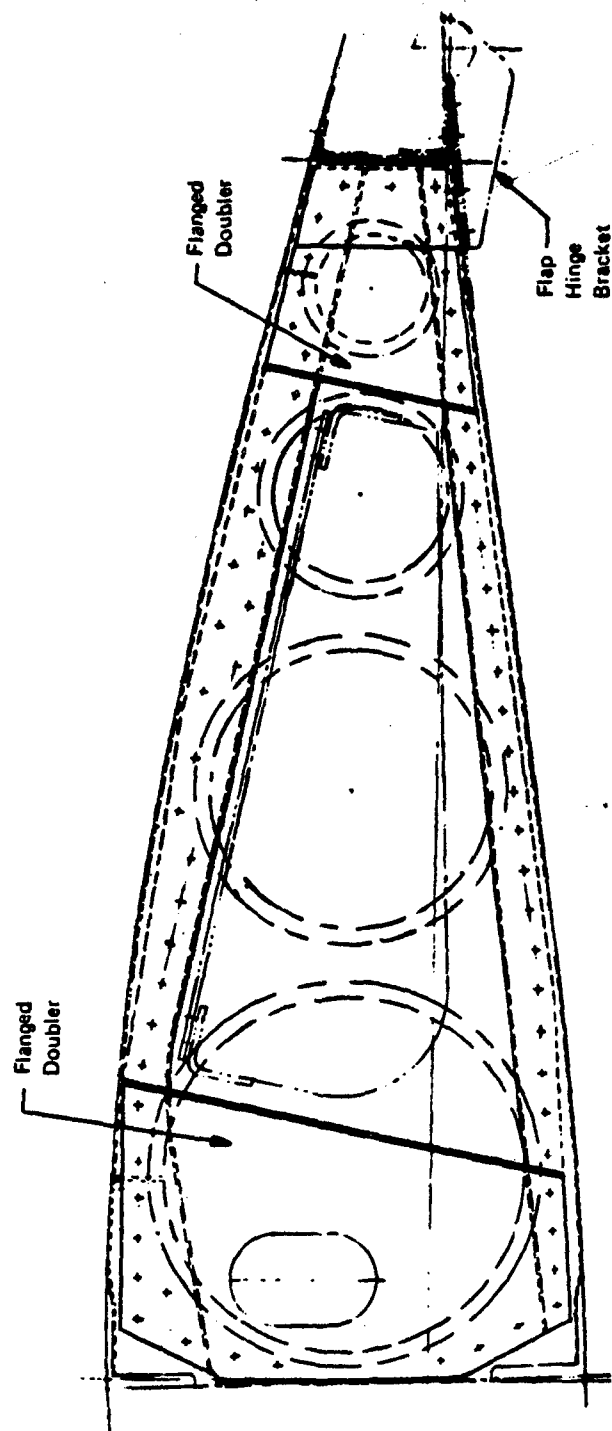
137

Flanged
Doubler

Flanged
Doubler

Flap
Hinge
Bracket

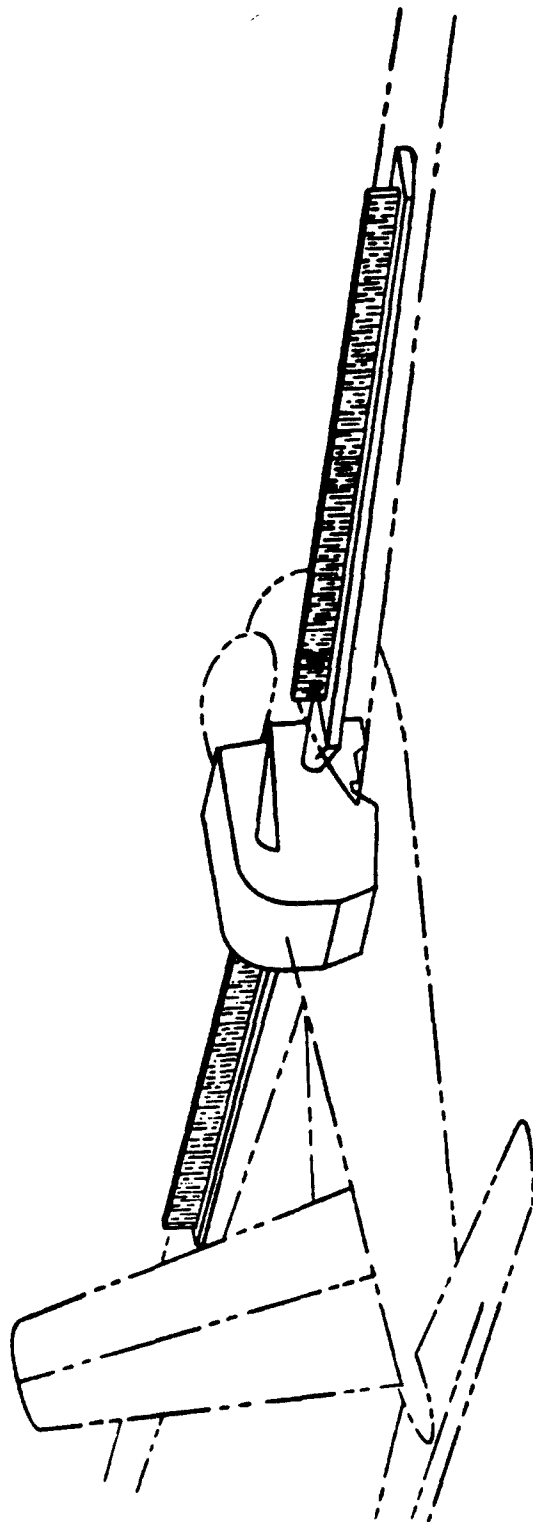Figure A-10. Typical Wing Rib Modification

Figure A-11. QRTV Propulsion System Installation Schematic

III. STRUCTURAL ANALYSIS

The Schweizer SGS 2-32 sailplane wing requires structural changes to accommodate installation of the wing duct which provides the mixed exhaust gas from the Williams Research Corporation WR-19 turbofan engine to an arrangement of microjet thrusting struts on the wing upper surface. Structural changes required include (a) a new root rib at wing station 18.75 to accommodate the exhaust duct transition section, (b) new wing ribs at all other rib stations aft of the main spar in the region of the spanwise wing ducts, (c) addition of local support points on the ribs for the spanwise wing duct, (d) addition of local doublers to reinforce the cutouts in the upper wing skin for the microjet thrusting struts.

The installation requires the riveting of the aerodynamic spoiler to make it inoperative. A trailing edge flap is added aft of the rear spar. Each flap section is supported on two hinges at wing stations 27.0 and 72.0 for the inboard flap and at wing stations 87.0 and 154.0 for the outboard flap. Ribs at these wing stations provide local support points for the flap hinge brackets.

Basically, the strength of the upper wing skin is maintained by doubler reinforcement around the cutouts for the struts. Each rib aft of the main spar outboard to wing station 166 is completely redesigned. The flexural and torsional characteristics of the wing are not affected. The redesigned ribs distribute the local aerodynamic airload pressures, inertia loads from the wing ducts, and flap hinge loads into the wing while maintaining the airfoil shape. Internal loads distribution in the wing main spar, upper and lower skin surfaces, rear spar, and root rib is assumed to be same as used in Reference (25).

Both the trailing edge flap and wing ducts are installed such that the wing is unrestrained in flexure and torsion. The clearances required are obtained from the static test deflection curves obtained from Reference (26). Thermally, the adjacent wing structure heats to various temperatures depending on operating conditions. Proper accounting due to reduced mechanical properties at temperatures are included in the analysis. The pertinent critical loading conditions, loads, deflections, internal stresses and strength margins of safety are summarized in this section.

A.   CRITICAL DESIGN CONDITIONS AND LOADS

The structural design criteria established in Section I.D. of this report were used. The critical design conditions for each major structural element of the wing modification are summarized in Table A-3.

The applied wing airload pressures, wing root attachment loads and wing skin shear flows are obtained from Reference (25). External airloads and consequent hinge moments for the trailing edge flap at various angular settings are obtained from Section I.B. of this Appendix.

The airload pressures and trailing edge flap loads are distributed into the wing box beam by the ribs. The method of reacting the running rib load due to the airload pressures is shown on Figure A-12 and due to the trailing edge flap hinge load in Figure A-13. The trailing edge flap loads are identified on Figure A-14 and shown in Table A-4. The design loads for the root attachment rib at wing station 18.75 are shown in Figure A-15. The internal rib load distribution (i.e., shear, axial load and bending moment) are presented with the strength analysis in Section C of this, Appendix.

140

TABLE A-3
## SUMMARY OF CRITICAL DESIGN CONDITIONS FOR THE WING MODIFICATION

Structural Element	Condition No.	Description
Wing Ribs	W-1	Airloads obtained from Reference 25, pages 57 through 59 reacted as shown on Figure A-12. Typical for all ribs.
	W-2	Hinge loads from the trailing edge flap as presented in Figure A-14 and Table A-4 reacted as shown in Figure A-13.
Root Rib at Wing Sta. 18.75	W-3	Wing attachment loads obtained from Reference 25, page 51 as shown in Figure A-15.
Wing Skin	W-4	Upper skin surface shear flows obtained from Reference 25 on pages 39 and 40.

TABLE A-4
SUMMARY OF TRAILING EDGE FLAP LIMIT LOADS

Load or Moment		Flap Setting, Degrees	
		30°	0°
Hinge Moment	(in-lb)	1357.2	499.4
q_i	(lb/in)	2.13	2.02
q_m	(lb/in)	1.80	1.70
q_t	(lb/in)	1.29	1.23
R_1	(lb)	156.22	53.10
R_2	(lb)	105.29	42.08
R_3	(lb)	183.63	67.69
R_4	(lb)	308.63	110.65
R_5	(lb)	79.72	25.74
R_6	(lb)	226.20	83.23
P_A	(lb)	226.20	83.23

Sign Convention   Positive up normal to the chord.
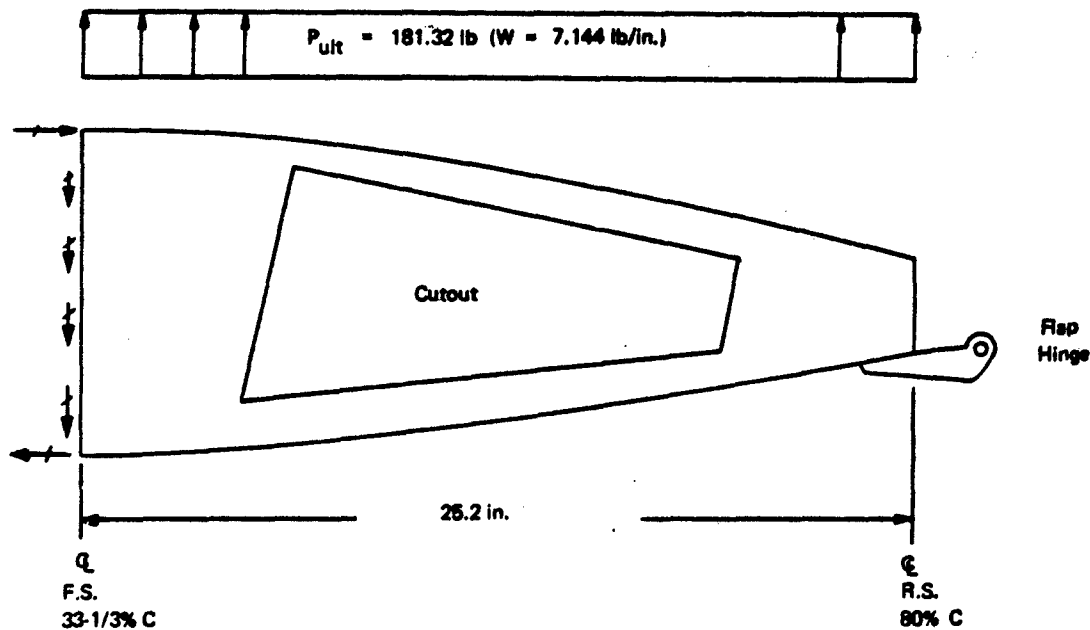
q_i, q_m, q_t

Chord

$+\theta$ R_3
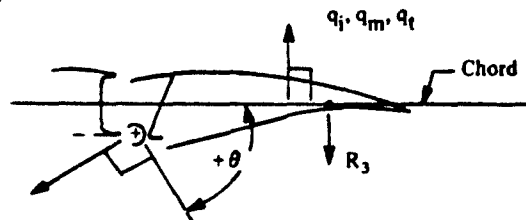
R_1, R_2, R_4, R_5

$+ P_A$ and $+ R_6$ -   As shown in Figure A-14 and in the fore and aft direction.

$+$ Hinge Moment - Airload moves trailing edge up.

141

$$P_{ult} = 181.32 \text{ lb} \quad (W = 7.144 \text{ lb/in.})$$

Cutout

Flap
Hinge

25.2 in.

℄
F.S.
33-1/3% C

℄
R.S.
80% C

Assume P_{ult} to be uniformly distributed between the forward and aft spars. Also assume the rib between the spars is cantilevered off the forward spar.

Distance between main spars = (0.80 - 0.333) 54.0 = 25.2 inches

> NOTE: Forward spar is at 33-1/3% C
> Rear spar is at 80% C
> Chord Length = 54.0 inches

Wing loading (applied) = 7.444 psf

Limit load factor - 5.25 g

Ultimate load factor - 5.25 × 1.5 = 8.25 g

Rib spacing at rib stations 18.75 to 27 = 8.25 in.
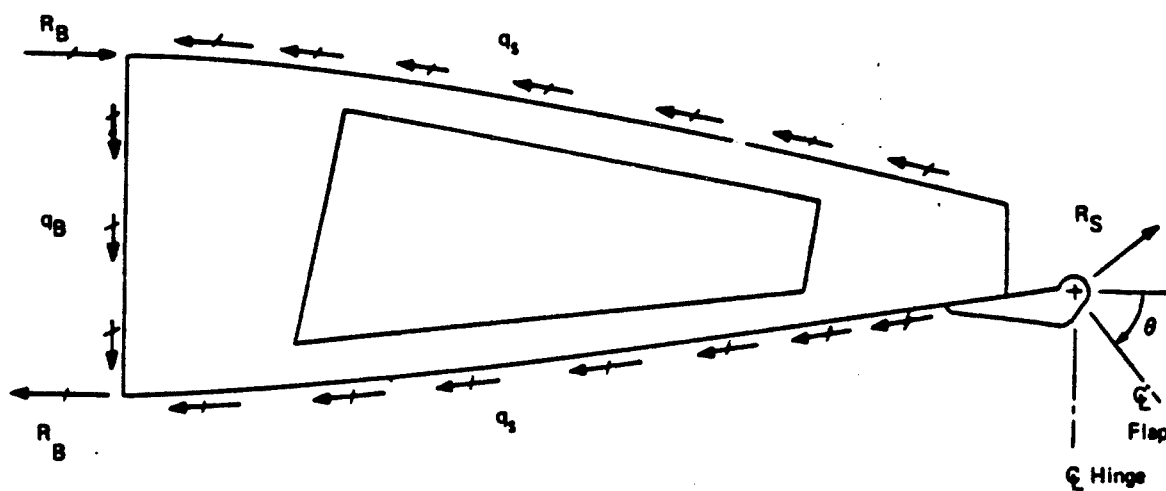27 to 34.5 = 7.50 in.

$$\text{Average rib spacing at Station 27} = \frac{8.25 + 7.50}{2} = 7.875 \text{ inches}$$

$$P_{ult} = \frac{7.444\,(8.25)}{144}\,(54)\,(7.875) = 181.32 \text{ lb}$$

$$W_{ult} = \frac{181.32}{25.38} = 7.144 \text{ lb/inch (ult)}$$

Figure A-12. Wing Station 27 Rib (Inboard Flap Hinge Support Rib) - Typical Rib Loading
Due to Airloads at All Stiffening Ribs

142

q_s	Reacting skin shear flows to the hinge load cordwise component
q_B	Reacting main spar web shear flow to hinge load vertical component
R_B	Reacting load at main spar to balance rib

Figure A-13. Wing Station 27 Rib (Inboard Flap Hinge Support Rib) - Typical Rib Loading
Due to Flap Loads at Flap Hinge Support Ribs

Figure A-14. General Arrangement - Trailing Edge Flap

144
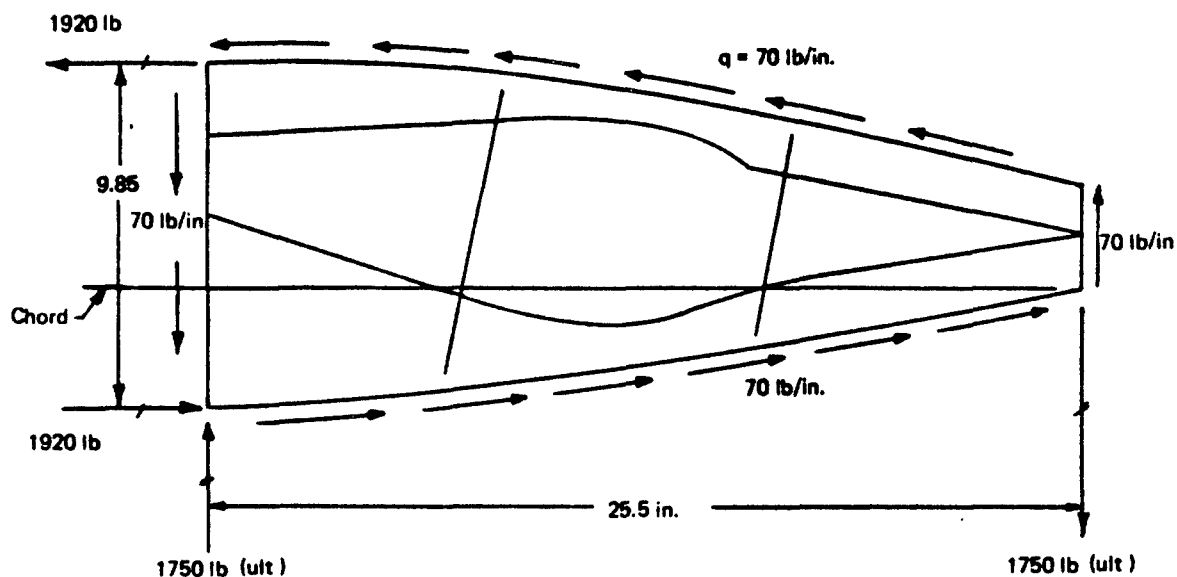
Page 27 for Limit Torsional Moment = 29,750 in-lb
Flight Condition IV is critical

Ultimate Torsional Moment = 1.5 (29,750) = 44,625 in-lb.

Couple Forces $= \dfrac{44,625}{25.5} = 1750$ lb (ult)

Pages 49 and 51 for Torsional Shear Flows

Applied q = 70 lb/in ultimate

Total enclosed area = 135.3 + 183.2 = 318.5 in^2
(nose) + (main to rear spar)

Torsion Check 70.0 x (2 x 318.5) = 44,625 in-lb

Reacting Load $= \dfrac{2(135.3)\,(70)}{9.85} = 1920$ lb

Figure A-15. Root Rib at Wing Station 18.75 - Design Loads

145

The method used for reacting the externally applied loads on the modified ribs is the same as the analysis used in Reference (25) for the existing ribs. The method is shown to be conservative by the following analysis: The SGS 2-32 wing in the outboard stations is a two-cell box beam with a main spar at 33-1/3 percent of the chord and a rear spar at 80 percent of the chord that reacts trailing edge loads with skin and rear spar shear flows aft of the main spar. Reacting shear flows, calculated for a unit trailing edge flap hinge load of 100 lbs., in the wing skins and spars are shown in Figure A-16. The analysis verifies the elastic axis location stated in Reference (25) as being practically on the main spar. Wing airload pressures to be distributed into the wing by each rib are similarly reacted. Therefore, the simplified analysis method used in Reference (25) is verified and was used for the remainder of the rib analyses.

B.   WING DEFLECTIONS AND CLEARANCES

The trailing edge flaps and spanwise wing ducts are installed in each wing in a determinate attachment arrangement. Vertical wing deflections are not restrained. Proper clearances, however, are required to prevent interference. Vertical deflections of the wing trailing and leading edges were measured during static test for the critical flight conditions as reported in Reference (26). These deflections are summarized in Table A-5 and plotted in Figure A-17. Each flap or duct section will span as a straight line between each of its respective attachment points. In the case of the trailing edge flap, a clearance greater than 0.250 inch is needed as shown in Figure A-17. For a duct section, a clearance greater than 0.100 inch was established.

C.   STRENGTH ANALYSIS

All the ribs are reinforced between wing stations 18.75 to 154.0 because of the cutout required for the wing duct installation. Each rib is reinforced in a similar manner. The most critical ribs are at the root for both wing stations 18.75 and 27.0, at the outboard hinge of the inboard flap at wing station 72.0 and at the most outboard hinge of the outboard flap at wing station 154.0. Analysis is presented in this section for these critical ribs. The root rib at wing station 18.75 requires reinforcing for the large cutout created by the engine exhaust duct transition section.

Each rib is analyzed as a redundant frame type structure using conventional methods. The internal load distributions are calculated and the margins of safety for strength are determined.

The structural reinforcement consists of cutting the existing rib to clear the wing duct, then riveting in the formed sheet metal stiffening members that are required. These consist of 2024-T3 Alclad-aluminum alloy formed channels along the main and rear spars and 2024-T3 Alclad-aluminum alloy formed angles along the upper and lower skin surfaces. For the rib at wing station 18.75, 7075 aluminum alloy is used. The angles overlap the channels to provide for load interchange around the edges of the cutout. At the rear spar, an additional formed 2024-T3 Alclad-aluminum alloy angle is placed along the web of the rear spar and the lower skin surface for added support for each flap hinge fitting.

a. Shear Flows Due to 100 lb Applied at the Shear Center
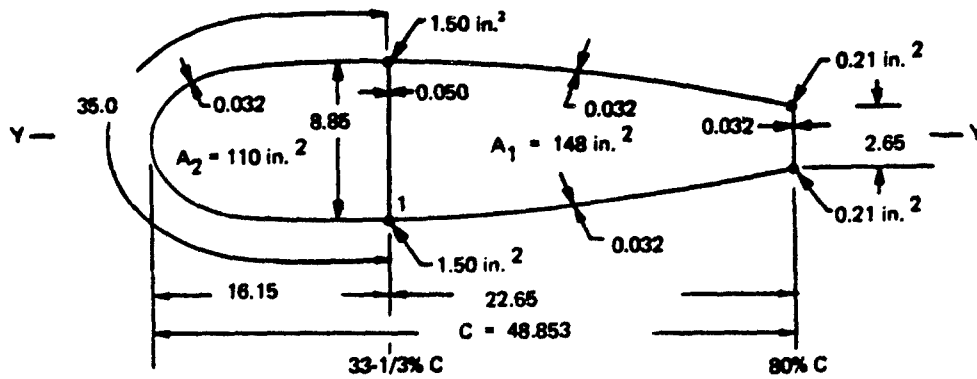
$I_{YY} = 2 (4.42)^2 1.50 + 2 (1.32)^2 0.21 = 58.5 + 0.73 = 59.23$ in.^{4}

11.18 lb/in.   0.47 lb/in
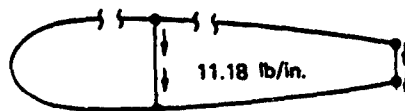
(Clockwise Shears are Positive)

For Cell 1 $\oint q\, ds/t = 1674\, q_1 - 177\, q_2 - 1941 = 0$ Solving $q_1 = 1.01$ lb/in.
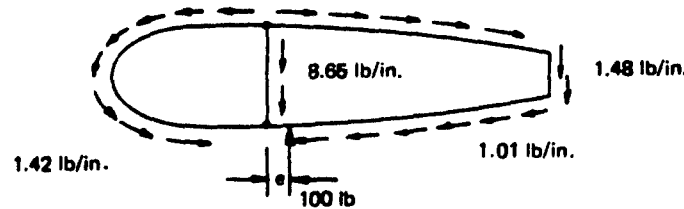For Cell 2 $\oint q\, ds/t = -177\, q_1 + 1268\, q_2 + 1980 = 0$ $q_2 = -1.42$ lb/in.
M at Point (1) Elastic Axis Location
$[-220 (1.42) + 296 (1.01) + 0.47 (2.65) (22.62)] / 100 = e = 12/100 = 0.12$ in.
Shear Center = 0.12 in. Aft of Main Spar

8.65 lb/in.   1.48 lb/in.

1.42 lb/in.   1.01 lb/in.

100 lb

b. Shear Flows Due to Applied Torsion Load of 100 lb X 24.6 in.

For Pure Torsion
Twist of Cell 1 = Twist of Cell 2 or $2A_1 G = 2A_2 G$

where $\theta_1 = \dfrac{q_1\, ds/t}{2A_1 G}$

$(1674\, q_1 - 177\, q_2) 220 = (-177\, q_1 + 1268\, q_2) 296$
$1912\, q_1 - 1877\, q_2 = 0$
$1.01\, q_1 - q_2 = 0$ Practically Equal
$T = 100 (24.6) = 516\, q_1$
$q_1 = q_2 = 2460/516 = 4.75$ lb/in.

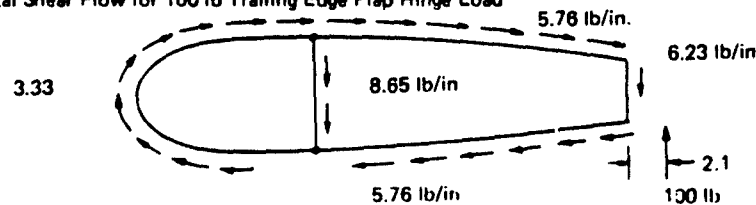c. Total Shear Flow for 100 lb Trailing Edge Flap Hinge Load

5.76 lb/in.

6.23 lb/in

3.33   8.65 lb/in

2.1

5.76 lb/in   100 lb

Figure A-16. Unit Wing Shear Flows at Sta. 72.0

147

TABLE A-5
VERTICAL WING DEFLECTIONS AT 100% UNIT LOAD

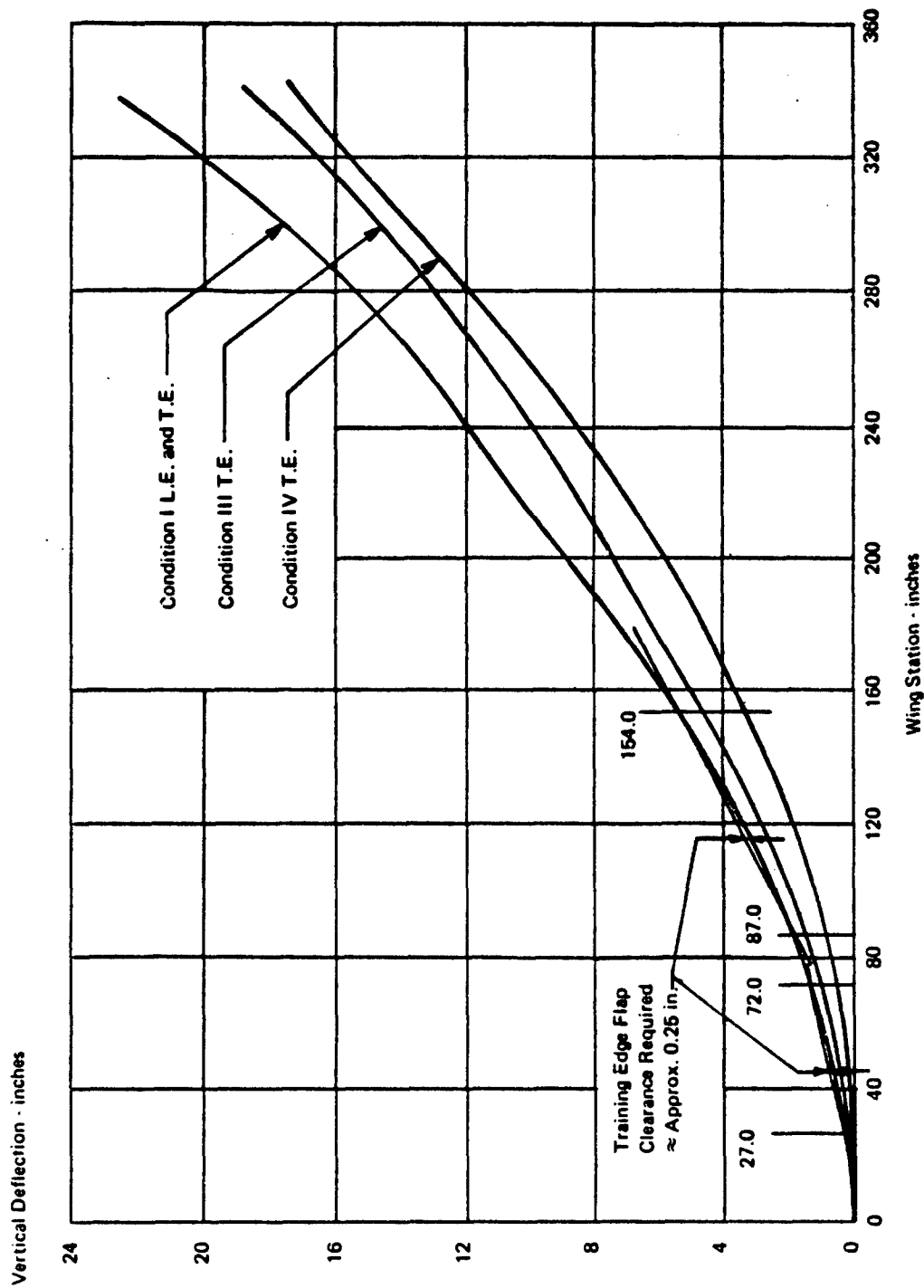| Scale No.	Wing Station	Flight Condition I	Flight Condition III	Flight Condition IV
4	17	3.31 - 3.28 = 0.03 in.	5.88 - 5.80 = 0.08 in.	5.05 - 4.93 = 0.12 in.
6	109	7.83 - 4.91 = 2.92 in.	4.85 - 2.27 = 2.58 in.	7.98 - 5.86 = 2.12 in.
8	202 L.E.	12.10 - 3.21 = 8.89 in.	11.16 - 3.27 = 7.89 in.	12.64 - 6.09 = 6.53 in.
10	270	17.97 - 3.62 = 14.35 in.	16.87 - 4.57 = 12.30 in.	14.68 - 3.18 = 11.70 in.
12	342	23.65 - 0.86 = 22.79 in.	23.25 - 3.95 = 19.30 in.	24.27 - 6.80 = 17.47 in.
5	17	2.42 - 2.39 = 0.03 in.	4.55 - 4.55 = 0 in.	3.80 - 3.85 = 0.05 in.
7	109	12.77 - 9.87 = 2.90 in.	11.50 - 9.10 = 2.40 in.	9.22 - 7.69 = 1.53 in.
9	202 T.E.	11.88 - 2.95 = 8.93 in.	13.29 - 5.91 = 7.38 in.	11.86 - 6.15 = 5.71 in.
11	270	17.24 - 3.09 = 14.15 in.	15.87 - 3.94 = 11.93 in.	13.18 - 2.28 = 10.90 in.

148

Figure A-17. Wing Vertical Deflections at 100% Limit Load at the Leading and Trailing Edges for Flight Conditions II, III, and IV

1. **Root Rib at Wing Station 18.75**

The critical loading condition is Condition W-3 with applied loads shown in Figure A-15. The frame is idealized as a series of finite elements. The design internal shear, axial load and bending moment variation is shown in Figure A-18. The critical sections are analyzed for the minimum margins of safety as follows:

Section at Element 8

$$A = 0.2875 \text{ in.}^2$$

$$I = 0.0192 \text{ in.}^4$$

$$\text{Temp} = 150°F$$
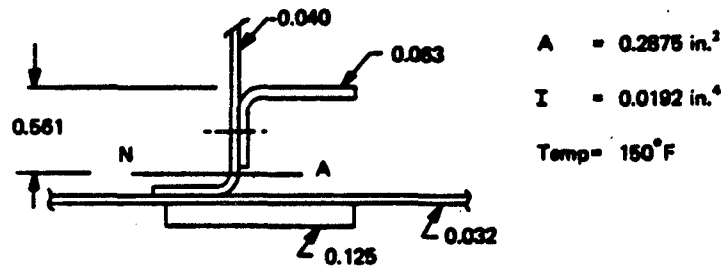
$$\left. \begin{array}{l} \text{Axial Load} = -2100 \text{ lb} \\ \text{Moment} = 1115 \text{ in.-lb} \end{array} \right\} \text{Ref. Figure A-18}$$

$$f = \frac{-2100}{0.2875} - \frac{1115\,(0.561)}{0.0192} = -7300 - 32{,}500 = -40{,}800 \text{ psi}$$

$$\frac{b}{t} = \frac{0.669}{0.063} = 10.62 \qquad \bar{\sigma}_F = 42{,}500 \text{ psi} \quad \text{Ref (8) 7075-T6 Aluminum Alloy}$$

$$\text{M.S.} = \frac{42{,}500}{40{,}800} - 1 = +0.042$$

<u>Shear Transfer from Angle to Web</u>

Angle:	Flange Force	=	40,800 (0.063) (0.70)	= 1799
	Web Force	=	1/2 (40,800) (0.063) (0.561)	= 721
	Total Angle Force	=	2520 lb (Ultimate)	
	6 Rivets (force/rivet)	=	420 lb	

Allowable for 5/16 in. Diameter Rivet in Shear = 596 lb

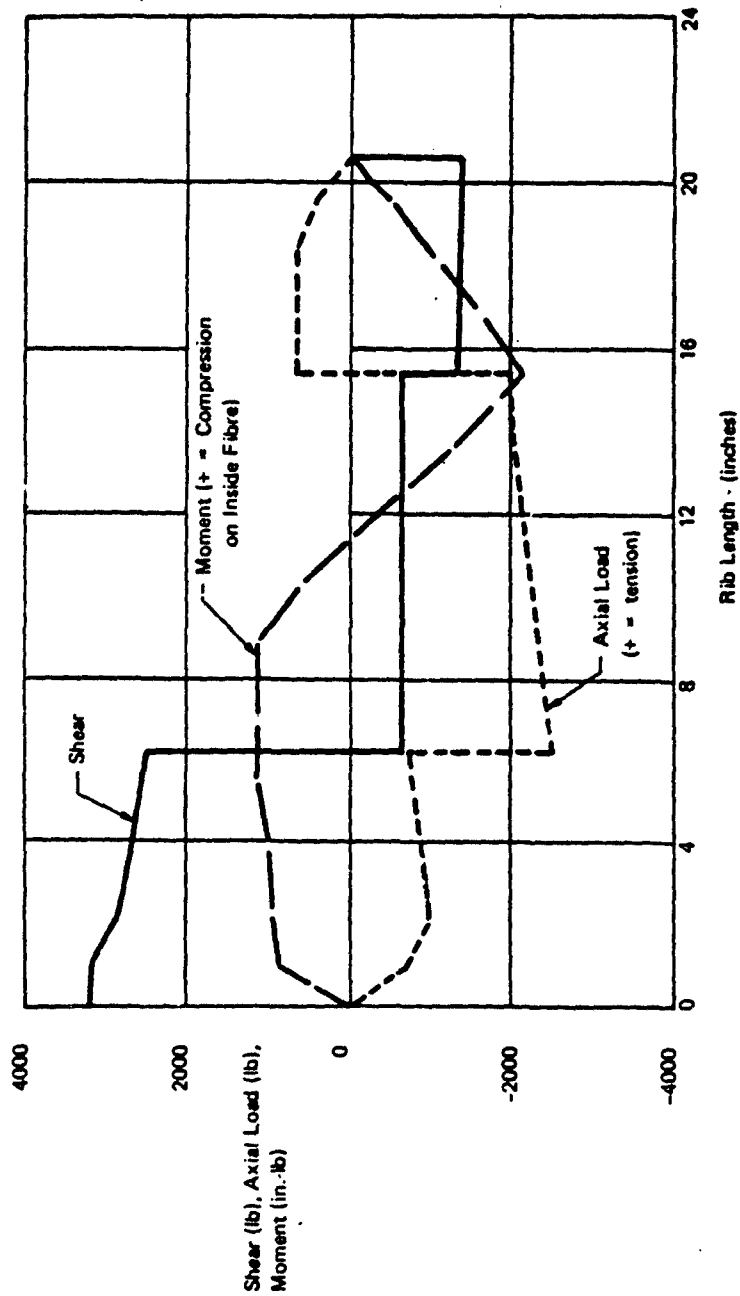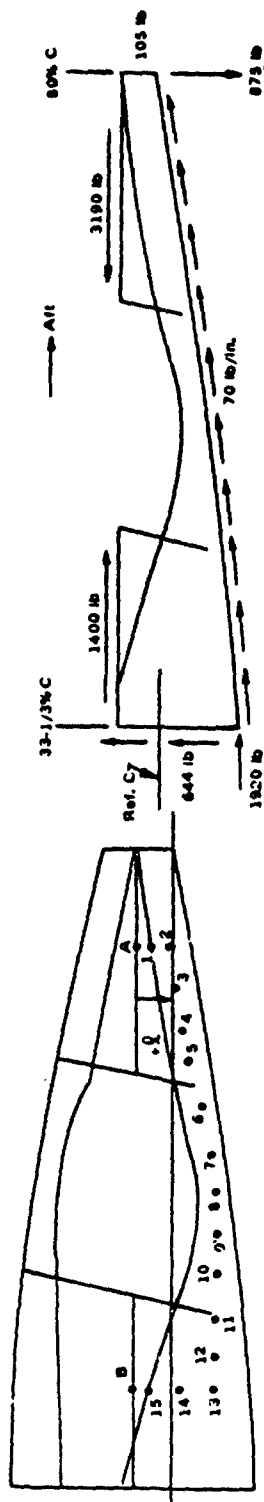$$\text{M.S.} = \frac{596}{420} - 1 = +0.42$$

Figure A-18. Internal Rib Ultimate Loads (Wing Station 18.75, Condition: W-3)

151

Section at Element 10
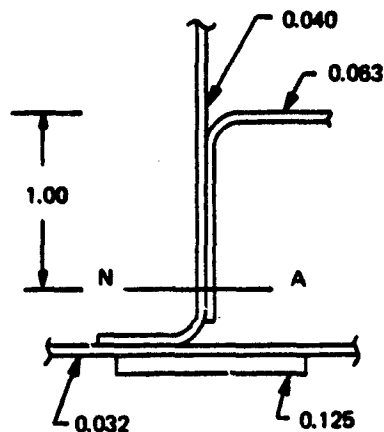
$A = 0.3512 \text{ in.}^2$

$I = 0.0970 \text{ in.}^4$

Temp = 150°F

Axial Load = − 2500 lb

Moment = 1200 in.-lb

Figure A-18

$$f = \frac{-2500}{0.3512} - \frac{1200 (1.00)}{0.0970} = -7120 - 12,350 = -19,470 \text{ psi}$$

$$\frac{b}{t} = \frac{0.669}{0.063} = 10.62 \quad \bar{\sigma}_F = 42,500 \text{ psi} \quad \text{Ref. (8) 7075-T6}$$
$$\text{Aluminum Alloy}$$

$$\text{M.S.} = \frac{42,500}{19,470} - 1 = +1.19$$

2.   Intermediate Rib at Wing Station 72.0

The rib at wing station 72.0 is the most highly loaded rib. The critical loading condition is a combination of conditions W-1 and W-2 as shown in Figures A-12 and A-13. The idealized frame of finite elements; applied loads; and internal shear, axial load and bending moment variation is shown in Figures A-19 and A-20. The critical section is analyzed for the minimum margin of safety as follows:

Section at Element 8
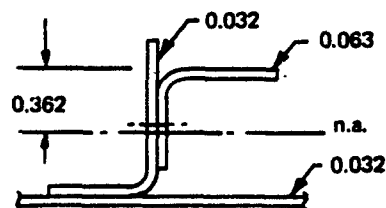
$A = 0.158 \text{ in.}^2$

$I = 0.01737 \text{ in.}^4$

Temp = 150°F

152

Figure A-19. Internal Rib Ultimate Loads (Wing Station 72.0, Condition: W-1)

153

Figure A-20. Internal Rib Ultimate Loads (Wing Station 72.0 Condition = W-2)

154

$$\text{Axial Load} = 1,090 \text{ lb}$$
$$\text{Moment} = -900 \text{ in. lb} \qquad \text{Ref. Figures A-19 and A-20}$$

$$f_{(skin)} = \frac{1090}{0.158} - \frac{900\,(0.362)}{0.01737}$$

$$= -17,000 \text{ psi (Ultimate)}$$
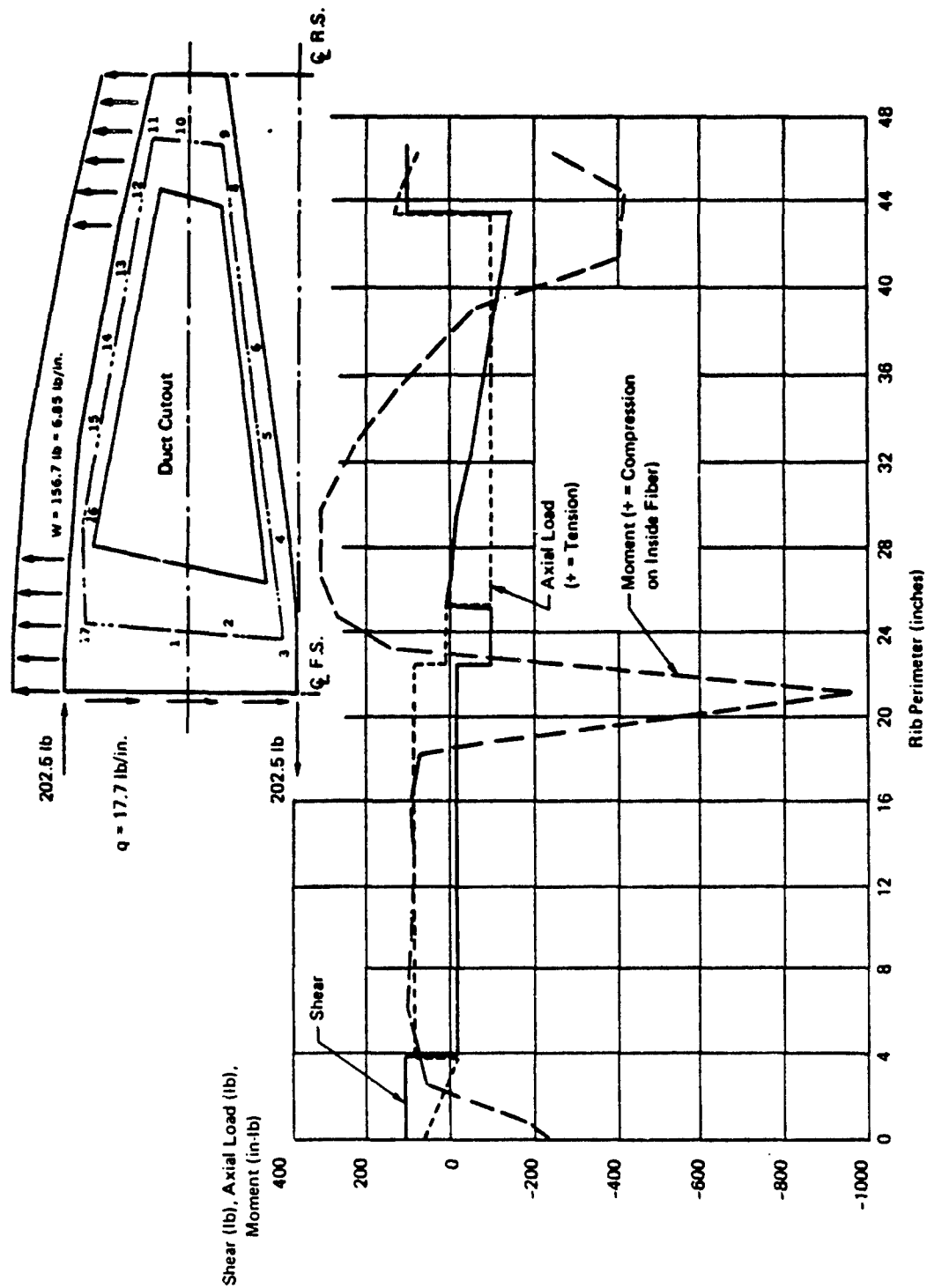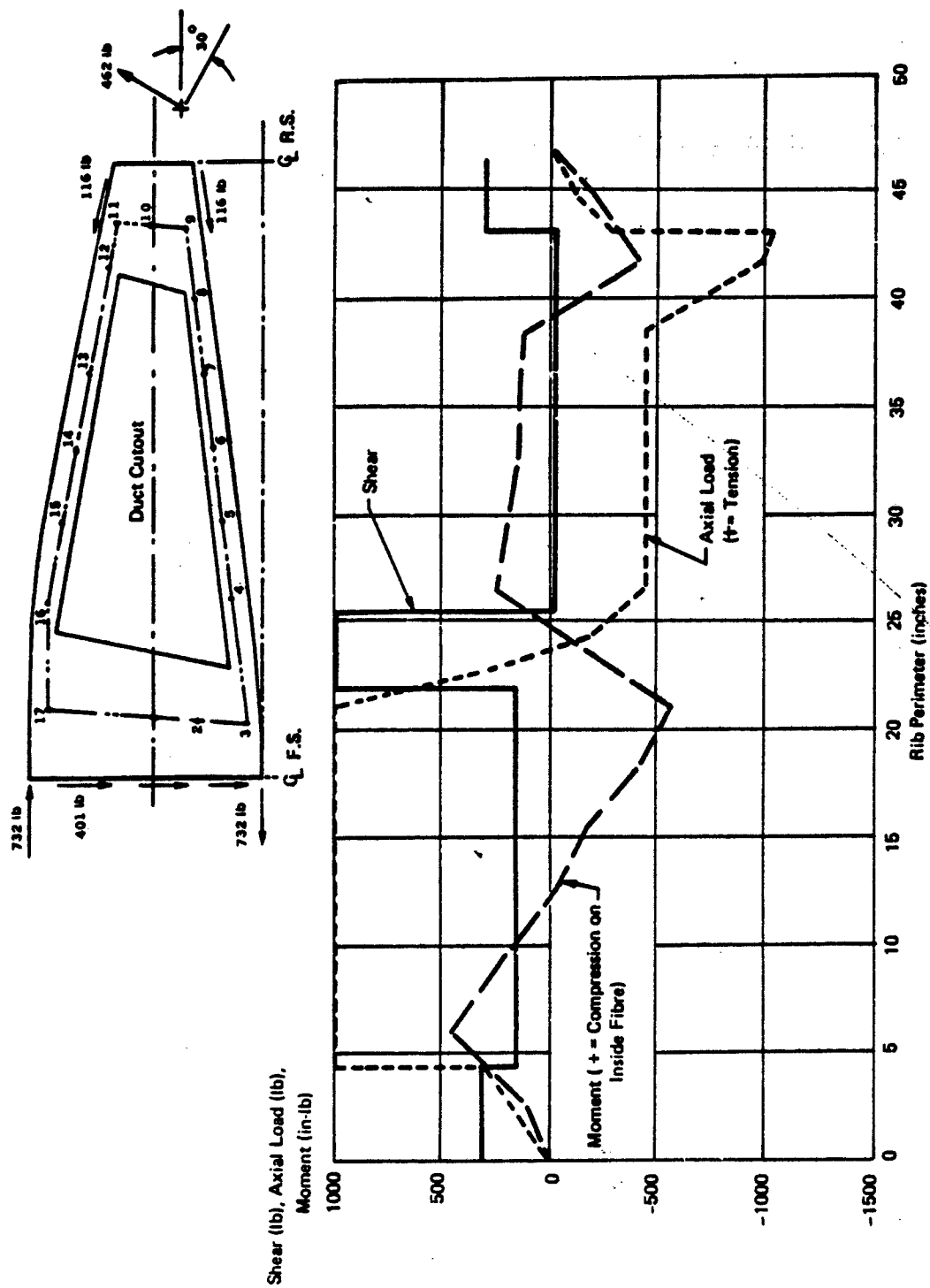
$$\frac{b}{t} = \frac{0.625 - 0.016}{0.032 + 0.016} = 12.7 \qquad \bar{\sigma}_F = 28,500 \text{ psi (at } 80^\circ\text{F)}$$
$$\text{Ref. (4) 2024-T3 Aluminum Alloy}$$

Temperature Factor for 150°F, 2024-T3 Aluminum Alloy $= 0.96$

$$\bar{\sigma}_F\,(150^\circ\text{F}) = 0.96\,(28,500) = 27,400 \text{ psi (Ultimate)}$$
$$\text{M.S.} = \frac{27,400}{17,000} - 1 = +0.61$$

3. **Other Wing Ribs**

The strength of all the other ribs is based on a comparison with the analysis presented for the rib at wing station 72.0. Ribs at wing stations 27, 87, and 154 also provide support for a trailing edge flap hinge. For the other lightly loaded ribs, the thickness of the reinforcement is reduced from 0.063 to 0.050 inch. The other ribs are nearly identical in construction with loadings lower than for wing station 72.0. Therefore, all the other ribs are considered structurally adequate.

4. **Wing Skin**

Cutouts are required in the upper wing skin where the struts are located above the wing ducts. The structural approach taken is that a 0.100 inch thick 2024-T3 aluminum alloy will be bonded to the 0.032 inch thick skin to provide sufficient strength to carry the applied ultimate shear flow. This approach assures no change in the basic wing structure which consists of a 2-cell box beam. Some stiffening will occur in the region of the cutout with some tendency of the doubler-skin combination to resist wing bending moment. This will be minimal since the material is located close to the wing section neutral axis.

In carrying shear loads across cutouts, the doubler-skin combination provides effective truss load paths between the cutouts. Allowables are based on buckling of the doubler-skin where compressive loadings occur. To verify the structural adequacy and design, an element shear test is recommended for this element. Standard shear load fixtures are available in the Bell Aerospace general laboratories for conducting a test on a representative section of the doubler reinforced skin.

APPENDIX B
HOT TEST OF A PRODUCTION STRUT

INTRODUCTION AND SUMMARY

The purpose of this test was to verify that the quiet propulsion struts (BAC drawing No. 7389-430065) as manufactured in production are structurally adequate for use on a test aircraft.

The criteria for structural adequacy were established as: ability to withstand takeoff temperature and 1.33 times takeoff pressure for repeated cycles without excessive growth (limit load), plus ability to withstand takeoff temperature and 2 times takeoff pressure without pulling out the rivet (ultimate load). (Even opening of a rivet hole would not affect flight safety, since opening of all of the rivets would only result in some thrust loss due to leakage, not flameout of the engine; the increase in drag due to swelling of all the struts after rivet pulling could increase drag by up to 30%, but this is well within the capability of the engine even with the increased nozzle area.)

After an initial failure, it was found that the rivets (used as tension posts) had not been upset properly. After some investigation of possible repairs, it was determined that the rivet could be replaced and properly upset, using "w-condition" ("as quenched" or "ice box") rivets. The test part was repaired using this technique and successfully passed the tests, plus an additional 3-hour 'creep' test at takeoff temperature and pressure. All of the production struts were reworked using the proven repair technique.

TEST ARTICLE

The test article was a production strut. For this test, the strut was welded to a test seal plate similar to the seal-plate to be used for multi-strut flight articles. The hole in the seal plate was made large enough to pass the largest production strut. The strut used was the smallest of approximately a dozen random samples of the production run. The weld was made in the same manner proposed for flight articles. A small leak (insignificant from propulsion or acoustic criteria) occurred at the strut leading edge. It is believed that this can be eliminated in production by a slight revision in the weld technique. A pretest photo of the test strut is shown in Figure B-1.

To permit static testing, the nozzles were plugged with a flexible elastomer. This permitted testing in a small closed oven. The resultant static loading is conservative (higher than the actual flight load) since the elastomer transmitted hydrostatic loads, while flow would reduce pressures in the vicinity of the nozzles. The temperature of the metal in the oven was set equal to the predicted exhaust-gas stagnation temperature. This is also conservative, since with the hot gas on the inside and ambient slip-stream flow on the outside, the metal temperature at takeoff has been calculated to be at least 50°F cooler than the internal gas temperature.

After initial failure of the rivet, a repair technique was established, consisting of drilling out the old rivet to accept a larger diameter soft rivet. When this repair was made to the test part, the hole was drilled off-center to the extent that half of the formed head of the old rivet was not removed; the resulting formed head of the new rivet had to be spread to fill both the old and new countersinks. This represented a 'worst case' for the repair technique, since any less desirable repair would require scrapping of the strut. If this strut passed the relatively severe hot pressure
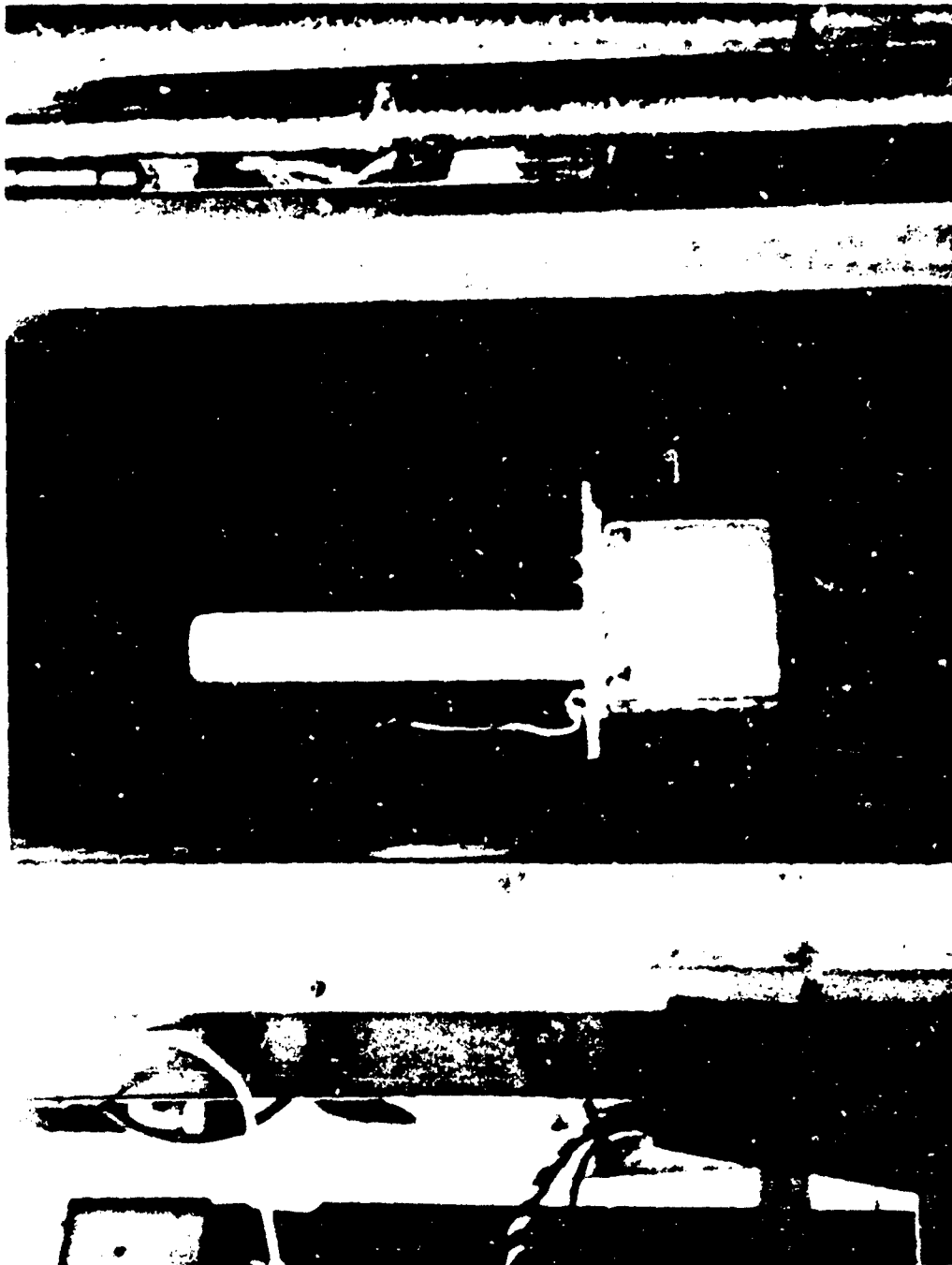
Figure B-1. Test Strut in Test Setup

tests, it was felt that the repaired production struts would indeed be flightworthy. The test part was assembled to a small plenum chamber with an asbestos gasket and a backup plate simulating the flight strut assembly.

TEST APPARATUS AND PROCEDURE

A thermostatically controlled electric oven was used. The oven contained a fan which forced hot air over the test part to ensure uniform temperature. Temperature of the strut metal was monitored by a chromel-alumel thermocouple close to the base of the strut (slowest to heat up). The specified temperature was maintained ± 10°F. Pressure (dry nitrogen) was supplied to the plenum chamber through a precision regulator valve; the leakage through the asbestos gasket was such that a continuous flow was required. Plenum pressure was monitored through a separate line to ensure that no line-pressure drops occurred. The pressure meter was a Heise precision gage, 0-60 psig, accurate to less than 0.1 psig. Specified pressures were maintained ±0.1 psig.

The test procedure consisted of repeated pressure cycling tests at a series of fixed temperatures. Each pressure cycle consisted of increasing pressure gradually from zero to the test level in about one minute, hold at test level for one minute, and decrease to zero in another minute. Strut thickness was measured at three locations away from the rivet heads with a micrometer or a micrometer caliper before and after each series of pressure cycles, with the strut at room temperature. The schedule of temperatures and pressure cycles is shown in Table B-1. An additional creep test was added, holding the strut at takeoff temperature and pressure for 3.0 hours (equivalent to approximately 200 takeoffs, representative of one or two years of experimental flight testing). This creep test was inserted prior to the 'ultimate' test.

TABLE B-1
TEST SCHEDULE OF TEMPERATURE AND PRESSURE CYCLES

Test	Temp °F	Pressure	No. of C	Remarks
0				Pretest Measurement
1	350°F	3 psig	1, 3, 10	Cruise
2	350	6	1, 3, 10	2 x Cruise
3	550	6	1, 3, 10	Takeoff
4A	550	6	1	Three Hour Creep Test (200 takeoffs)
5	550	8	1, 3, 10	1.33 x Takeoff
6	550	12	1, 3, 10	2 x Takeoff

TEST RESULTS

Initial Tests

Results of Tests 1 through 3 are shown in Table B-2. After 22 minutes of Test 4A, the lower rivet pulled through the skin, terminating the test. Prior to this failure, the growth of the strut was insignificant.

Analysis of Failure and Repairs

A photograph of the strut with the failed rivet is shown in Figure B-2; a closeup of the pulled out rivet head is shown in Figure B-3.

The reason for the failure was determined by sectioning several of the riveted struts (not the test strut). Typical rivet appearances were found to be as shown in Figure B-4a. It is apparent that the forming of the rivet head has not resulted in mushrooming and clamping of the skin, but instead the rivet shank has increased in diameter by nearly 20%, enlarging the hole in the post, displacing the countersunk skin material, raising the skin away from the post, and providing no appreciable clamping action.

The first attempt at a repair was to weld the rivet to the skin. This would make a gas-tight seal and a good mechanical connection, if good fusion to the rivet could be achieved. The typical results of several tests are illustrated in Figure B-4b. Some good welds to the rivet were successful (lower) but frequently the rivet did not bond to the skin (upper). Two reasons for this appeared to be (a) the lack of good clamping of the skin, after the rivet was melted, and (b) the rivet material (4117) is not considered readily weldable.
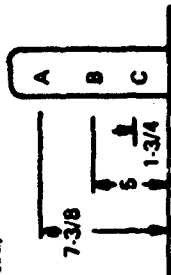
The next attempt at repair was to weld the skin directly to the post. The skin (6061-T0) is readily weldable with the 4043 weld wire and the post is cast 356 aluminum, also readily weldable. To clean the material and the casting scale, a hole of 0.093 inch to 0.125 inch diameter was drilled through the skin into the post, about 1/4 inch from the rivet. The arrangement is self-fixturing to a degree, since the rivet should retain the skin. A copper 'chill' consisting of a 1/4 inch thick copper plate with a 3/8 inch diameter, 100° countersink hole was fabricated to be placed over the weld to keep the heating and distortion of the strut to a minimum.

The resulting welds and problems are illustrated in Figure B-4c. The clamping action of the rivet and chill was not adequate to prevent the skin from lifting off the post. The residual material on the interior surfaces (casting scale, mill scale, zinc chromate) could not be adequately cleaned, resulting in cracked and porous welds. No assurance could be given of adequate welds by external inspection or X-Ray. The welding approach was therefore abandoned, in favor of mechanical methods.

Two mechanical approaches were tried. In one, a 4-40 screw hole was drilled, tapped and countersunk next to the existing rivet (same location as the welds of Figure B-4c all the way through the strut). A flat-headed aluminum screw slightly longer than the strut thickness was used. The threaded end of the screw was riveted or peened to prevent the screw from backing out. This appeared acceptable, except that a tolerance problem might exist because the posts in the production struts might be slightly cocked, and leakage around the screwhead would be hard to avoid. The method appeared expensive, and also would not prevent leakage around the old rivet.

TABLE B-2
RESULTS OF TESTS 1 THRU 3

Test No.	Date	Temp °F	Press. psig	Cycles Comp	Total Cycles Per Test	A Top	B Center	C Lower	Remarks
Base 1	8/21/73	Room	-	-	1	0.262	0.290	0.303	(1 in. Micrometer used)
		355	3	1		0.257	0.278	0.291	
		355	3	3	4	0.256	0.278	0.291	
		359	3	10	14	0.256	0.277	0.291	
2	8/22/73	360	6	1	1	0.256	0.277	0.291	
			6	3	4	0.256	0.277	0.291	
			6	10	14	0.256	0.276	0.289	
3	8/23/73	550	6	1	1	0.257	0.280	0.293	Noted lower rivet pulling through
			6	3	4	0.257	0.282	0.295	
			6	10	14	0.2576	0.290	0.303	
4		550	8	1					
			8	3					
			8	10					
4A	8/24/73	550	8			0.257	0.296	0.310	End test after 22 min. on 8/24/73 dimensions made on 8/27/73 8/27/73
5		550	12	1					8/27/73 - Strut removed for examination
				10					

Remarks diagram:

7-3/8

5

1-3/4

A

B

C

Figure B-3. Closeup of Failed Rivet Head
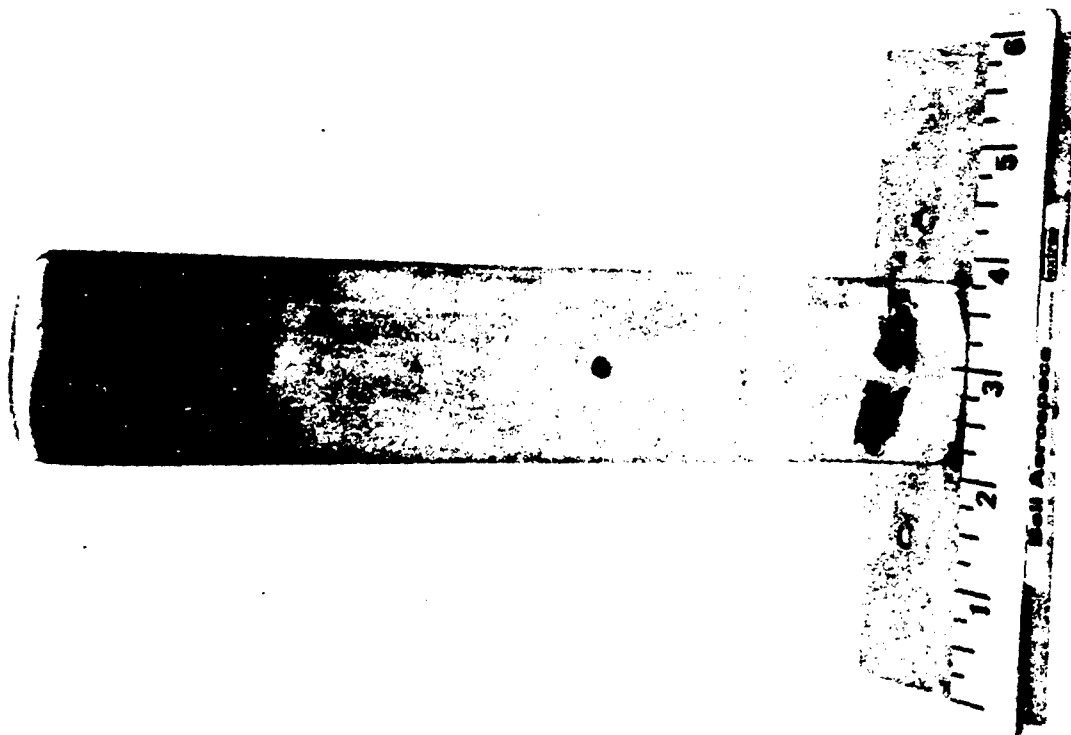
Figure B-2. Test Strut After Failure

(a) Typical Production Rivets

(b) Weld to Rivet Head
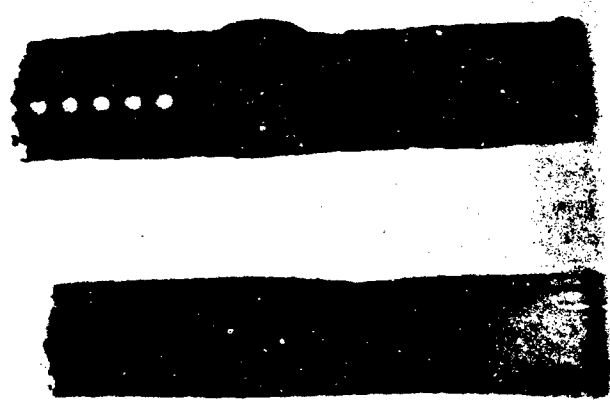
(c) Weld to Post

(d) Larger Soft Rivet

Figure B-4. Rivet and Repair Cross Section

162

The second mechanical approach was to replace the existing rivet. It was believed that the reason that the existing rivet was unsatisfactory was due to the fact that the rivet was harder than the material around it. The 4117-(T4) rivet shank was not being restrained by the relatively thin walls of the (cast Al 356) post, or by the 6061-(O) annealed skin. However, if the rivet were in either the annealed or quenched condition, it could be properly upset into the countersunk skin. This was demonstrated by reheat treating some of the original rivets and inserting them in drilled-out holes. This was partially successful, but two problems arose. In the drilling process, the posts were frequently rotated by the drill to about a 45° position with respect to the strut. Secondly, the enlarged shank of the old rivet frequently came out, leaving a hole too large for the rivet, resulting in insufficient rivet material to form a proper head.

The problem of the twisting posts was solved by fabricating a pair of tongs (Figure B-5) which could be used to restrain the post in its proper position during the drilling operation. The problem of the enlarged shank was solved by employing the next larger size rivet; the hole for this rivet removed all of the original rivet.

In order to form a good head, a rather long rivet was used, and hand-peened to form an oversize 'mushroom'. In order to ensure that the head could be formed properly, it was necessary to restrict the diameter of the countersink to be less than the width of the post (0.205 inch minimum). This is smaller than the specified diameter of countersink for this size rivet (0.228 inch). Therefore the manufactured head and the formed head both protrude from the skin. The manufactured head was peened down slightly, and then both sides were cleaned by grinding flush to the skin. The resulting rivet sections proved very reproducible, appearing typically as shown in Figure B-4d. These appeared satisfactory for continuation of the test.

It should be noted that this repair procedure differs from the riveting specifications in three respects: use of W-condition 'as-quenched' rivets; working the manufactured head; and reducing the diameter of the flat head by grinding. The justification for these deviations is the use only for this repair, under strict surveillance. For future production a redesign is required.

Following the demonstration of a reproducible repair procedure, both rivets of the test strut were repaired for continuation of the test. In drilling out the failed (lower) rivet, the hole was drilled so that half of the formed head of the old rivet was not removed. The countersink operation removed the old head, and also champfered around the new hole. The formed head of the new rivet thus had to be spread to fill both the old and the new countersinks. This represented a 'worst-case' for the repair technique, since any less desirable repair would require scrapping of the strut.

The repaired strut is shown in Figure B-6.

Completion of the Test

The repaired strut was subjected to tests 4A, 4, and 5. The results of these tests are shown on Table B-3. The 3-hour creep test resulted in a growth in thickness of 0.007 inch, 0.017 inch, and 0.015 inch respectively at the three measurement locations. Ten pressure cycles to 1.33 times takeoff condition resulted in barely measurable further growth. and started very small leaks around the rivets.

At the ultimate load condition (2 times takeoff) continued growth is apparent, and increased leakage. However no failure occurred.
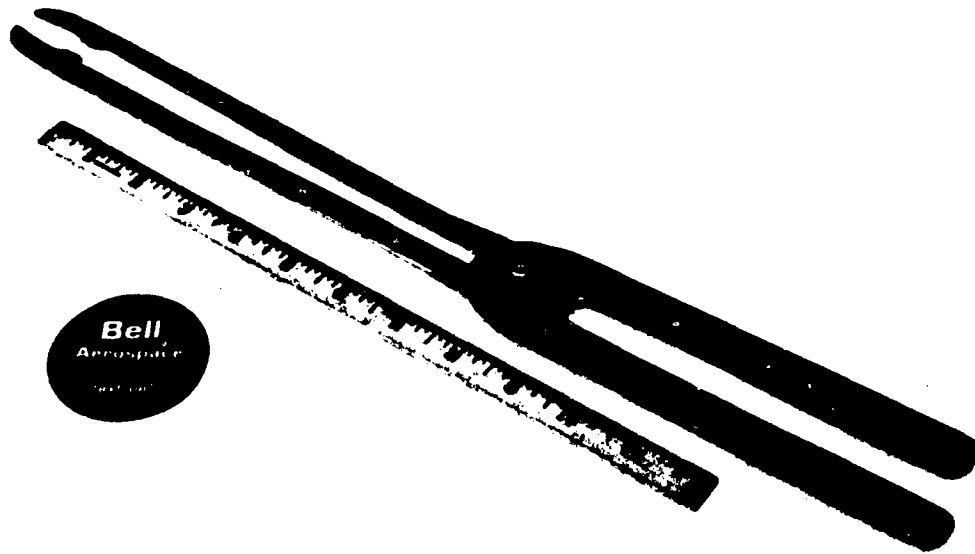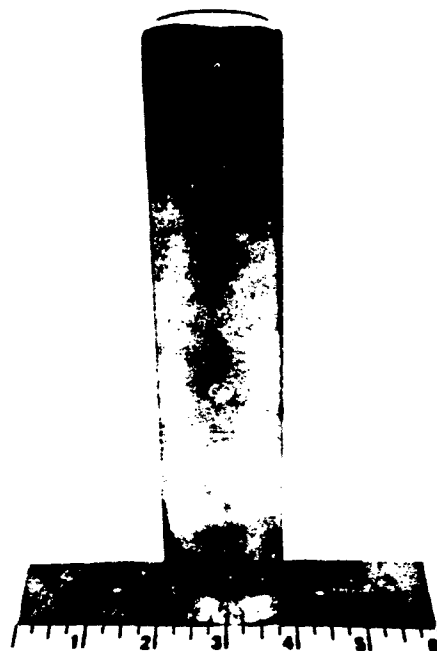
Figure B-5. Tongs to Hold Parts for Drilling

Figure B-6. Test Strut After Repair

TABLE B-3
RESULTS OF TESTS 4A THRU 5 AFTER STRUT REPAIR

Test No.	Date	Temp °F	Pres psig	Cycles	Total Cycles	Arm Prop			Remarks
						A Top	B Center	C Lower	
4A	9/10/73	Room	3	...	...	0.269	0.267	0.302	No leakage at rivets at 3. psi.
		Room	0	...	...	0.269	0.271	0.302	Prior to heat to 550° (Dial vernier caliper used)
		Room	0	...	...	0.276	0.288	0.317	After heat to 550°
		550	6	Soak 3.0 hrs	.				
4	9/11/73	550	8	1	1	0.276	0.288	0.318	Leak at top rivet Mfg end. Shop ends OK.
				3	4	0.276	0.289	0.318	
				10	14	0.278	0.291	0.320	Leak at top rivet both ends. Bottom at Mfg end.
5	9/12/73	550	12	1	1	0.278	0.298	0.335	Top, Mfg end - slight leak.
		550	12	3	4	0.300	0.325	0.366	Top, Shop end - moderate leak.
		550	12	10	14	0.301	0.350	0.385	Bottom, Mfg end - slight leak.
									Bottom, Shop end - slight leak.

Appearance of the strut after completion of the test is shown in Figure B-7 (strut was buffed to emphasize skin dimpling) and Figure B-8 where the left strut (after test) is compared with an untested strut. The bulging is seen to be quite general, and the rivet is effective only over a relatively small part of the skin.

CONCLUSIONS

a.   The struts as manufactured were not satisfactory for use due to inadequate formed rivet heads.

b.   The replacement of the inadequate rivets with an appropriate rivet procedure is reproducible.

c.   The repaired struts will have sufficient strength to withstand extended ground testing and flight testing appropriate to test aircraft.

d.   All of the 482 production struts were repaired using the demonstrated repair technique.

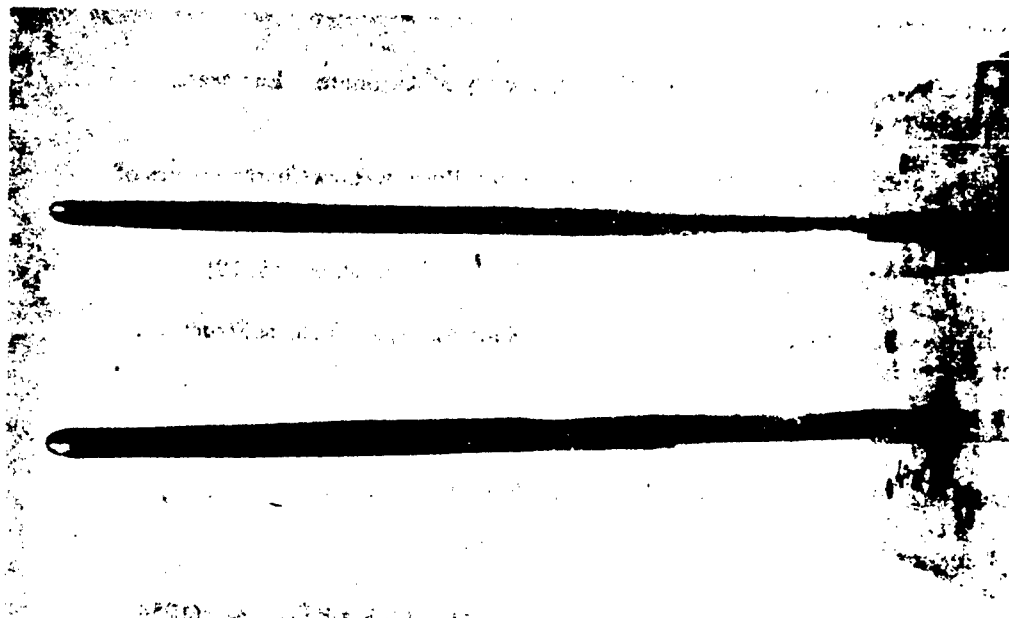e.   A redesign is required for any future production.

Figure B-8. Test Strut (left) After Test to Ultimate Stress (front view)
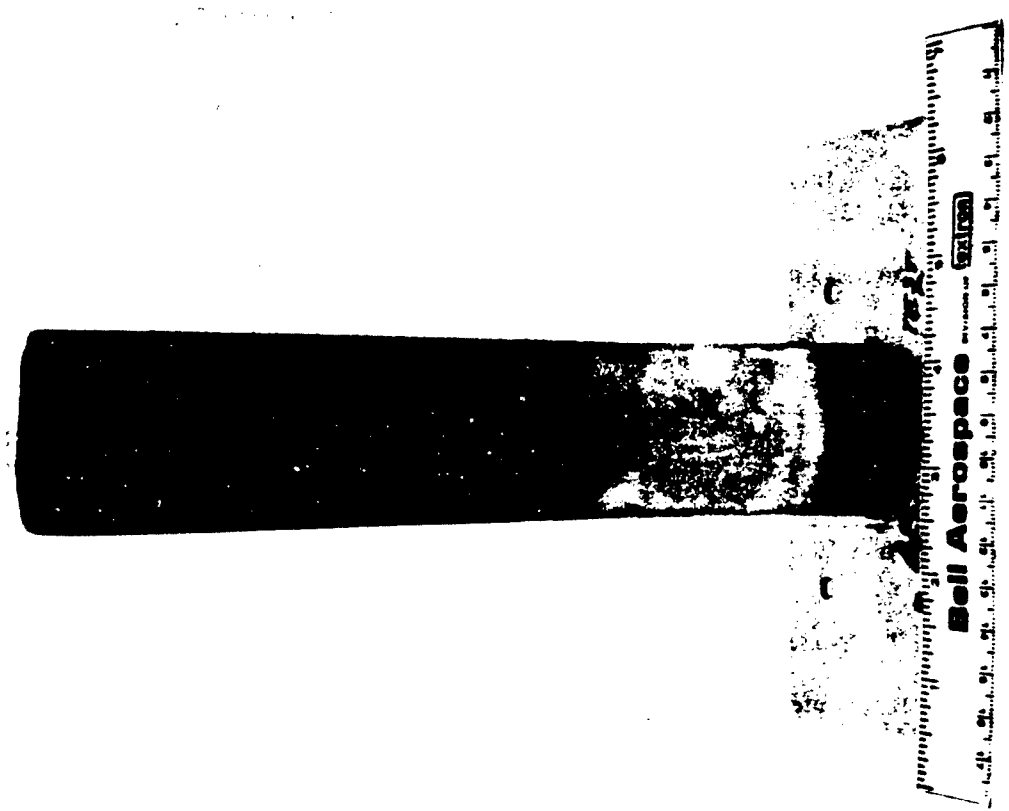Compared to Untest Strut (right)

Figure B-7. Test Strut After Test to Ultimate Stress (Side View)

167

VI. REFERENCES

1. Fluid Flow Data Book, General Electric Co., Schenectady, N.Y., Section 6405.6, December 1969.

2. Aerospace Applied Thermodynamics Manual, Society of Automotive Engineers, February 1960.

3. Henry, John R., "Design of Powerplant Installations, Pressure-Loss Characteristics of Duct Components," NACA ARR No. L4F26, 1944.

4. "Individual Lift Devices," BAC Report No. 2203-933023, December 15, 1967.

5. MIL-HNBK-5B, "Metallic Materials and Elements for Aerospace Vehicle Structures," 1 September 1971.

6. "Fuselage Stress Analysis," Schweizer Aircraft Corp., Report No. 32-3.

7. "Basic Design Data," Schweizer Aircraft Corp., Report No. 32-1A.

8. Bell Aircraft Corporation Structures Manual.

9. Roark, R.J., "Formulas For Stress and Strain," McGraw-Hill Book Co., Inc., (1954).

10. Bruhn, E.F., "Analysis and Design of Flight Vehicle Structures," Tri-State Offset Co., (1965).

11. Timoshenko, "Strength of Materials PT.I.," D. Van Nostrand Co., Inc., (1940).

12. Sechler, E.E. and Dunn, L.G., "Airplane Structural Analysis and Design," John Wiley & Sons, Inc., (1942).

13. Schweizer Aircraft Corporation Form I-4356, pages 1-3, dated 11 July 1966.

14. Bisplinghoff, R.L., Ashley, H., Halfman, R.L., "Aeroelasticity," Addison-Wesley Publishing Co., Inc. 1955.

15. "Investigation of Damping Methods for Augmentor Combustion Instability," AFADL-TR-72-84, October 1972.

16. "Study and Development of Turbofan Nacelle Modifications to Minimize Fan-Compressor Noise Radiation, Volume II - Acoustic Lining Development," NASA CR-1712, January 1971.

17. Beranek, L.L., "Noise and Vibration Control," Chapter 11, McGraw Hill, 1971.

18. Bossler, F.B., Barsotelli, M.V., Krishnamoorthy, V., et. al., "Jet Noise Reduction Technique for Military Reconnaissance/Surveillance Aircraft (Phase I - Bench/Wind Tunnel Tests)," AFFDL TR-72-107, August 1973.

19. Krishnamoorthy, V., Bossler, F.B.; Bell Aerospace Co. Report No. 7389-945005A, "Jet Noise Reduction for Military Reconnaissance/Surveillance Aircraft, Task Summary Report Phase I, Task 5 Wind Tunnel Tests A. Aerodynamic Tests," April 1972.

20. Abbott, I.H. and vonDoenhoff, A.E., "Theory of Wing Sections," McGraw-Hill Book Co., Inc., 1949.

21. Toll, T.A., NACA Report No. 868, "Summary of Lateral-Control Research," 1947.

22. Basic Design Data Report No. 32-1A, Schweizer Aircraft Corp.

23. Flutter Test and Analysis Report No. 32-7, Part II, Schweizer Aircraft Corp.

24. Manual on Aero-Elasticity. Agard. Vol. V, Chapter 6.

25. "Wing Stress Analysis," Schweizer Aircraft Corp. Engineering Report. 32-6.

26. "2-32 Static Test Report," Schweizer Aircraft Corp., Report No. 32-5.

27. "Determination of Wing Airloads," Schweizer Aircraft Corp., Report No. 32-2, 1 Sept. 1971.

28. "Measurements of the Radiated Noise from a Schweizer 2-32 Sailplane with and without a Wing Mounted Multi-Strut Assembly," Air Force Flight Dynamics Laboratory, AFSC, Wright Patterson Air Force Base, Ohio; Report No. AFFDL/FYA-73-5, 1 May 1973.

DOCUMENT CONTROL DATA - R & D

(Security classification of title, body of abstract and indexing annotation must be entered when the overall report is classified)

1. ORIGINATING ACTIVITY (Corporate author)	2a. REPORT SECURITY CLASSIFICATION
Bell Aerospace Company	Unclassified
Buffalo, New York 14240	2b. GROUP
	N/A

3. REPORT TITLE

JET NOISE REDUCTION FOR MILITARY RECONNAISSANCE/SURVEILLANCE AIRCRAFT PHASE II: ANALYSIS AND DESIGN OF A QUIET RESEARCH TEST VEHICLE

4. DESCRIPTIVE NOTES (Type of report and inclusive dates)

Final Technical Report   72 October to 74 February

5. AUTHOR(S) (First name, middle initial, last name)

Robert F. Speth, et. al.

6. REPORT DATE	7a. TOTAL NO. OF PAGES	7b. NO. OF REFS
April 1974	169	28

8a. CONTRACT OR GRANT NO.	9a. ORIGINATOR'S REPORT NUMBER(S)
F33615-71-C-1840	BAC 7389-927004
b. PROJECT NO.	
AFFDL 1471 and AFAPL 3006	
c.	9b. OTHER REPORT NO(S) (Any other numbers that may be assigned this report)
Task No. - AFFDL 02 and AFAPL 14	AFFDL-TR-73-158
d. Work Element No. AFFDL 018 and AFAPL 005	

10. DISTRIBUTION STATEMENT

Distribution limited to U.S. Government Agencies only; test and evaluation; statement applied February 1974. Other requests for this document must be referred to AF Flight Dynamics Laboratory (FYA) Wright-Patterson AFB, Ohio 45433.

11. SUPPLEMENTARY NOTES	12. SPONSORING MILITARY ACTIVITY
N/A	Air Force Flight Dynamics and Aero Propulsion Laboratory, Wright-Patterson Air Force Base. Ohio 45433

13. ABSTRACT

This report presents the results of the analysis and design of a static ground test version of a Quiet Research Test Vehicle (QRTV) utilizing flightworthy propulsion system components. Also included is a discussion of the fabrication of a sufficient number of propulsive struts, employing multiple micro-jets, to propel a Schweizer SGS 2-32 sailplane up to 123 knots airspeed.

The analysis and design encompasses the information required to modify the sailplane structure to incorporate the propulsion system for basic ground tests. The design of the static ground test is not covered completely. Overall consideration of the ultimate QRTV flight version has been a primary goal in the analysis and design phase of this program.

As negotiated originally, the modification to the wing structure necessary to install the spanwise ducts was not a task in Phase II. Late in the program, the analysis and design of the spanwise wing duct installation was added to the program. Furthermore, hot pressure tests of a sample production propulsive strut were also included. Results of these two additional tasks have been incorporated as appendices in this report.

DD FORM 1 NOV 65 1473

14. KEY WORDS	LINK A		LINK B		LINK C	
	ROLE	WT	ROLE	WT	ROLE	WT
Acoustics						
Acoustic Research Aircraft						
Jet Noise Reduction						
Propulsion						
Quiet Propulsion						